ESTIMATING SOIL WATER CONTENT USING SOIL TEMPERATURES AND A NEURAL NETWORK

By

CHRISTINE THERESA ALTENDORF

Bachelor of Science
Oklahoma State University
Stillwater, Oklahoma
1985

Master of Science
Oklahoma State University
Stillwater, Oklahoma
1987

Submitted to the Faculty of the
Graduate College of the
Oklahoma State University
in partial fulfillment of
the requirements for
the Degree of
DOCTOR OF PHILOSOPHY
December, 1993

ESTIMATING SOIL WATER CONTENT USING

SOIL TEMPERATURES AND A

NEURAL NETWORK

Thesis Approved:

Ronald L. Elliott

Thesis Advisor

Donald R. Snethen

Thomas C. Collins

Dean of the Graduate College

PREFACE

This research is the development of a soil water content measurement system which uses soil temperatures and a neural network to predict soil moisture. Weather stations were placed at various locations to collect soil and weather data to be used as input parameters in the neural network. Thermocouple probes were designed to measure soil temperature at various depths. Several different neural network strategies were developed and tested until a "final" model which uses only soil temperatures was selected. The basis for the network design was dependent on the theoretical soil water - temperature relationship. The final model was tested, and proved to be an efficient, accurate method for measuring soil water content.

I would like to thank Dr. Ronald L. Elliott, my adviser, for his input and guidance during this research, and for his patience through all of my gripe sessions. I would also like to thank Dr. Marvin L. Stone who let me experience all the phases of running the grant from which this research was funded. It was an insight into my future if I choose to remain in University life. Also appreciated is the input from Dr. Dan Storm for his service on my committee and for his help in preparing this document. I would also like to thank the committee member from outside my department, Dr. Don Snethen, for his time and commitment to this project. Although I did not make it to Engineering South very often, his words of encouragement and wisdom from the shrimp stand were valued.

I would also like to acknowledge Dr. Tom Haan. The time he spent analyzing data was greatly appreciated. Thanks also goes to Dr. Mike Kizer who took many trips to the field to check datalogger problems. His guidance and input to this project, and life in general, will always be remembered.

Special thanks are due to all of the hourly employees that gathered field data for me over the past several years - Arvil Bass, Mark Dahlke, John Ringer, Chad Dow and Degaga Kumera. The ups and downs of being a supervisor for this group surely has prepared me for the real world. I would also like to thank Tung-Ming Koo, Meishan Cheng and Liu Xiaoji who were the computer programmers who worked on the neural network for me.

Other thanks goes to all the members of the Biosystems and Agricultural Engineering Department. The friendships that I have made over the years will always be treasured. I would like to especially thank Marge Johnston, who let me know how I was supposed to act each day with the morning reading of my horoscope, and Tracie Brown who handled the money side of this research, but more importantly, walked daily with me to the Little Bakery for chocolate muffins. I would also like to thank my pseudo big brothers - Sam Harp, Ray Huhnke, Dick Whitney, and John Solie. Without them to argue and fight with, I probably would have finished this dissertation years earlier, but chose to harass them as long as possible.

I would finally like to thank my friends and family for their support and encouragement through these many years of school. My parents, Harold and Catherine have always been there when needed and have always supported my decisions. I would also like to thank Richard Norman for always telling me that I could do it and that the future was limitless. For this I will always be grateful.

TABLE OF CONTENTS

Chapter | Page

1. INTRODUCTION 1
    Background 1
    Objectives of Study 3

2. REVIEW OF SOIL WATER CONTENT MEASUREMENT METHODS . . . 4
    Introduction 4
    Laboratory Methods 4
    Field Methods 7
        Tensiometers 7
        Electrical Resistance Blocks 8
        Heat Dissipation Sensor 10
        Thermocouple Psychrometer 11
        Neutron Scattering Method 12
        Near Infrared Reflectance Spectrometry (NIR) 13
        Dielectric and Time Domain Reflectrometry Sensors 15

3. SOIL WATER AND THERMAL RELATIONSHIPS 18
    Heat Flow in Soil 18
    Thermal Properties of Soils 21
        Volumetric Heat Capacity 21
        Thermal Conductivity of Soil 22
        Thermal Diffusivity 26
            Thermal Regime of Soil Profiles 27
            Thermal Diffusivity Solutions 29
    Simultaneous Transport of Heat and Moisture 33

4. NEURAL NETWORK THEORY 35
    Background 35
    Learning 38
    Types of Neural Networks 40
        Mapping 40
        Associative Memory 40
        Prototype 42
    Backpropagation 44
        Description 44
        Operation and Function 45
        Learning Algorithm 48

Chapter | Page

Error 49
Summary 54
Neural Network Applications 54

5. FIELD PROCEDURES 57
General 57
Site Locations and Layout 57
Datalogger 60
Measured Varaiables 62
Wind Speed 62
Rainfall 62
Solar Radiation 62
Net Radiation 63
Soil Heat Flux 63
Soil Temperature 64
Air Temperature 66
Soil Water Content 66

6. MODEL DEVELOPMENT 68
Preliminary Data Analysis 68
Bulk Density 68
Soil Temperature 68
Thermal Diffusivity Calculation 70
Thermal Conductivity Calculation 73
Neural Network Design 75
ExploreNet 77
NeuralWare 82
Final Network Development 93
Thermocouple Probe Installation Comparison 111
Network Optimization 112
Multiple Variable Linear Regression 115

7. MODEL VALIDATION 119
Soil Coefficient Values 119
Model Testing 120
Efaw 122
Perkins 123
Hyd 123
General 144
Repeatability of Measured Soil Water Content 152
Multiple Variable Linear Regression Results 154

8. SUMMARY, CONCLUSIONS AND RECOMMENDATIONS 163
Summary and Conclusions 163
Recommendations 166

REFERENCES 168

APPENDICES 176

APPENDIX A - CAMPBELL SCIENTIFIC DATALOGGER PROGRAM 177

APPENDIX B -THERMAL DIFFUSIVITY PROGRAM 181

APPENDIX C - EXAMPLE RAW DATA COLLECTED FROM DATALOGGER 186

APPENDIX D - NEURAL NETWORK COEFFICIENT INFORMATION 191

APPENDIX E - PROCESSING ELEMENT INFORMATION 194

APPENDIX F - C CODE OF NEURAL NETWORK MODEL 204

APPENDIX G - FOURIER ANALYSIS PERIODOGRAMS 208

LIST OF TABLES

Table Page

5.1. Particle Size Distribution for Soil Types 58

6.1. Original Neural Network Designs 79

6.2. Network Summary for Various Inputs 85

6.3. Root Mean Square Error Analysis for Various Networks and Depths 88

6.4. MinMax Table for Neural Network Input Parameters 95

6.5. Root Mean Square Error Analysis for Improved Networks and Depths 97

6.6. Regression Analysis Results of Combined Network 106

6.7. Root Mean Square Error Analysis for the Individual Probes 112

6.8. MinMax Table for Final Network Input Parameters 113

7.1. Hyd Data Soil Coefficient Values 121

7.2. Statistics of Neural Network Results 145

7.3. Network Prediction Capabilities for Various Error Values 151

7.4. Neutron Moisture Gauge Readings 155

7.5. Correlation Coefficients of Multivariate Linear Regression 156

LIST OF FIGURES

Figure Page

4.1. Neural Network Processing Element and Connections 36

4.2. Typical Backpropagation Network 45

4.3. Backpropagation Processing Element 47

4.4. Sigmoid Function 50

4.5. Hyperbolic Tangent Function 51

5.1. Layout of Data Collection Sites 59

5.2. CR10 Datalogger and Multiplexer 61

5.3. Thermocouple Probe Used to Measure Soil Temperatures 67

6.1. Bulk Density Values for Efaw 69

6.2. Bulk Density Values for Perkins 69

6.3. Hourly Soil Temperatures for 4 Depths 71

6.4. Daily Soil Temperatures for 4 Depths 71

6.5. Calculated Thermal Diffusivity (α) Values for Efaw 74

6.6. Calculated Thermal Conductivity (λ) Values for Efaw 74

6.7. Active Range of a Transfer Function 80

6.8. Change in Temperature with Depth and Time 86

6.9. Perkins Networks Tested with Perkins Test Data 91

6.10. Efaw Networks Tested with Efaw Test Data 92

6.11. Predicted and Measured Values Using Efaw-Trained Network (15 cm) . . . 98

Figure Page

6.12. Predicted and Measured Values Using Efaw-Trained Network (30 cm) . . . 99

6.13. Predicted and Measured Values Using Efaw-Trained Network (60 cm) . . . 100

6.14. Predicted and Measured Values Using Efaw-Trained Network (120 cm) . . 101

6.15. Predicted and Measured Values Using Perk-Trained Network (15 cm) . . . 102

6.16. Predicted and Measured Values Using Perk-Trained Network (30 cm) . . . 103

6.17. Predicted and Measured Values Using Perk-Trained Network (60 cm) . . . 104

6.18. Predicted and Measured Values Using Perk-Trained Network (120 cm) . . 105

6.19. Measured and Predicted Values of Combined Model (15 cm) 107

6.20. Measured and Predicted Values of Combined Model (30 cm) 108

6.21. Measured and Predicted Values of Combined Model (60 cm) 109

6.22. Measured and Predicted Values of Combined Model (120 cm) 110

7.1. Measured and Predicted Test Results for Efaw (15 cm) 124

7.2. Residual Plots for Efaw (15 cm) 125

7.3. Measured and Predicted Test Results for Efaw (30 cm) 126

7.4. Residual Plots for Efaw (30 cm) 127

7.5. Measured and Predicted Test Results for Efaw (60 cm) 128

7.6. Residual Plots for Efaw (60 cm) 129

7.7. Measured and Predicted Test Results for Efaw (120 cm) 130

7.8. Residual Plots for Efaw (120 cm) 131

7.9. Measured and Predicted Test Results for Perkins (15 cm) 132

7.10. Residual Plots for Perkins (15 cm) 133

7.11. Measured and Predicted Test Results for Perkins (30 cm) 134

7.12. Residual Plots for Perkins (30 cm) 135

Figure Page

7.13. Measured and Predicted Test Results for Perkins (60 cm) 136

7.14. Residual Plots for Perkins (60 cm) 137

7.15. Measured and Predicted Test Results for Perkins (120 cm) 138

7.16. Residual Plots for Perkins (120 cm) 139

7.17. Measured and Predicted Test Results for Hyd (15 cm) 140

7.18. Residual Plots for Hyd (15 cm) 141

7.19. Measured and Predicted Test Results for Hyd (30 cm) 142

7.20. Residual Plots for Hyd (30 cm) 143

7.21. Frequency Distribution of Error for Efaw at 15 and 30 cm 146

7.22. Frequency Distribution of Error for Efaw at 60 and 120 cm 147

7.23. Frequency Distribution of Error for Perkins at 15 and 30 cm 148

7.24. Frequency Distribution of Error for Perkins at 60 and 120 cm 149

7.25. Frequency Distribution of Error for Hyd at 15 and 30 cm 150

7.26. Individual Temperatures Test Results for Efaw (15 cm) 157

7.27. ΔT with Time Test Results for Efaw (15 cm) 158

7.28. ΔT with Depth Test Results for Efaw (15 cm) 159

7.29. Individual Temperatures Test Results for Perkins (15 cm) 160

7.30. ΔT with Time Test Results for Perkins (15 cm) 161

7.31. ΔT with Depth Test Results for Perkins (15 cm) 162

CHAPTER 1

INTRODUCTION

Background

The water content of a soil can vary with depth, time, texture, bulk density, climate, and many other factors. Knowledge of soil water content is important in many agricultural, environmental and structural applications including irrigation scheduling, leachate control, contaminant transport, soil strength and stability, and drought assessment. Changes in moisture content are the primary cause of variability in a soil's heat transfer properties for a given soil composition and density. Complicating the characterization of thermal properties is the fact that moisture content within a soil profile will vary based on the processes of precipitation/irrigation, evaporation, transpiration, and temperature induced moisture migration.

The measurement of water content in the soil has always posed an interesting problem. Methods of determination vary quite extensively, and all have drawbacks. Current soil moisture measurement methods include gravimetric sampling, radioactive techniques, and the use of moisture sensors. The gravimetric sampling method is laborious and destructive. Radioactive techniques are reproducible, but continuous temporal monitoring is very difficult. In addition, because of the radioactive sources and required licenses, general application of this technique is impractical. Soil water content can be measured using moisture sensors buried in the soil. There are several moisture sensors commercially available, none of which has proved to be entirely satisfactory. An improved soil moisture sensor system is needed which allows continuous in-field monitoring of soil water content. Ideally, the sensor should satisfy the following basic criteria:

a) mechanical construction allowing for installation with minimal impact on soil structure
b) sensitivity to moisture variations from air dry to full saturation
c) insensitivity to soil texture
d) insensitivity to soil solution composition
e) long-term calibration stability
f) long life with minimal maintenance requirements
g) economical.

This research is based on the knowledge that the rate of heat flow in soil is sensitive to water content. Basically, air is a better thermal insulator than water, so that as water is replaced by air, the remaining water films become thinner and the path length for and resistance to heat conduction increases. Using this theory, it is proposed that soil moisture content can be determined based on soil thermal properties, more specifically, temperatures. Accurate soil temperatures are relatively easy and inexpensive to determine.

Although soil water content and soil temperature are definitely interrelated, a problem arises in that there are other factors affecting the relationship, including soil thermal conductivity and bulk density. Both of these parameters are difficult to measure. To circumvent these uncertainties, a neural network modeling approach is proposed.

In using a neural network, the objective is to provide sufficient data to train the network to estimate the desired outcome. A neural network could potentially relate soil temperature and moisture without necessarily knowing the values of all the governing parameters. Neural networks are typically used to develop a relationship between several inputs and several outputs. Rather than being given information about how to process the input, neural networks determine the procedure by looking at several examples of input/output pairs. This process of self-organizing is called learning. With this concept in mind, a neural network was selected so that easily measured soil parameters could be used as input data resulting in soil water content as the output data.

Objectives of Study

The overall objective of this study was to develop a system which can measure soil water content accurately and inexpensively based on soil thermal properties, mainly temperature. The specific supporting objectives included in the main objective are:

1. Design and deploy a sensor system to collect field data at three different sites, each consisting of a different soil type.
2. Develop a model which uses the collected data to predict soil water content.
3. Validate the model using test data.

CHAPTER 2

REVIEW OF SOIL WATER CONTENT MEASUREMENT METHODS

Introduction

Soil water is usually measured as water content (either mass or volume fraction) or as soil water potential (the amount of useful work per unit quantity of pure water that must be done by means of externally applied forces to transfer reversibly and isothermally an infinitesimal amount of water from the standard state to the soil liquid phase at the point under consideration - Bolt, 1976). The need for quantitative information on soil moisture has led to the development of a number of methods for its measurement, with various principles employed. All techniques possess certain limitations and shortcomings.

Laboratory Methods

Laboratory methods for determining the moisture content of a soil are useful for verification or calibration of many types of in situ field instruments. The basic testing approaches are thermo-gravimetric, chemical extraction, mechanical extraction, and immersion (Morrison, 1983).

Gravimetric methods consist of weighing a wet soil sample followed by oven drying at 105°C until a constant weight is attained. Microwave, infrared, and vacuum drying have also been used. To calculate the water content on a mass basis, the weight of the evaporated water is expressed as a fraction of the dry soil weight. Soil bulk density must be known to convert this gravimetric water content to a volumetric water content:

$$\theta = \frac{W_w \, \rho_s}{W_s \, \rho_w} \tag{2.1}$$

where

θ = volumetric water content
W_w = weight of water (g)
W_s = dry weight of soil (g)
ρ_s = oven dry bulk density (g/cm^3)
ρ_w = water density (g/cm^3)

This method is labor intensive and time consuming, especially if samples from deep in the root zone are needed. Because of spatial variability, several samples may be needed to obtain representative values of water content. Also, because of drying time, there is at least a 24 hour delay between the time of sampling and the time at which results are known (Hillel, 1980). Variations of this method include freeze drying (lyophilization), distillation, heating in oil, desiccant weight gain, and alcohol burning.

The three types of chemical extraction employ alcohol, calcium carbide (hydride), and the Karl Fischer approach (Morrison, 1983). In the alcohol extraction method, the moisture content is determined by the density (hydrometer method) of the alcohol and water mixture after extraction from the soil sample. The calcium carbide method is usually related to the decrease in the weight of the carbide mixture after evolution of acetylene, and the rise in pressure in a closed vessel containing the mixture, which measures the volume of gas produced. The calcium carbide reaction with the soil water proceeds as:

$$CaC_2 + 2H_2O \rightarrow Ca(OH)_2 + C_2H_2$$

The pressure of the C_2H_2 gas produced within the vessel is correlated with the moisture content. A similar procedure is employed in the hydride reaction:

$$CaH_2 + 2H_2O \rightarrow Ca(OH)_2 + 2H_2$$

In the Karl Fischer method, the soil sample is dissolved or leached with a solvent followed by titration with an iodine sulfur dioxide and pyridine in methanol solution. Determination of the titrated end point is related to the soil moisture content using electro-chemical endpoint detection.

For soils with a high moisture content, mechanical extraction is possible using pneumatic or hydraulic presses. The weight before and after compression is used to calculate the water content.

Immersion techniques measure the change in the specific gravity of the soil sample in various liquids. Water, alcohol, and alcohol acetone salt solutions have been employed. One technique relies upon the change in soil conductivity created with the displacing fluid. This value is corrected for temperature and correlated with the soil moisture content.

Errors due to soil sampling method can be reduced by increasing the size and number of samples. However, the sampling method is destructive and may disturb an observation or experimental plot sufficiently to distort the results. For these reasons, many workers prefer non-destructive, indirect methods, which permit making frequent or continuous measurements at the same points.

Field Methods

Tensiometers

There are a number of ways to make point evaluations of soil moisture indirectly. One method used for many years is measurement of soil water potential with tensiometers. A tensiometer is an air-tight system which consists of a ceramic cup connected through an impervious tube to a pressure-sensing device, with the cup and tube filled with water. When the tensiometer is initially placed in the soil, the water contained in the tensiometer is at atmospheric pressure. The soil, which is usually at less than atmospheric pressure, creates a suction. This suction draws a portion of the water out of the tensiometer through the ceramic cup, causing a vacuum in the plastic tube. This vacuum can be measured using a pressure transducer. The vacuum can also be measured with a vacuum gauge or a manometer. Through the use of a soil water potential curve, the volumetric water content at that potential is determined.

This method requires laboratory determination of the soil water potential curve (calibration of suction to water content), usually with a pressure plate apparatus. Another disadvantage of the tensiometer is the high maintenance required. It must be filled with de-aired water regularly. Also, tensiometers cannot be used in an extremely cold environment because the water inside the tensiometer will freeze. A further limitation is that tensiometers work effectively only up to suctions of approximately 0.8 bars which in many agricultural soils covers only about the upper 1/4 of the range of plant-available soil water.

There are two basic types of pressure transducers used with tensiometers. Enfield and Gillaspy (1980) described a pressure transducer that has a frequency output and is linearly temperature dependent. The more common type, described by Long (1982), uses a temperature compensated strain gage. The cost of the pressure transducer is a significant portion of the system cost. Thus, systems may have one pressure transducer serving several tensiometers. Anderson and Burt (1977) and Long and Huck (1980) used this principle in their designs. Another system that uses scanning photocells to measure mercury levels in manometer type tensiometers is described by Bottcher and Miller (1982).

Electrical Resistance Blocks

The electrical resistance of porous bodies placed in the soil and left to equilibrate with soil moisture can sometimes be calibrated against soil water content. The blocks are made of a porous material such as gypsum, fiberglass or spun nylon. Electrical contacts are imbedded in the block at a measured distance apart. When the block is buried in the soil, its water content varies with the surrounding soil, and the ease with which a calibrated current is passed between the imbedded contacts varies accordingly.

Electrical resistance blocks are inexpensive but have enjoyed rather limited success in measuring soil water content. Much of the difficulty in using the blocks stems from variations in the calibration relationship. The electrical resistance of a soil volume depends not only upon its water content, but also upon its composition, texture, and soluble-salt concentration. For the fiberglass resistance cell (FRC), Servick (1972) found that as the electrical conductivity of the soil increases, the impedance of the FRC decreases. Another difficulty discussed by England (1965) is the gradual degradation of the FRC sensitivity and gradual changes in calibration due to the impregnation of soil constituents into the fiberglass. The reduced sensitivity and change in calibration were found to occur during the first five to six years of use. A major limitation with gypsum blocks is a short life span of approximately 1 to 5 years, depending on the soil characteristics. Gypsum blocks have a shorter life span in alkaline soils and in soils that are saturated for extended periods of time. Another problem is the effects of salt on the life of the sensor and the associated degradation of the measurements. Aitchison et al. (1950) found that gypsum blocks placed in soil containing 0.3% or more total soluble salts with at least 0.2% NaCl were "completely unserviceable" after two years. They also found that salt contents exceeding 0.07% total soluble salts and 0.02% NaCl lowered the block resistance significantly.

Malicki and Hanks (1989) showed that within the range of commonly applied frequencies, readings of sensors' electrical capacitance are totally masked by interfacial pseudocapacitance while the readings of the sensor electrical resistance are influenced by interfacial phenomena unless the read-out device compensates for the capacitive component of the sensor impedance. Two electrical resistance methods were developed for making a continuous measurement of soil moisture under field conditions by Bouyoucos (1955). One employed a plaster block and the other a nylon unit encased in a plaster casting. The effective range of the plaster block was from field capacity to somewhat beyond the wilting point of plants. The effective range of the nylon cell was from near saturation to a point above the air dry condition. One major disadvantage of the gypsum units, especially for research purposes, is that they are not sensitive at tensions less than 300 cm.

A sensor which consists of two concentric electrodes buried in a particle matrix was tested and calibrated by Armstrong et al. (1985). Their research included the development of an equation which relates sensor resistance to soil water tension and temperature.

Heat Dissipation Sensor

The heat dissipation sensor operates on the principle of the difference in thermal conductivity between water and air. Shaw and Baver (1939) showed that in response to a short heat pulse, the rise in temperature (ΔT) of a porous medium containing water is inversely proportional to the water content of the medium. The dynamics of this phenomenon and of devices used to measure it have been studied for several decades (Shaw and Baver, 1939; Johnston, 1942; Bloodworth and Page, 1957; Phene et al., 1971, 1981; Wong and Ho, 1987). Phene et al.(1971) described a heat dissipation sensor (HDS) made of a micro-thermometer and heater embedded on opposite sides of a ceramic cylinder. The thermal dissipation properties of the ceramic vary with its moisture content, which is assumed to be in equilibrium with the surrounding soil. The HDS is sensitive to the matric potential of the soil in the range of approximately -0.1 to -1.0 bar. The HDS is independent of temperature, pH, and salinity effects but cell uniformity is a problem. Thus, each sensor should be calibrated for accurate results. Cardon et al. (1993) describe the physical equipment and data processing methodology for calibration of a soil matric potential sensor based on heat dissipation principles. Work by Gardner (1955) has shown that temperature changes in soil greatly influence soil water tension, therefore thermal techniques may change the parameter which is to be measured. A review of the present status of heat dissipation devices and their use is given by Phene et al. (1992).

Thermocouple Psychrometer

A thermocouple psychrometer measures the relative humidity of the soil pore air which is related to the total water potential of the soil. The total water potential is the sum of the matrix potential and the osmotic potential. A single junction thermocouple psychrometer consists of a sensing junction made of a chromel-constantan thermocouple. The thermocouple is enclosed in either a hollow porous ceramic cup or in a screen cage, and has a reference junction in the base. A thermocouple psychrometer can operate in two different modes. Both modes start by condensing a drop of water on the sensing junction. This process is accomplished by cooling the sensing junction below the dew point using the Peltier cooling effect described by Roeser (1940). The first mode, called the psychrometric mode, allows the water on the sensing junction to evaporate, during which time the wet-bulb depression is measured. In the second mode, called the dew point mode, a series of cooling currents is passed through the sensing junction, causing the junction to converge on the dew point. The wet-bulb depression and the dew point are linearly related to the total water potential, with a useful range of approximately -1.0 to -80 bars.

Weibe et al. (1977,1979) found that a major source of error associated with the thermocouple psychrometer is the thermal gradient which occurs when there is a difference between the temperature of the sensing junction and that of the reference junction. The thermal gradient causes extraneous output voltage which leads to error.

However, this error can be eliminated by using a model developed by Brown and Bartos (1982). Another problem is the contamination of the sensing junction which causes a shift in the calibration of the sensor. Merrill and Rawlins (1972) found that it was necessary to clean and recalibrate the thermocouple psychrometer every six months. In addition, Daniel et al. (1981) found that corrosion of the thermocouple wire was a problem in acidic clays. The device is also inaccurate at high moisture contents.

Neutron Scattering Method

Neutron scattering, which was first developed in the 1950's, has gained widespread acceptance as an efficient and reliable technique for monitoring soil moisture in the field (Holmes,1956; van Bavel,1963). Its principal advantages are that it allows less laborious, more rapid, non-destructive and periodically repeatable measurements (at the same locations and depths) of the volumetric wetness of a representative volume of soil. The method is practically independent of temperature and pressure. A source of fast neutrons is lowered into an access tube that has been installed in the soil. A sensor connected with the source measures the number of low energy neutrons that bounce back after colliding with hydrogen nuclei. In most agricultural soils, the predominant source of hydrogen is water, so a calibration relationship between neutrons measured and water content is possible. The main limitations of this method are the high initial cost of the instrument, the relatively low degree of spatial resolution, difficulty of measuring moisture in the soil surface zone and the labor involved in installing the access tubes. Also, the inconvenience and federal regulations associated with maintaining a radiation source, and the necessary recalibration as the radiation source decays can be difficult.

Near Infrared Reflectance Spectrometry (NIR)

The near infrared region of the electromagnetic spectrum extends from the visible region to the middle of the infrared region, or from approximately 800-2800 nm. Near infrared reflectance is a viable method of moisture determination because of the occurrence of absorption bands at 970,1190, 1450 and 1940 nm due to water (Curcio and Petty, 1951). Absorption bands occur when the frequency of the incident energy equals the frequency of overtones or combinations of the fundamental vibration modes of a molecule (Hunt and Salisbury, 1970). The greater the concentration of the molecule, in this case water, the more absorption occurs.

The possibility of using NIR methods in measuring the moisture content of soils was introduced almost three decades ago by Bowers and Hanks (1965). They found excellent correlation between percent reflectance at 1900 nm and the moisture content of Newtonia silt loam. Dalal and Henry (1985) used the NIR method to predict the moisture, organic carbon and total nitrogen contents of air dried soil.

Soil-methanol extracts have been prepared and analyzed in laboratory spectrophotometers. Bowers and Smith (1972) found a linear relationship between moisture content and the absorption of the methanol extracts of three soils at a wavelength of 1940 nm. Bowers et al. (1975) reported a curvilinear relationship between the absorbtion at 1940 nm and the moisture content of 16 soils using a portable spectrophotometer of their design. Both of these spectrophotometers require the collection of a soil sample to obtain the moisture content through the soil profile. The time to take the soil core and to prepare the soil-methanol extracts would prohibit real-time analysis. To allow real-time soil moisture content measurements at discrete intervals to be made with the NIR method, a fiber optic attachment similar to the ones used by Birth (1967) and Beroza et al. (1968) might be used. These two instruments used bifurcated bundles, in which a bundle of optical fibers from a light source and a bundle from a detector are joined together to form a common leg. The fibers at the end of the common leg were randomized so that the light from the source was reflected off the object and into the fibers leading to the detector. A common end bundle diameter of 6.35 mm allowed the reflection measurements to be taken over a small area.

Christensen and Hummel (1985) built a system which used the difference of two wave-lengths in an optical density calculation to predict gravimetric moisture content. They tested wavelength combinations ranging from 800 to 2600 nm. Kano et al. (1985) built a soil moisture sensor that determines the difference between two reflectance readings. The results showed a high correlation but the study was limited by the fact that the sensor was only tested on two soil types. Peterson and Baumgardner (1981) calculated the difference between an oven dry reflectance and the reflectance at a specific matric potential. Their results indicate that 52 different soils tend to fall on a straight line when the difference is plotted against oven dry reflectance. Price et al. (1990) developed and tested an NIR sensor to predict corn seed planting depth based on moisture content and matric potential. The sensor was tested on 29 different soils and was able to predict the -10, -30, and -50 kPa potentials from the -100 and -1500 kPa potentials with an 80% accuracy.

Dielectric and Time Domain Reflectrometry Sensors

Dielectric sensors are based upon the relationship between the soil moisture content and the capacitance of the soil measured by a pair of embedded electrodes. Capacitance sensors incorporate the soil as the dielectric (i.e., part of the measurement circuit) as opposed to methods which absorb moisture into a resistive or dielectric element. A fundamental electrical property of a material is its dielectric permittivity (ϵ) which is proportional to the dielectric constant (k) by:

$$\epsilon = k \epsilon_o \tag{2.2}$$

where ϵ_0 is the permittivity of a vacuum. Since ϵ and ϵ_0 have the same dimensions, k is dimensionless. The relationship between the dielectric constant and the capacitance (C) of a sensor consisting of two electrodes embedded in a soil is:

$$C = \alpha \epsilon_o k \tag{2.3}$$

where α is the electrode geometry constant. For most solid soil components, the dielectric constant ranges from about 2 to 4 while the dielectric constant for free water is approximately 79 between 15 and 35°C. The dielectric constant varies primarily with the number of water molecules present per unit volume of soil in the zone of influence between the electrodes. The resonant circuit containing the electrodes and moist soil will therefore oscillate at a frequency dependent on the soil moisture content.

A calibration curve is required for each capacitance sensor using a representative soil sample from the installation site. Capacitance sensors can be permanently installed in the soil, for continuous measurement, or lowered down an access tube, for soil moisture profiling. In situ placement requires minimum soil disturbance around the sensor; contact between the sensor and soil is essential. Variations in bulk density with time exert an indirect effect upon the relationship between the dielectric constant and soil moisture (Morrison, 1983).

Time domain reflectometry devices have been a relatively recent addition to the array of instruments that determine soil water content. These devices send a high frequency electromagnetic pulse along two wave guides that are placed in the soil. The transit time of the pulse is a function of the dielectric properties of the soil, which in turn are solely a function of the volumetric water content in the given frequency range. This method is accurate but the instrument is expensive. It is further limited by the depth to which wave guides can be installed easily. The only commercial units available are not effective in wetter soil, being functional only in about the lower 3/4 of the range of plant-available soil water.

There have been several successful attempts at using dielectric properties to determine soil moisture content. Topp et al. (1980) showed that with time domain reflectometry (TDR), the dielectric constant could be correlated directly with volumentric water content with a "universal" calibration curve which is independent of soil type and density. Herkelrath et al. (1991) and van Wesenbeeck and Kachanoski (1988) have successfully used time domain reflectometry to measure soil moisture in field experiments. Dean et al. (1987) used a capacitance method to determine the moisture content of soils, but most of the soil types used in their experiment were not typical agricultural soils. Selig and Mansukhani (1975) provide an excellent review of literature on dielectric properties of soil and suggest that a good frequency range for using the soil dielectric constant to measure soil moisture is 1 MHz to 100 MHz. It is important to note that the dielectric methods have been shown to work well for determing volumetric moisture content, but not for mass basis moisture content. Arnold et al. (1992) developed a dielectric sensor and analyzed dielectric constants for several Oklahoma soils as a function of frequency, soil type, density, and volumetric water content.

CHAPTER 3

SOIL WATER AND THERMAL RELATIONSHIPS

Heat Flow in Soil

Temperature influences physical, chemical, and biological processes which occur in the soil. Heat energy may be transported through soil by a number of different mechanisms, including conduction, radiation, convection in liquid water, and convection of sensible and latent heat in air. Under normal conditions, the two most important processes of heat transport in soil are conduction and convection of latent heat.

Conduction refers to the transport of heat by molecular collisions. For a pure solid substance, the conductive heat flux (q) in one dimension is described by Fourier's law as:

$$q = -\lambda \frac{\delta T}{\delta z} \tag{3.1}$$

where q is heat flux (W/cm^2), λ is thermal conductivity (W/cm °C), T is temperature (°C) and z is the distance (cm). This equation describes the heat flow in rigid bodies whose composition remains unchanged during the transport of heat.

The heat conservation equation is derived by performing a heat energy balance on a small cubic soil volume. The heat balance is recorded during a short time interval Δt between t and $t+\Delta t$. The principle of heat conservation may be stated as follows:

the amount of heat energy flowing into a soil volume during Δt (term 1) is equal to the amount of heat energy flowing out of the soil volume during Δt (term 2) plus the increase in heat energy stored in the soil volume during Δt (term 3) plus the amount of heat energy that has been removed from the soil volume during Δt by reactions (term 4). For one-dimensional vertical heat flow, the first term may be written as

$$q(x,y,z,t+\frac{1}{2}\Delta t)\Delta x\Delta y\Delta t \tag{3.2}$$

where q is the soil heat flux evaluated at the average time $t+1/2\Delta t$ and $\Delta x\Delta y$ is the cross-sectional area of the soil volume element. Similarly, the second term may be written as

$$q(x,y,z+\Delta z,t+\frac{1}{2}\Delta t)\Delta x\Delta y\Delta t \tag{3.3}$$

The third term which is the increase in heat energy stored in the soil volume can be expressed in terms of the heat content per unit soil volume (h):

$$[h(x,y,z+\frac{1}{2}\Delta z,t+\Delta t)\ -\ h(x,y,z+\frac{1}{2}\Delta z,t)]\Delta x\Delta y\Delta z \tag{3.4}$$

where h is evaluated at the midpoint $z+1/2\Delta z$ of the volume element. The final term is the amount of heat removed by reactions from the volume and is expressed as

$$r_h\Delta x\Delta y\Delta z\Delta t \tag{3.5}$$

where r_h is the rate of loss per unit soil volume.

Using these definitions, substituting into the heat balance equation, and rearranging terms, the result is

$$\frac{q(x,y,z+\Delta z,t+\frac{1}{2}\Delta t) - q(x,y,z,t+\frac{1}{2}\Delta t)}{\Delta z}$$

$$+ \frac{h(x,y,z+\frac{1}{2}\Delta z,t+\Delta t) - h(x,y,z+\frac{1}{2}\Delta z,t)}{\Delta t} \tag{3.6}$$

$$+r_h = 0$$

As the size of the volume shrinks ($\Delta z \to 0$) and the time interval $\Delta t \to 0$, the previous equation reduces to the differential heat conservation equation

$$\frac{\partial q}{\partial z} + \frac{\partial h}{\partial t} + r_h = 0 \tag{3.7}$$

The heat sink term r_h should be included in the heat balance whenever a source or sink of heat generates or consumes non-negligible quantities of heat. Normally it is assumed that $r_h=0$. The heat content per unit volume (h) may be written as

$$h = C_{soil}(T - T_{ref}) \tag{3.8}$$

in which

$$C_{soil} = \rho c_m \tag{3.9}$$

where C_{soil} is the soil volumetric heat capacity, T_{ref} is an arbitrary reference temperature at which $h=0$, ρ is the bulk density, and c_m is the specific heat capacity.

When the heat flux equation (Equation 3.1) and the heat content (Equation 3.8) are inserted into the heat conservation equation (Equation 3.7), the following equation is obtained

$$C_{soil}\frac{\partial T}{\partial t} = \frac{\partial}{\partial z}(\lambda\frac{\partial T}{\partial z}) \tag{3.10}$$

If the z dependence of λ is neglected, the equation reduces to the commonly known differential heat flow equation

$$\frac{\partial T}{\partial t} = \alpha\frac{\partial^2 T}{\partial z^2} \tag{3.11}$$

where α is the soil thermal diffusivity(λ/C_{soil}).

To solve the foregoing equations so as to obtain a description of how temperature varies in both space and time, it is necessary to know, by means of measurement or calculation, the values of the three parameters just defined, namely, the volumetric heat capacity C_{soil}, thermal conductivity λ, and thermal diffusivity α. Collectively, they may be referred to as the thermal properties of soils.

Thermal Properties of Soils

Volumetric Heat Capacity

The volumetric heat capacity of a soil (C_{soil}) is defined as the change in heat content of a unit bulk volume of soil per unit change in temperature. For a mixture of materials such as soil, the heat capacity per volume of the composite material is the sum of the heat capacities of the constituents weighted by their volume fractions. As given by de Vries (1975),

$$C_{soil} = \sum f_{si}C_{si} + f_w C_w + f_a C_a \tag{3.12}$$

Here, f denotes the volume fraction of each phase: solid (subscripted s), water (w), and air (a). The solid phase includes a number of components, subscripted i, such as various minerals and organic matter. Most of the minerals composing soils have nearly the same values of density (approximately 2.65 g/cm^3) and of heat capacity (0.48 cal/cm$^{3\circ}$K). Since it is difficult to separate the different kinds of organic matter present in soils, it is acceptable to lump them all into a single constituent. Since the density of air is very small compared to that of water, its contribution to the specific heat of the composite soil can generally be neglected (Hillel, 1980). Equation 3.12 can then be simplified as follows:

$$C_{soil} = f_m C_m + f_o C_o + f_w C_w \tag{3.13}$$

where the subscripts m, o, and w refer to mineral matter, organic matter, and water, respectively. Note that $f_m+f_o+f_w=1-f_a$, and the total porosity $\phi=f_a+f_w$. The volume fraction of water f_w is commonly known as θ. In mineral soils, the contribution from organic matter need not be differentiated (Campbell, 1985) because the volumetric specific heats of mineral and organic materials are so similar. The volumetric specific heat of soil therefore becomes

$$C_{soil} = C_m(1-\phi)+C_w\theta \tag{3.14}$$

Thermal Conductivity of Soil

Since soil is a granular medium consisting of solid, liquid and gaseous phases, the thermal conductivity will depend upon the volumetric proportions of these components, the size and arrangement of the solid particles, and the interfacial contact between the solid and liquid phases. Thermal conductivity (λ) is defined as the amount of heat transferred through a unit area in unit time under a unit temperature gradient. Moisture content has a pronounced effect upon soil thermal conductivity. As moisture is added to a soil, a thin water film develops around the soil particles which bridges the gaps in the soil. This "bridging" increases the effective contact area between the soil particles, which increases the heat flow and results in higher thermal conductivity. As more moisture is added the voids between the soil particles become completely filled with moisture and the soil thermal conductivity no longer increases with increasing moisture content (Salomone et al., 1984).

Soil thermal conductivity also increases with the dry density of the soil. With an increase in soil dry density, more soil particles are packed into a unit volume and, thus, the number of contact points between the particles increases. This increase in contact points provides a larger heat flow path resulting in higher soil thermal conductivity (Misra, 1992). The mineral composition of a soil also influences its thermal conductivity. For example, sands with a high quartz content generally have a greater thermal conductivity than sands with high contents of plagioclase feldspar and pyroxene (Kersten, 1949). Soil texture is another factor which may influence thermal conductivity. For a given moisture content and dry density, the thermal conductivity of coarse textured, angular grained soils is higher than that of fine textured soils. Also, uniformly graded soils exhibit lower thermal conductivity than well graded soils (Salomone and Marlow, 1989).

Thermal conductivity also depends upon the shape of the mineral constituents and the soil structure (de Vries, 1963). A model developed by de Vries allows calculation of the thermal conductivity of soils from the volume fractions of its constituents and the shape of the soil particles. This model has been tested on disturbed samples in the laboratory and found to give reliable results for wet soils (Cochran et al., 1967; Skaggs and Smith, 1967; Woodside and Cliffe, 1959). A correction factor was needed for some dry soils (de Vries, 1952; Skaggs and Smith, 1967), but not for others (Woodside and Cliffe, 1959). This model was used by Wierenga et al. (1969) to predict the effects of irrigation on the thermal behavior of soils.

Many other relationships for estimating soil thermal conductivity have been proposed (van Rooyen and Winterkorn, 1957; Johansen, 1975; Gemant, 1952; Kersten, 1949). These relationships vary in complexity, and each method is limited to only certain soil types under specific conditions.

In steady-state testing, a temperature gradient is imposed across a soil sample. When the temperatures within the sample stabilize, the power required to maintain the temperature gradient is used to determine the thermal conductivity by using the following equation (Misra et al., 1993):

$$\lambda = \frac{q}{A}\frac{\Delta x}{\Delta T} \tag{3.15}$$

where q is the input power, A is the cross-sectional area of the sample, Δx is the length of the sample and ΔT is the temperature difference imposed on the sample. The steady-state method for determining the thermal conductivity of moist soils has two major weaknesses. First, water will redistribute under the influence of a steady-state temperature gradient (Jury and Miller, 1974), creating a nonuniform profile within the column. Second, this method is strictly a laboratory technique and cannot be used in situ.

The transient state cylindrical probe (Jackson and Taylor, 1965; de Vries and Peck, 1968) overcomes these difficulties, although there is some temperature induced moisture flow. The method consists of a thin, electrically heated, metal wire that serves as the heat source and a thermocouple to measure the temperature rise. These are placed inside a cylindrical tube, which is inserted into the soil. When the wire is connected to a voltage source, the wire heats up, causing heat to flow radially. The temperature of the thermocouple probe in contact with the soil is given by the following equation

$$T - T_o = \frac{q}{4\pi\lambda}[d+\ln(t+t_o)] \tag{3.16}$$

where T_o is the temperature at time t_o, $T-T_o$ is the temperature rise, q is the heat flowing per unit time and unit length of wire, and d is a constant that depends on the location of the thermocouple (Jury et al., 1991).

Equation 3.16 is obtained by solving the heat flow equation in cylindrical coordinates for the appropriate initial and boundary conditions (Carslaw and Jaeger, 1959). If $T-T_o$ is plotted against ln(t), a straight line is obtained for time $t >> t_o$. The thermal conductivity is then calculated by the revised equation

$$\lambda = \frac{q}{4\pi S} \tag{3.17}$$

where S is the measured slope of T versus ln(t). The value of the power dissipation per unit length (q) is calculated from the current applied to the wire and the measured resistance per unit length of wire.

Thermal Diffusivity

The soil thermal diffusivity (α) can be defined as the change in temperature produced in a unit volume by the quantity of heat flowing through the volume in a unit time under a unit temperature gradient. Alternatively, the thermal diffusivity is the ratio of the conductivity to the volumetric heat capacity:

$$\alpha = \frac{\lambda}{C_{soil}} \tag{3.18}$$

The thermal diffusivity can be calculated from measurements of thermal conductivity and volumetric heat capacity, or it can be measured directly as described by Jackson and Taylor (1965).

Several methods are available to determine the thermal diffusivity of field soil from observed temperature variations. Most of these methods are based on solutions of the one-dimensional conduction heat equation with constant diffusivity (van Wijk, 1963; Neprin and Chudnovskii, 1967), and thus apply to uniform soils only. Lettau (1954) described methods for determining the thermal diffusivity in non-homogenous soil. In his methods the thermal diffusivity is determined as a function of depth below the soil surface. In order to utilize the methods presented by Lettau, measurements of soil temperature with time are required at the soil surface, and at several subsurface depths. However, often the lack of soil temperature data limits the utility of Lettau's methods, and methods that assume independence of thermal diffusivity with depth must be utilized. While these apparently yield reasonable values for the thermal diffusivity of the subsoil, they are less successful when applied to the upper 10 cm of the soil profile (Lettau, 1954; Wierenga et al., 1969). Reasons for the poor results are that the assumptions made for obtaining solutions of the heat equation near the soil surface are generally not met.

Singh and Sinha (1977) developed solutions of the heat conduction equation for four different functional forms of the surface boundary temperature by specifying the boundary condition in terms of thermal gradients as well as temperatures at the soil surface. Their methods provide expressions for the thermal diffusivity which pertain to periods in which one of the four functions adequately describes the measured temperatures. Unfortunately, thermal gradients at the soil surface are extremely difficult to ascertain. Although surface temperature is somewhat easier to measure, it is often assumed to be approximated by a sinusoidal function when estimating the thermal diffusivity. Errors due to the assumption of a sinusoidal temperature wave at the soil surface can be reduced by using a Fourier series to accurately describe the variation in surface soil temperature with time (Lettau, 1954; van Wijk, 1963), or by using the observed data and a numerical interpolation scheme (Wierenga and de Wit, 1970).

Horton et al.(1983) compared several methods for calculating the thermal diffusivity of field soils from observations of soil temperature restricted to the upper 10 cm of soil. Inasmuch as soil temperature data are frequently limited, only methods based on depth independence of the diffusivity were considered.

Thermal Regime of Soil Profiles. In nature, soil temperature varies continuously in response to the everchanging meteorological regime acting upon the soil-atmosphere interface. That regime is characterized by a regular periodic succession of days and nights, and of summers and winters. Yet the regular diurnal and annual cycles are perturbed by such irregular episodic phenomena as cloudiness, cold waves, warm waves, rainstorms, etc. Add to these external influences the soil's own changing properties (temporal changes in reflectivity, heat capacity, and thermal conductivity), as well as the influences of geographic location and vegetation, and the thermal regime of soil profiles becomes quite complex, yet not altogether unpredictable.

A relatively simple mathematical representation of nature's fluctuating thermal regime is to assume that at all depths in the soil, the temperature oscillates as a pure harmonic (sinusoidal) function of time around an average value. Although soil temperature varies with depth, it will be assumed for the time being that the average temperature is the same for all depths. A starting time (t=0) is chosen such that the surface is at the average temperature. The temperature at the surface can then be expressed as a function of time:

$$T(0,t) = T_{avg} + A_o \sin\omega t \tag{3.19}$$

where T(0,t) is the temperature at z=0 (soil surface) as a function of time t, T_{avg} is the average temperature of the surface, A_o is the amplitude of the surface temperature fluctuation (the range from maximum to average temperature), and ω is the radial frequency ($2\pi f$).

Equation 3.19 is the boundary condition for z=0. If an infinite depth is assumed ($z=\infty$), then the temperature at that boundary is constant and equal to T_{avg}. Under these circumstances, temperature at any depth z and time t is also a sine function of time:

$$T(z,t) = T_{avg} + A_z \sin[\omega t + \phi(z)] \tag{3.20}$$

in which A_z is the amplitude at depth z and $\phi(z)$ is the phase angle at depth d. Both A_z and $\phi(z)$ are functions of z but not of t. They can be determined by substituting the solution of equation 3.19 in the differential heat flow equation (Equation 3.11) which leads to the following solution

$$T(z,t) = T_{avg} + A_o e^{\left(-\frac{z}{z_d}\right)} \sin\left[\omega t - \frac{z}{z_d}\right] \tag{3.21}$$

The constant z_d is a characteristic depth, called the damping depth, at which the temperature amplitude decreases to the fraction 1/e of the amplitude at the soil surface A_o. The damping depth is related to the thermal properties of the soil and the frequency of the temperature fluctuation as follows:

$$z_d = \left[\frac{2\alpha}{\omega}\right]^{\frac{1}{2}} \tag{3.22}$$

Thermal Diffusivity Solutions. Using the previous relationships, several methods have been developed to calculate thermal diffusivity. The methods which are most commonly used are (1) amplitude, (2) phase, (3) arctangent, (4) logarithmic, (5) numerical and (6) harmonic. Using Equations 3.21 and 3.22, the thermal diffusivity can be determined explicitly using the following amplitude equation:

$$\alpha = \frac{\omega}{2}\left[\frac{z_2 - z_1}{\ln\frac{A_1}{A_2}}\right]^2 \tag{3.23}$$

where A_1 is the amplitude at z_1, and A_2 is the amplitude at z_2. Temperature records at depths z_1 and z_2 would provide measures of A_1 and A_2 even though the temperatures might not necessarily fluctuate in a strictly sinusoidal manner. In order to determine the values of A_1 and A_2, four temperature observations are required - the maximum and minimum values at each of the two depths. Unlike the following method, information on their time occurrence is not required.

If the time interval between measured occurrences of maximum soil temperature at depths z_1 and z_2 is $\delta t=(t_2-t_1)$, the phase equation stemming from equations 3.21 and 3.22 is

$$\alpha = \frac{1}{2\omega}\left[\frac{z_2-z_1}{\delta t}\right]^2 \qquad (3.24)$$

Frequent observations of T are necessary to ensure accurate estimates of t_1 and t_2. Furthermore, on cloudy days, several relative maxima of T may be manifested rendering the value of δt somewhat subjective.

Soil temperature near the surface can be described by a series of sine terms. Measured values of temperature at a specific depth can be fitted to Fourier series using standard linear least square regression techniques (Draper and Smith, 1966), resulting in:

$$T(t) = T_{avg} + \sum_{n=1}^{M} [A_n\cos(n\omega t) + B_n\sin(n\omega t)] \qquad (3.25)$$

where T_{avg} is the mean value of the temperature in the time interval considered, M is the number of harmonics, and A_n and B_n are the amplitudes. If the first four terms (M=2) of the above series are assumed to describe an upper boundary condition at $z=z_1$, where z_1 may be zero (soil surface) or greater, the thermal diffusivity can be calculated from

$$\alpha = \frac{\omega(z_2-z_1)^2}{2\left[\arctan\left[\frac{(T_1-T_3)(T_2'-T_4') - (T_2-T_4)(T_1'-T_3')}{(T_1-T_3)(T_1'-T_3') + (T_2-T_4)(T_2'-T_4')}\right]\right]^2} \tag{3.26}$$

where temperatures T_i and T'_i are recorded each 6 hours at two depths, z_1 and z_2, respectively. For example, if the first reading is taken in the morning at 0700 h, the second at 1300 h, the third at 1900 h and the fourth at 0100 h, values T_1, T_2, T_3, and T_4 at depth z_1 and values T_1', T_2', T_3' and T_4' at depth z_2 would be obtained (Neprin and Chudnovskii, 1967).

Using the same assumption as in the arctangent equation, Seemann (1979) showed that the thermal diffusivity can be calculated using a logarithmic form:

$$\alpha = \left[\frac{0.0121(z_2-z_1)}{\ln\left[\frac{(T_1-T_3)^2 + (T_2-T_4)^2}{(T_1'-T_3')^2 + (T_2'-T_4')^2}\right]}\right]^2 \tag{3.27}$$

The arctangent and logarithmic equations are analogous to the amplitude and phase equations but take advantage of a greater number of temperature observations to approximate a potentially nonsinusoidal behavior.

For homogenous soils with constant thermal diffusivity, the differential heat flow equation (Equation 3.11) can be approximated with an explicit finite difference equation (Richtmeyer and Morton, 1967):

$$\frac{T_j^{n+1} - T_j^n}{\alpha \Delta t} = \frac{T_{j+1}^n - 2T_j^n + T_{j-1}^n}{(\Delta z)^2} \tag{3.28}$$

where j is the depth index and n the time index. Equation 3.28 can be used to estimate the thermal diffusivity from observed temperature values at several depths. Stability in the numerical solution is ensured if

$$\frac{\alpha \Delta t}{(\Delta z)^2} < 0.5 \tag{3.29}$$

If temperature measurements at an upper and a lower boundary and an initial temperature distribution are provided, a value of α can be selected to calculate the temperature variation at an intermediate depth (Wierenga et al., 1969). The procedure, repeated for different values of α, ascertains the appropriate value of α (the value which gives the smallest difference between observed and computed soil temperature at the intermediate depth for the time period). A disadvantage to this method is that temperature must be measured at three depths while the other methods require temperature measurements at only two depths.

An equivalent representation of Equation 3.25 is

$$T(t) = T_{avg} + \sum_{n=1}^{M} [C_n \sin(n\omega t + \phi_n)] \tag{3.30}$$

where C_n is the amplitude of the n^{th} harmonic equal to $(A_n^2+B_n^2)^{1/2}$ and ϕ_n is a phase angle equal to $\arctan(A_n/B_n)$ as well as $\arcsin(A_n/C_n)$ (Conrad and Pollak, 1950). For the following boundary conditions, where variation in the surface temperature of a homogeneous soil is described by M harmonics,

$$T(0,t) = T_{avg} + \sum_{n=1}^{M} C_{on} \sin(n\omega t + \phi_{om}) \tag{3.31}$$

$$T(\infty,t) = T_{avg} \tag{3.32}$$

the solution of the differential heat equation (Equation 3.11) developed from the sinusoidal temperature equations (Equations 3.21 and 3.22) using superposition is (Van Wijk, 1963)

$$T(z,t) = T_{avg} + \sum_{n+1}^{M} [C_{on} \exp(-z\sqrt{n\omega/2\alpha}) \sin(n\omega t + \phi_{on} - \sqrt{n\omega/2\alpha})] \quad (3.33)$$

where C_{on} and ϕ_{on} are the amplitude and phase angles, respectively, of the n^{th} harmonic for the upper boundary. The thermal diffusivity can be solved implicitly from Equation 3.33 if temperature measurements at one depth in addition to those at the upper boundary are available. The value of α is selected to minimize the sum of squared differences between the calculated and measured temperature values. The number of measurements required depends upon the rate at which the temperature at the soil surface fluctuates.

Simultaneous Transport of Heat and Moisture

The flows of water and thermal energy in the soil are interactive phenomena -- one entails the other. Temperature gradients affect the moisture potential field and induce both liquid and vapor movement. Reciprocally, moisture gradients move water which carries heat. This combined transport of heat and moisture can generally be ignored in the extreme cases of a relatively wet soil and a nearly dry soil. In the wet soil, the influence of temperature gradients on liquid water flow is generally small in comparison to the influence of moisture gradients. In the dry soil, the movement of heat can entail no significant movement of either liquid water or vapor. The problem arises in situations in which transport of liquid water and of vapor are quantitatively similar, and in which thermal gradients are more important than other moisture potential gradients (Hillel, 1980).

Two separate approaches to the combined transfer of heat and moisture have been attempted: (1) a mechanistic approach based on a physical model of the soil system, and (2) a thermodynamic approach based on an attempt to formulate the phenomenology of irreversible processes in terms of coupled forces and fluxes. Though starting from different points of view, the two approaches have been shown to be related and can be cast into an equivalent mold(Groenvelt and Bolt, 1969; Jury, 1973). Neither approach has yet been developed sufficiently to encompass the full complexity of the interactive set of transport processes involved in simultaneous heat and moisture transport.

CHAPTER 4

NEURAL NETWORK THEORY

Background

One possible way to model soil water content based on soil temperatures is to use a neural network. In the preceding sections, the relationships between soil water content and soil temperature were discussed. If soil temperatures are measured at various depths, then a relationship between temperature and soil moisture can be developed, but not without knowing the soil's thermal diffusivity or conductivity and bulk density. Neither thermal conductivity nor bulk density is easily measured. One reason for using a neural network is to circumvent these measurement "unknowns". A neural network could potentially relate soil temperature and moisture without knowing all the quantities necessary for a direct solution.

In the past few years, research on neural networks has greatly expanded. They constitute a radically different approach to computation. The basic building blocks of neural networks are the processing element and the connections (Figure 4.1). Processing elements are loosely analogous to human neurons. The processing element combines several inputs together, modulating them by weights (or connection strengths). The result of this weighted sum is typically transformed by some nonlinear function called a "transfer" or "activation" function. The result of the transfer function is the output of the processing element. This output is also called the processing element's "activation." Within a neural network, processing elements are often grouped together into linear arrays called layers. In general, processing elements that reside on the same level share the same transfer function and learning laws. Data is applied to the input layer. Connections transfer information from the input layer to the hidden layers to the output layer. The middle layers are called "hidden layers" because neither their inputs nor outputs are available to the outside world (Reid, 1988).

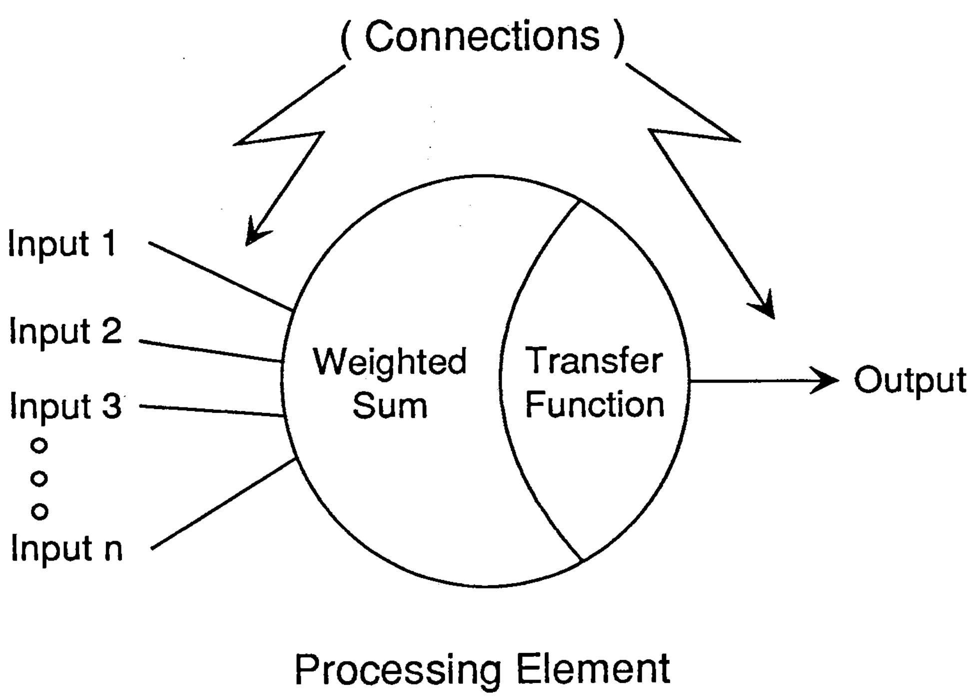

Figure 4.1. Neural Network Processing Element and Connections.

Neural networks are typically used to develop a relationship between several inputs and several outputs. In a computer program, the algorithm implemented by the programmer maps the programs inputs to the desired outputs. In expert systems, higher level concepts (rules) are used to specify relationships between various inputs and outputs. In contrast, neural networks need not be given any information about how to process the input data.

Networks use feedforward connections and may also have feedback connections. In a purely feedforward network, the input simply flows through the connections. As it passes through intermediate processing elements, it is transformed until it ultimately reaches its final form at the output processing elements. The only time related factor is that sending processing elements must compute their states before the receiving processing elements can use them to compute their own states. Once the flow of information reaches the output processing elements, processing ends until new input values are fed into the network. Thus, a simple functional relationship exists between inputs and outputs.

A typical example of a feedforward network is the backpropagation network. Backpropagation passes an input vector through several layers of processing elements and transforms it into an output vector. It implements a mapping from the space of inputs to the space of outputs. The mapping implemented depends on the weight vectors of the backpropagation processing elements. Therefore the important task for a backpropagation network is to find a set of weights which implement the desired mapping.

With feedback connections, the simple functional relationship of inputs to outputs goes away. In this case, the output values of higher level processing elements are fed back to lower levels. Therefore, it is no longer true that once the flow of information reaches the output processing elements nothing changes until new input values are presented to the network. If the higher level outputs differ from their previous values, which they generally will, the processing cycle will continue, possibly indefinitely. Many feedback networks have convergence properties which guarantee that the evolution of the network's state vector will reach some limiting state vector and will no longer change. In this case there is a functional relationship between the network's initial states (including the states of the input layer) and its final states. The simplest type of feedback is from a processing element to itself. In this case the output state value of the processing element depends on its current values as well as the values from incoming connections.

Learning

A higher level form of feedback is adaptation or learning. A network is said to learn if over time the way in which it transforms inputs into outputs changes (preferably for the better). The changes are generally produced by changes in the weights. Weights are values associated with each interconnection between processing elements in the different layers. Before training, they are initialized to random small numbers and are adjusted as learning progresses. The way in which the weights change is determined by the learning laws of the processing elements. The learning laws are of a fixed form but depend on the states, local memory, and weights. With feedback connections, one state depends on another state, which in turn depends on the previous value of the first state.

With learning, a state depends on a weight, which depends on the previous value of that state.

From the standpoint of the amount of information required for a network to operate, there are three major categories of learning. From a practical standpoint, networks which require less information are preferable because less must be known about the problem in order to use these networks. On the other hand, the more information provided to a network, the faster it is generally able to learn.

The most information is required by supervised-learning networks. For every input, these networks should generate a particular output. During learning, the network needs to be supplied with the desired output for every input it sees. The actual output is then compared with the desired output to produce a measurement of "error". This measurement is used to drive the learning process. Less information is required by the graded-learning (or reinforcement-learning) networks. Instead of being told the desired output for each input, they are graded on how appropriate their output is. Depending on the specific learning law, the grade may be supplied either for every input/output pair, or less frequently. Graded learning is extremely useful in cases where one does not know what the output of the network should be, but can test whether the output is appropriate. The unsupervised network does not use a training input as its guideline for determining a correct response. The specific functions and outputs of unsupervised learning networks depend on the network.

Recall refers to how the network processes a stimulus presented at its input buffer and creates a response at the output buffer. Often a recall is an integral part of the learning process such as when a desired response of the network must be compared to the actual output of the network to create an error signal.

Types of Neural Networks

There are several different paradigms of neural networks. Each neural network architecture and training system is better at some kinds of problems than others. The general applications of neural networks fall into several categories: (1) mapping, (2) associative memory, and (3) prototype or categorization.

Mapping

A mapping problem is one in which an input pattern is associated with a particular output pattern as described earlier. For example, the input pattern that consists of a pixel image of a character may be mapped to the output pattern of that character's ASCII code, or a pattern of sensor readings may map to a pattern of valve settings. In the case of this particular research, a set of temperature readings is being mapped to a set of moisture readings. Backpropagation networks are very appropriate for these types of problems and will be discussed in detail in a later section.

Associative Memory

An associative memory network stores information by associating it with other information. Recall is performed by providing the association and having the network produce the stored information. One way to distinguish an associative memory problem from a mapping problem is to determine if the network should reproduce one of the output patterns which it was trained with or if the network is used to generate a new output. If a reproduction is necessary, then an associative memory paradigm should be utilized (NeuralWare, Inc., 1991).

Feedback associative networks fall into two classes: binary and continuous. Most of them have both binary and continuous versions which are closely related. Most can also have learning laws defined for them, although many are generally used with off-line weight generation strategies. One of the most useful features of many feedback associative networks is their automatic minimization of system "energy." Energy minimization guarantees convergence of the states and makes these networks applicable to optimization problems. The feedback associative networks are even more homogeneous than the backpropagation family because not only do the processing elements have the same transfer function, but all processing elements are equivalent with respect to the connection structure. Some examples of feedback associative networks include the Hopfield Network (HOP), the Bidirectional Associative Memory Network (BAM) and the Brain-State-in-a-Box Network (BSB).

HOP is a continuous valued associative network. In addition to its main processing layer, it also has an input layer. Its main processing layer is fully connected. BAM is a binary valued associative network. Its main processing layer is divided into two parts. Each processing element on each layer is fully connected to each processing element on the other layer, but not to any processing elements on its own layer. The BAM has no input layer and does not have a learning law.

BSB is a continuous valued associative network. Like the Hopfield Network, the function layer is fully interconnected. The single functional layer is divided into two layers, called fields, and the connections are divided into four sets depending on what fields contain their source and target processing elements (HNC, Inc., 1991; NeuralWare, Inc., 1991).

Prototype

In a categorization problem the inputs are to be clustered into categories. Typically, the network is provided with an input pattern and it responds with the category to which the pattern belongs. One strategy often used by neural networks is vector quantization, or the representation of large numbers of vectors by a smaller set of prototypes stored as processing element weight vectors. The important task for a network which uses vector quantization is to find a set of weight vectors which represent the input vectors in a suitable manner. Networks using this approach are called prototype-based networks. There are several networks which fall under this category including the Kohonen Network, Counterpropagation (CPN), Self-Organizing Map (SOM) and Probabilistic Network.

For the Kohonen Network, vector quantization is only part of the network's processing. There is some fixed number of processing elements with modifiable weight vectors. For each network input, a subset of the processing elements is allowed to modify its weight vectors so they become either more or less like the input vector. As learning progresses, the weight vectors differentiate and spread out so that each weight vector has its region in the input space in which some inputs are closer to it than to any other weight vector. Each weight vector becomes the prototype example for inputs in that region. This is an unsupervised learning procedure.

CPN, like BPN is designed to learn mappings, but in a very different way than

BPN. CPN has two function layers. The first uses a form of Kohonen learning in which only the processing elements whose weight vector is most like the input vector modifies its weights. This processing element's weight vector is adjusted to become more like the input vector. Different from the Kohonen learning, CPN network processing uses the following rules: (1) only the processing element whose weight vector is closest to the input vector can output a non-zero value, (2) the processing elements in the second functional layer output different values depending on which first layer processing element outputs a non-zero value, (3) the value of a processing element output is determined by its own weight, and (4) the vector of second layer processing element outputs is the output for the network.

The SOM network is like the first layer of CPN, except that not just the closest vector to the input is allowed to modify its weights. Its topological neighbors can slow modify their weights to become more like the input vector. First layer processing elements are connected to each other topologically, in a rectangular lattice, so that each processing element has four layers. This topological order is predefined and is entirely independent of whether the weight vectors are metrically near each other. Therefore, the firs layer processing elements become a set of ordered prototypes, in contrast to the unrelated prototypes produced by normal Kohonen learning.

The Probabilistic Neural Network is not a competitive learning network. Instead of using input vectors to organize a fixed set of prototype weight vectors, it stores input vectors themselves as the prototypes. When an unknown input is to be classified, all the stored input prototypes vote in a manner in which the processing elements which are closer to the input have a greater voting strength (HNC, Inc., 1991; NeuralWare, Inc., 1991; Dayhoff, 1990).

There are many different neural networks available for problem solving. The network emphasized in this research is the backpropagation method due to the nature of the non-linear relationship between soil temperature and soil moisture and the performance of backpropagation for data modeling with missing information.

Backpropagation

Description

The backpropagation network is currently the most widely used type of neural network. Backpropagation implements a feed forward mapping which is determined by the network's weights. Backpropagation learns by comparing the actual outputs produced using its current weights with the desired outputs for the mapping it is supposed to implement. It uses the differences to adjust its weights and reduce the average error. What makes backpropagation a supervised learning network is that it must be provided with a desired output that corresponds to each input. Backpropagation networks are homogeneous in that all processing elements have basically the same transfer function regardless of their position in the network. They are very versatile because their transfer functions can implement a wide variety of mappings with appropriate weights.

The typical backpropagation network has an input layer, an output layer and at least one hidden layer. There is also a training layer. There is no theoretical limit on the number of hidden layers but typically there will be one or two. The basic form of this network is illustrated in Figure 4.2. Each layer is fully connected to the next higher-level layer, with the highest level hidden layer feeding into the output layer. The dashed lines going from the input layer processing elements to output layer processing elements indicate that these connections can be enabled or disabled depending on the needs of a given application. If these connections are enabled, each output layer processing element receives an input from each input layer processing element. The training layer is connected to the output layer in a one-to-one manner (HNC, 1991; Caudill, 1991).

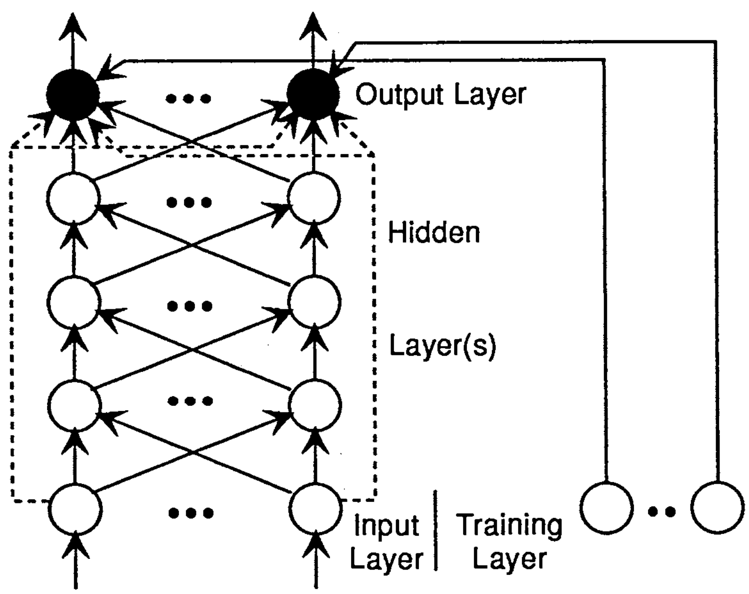

Figure 4.2. Typical Backpropagation Network.

Operation and Function

There are two modes of backpropagation operation: training and production. The goal of the training is for the network to learn to reproduce a mapping or functional relationship from an example set of input vectors and a corresponding set of desired output vectors (training data). After training, the network is used in production mode. If trained correctly, the network should be able to produce appropriate output responses when presented with input vectors it has not previously experienced. Input vectors are presented via the input layer, and corresponding desired output vectors are presented via the training layer. The input layer fans out the input data without making calculations. The data flow along the connections toward the hidden layers and the output layer. Each hidden layer processing element transforms the incoming data by executing specified equations. It then outputs the transformed data to the next layer. Each output layer processing element makes a similar transformation on the data from the last hidden layer and, optionally, from the input layer. The final result is that the input vector is mapped or transformed into some corresponding output vector at the output layer. To avoid getting confused from one layer to another, a clear notation is needed for describing the learning rule. A superscript in square brackets is used to indicate which layer of the network is being considered. A backpropagation element transfers its inputs as follows:

$$x_j^{[s]} = f\left[\sum_i (w_{ji}^{[s]}\, x_i^{[s-1]}) \right] \tag{4.1}$$

$$= f\left(I_j^{[s]}\right) \tag{4.2}$$

where $x_j^{[s]}$ = current output state of jth neuron in layer s, $w_{ji}^{[s]}$ = weight on connection joining ith neuron in layer (s-1) to jth neuron in layer s, $I_j^{[s]}$ = weighted summation of inputs to jth neuron in layer s, and f is traditionally the sigmoid function, but can be any differentiable function such as a hyperbolic tangent or sine function. A typical backpropagation processing element can be seen in Figure 4.3.

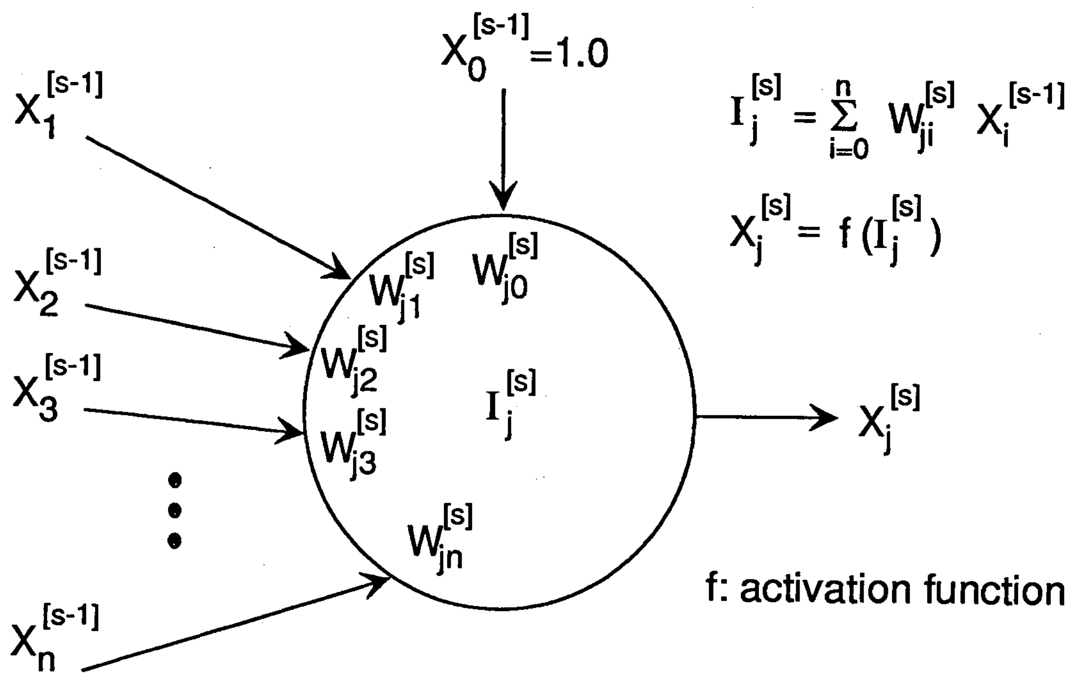

Figure 4.3. Backpropagation Processing Element.

As seen from Figure 4.3, every processing element has inputs, weights, an activation function, bias input (x_0) and outputs. The bias input is usually set to one. The bias can be viewed as a threshold of a processing element which determines the activation level. The weights are numbers associated with each interconnection between neurons in the different layers. Before training, they are initialized to random small numbers and are adjusted during learning. After learning is completed, the weights are fixed and then can be used during "recall" sessions.

If learning is enabled the actual output vector is then compared to the desired output vector, and the errors between the two vectors are calculated. The error values are then used to calculate the weights for all output and hidden layer processing elements and thereby reduce the error in network output. This process is repeated until the mapping has been trained to the desired accuracy or until it appears that the network has learned as well as it can. For a given set of training data, a particular set of weight values will result in some degree of mapping accuracy. The idea is to find a set of weight values that result in maximum accuracy and minimum error. The error criterion used is the Mean Squared Error (MSE). For a given set of input/training pairs, the MSE is the average over all pairs of the squared differences between the desired output and the actual output.

Learning Algorithm

The backpropagation learning algorithm involves a forward propagating step followed by a backward propagating step. Both the forward and backward propagation steps are done for each input vector and the corresponding output vector. Once the forward propagation and backward propagation are completed on one set of input/output vectors, this iteration of the network is complete and the next iteration of the network is started.

The forward propagation step begins when the input vector is presented to the input layer. The input layer fans out the inputs to each processing element in the first hidden layer. The processing elements in the first hidden layer calculate their outputs by applying a non-linear transfer function (most commonly, sigmoid) to the summation of all the inputs to the processing elements. The processing elements of the first hidden layer then fan out the calculated outputs to the processing elements of the next layer. This process continues on each successive layer. Finally, the processing elements of the output layer calculate the actual output of the network.

After the forward propagation step, the network calculates the error by comparing the actual output of the network with the desired output vector. The network then changes the weights associated with each processing element in the output layer. The changing of the weights usually is based on the learning rule of the specific network. Backpropagation networks use the generalized delta rule. This process continues backward, starting with the output layer and moving to the first hidden layer. This process is known as the backpropagation step. The backpropagation step stops when all the weights in the network have been changed. During this back stepping, the network corrects its weights in such a way as to decrease the network calculated error.

Error

The neural network has a global error function E asssociated with it which is a differentiable function of all the connection weights in the network. The critical parameter that is passed back through the layers is defined by

$$e_j^{[s]} = -\frac{\partial E}{\partial I_j^{[s]}} \tag{4.3}$$

where $e_j^{[s]}$ is a measure of the local error at processing element j in level s. Using the chain rule twice in succession gives a relationship between the local error at a particular processing element at level s and all the local errors at the level s+1:

$$e_j^{[s]} = f'\left(I_j^{[s]}\right) \sum_k \left(e_k^{[s+1]}\ w_{kj}^{[s+1]}\right) \tag{4.4}$$

Note that in Equation 4.4 there is a layer above layer s; therefore the equation can only be used for non-output layers. If f is the sigmoid function (Figure 4.4),

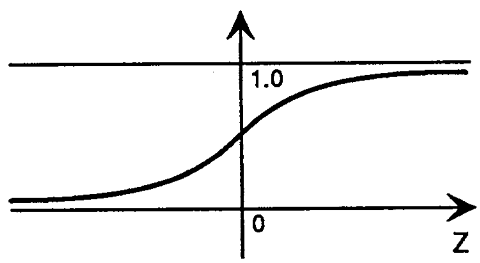

Figure 4.4. Sigmoid Function.

$$f(z) = \frac{1}{1.0+e^{-z}} \tag{4.5}$$

then its derivative can be expressed as a simple function of itself as follows:

$$f'(z) = f(z)\ (1.0\ - f(z)) \tag{4.6}$$

Therefore, from Equation 4.1, Equation 4.4 can be rewritten as:

$$e_j^{[s]} = x_j^{[s]} \, (1.0 - x_j^{[s]}) \sum_k \left(e_k^{[s+1]} \, w_{jk}^{[s+1]} \right) \tag{4.7}$$

If the hyperbolic tangent function is selected as the transfer function (Figure 4.5)

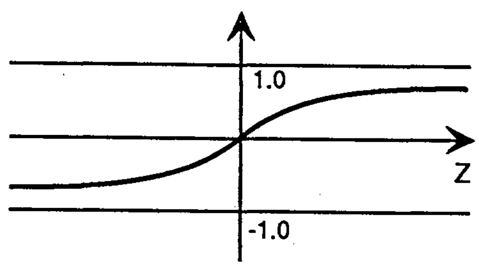

Figure 4.5. Hyperbolic Tangent Function.

$$f(z) = \frac{e^{z} - e^{-z}}{e^{z} + e^{-z}} \tag{4.8}$$

then the derivative can also be expressed in terms of itself:

$$f'(z) = (1.0 + f(z)) \, (1.0 - f(z)) \tag{4.9}$$

Thus with this type of transfer function the error propagation equation (Equation 4.4) is modified to

$$e_j^{[s]} = (1.0 + x_j^{[s]}) \, (1.0 - x_j^{[s]}) \sum_k \left(e_k^{[s+1]} \, w_{kj}^{[s+1]} \right) \tag{4.10}$$

The summation term in Equations 4.7 and 4.10 which is used to backpropagate errors is analogous to the summation term in Equation 4.1 which is used to forward propagate the input through the network. Thus the main mechanism in a backpropagation network is to forward propagate the input through the layers to the output layer, determine the error at the output layer, and then propagate the errors back through the network from the output layer to the input layer using Equation 4.7 or 4.10, or more generally Equation 4.4. The multiplication of the error by the derivative of the transfer function scales the error.

The aim of the learning process is to minimize the global error E of the system by modifying the weights. This can be accomplished based on knowledge of the local error at each processing element. Given the current set of weights $w_{ji}^{[s]}$, the incrementation or decrementation of these weights must be determined in order to decrease the global error. This can be done using a gradient descent rule as follows:

$$\Delta w_{ji}^{[s]} = -lcoeff \left(\frac{\partial E}{\partial w_{ji}^{[s]}} \right) \tag{4.11}$$

where lcoeff is a learning coefficient. In other words change each weight according to the size and direction of negative gradient on the error surface.

The partial derivatives in Equation 4.11 can be calculated directly from the local error values discussed in the previous section because by the chain rule and Equation 4.1:

$$\frac{\partial E}{\partial w_{ij}^{[s]}} = \left(\frac{\partial E}{\partial I_j^{[s]}} \right) \left(\frac{\partial I_j^{[s]}}{\partial w_{ji}^{[s]}} \right) \tag{4.12}$$

$$= -e_j^{[s]} \, x_i^{[s-1]} \tag{4.13}$$

By combining Equations 4.11 and 4.13, the equation to determine the change in the weights is as follows:

$$\Delta w_{ji}^{[s]} = lcoeff\ e_j^{[s]}\ x_i^{[s-1]} \tag{4.14}$$

The above discussion has assumed the existence of a global error function without actually specifying it. This function is needed to define the local errors at the output layer so that they can be propagated back through the network. If vector i is presented at the input edge layer of the network and the desired output d is specified by a teacher, and o denotes the actual output produced by the network with its current set of weights, then a measure of the error in achieving that desired output is given by

$$E = \sum_k (d_k - o_k)^2 \tag{4.15}$$

where the subscript k indexes the components of d and o. Here, the raw local error is given by d_k-o_k. From Equation 4.3, the scaled "local error" at each processing element of the output layer is given by

$$\begin{aligned} e_k^{(o)} &= -\frac{\partial E}{\partial I_k^{(o)}} \\ &= -\frac{\partial E}{\partial o_k}\frac{\partial o_k}{\partial I_k} \\ &= (d_k - o_k)\, f'(I_k) \end{aligned} \tag{4.16}$$

The scaled local error which is backpropagated is stored in the error field of each processing element. The raw local error is stored in the current field.

E as defined in Equation 4.15 defines the global error of the network for a particular (i,d). An overall global error function can be defined as the sum of all the pattern specific error functions. Then each time a particular (i,d) is shown, the backpropagation algorithm modifies the weights to reduce the particular component of the overall error function.

Summary

The standard backpropagation algorithm can be summarized in the following steps assuming an input vector i and a desired output vector d:

1. Present i to the input edge layer of the network and propagate it through to the output edge to obtain an output vector o.

   As this information propagates through the network it will also set all the summed inputs I_j and output states x_j for each processing element in the network.

2. For each processing element in the output layer, calculate the scaled local error as given in Equation 4.16 and then calculate the delta weight using Equation 4.14.

3. For each layer s starting at the layer below the output layer and ending with the layer above the input layer, and for each processing element in layer s calculate the scaled local error as given in Equation 4.7 or 4.10 and then calculate the delta weight using Equation 4.14.

4. Update all weights in the network by adding the delta weights to the corresponding previous weights.

Neural Network Applications

In the past several years, many studies have been done involving the development, improvement, and application of neural networks. Neural networks have been used for things such as encoding and data compression, signal processing, noise filtering, stock market predictions, pattern classifications and modeling (NeuralWare, 1991).

A backpropagation network can be considered as an encoder where the encoding is contained in hidden layer states of the network when the network with one hidden layer is used in an auto-associative manner. If the hidden layer has fewer processing elements than the input or output layer, then this encoding can be considered to be a method of compressing data. Ackley et al. (1985) were the first to apply this technique when they successfully used it to encode orthogonal binary vectors. Cottrell et al. (1987) have applied the technique to do gray-scale image compression.

Pattern classifications have been performed extensively using neural networks. Rigney and Kranzler (1989) used a neural network in an attempt to improve the classification performance of a prototype machine vision based tree seedling grading system. The neural network provided accurate classification performance when given noisy seedling data. Neural networks have also been applied to pattern recognition tasks which include diagnosing engine faults (Schwartz, 1989), detection of explosives in baggage (Shea and Lin, 1988), mortgage underwriting (Collins et al., 1988) and handwritten digit recognition (Pawlicki et al., 1988). Other classifaction applications include natural language processing (Zeidenberg, 1987), visual pattern recognition and associative recall (Fukushima, 1987) and image vector quantization (Jackel et al., 1987). In research conducted by Zhuang and Engel (1990), back-propagation neural networks were compared with statistical classification methods to classify multispectral remotely sensed data. Neuro-computing techniques were applied to the determination of mathematical relationships linking human sensory judgements to physical measurements of external color for tomato and peach (Thai and Shewfelt, 1990).

Backpropagation has been used by Lapedes and Farber (1987) for doing prediction and system modeling. They showed that for "chaotic" time series prediction, backpropagation exceeds conventional linear and polynomial predictive methods by many orders of magnitude. Bolte (1989) used neural networks for applications in agriculture including grain price prediction and alfalfa cultivar selection. Shackleford (1989) discussed the uses of networks of neurons to find solutions to many optimization problems. Systems-analysis problems solved using neural networks have been described by Hillman (1991) and Waite and Hardenbergh (1989) discussed digital implementations of neural nets.

Other research has been involved with improvements of neural networks. Arsenault and Macukow (1989) described an approach to learning in a multilayer network by creating interconnections between the input layer and the intermediate layer. Wieland and Leighton (1989) presented a geometric analysis of neural networks to lend a basis for understanding network capabilities, network topologies, and network dynamics.

CHAPTER 5

FIELD PROCEDURES

General

In order to use a neural network to predict soil water contents, various parameters must be used as inputs to the network. Since soil water content is interdependent on many other soil and weather properties, several related measurements were made using various sensors so that a complete set of possible input parameters could be obtained. These sensors included: a cup anemometer, a net radiometer, a solar pyranometer, a tipping bucket rain gage, a thermocouple for average ambient temperature, six soil heat flux plates, and three soil thermocouple temperature probes. All of the sensors were connected to a datalogger which collected and stored the information from each sensor. The data were collected from three sites each with a different soil type.

Site Locations and Layout

Since the objective of this research is to determine soil moisture content by using a neural network, data were collected in the field to be used for network model development, training and testing. Two sites were initially selected with a third one added later to increase the amount and diversity of the test data.

The first site is located at an Agronomy Research Station (Efaw) west of

Stillwater, Oklahoma (36°08'N, 97°10' W,). The location was selected and a weather station with soil sensors was set up in October, 1991. The second site is also at an Agronomy Research Station (Perkins) which is located near Perkins, Oklahoma (36°0'N, 97°07'W). An identical weather station was placed at the site in March, 1992. The third site consists of a scaled down data collection unit which is located at the USDA Hydraulics Lab near Lake Carl Blackwell (Hyd) nine miles west of Stillwater (36°09'N, 97°11'W). Data collection for site three began in April, 1993. All three sites have bermuda grass cover. The soil at Efaw is Easpur clay loam, the Perkins soil is Teller sandy loam and the Hyd soil is Ashport loam. Particle size analyses had been performed on these three types of soil and recorded. The distribution can be seen in Table 5.1.

Soil Type	Component	Particle Size (μm)	Proportion (%)
Easpur	Sand	> 50	34
	Silt	2-50	29
	Clay	< 2	37
Teller	Sand	> 50	72
	Silt	2-50	18
	Clay	< 2	10
Ashport	Sand	> 50	44
	Silt	2-50	34
	Clay	< 2	22

Table 5.1. Particle Size Distribution for Soil Types.

Sites 1 and 2 (Efaw and Perkins) have a plot area of approximately 36 square meters (Figure 5.1). The temperature probes alternate with the soil moisture access tubes with a spacing of 1 m running east and west. Two heat flux plates are buried two meters south of each thermocouple probe resulting in a total of six plates at each site. The weather station complete with sensors is located 2 meters north of the temperature probes and access tubes.

Site 3 (Hyd) was used specifically to gather test data. Therefore a scaled down version of the other two sites was used. The parameters measured were soil temperatures, air temperature and soil water contents. Like the first two sites, the thermocouple probes alternated with the mositure access tubes in a line approximately 2 m from the datalogger.

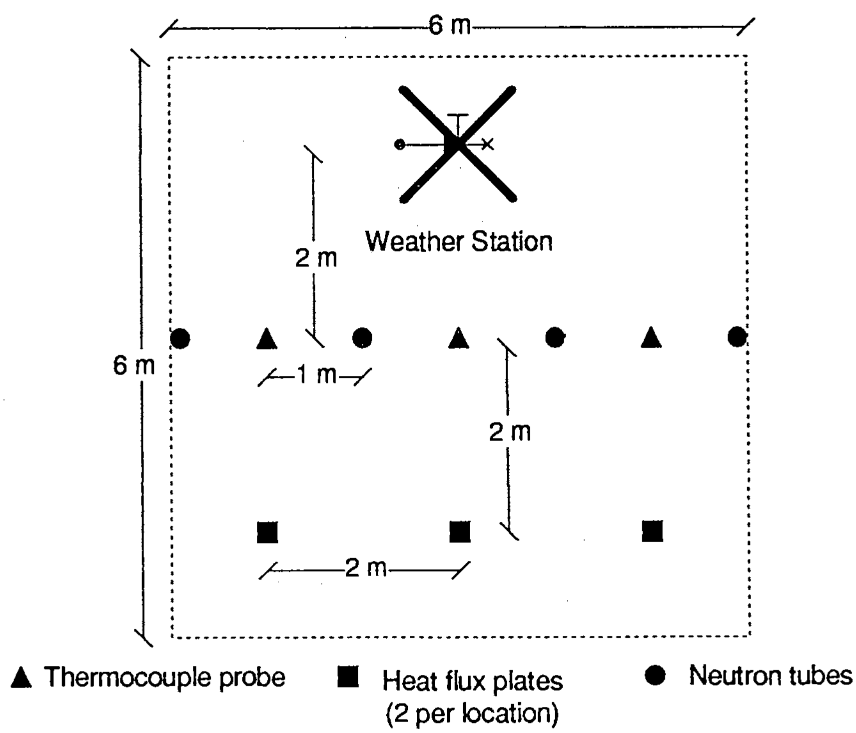

Figure 5.1. Layout of Data Collection Sites.

Datalogger

All of the weather and soil instrumentation is controlled by a Campbell Scientific CR10 datalogger enclosed in a weather proof housing. The datalogger reads the signals from the various sensors, processes the data into a usable form, and stores the data internally. A listing of the datalogger program is provided in Appendix A. All sensors are read by the datalogger every 60 seconds; the data are averaged and recorded hourly. Fifty-three different sensor readings are recorded. They include wind speed, net radiation, rainfall, solar radiation, air temperature, six heat flow measurements and 42 soil temperatures. The datalogger is downloaded weekly to a Campbell Scientific Storage Module (SM-192) and then to a personal computer.

Since the standard CR10 does not have enough analog input ports to measure all the required data, a multiplexer (Campbell Scientific AM416) was used to increase the number of sensors that may be scanned by the datalogger. The multiplexer was positioned between the sensors and the datalogger; mechanical relays were used to switch the desired sensor signals through the system. All of the thermocouples (soil temperatures and air temperatures) were wired to the multiplexer. The CR10 and multiplexer are pictured in Figure 5.2.

A thermocouple reference (Campbell Scientific, 10TCRT) was installed with the CR10 measurement and control module. The thermocouple reference lies between the two analog input terminal strips of the CR10. The CR10 provides a 2 VAC excitation, makes a single ended measurement and linearizes the result with a fifth order polynomial to output the temperature in °C.

The datalogger is powered using a 12 V lead acid battery. A solar panel, which is mounted facing south on the mast of the tripod, is used for charging the battery. The solar panel is an MSX18R which is a regulated panel with two stripped and tinned leads for direct connection to an external 12 volt battery.

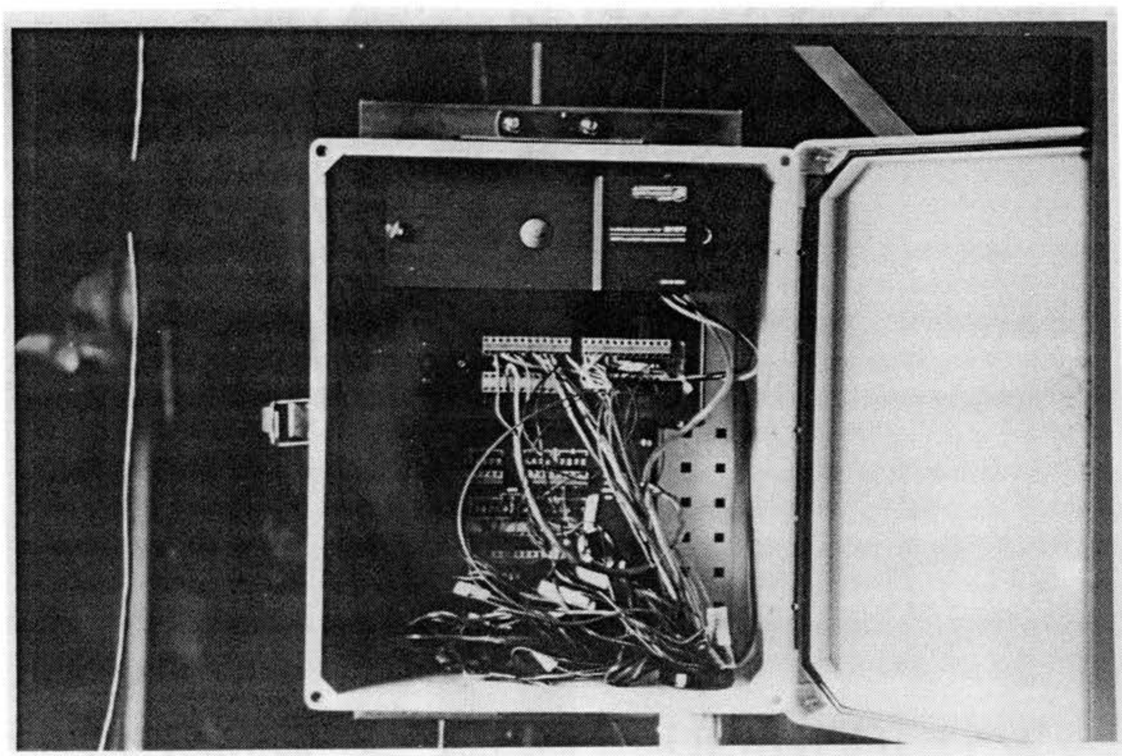

Figure 5.2. CR10 Datalogger and Multiplexer.

Measured Varaiables

Wind Speed

The horizontal wind speed sensor used is a Met-One 014A three cup anemometer. It utilizes a magnet activated reed switch to produce a pulse output with a frequency proportional to wind speed. It can measure wind speed in the range of 0-45 m/s and has a threshold velocity of 0.45 m/s. It is mounted on the main axis cross arm at a height of 2.0 m.

Rainfall

The rain gage is manufactured by Texas Electronics. The TE525 is a smaller adaptation of the standard Weather Bureau tipping bucket rain gage. It measures rainfall at rates up to 5.08 cm/hr (2 in/hr) with an accuracy of $\pm 1\%$. Output is a switch closure for each bucket tip. A tip occurs with each 0.01 inch of rainfall. The rain gage is also mounted on a cross arm on the tripod at a height of 2 m.

Solar Radiation

The solar pyranometer used is a Li-Cor LI200S silicon pyranometer. It uses a silicon photodiode to produce an electrical output proportional to the intensity of incoming short-wave radiation. It is mounted on an arm extending from the main tripod mast at a height of approximately 2 m. The pyranometer outputs a low level voltage ranging from 0 to a maximum of about 10 mV. A multiplier is used to convert the millivolt reading to engineering units.

Net Radiation

The net radiometer is a REBS (Radiation and Energy Balance Systems, Inc.) Q-6. It measures net radiation which is defined as the sum of incoming radiation minus the sum of outgoing radiation. Incoming radiation consists of direct beam and diffuse solar radiation and longwave sky radiation. Outgoing radiation consists of reflected radiation and terrestrial longwave radiation. The net radiometer has sensing surfaces which are black and white and protected from convective cooling by hemispherical polyethylene domes. The domes require no pressurization. Air spaces inside the domes are connected to a dryer filled with silica gel to prevent internal condensation. The device was factory calibrated before placement in the field. The instrument was mounted horizontally on a cross bar on the tripod approximately 2 m above ground level. Net radiation is computed from the thermopile voltage which is recorded by the datalogger.

The net radiometer proved to be unreliable due to persistent attack by birds. The domes were easily clawed or pecked, resulting in large holes. Several scare tactics were tried to keep the destruction from occurring, but none proved capable.

Soil Heat Flux

The soil heat flow transducers used were REBS HFT-3. A thermopile is encapsulated in high thermal conductivity epoxy to prevent ground potential pickup. The heat flow is computed by multiplying the thermopile voltage by a calibration factor. Calibration of the heat flux transducers was performed at the factory, resulting in a separate factor for each heat flux plate. Six heat flow transducers were placed at each site. A shallow hole was dug and a large flat bladed knife was used to make a slit about 5 cm wide horizontally into the wall of the hole approximately 2.5 cm and 7.5 cm below the soil surface. A thin wooden splint was then used to push the heat flux plates into the two slits until they were a minimum of 5 cm beyond the rim of the hole. This procedure was repeated at two other locations with each hole containing two heat flux plates. The excess lead wire was coiled in the holes and covered with the extracted soil.

Soil Temperature

Thermocouples were used to measure the soil temperature at various depths. A thermocouple consists of two wires, each of a different metal or alloy, which are joined together at each end. If the two junctions are at different temperatures, a voltage proportional to the difference in temperatures is induced in the wires. When a thermocouple is used for temperature measurement, the wires are soldered or welded together at the measuring junction. The second junction, which becomes the reference, is formed where the other ends of the wires are connected to the measuring device. (With the connectors at the same temperature, the chemical dissimilarity between the thermocouple wire and the connector does not induce any voltage.) When the temperature of the reference junction is known, the temperature of the measuring junction can be determined by measuring the thermocouple voltage and adding the corresponding temperature difference to the reference temperature.

The CR10 determines thermocouple temperatures using the following sequence. First, the temperature of the reference junction is measured. The reference junction temperature is stored in an input location which is accessed by the thermocouple measurement instruction. The CR10 calculates the voltage that a thermocouple would output at the reference junction temperature if its reference junction were at 0°C, and adds this voltage to the measured thermocouple voltage. The temperature of the measuring junction is then calculated from a polynomial approximation of the National Bureau of Standards calibrations.

Soil temperatures are measured at 14 depths ranging from the surface to 150 cm for Efaw and Perkins, and from the surface to 50 cm for Hyd. Using type T thermocouple wire, thermocouples were mounted on a 1.9 cm diameter wooden dowel rod at 0, 5, 10, 15, 20, 25, 30, 40, 50, 60, 70, 90, 120 and 150 cm. For Hyd, the top nine locations were used. This frequency gradient was chosen because soil temperatures tend to vary more near the surface making it necessary for temperatures to be monitored at smaller increments. Three extra thermocouples were located at 80, 105 and 135 cm to compensate for possible thermocouple failure at the greater depths. Small holes were drilled through the rod so that the wire could be placed through it, allowing direct contact with the soil. The wire is run up the outside of the rod and directly to the datalogger. The thermocouples are covered with epoxy and the rod was painted to provide some protection from the soil environment. There are three soil temperature probes at each site resulting in 42 soil temperature measurements at Efaw and Perkins and 27 soil temperature measurements at Hyd. One of the thermocouple probes can be seen in Figure 5.3.

To insert the temperature probes into the ground, an auger was used to drill holes slightly smaller than the probe. A rubber mallet was then used to gently pound the rod into the ground making sure that the thermocouples had direct contact with the soil. The probe was placed so that the top thermocouple was at the soil surface. The wires that ran from the thermocouple probes to the datalogger were covered with radiator hose to protect them from weathering and rodent damage.

Air Temperature

Air temperature was also measured using a type T thermocouple. The thermocouple was placed in the shade beneath the datalogger shelter to avoid temperature elevation due to solar radiation loading. The temperature sensor is located at approximately 0.5 m above the ground.

Soil Water Content

A calibrated neutron moisture gauge (Troxler Electronic Laboratories, Model 3333) was used to measure volumetric soil water content at various depths and locations within the plot. The access tubes for the soil water readings were made of 3.81 cm diameter electro-mechanical tubing and were installed when the weather stations were erected and the temperature probes were placed. A tractor mounted hydraulic core sampler, was used to core out a hole so the access tubes could be installed in the ground. The soil core which was taken from the ground was used for bulk density measurements for the various depths. Four tubes were installed at each site in locations which were representative of the thermocouple probe locations. Water content readings were taken manually two to three times per week. Data were collected in the field and downloaded each time to a personal computer. Soil water content was measured every 15 cm to a depth of 150 cm resulting in 10 moisture depths moisture depths for Efaw and Perkins and to a depth of 30 cm for Hyd resulting in two readings per tube.

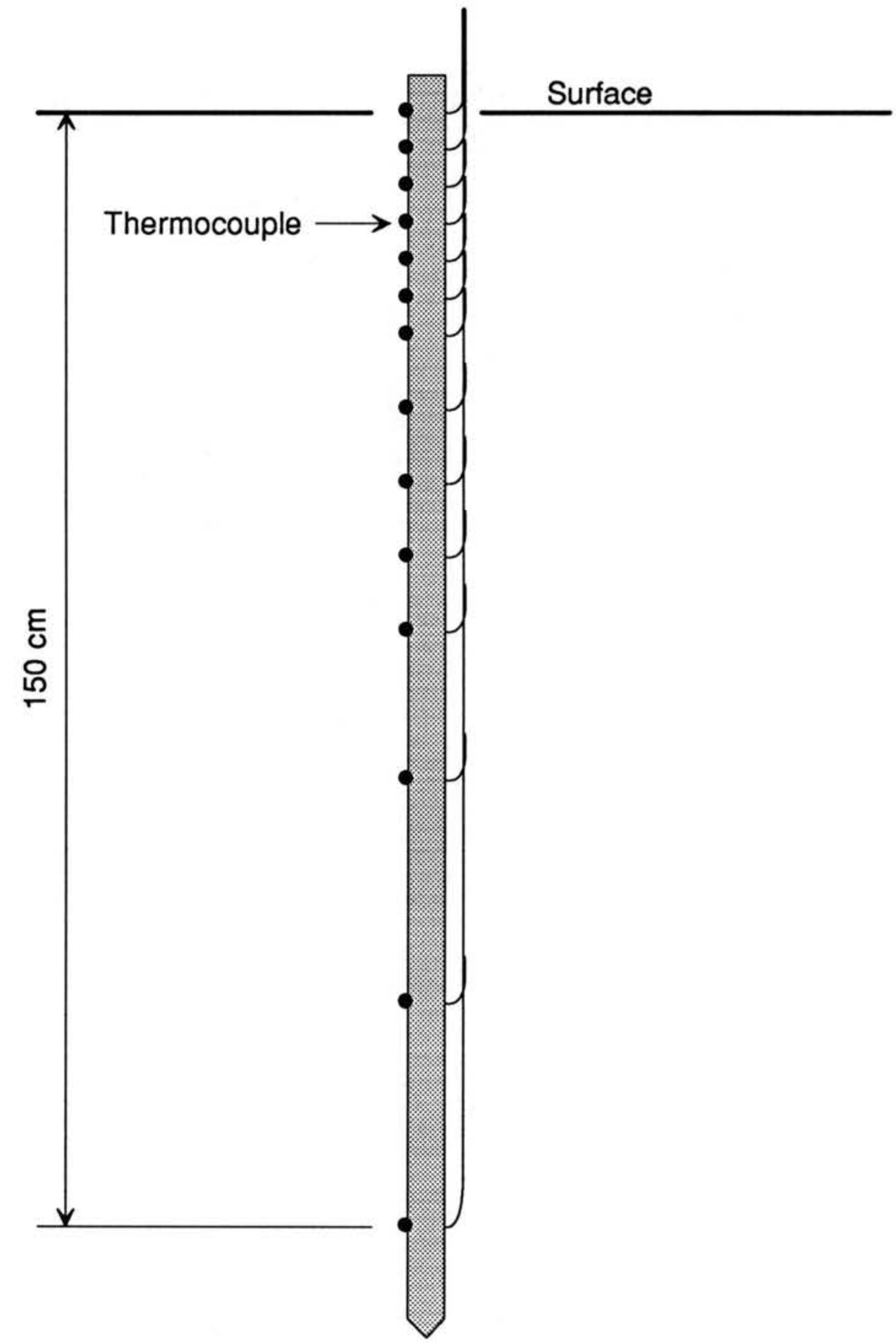

Figure 5.3. Thermocouple Probe Used to Measure Soil Temperatures.

CHAPTER 6

MODEL DEVELOPMENT

Preliminary Data Analysis

Bulk Density

Soil porosity, which is a function of soil bulk density, is an important parameter in the specific heat - moisture relationship (Equation 3.14). For the Efaw and Perkins sites, the bulk densities were obtained by dividing the soil dry weight by the soil volume. The soil cores removed to install the neutron access tubes were sliced into 7.5 cm lengths. The soil volume was the product of this length and the cross-sectional area (11.4 cm^2 for a 3.81 cm diameter soil core). Figures 6.1 and 6.2 show the scatter plots of the bulk density with depth for Efaw and Perkins, respectively. The average bulk densities were 1.23 g/cm^3 and 1.55 g/cm^3 for the Efaw and Perkins soils, respectively. Bulk density samples were not taken at the Hyd site but previous studies have shown that the average bulk density is about 1.34 g/cm^3 (Hansen, 1993).

Soil Temperature

Since the soil temperatures were recorded hourly at 14 different depths in triplicate, a great deal of data was collected over the course of the study. Figures 6.3

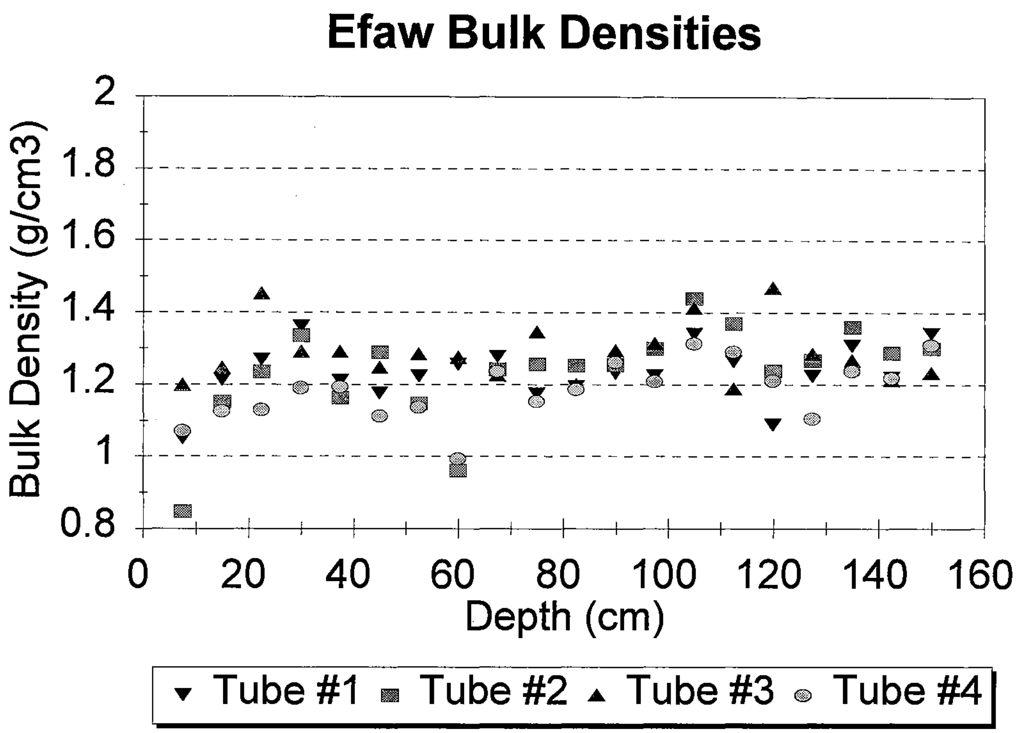

Figure 6.1. Bulk Density Values for Efaw.

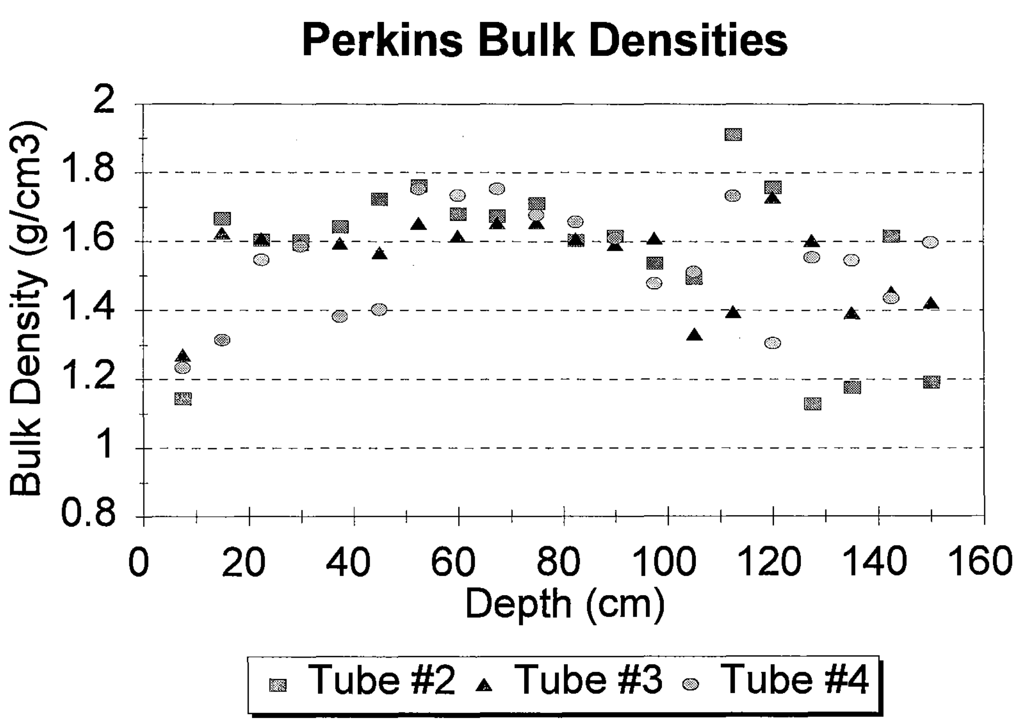

Figure 6.2. Bulk Density Values for Perkins.

and 6.4 show examples of the temperature data collected at Efaw. As seen from the figures, the soil temperatures tend to follow the sinusoidal pattern mentioned in Chapter 3. It is also evident that the amplitude of the diurnal wave decreases with depth which is consistent with the concept of a damping depth (z_d) discussed previously.

Thermal Diffusivity Calculation

Thermal diffusivity was calculated using one of the previously described methods. Horton et al. (1983) recommended that the harmonic equation method be used because it proved to be very consistent with the least amount of data required. They also stated that the numerical method was very reliable if sufficient temperature data were available as was the case with this study.

The alpha calculations were performed on the Efaw soil to determine if α and λ had a strong relationship with θ (soil water content). If a relationship does exist for this data, then soil water content values could be determined using previously discussed equations (Chapter 3). On the other hand, if a relationship does not exist then a procedure which bypasses these properties must be utilized. Since this was a preliminary analysis, calculations were done on the Efaw soil (the Efaw site was set up six months before the Perkins site). The soil was assumed to be homogeneous with constant thermal diffusivity. Equation 3.28 was used with $\Delta t=1$ hour and $\Delta z=10$ cm. Since temperatures tend to vary more in the upper portion of the soil profile the following values were chosen:

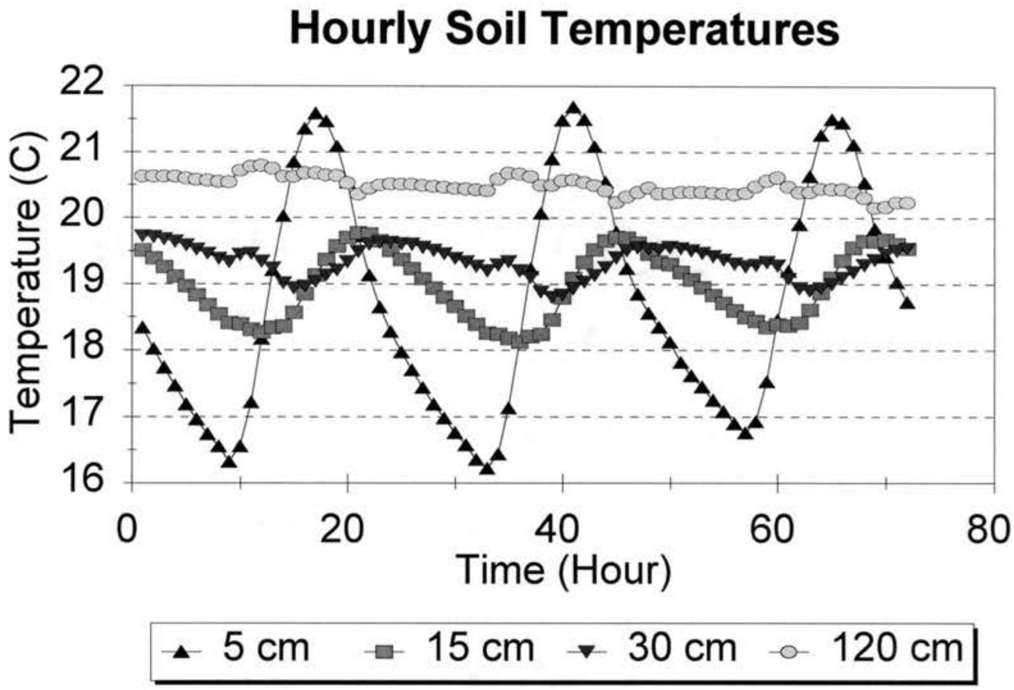

Figure 6.3. Hourly Soil Temperatures for 4 Depths.

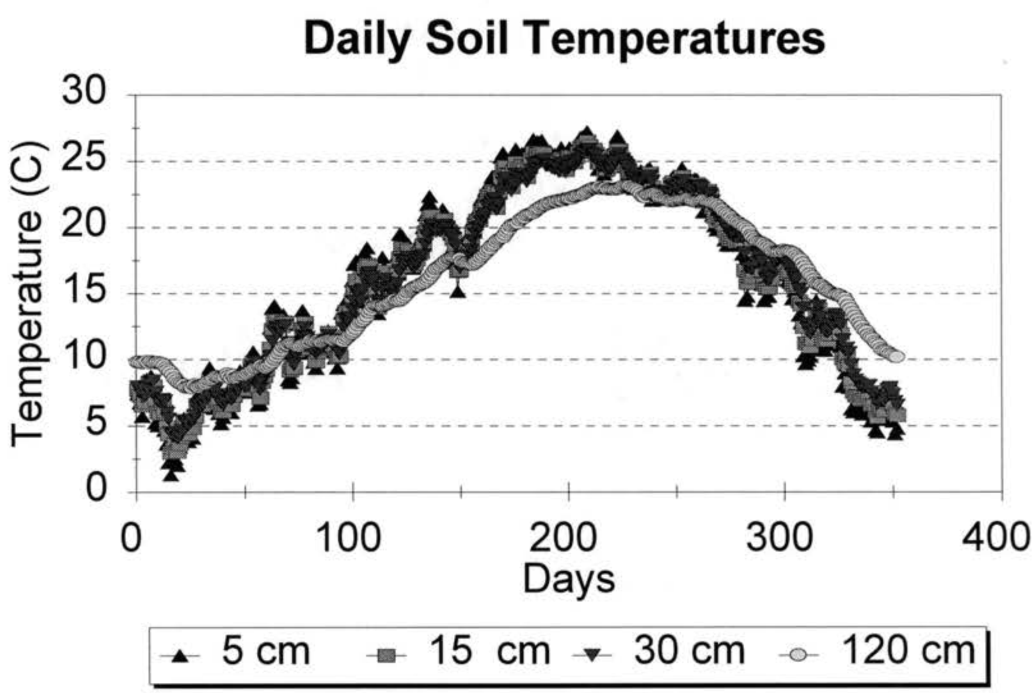

Figure 6.4. Daily Soil Temperatures for 4 Depths.

$j = 20$ cm
$j+1 = 30$ cm
$j-1 = 10$ cm
$n =$ current time
$n+1 =$ current time + 1 hour

Each calculation was checked for stability using Equation 3.29. The C program listing used to calculate α can be found in Appendix B.

Thermal diffusivity values were calculated for a period of about one year. The "current" temperatures used were values which were collected at approximately the same time as the moisture readings were taken (2:00p). The values represented the average of the three temperature probes. Once the α values were determined, they were matched with a corresponding moisture content for that day. Since moisture contents were measured only every two to three days, a daily time series was obtained through interpolation. The moisture contents were the average of the 15 cm reading and 30 cm reading for the four tubes. A graph of the calculated thermal diffusivity versus volumetric moisture content is shown in Figure 6.5.

It can be seen from the figure that thermal diffusivity appears to be relatively constant for the observed range of moisture contents. Most values were between 0 and 0.02 cm^2/s, with the average α equal to 0.009 cm^2/s. Normally, thermal diffusivity first increases rapidly with increasing water content to a maximum and then decreases (Patten, 1909). This is explained by the fact that heat capacity rises linearly with water content, whereas thermal conductivity experiences its most rapid rise at low moisture contents, causing λ/C_{soil} to have an internal maximum as a function of θ. A peak is not seen in Figure 6.5 due to the measured range of moisture contents (16 to 32%). The peak will usually occur at moisture content values drier than 16% (e.g., 10-12%).

Thermal Conductivity Calculation

Once the thermal diffusivity and bulk density values were calculated, they were used along with the measured moisture contents to determine volumetric heat capacity (C_{soil}) and thermal conductivity (λ) of the soil. The average bulk density value (ρ) of 1.23 g/cm^3 for the Efaw soil was used to determine porosity given by the following equation:

$$\phi = 1.0 - \left(\frac{\rho}{\rho_p}\right) \tag{6.1}$$

where ρ_p is the soil particle density assumed to be 2.65 g/cm^3, a typical value for quartz and clay minerals (Campbell, 1985).

The volumetric heat capacity was then calculated for the same soil water content values (θ) used in the thermal diffusivity calculations by using Equation 3.14. When calculating C_{soil}, a value of 2.39 J/cm^3°C was used for the volumetric heat capacity of the mineral component of the soil and a value of 4.18 J/cm^3°C was used as the volumetric heat capacity of water. The average value over time for the volumetric heat capacity for the Efaw soil was 2.24 J/cm^3°C, which is in line with other studies on clay type soils.

The thermal conductivities for the various moisture contents were calculated using Equation 3.18. The λ values are plotted in Figure 6.6. The average value of 0.020 W/cm°C is physically reasonable. It can be seen that the computed thermal properties of the Efaw soil remained relatively constant over the measured moisture content range. This is due to the fact that the measured range of moisture values was above the critical moisture content for that soil. Thus, it would be very difficult to infer soil moisture

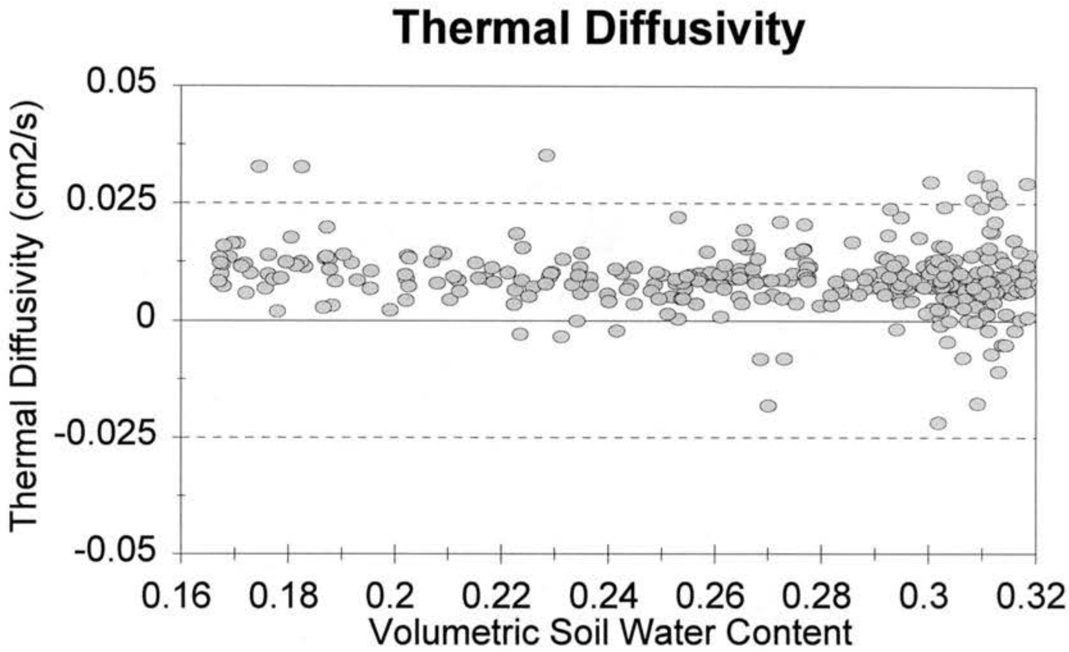

Figure 6.5. Calculated Thermal Diffusivity (α) Values for Efaw.

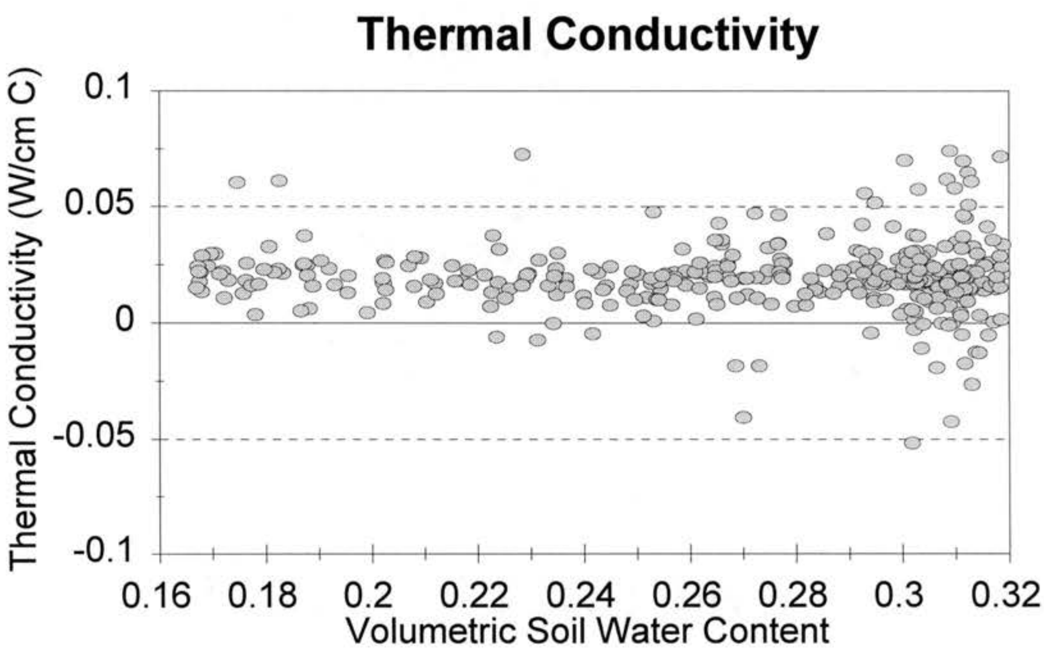

Figure 6.6. Calculated Thermal Conductivity (λ) Values for Efaw.

content based on the calculated values of thermal diffusivity or thermal conductivity and using heat flow equation (Equation 3.11). It should be pointed out, however, that the techniques used to calculate α and λ were rather limited (using averages and assuming homogeneity over a limited range of soil water contents) and these results do not invalidate the heat flow equation.

Neural Network Design

A neural network was chosen as the modeling scheme for this project because of the non-linearity of the system and the difficulty in performing a direct calculation. A neural network has the capability to use a large number of inputs, therefore decreasing the restrictiveness of the calculations (which occurred when using the "direct" approach). The building of a neural network is performed in two stages - the concept phase and the design phase (Bailey and Thompson,1990).

The concept phase develops the approach to building the neural network application. It determines which type of application to consider. Then according to the type and requirements of the application, the proper neural network paradigm is selected. Finally, the neural network size, output type and training method are decided on the basis of the chosen network paradigm. The design phase specifies initial values and conditions for the selected neural paradigm at the node, network and training levels. The design phase comprises several steps to determine the type of nodes or processing elements, size and connectivity of the network layers, and learning algorithm and parameters (Bailey and Thompson, 1990).

There are at least 24 neural network paradigms. To select a proper paradigm, the type of application represented by the project must be determined. This research involves estimating soil water content based on measured input variables. An accurate result is desired given a minimum amount of input data. This project is a data modeling or functional mapping application. As discussed in the Chapter 4, backpropagation is an excellent paradigm for this type of application and therefore was chosen.

The output of a backpropagation neural network can be pattern, real number or classification output depending on what is desired. Since soil water content is a real number, the output of the network must also be a real number. The training method of the backpropagation paradigm is limited to supervised training. Supervised training requires pairs of data consisting of an input vector and the correct result. For this study, the training data is weather and soil data collected at the Efaw and Perkins locations and the corresponding soil moisture content. In the training data, the desired output is the soil water content at various depths. It is fed into the training layer to teach the network. A variety of networks were designed, first to learn the system and later to come up with the "best" network.

Two different neural network packages were used in this study. Originally, the multilayer backpropagation paradigm in ExploreNet 3000 by HNC was used. This was a PC-based package which worked well, but as the size of the database increased and comparison networks were developed, a workstation proved to be more efficient. The majority of the network design and testing was done using NeuralWorks Professional II/Plus by NeuralWare, on a SUN IPX workstation.

ExploreNet

The initial use of ExploreNet was to determine whether or not the use of a neural network for this project was feasible. This package was used at the beginning of the project and therefore was only used with Efaw data. The monitoring station had been functional for only six months resulting in a limited amount of training data. The first step of the neural network process involved becoming familiar with the data and the system. The ExploreNet package was used to set up and test a simple network system using a small portion of the data collected at the beginning of the project. Soil temperatures were extracted from the data file. Soil temperature was used for four consecutive days at a depth of 30 cm and the fifth day provided the training data. The neural network consisted of an input layer with training data, one hidden layer, and an output layer. The objective was for the neural network to predict the fifth day's temperature. Ten thousand epochs (training sessions) were run with the results being quite good. Although this was a simple model and the learning for the network did not require very many epochs, it was a good way to become familiar with the system.

The data preparation and manipulation for this project included retrieving the data from the datalogger and putting it into a format which was usable by the neural network. An example of the raw downloaded data can be seen in Appendix C. There are 58 output storage fields for each hour of the day. The fields are described below:

Field	Description
1	Identifier Number
2	Julian Day
3	Time
4	Thermocouple Reference Temperature

5	Solar Radiation
6	Net Radiation
7-12	6 Heat Flux Plates
13	Wind Speed
14	Rainfall
15-28	Soil Temperature Probe 1 (14 depths)
29-42	Soil Temperature Probe 2 (14 depths)
42-56	Soil Temperature Probe 3 (14 depths)
57	Air Temperature
58	Battery Voltage

ExploreNet is capable of selecting specified data directly from this raw data file, but since the process is rather slow, computer programs were written to get the data in the desired format. Soil temperature, air temperature and rainfall data were used for the initial training network with the concept that if the network did not learn, more input parameters could be added such as net radiation, solar radiation, soil heat flux, etc.

The first network used hourly averages of the three soil temperature probes for each of the 14 depths. The input module was constructed with one array consisting of an input layer with 384 neurons (24 hourly averages each for rainfall, air temperature, and 14 soil temperatures). The training layer consisted of 10 neurons which corresponded to the moisture readings taken at the 10 depths (averages of the four replicated measurements).

A second network was developed to try to train the surface moistures with more accuracy. Near the surface, soil temperature and moisture tend to fluctuate more and are more directly affected by above-ground conditions. Therefore, solar radiation was added as another input. It was also desirable to have more training data so rather than averaging the four neutron readings and matching those with the averaged temperature data to create a single array, three input arrays were used. The data from each temperature probe were treated separately and readings from the two neutron tubes on either side of the temperature probe were averaged and used as the training input data. To reduce the size of the input layer, the input data were averaged every two hours which resulted in 12 values for each 24 hour period. Each of the three input arrays consisted of 204 values (14 temperatures, rainfall, air temperature, and solar radiation averaged every two hours for one day).

There seems to be no rule of thumb except trial and error for the number of hidden layers and the number of neurons in each hidden layer. Of course, more layers and neurons lead to more computer time. Since some unknowns are involved when deducing soil moisture given soil temperature, it was decided to use the maximum number of hidden layers for this paradigm (three). The number of neurons in each layer was selected with the idea of funneling a large number of input neurons down to 10 output neurons. Computer memory also was a consideration in selecting the number of neurons. The initial neural network designs are summarized in the Table 6.1.

	Input Layer Neurons		Hidden Layer Neurons			Output Layer Neurons
	Input	Training	1	2	3	
Network 1	384	10	42	30	20	10
Network 2	204	10	60	50	40	10

Table 6.1. Original Neural Network Designs.

The activation function chosen was the most commonly used logistic, which is a sigmoid function. The active range of a transfer function is shown in Figure 6.7.

Unless the training vector values are in the range of the activation of the output layer, the mapping cannot possibly be reproduced accurately. Qualitatively, the sigmoid function allows a backpropagation processing element to define one half of the space of its inputs as calling for a high output value, and the other half a low output value. (The half-spaces are on either side of the hyperplane I = 0.)

An error tolerance of 0.01 was selected. The inputs were connected to the outputs and the initial weights began at 0.5. Once the network begins to run, it can be halted and the current weights can be saved which will allow the network to begin again later without losing what it has already learned. For these two particular configurations,

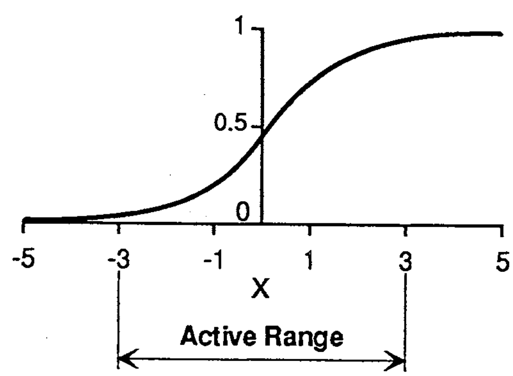

Figure 6.7. Active Range of a Transfer Function.

100000 iterations were run, which on a 486 machine took approximately 1.5 days.

The neural network did a very good job of compensating for the unknowns in the soil moisture-temperature relationship. First of all, the networks were observed to determine if they could even learn at all. The first network configuration performed fairly well in predicting soil moistures for all of the depths except near the surface. These results were displayed graphically in the ExploreNet package. Each depth was represented by a different color along with the corresponding training data. As the network learned the output from the network began to converge with the measured data. The network seemed to have a difficult time learning for the 15 cm depth. This was not too surprising knowing that the surface layer can and will change rapidly depending on above-ground conditions. The results of the second network were similar to the first one with the exception that there was less scatter for the 15 cm depth because solar radiation had been added. It was assumed that with this addition, the network could learn and predict moisture contents better for the shallower depths because the network was given some surface changes as inputs.

Once both networks were trained within the desired tolerance, data which was not used in the training was used to test how well the network could perform. Although the results were not quite as good as for the training data (which is to be expected), they were still promising when taking into consideration the amount of training data and the unsureness of the input data preparation.

Although the results of the ExploreNet package were a bit vague and based on visuals, they proved to be very encouraging. It was shown that soil water content could be predicted based on the measured input parameters and the next step would involve working with the input data to determine the optimal input layer to produce the minimal error between predicted and measured soil water contents.

NeuralWare

After determining that a neural network would have the capability of learning to predict soil water content with the measured inputs, the goal was to develop an optimal model. Also desired was the development of a "universal" model which could predict well regardless of soil type or conditions. Since the PC neural network version was relatively slow and it was desired to run several networks at once for comparative purposes, a SUN workstation neural network package (NeuralWare) was used.

When beginning the neural network application, the only thing which was known was the desired output (soil water content). Although through using the ExploreNet package there was confidence that an efficient network could be developed, the formation of the input layer (number of neurons, input parameters or combination of input parameters) and the hidden layers had to be determined by trial and error. With the many parameters measured in the field, the input combinations could be endless, so the theoretical relationships between temperature and moisture were used to come up with a reasonable input strategy. As time progressed throughout the study, the field database was continually increasing resulting in a larger set of training data. When using ExploreNet, several of the collected input parameters were used initially as input to the neural network without actually knowing what contribution the particular input was making to the network as a whole. Therefore, a test was performed to determine parameter importance as it related to the output.

Five separate network cases were developed for each site location (2 different soil types) with varying input parameters. Soil moisture data was used to train the network for estimation of soil moisture content at four of the 10 measured depths. It was decided to train the particular depths individually rather than all together because the soil variables behave differently at different depths. This cleaned up the network allowing it to "concentrate" on one particular depth at a time. Each network was trained to a convergence threshold of 0.015 (RMS error in volumetric water content). Once the networks were trained, test data (data never exposed to the network during training) were used to estimate soil moisture content at the four selected depths. The predicted soil moisture content was then compared to measured values at those same depths and error analysis was performed.

The first network case had an input layer of soil temperatures measured at 10 cm and 20 cm at the time of day the moisture content readings were recorded (approximately 2:00p) and temperatures at the same depths at a time 12 hours previous to the moisture readings (2:00a) for each of the three temperature probes, resulting in 12 input neurons. The training data consisted of a single moisture value at a 15 cm depth which was an average of the four neutron tube readings. The network consisted of one hidden layer with 5 neurons and a single neuron (moisture content) in the output layer.

The second case was similar to the first network except temperature values at 5 cm and 25 cm depth were added to the input layer resulting in a layer of 24 neurons. The third case added in the daily average air temperature for the preceding 24 hours. Average solar radiation was then added to the input layer for the fourth case followed by cumulative rainfall for the day previous to the moisture measurement for the fifth case. Similar designs were also used to train the networks to estimate moisture contents at 30 cm, 60 cm and 120 cm. At the 120 cm depth, only 4 cases were used because of the limited temperatures surrounding that depth. The networks used for both soil types are summarized in Table 6.2.

Only one hidden layer was used which had five processing elements. This was a reduction from the previous runs because most backpropagation models will eventually give the same result with one hidden layer as with several and at the same time use much less computer power (NeuralWare, 1991). The number of processing elements (PEs) in the hidden layer usually falls somewhere between the total number of input and output processing elements. For fully connected feedforward networks with one hidden layer, there are some general guidelines for deciding how many Pes should be placed in the hidden layer. There are two factors to consider: complexity and the amount of training data available.

1. The more complex the relationship between the input data and the desired output, the more processing elements are normally required in the hidden layer.

2. Based on the amount of training data available, an upper bound for the number of processing elements in the hidden layer can be estimated. To calculate the upper bound, the following formula can be used:

$$h = \frac{cases}{10(m+n)} \tag{6.2}$$

where cases is the number of vectors in the training file, m is the number of processing elements in the output layer, n is the number of processing elements in the input layer and h is the number of processing elements in the hidden layer. The value of 10 is the top of a range of 5 to 10, where 10 is used for relatively "noisy" data.

With too few neurons in the hidden layer, the network can not perform the complex mapping. On the other hand, with too many neurons, the network can easily

Case	Inputs	Input	Hidden	Output
1	T_{10}, T_{20}	12	5	1(= MC_{15})
2	Add T_5, T_{25}	24	5	1
3	Add T_{air}	25	5	1
4	Add Avg Solar Rad	26	5	1
5	Add Cumm Rainfall	27	5	1

Case	Inputs	Input	Hidden	Output
1	T_{20}, T_{40}	12	5	1(= MC_{30})
2	Add T_{10}, T_{50}	24	5	1
3	Add T_{air}	25	5	1
4	Add Avg Solar Rad	26	5	1
5	Add Cumm Rainfall	27	5	1

Case	Inputs	Input	Hidden	Output
1	T_{50}, T_{70}	12	5	1(= MC_{60})
2	Add T_{30}, T_{90}	24	5	1
3	Add T_{air}	25	5	1
4	Add Avg Solar Rad	26	5	1
5	Add Cumm Rainfall	27	5	1

Case	Inputs	Input	Hidden	Output
1	T_{90}, T_{150}	12	5	1(= MC_{120})
3	Add T_{air}	25	5	1
4	Add Avg Solar Rad	26	5	1
5	Add Cumm Rainfall	27	5	1

Table 6.2. Network Summary for Various Inputs.

find a set of weights to memorize all the input patterns. This is called table lookup. In this case, the network just memorizes all the input patterns which have been presented to the network. The network actually does not extract the salient features of input patterns. When new input patterns are presented to the network, the network will give an incorrect response. Therefore, the network loses the capability of generalization.

The soil temperatures which were used in the input layer were values recorded at 2:00a and 2:00p. These times were selected for two reasons: 1) the 2:00p measurements were approximately at the same time as the neutron probe readings and 2) by selecting a current time and 12 hours previous, the theoretical sinusoidal temperature change with time could be incorporated. By selecting these times, it was possible to capture (at least partially) the diurnal temperature change. The temperatures which were used on either side of the estimated moisture content were chosen because the change in temperature over depth relates to the thermal properties of the soil and ultimately to the moisture content. Figure 6.8 demonstrates this concept.

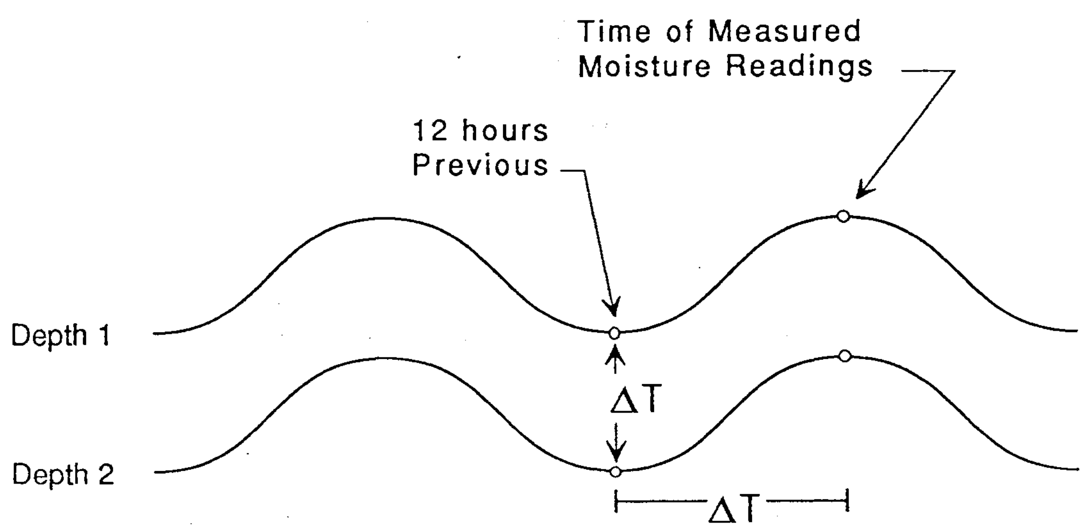

Figure 6.8. Change in Temperature with Depth and Time.

The Efaw networks consisted of approximately one year of data (October 1991-October 1992). Half of the data was used for training and the other half was used for testing. The training data was selected so that maximum variability of the moisture content could be taken into consideration. The data was handled in the same manner for both locations except Perkins (sandy soil) used 8 months of total data (March 1992-October 1992) instead of 12 months.

As stated earlier, the networks were trained to a tolerance of 0.015 volumetric water content. The selection of this value was influenced by the CPU time that it took the network to train. On average, each network required approximately 6 hours to train with the clay networks taking more time and the sand networks less time. Because of the time needed for training, several networks were run simultaneously. The learning rule used was the Delta Rule (described in Chapter 4) and the activation function was the sigmoid function. A computer program was used to normalize the input and training data to values between 0 and 1 so that the sigmoid function could be operable. The two lower depths (60 and 120 cm) trained much faster than the upper two depths (15 and 30 cm) because the training moisture data and input temperature data were much more constant at the lower depths.

Once the networks were trained, test data was used to determine how well the networks could predict soil moisture content. Perkins test data were initially used to test the sandy soil network just as Efaw test data were used in the clayey soil network. The predicted moisture contents were then compared to field measurements and a root mean square error was calculated. The Perkins test data were then used in the Efaw trained network and vice-versa to determine how well a "clay-trained" network predicted

		Independent Verification from Same Location		Independent Verification from Alternate Location	
Depth (cm)	Network	Efaw RMSE	Perkins RMSE	Efaw RMSE	Perkins RMSE
15	1	.0587	.0405	.0674	.1038
	2	.0583	.0398	.0647	.1103
	3	.0584	.0399	.0651	.1069
	4	.0584	.0399	.0672	.1092
	5	.0569	.0419	.0646	.1033
30	1	.0438	.0370	.0401	.0549
	2	.0435	.0369	.0407	.0574
	3	.0436	.0371	.0399	.0569
	4	.0435	.0370	.0401	.0574
	5	.0436	.0391	.0393	.0542
60	1	.0364	.0144	.0209	.0434
	2	.0359	.0142	.0218	.0437
	3	.0363	.0144	.0207	.0437
	4	.0359	.0150	.0214	.0428
	5	.0360	.0145	.0233	.0438
120	1	.0312	.0118	.0497	.0623
	3	.0311	.0119	.0489	.0627
	4	.0310	.0121	.0489	.0635
	5	.0307	.0115	.0495	.0627

Table 6.3. Root Mean Square Error Analysis for the Various Networks and Depths. (Error in Units of Volumetric Water Content)

moisture in a sandy soil and how well the "sandy" network predicted moisture content given temperature inputs form a clay soil.

The results for the various input parameter cases are shown in Table 6.3. It can be seen that the addition of air temperature, solar radiation and rainfall (network cases 3 through 5) did not have much of an impact on the overall network performance. Therefore, it could be said that the networks can predict to their best capability by using only soil temperatures as inputs. The first two columns of RMSE values are the root mean square error values for each of the networks when tested with independent data taken at the same location as the training data. The last two columns are the mean square error values which use the trained network from one location with independent test data from another location. It can be seen from the table that for the networks tested with the same location data, the Perkins (sand) networks predicted better than the Efaw (clay) networks. For both networks the deeper depths had lower RMS error values than the upper depths. The moisture contents at depths of 60 and 120 cm are much more consistent and are less dependent on what is happening at the surface. The moisture contents at 15 and 30 cm on the other hand can vary markedly and are much more apt to show distinct wetting and drying cycles. The networks can obviously train and predict more consistently when the variation is minimized.

The average RMS error for the clay (Efaw) soil network for the 4 depths which span the profile using temperatures only (case 2) is 0.0422 volumetric water content. For the sand (Perkins) network the average RMS error for the same conditions is 0.0257 volumetric water content. This difference could be due to lower variability in the Perkins data. The RMSE values of the Perkins test data used in the Efaw trained network (column 5) were similar to those when the Efaw test data was used. The average RMSE value was 0.044 volumetric water content. When the Efaw test data was used in the Perkins trained network (column 6), the RMSE values were considerably higher, resulting in an average of 0.0684 volumetric water content. The worst predictions for the Perkins trained network were at the 15 cm depth. These results are understandable because the clay moisture data had considerable variability, but the sand network was trained on fairly constant moisture values.

The measured and predicted data for both soil types (trained and tested at the same location) can be seen in Figures 6.9 and 6.10. Both figures are of the test results of case 2 (2 temperatures on each side of desired moisture content depth at time of measured reading and 12 hours previous). The comparisons are shown for soil moisture depths of 15, 30 and 60 cm, respectively. The sequential observations are the times when neutron probe readings were collected. The data are presented chronologically, but not necessarily at set time increments. It can be seen for the Perkins data (Figure 6.9), that the network predictions follow the basic trends of the measured data, but do not respond when there is a dramatic drop or increase in moisture content. Figure 6.10 shows the results for the clay network. The measured soil moisture values for the clay are much more varied than those measured for the sand. The network once again can follow major trends but has difficulties if any data points are extreme. One possible reason for these discrepancies is that there are not enough high and low moisture content values in the training set for the network to learn sufficiently.

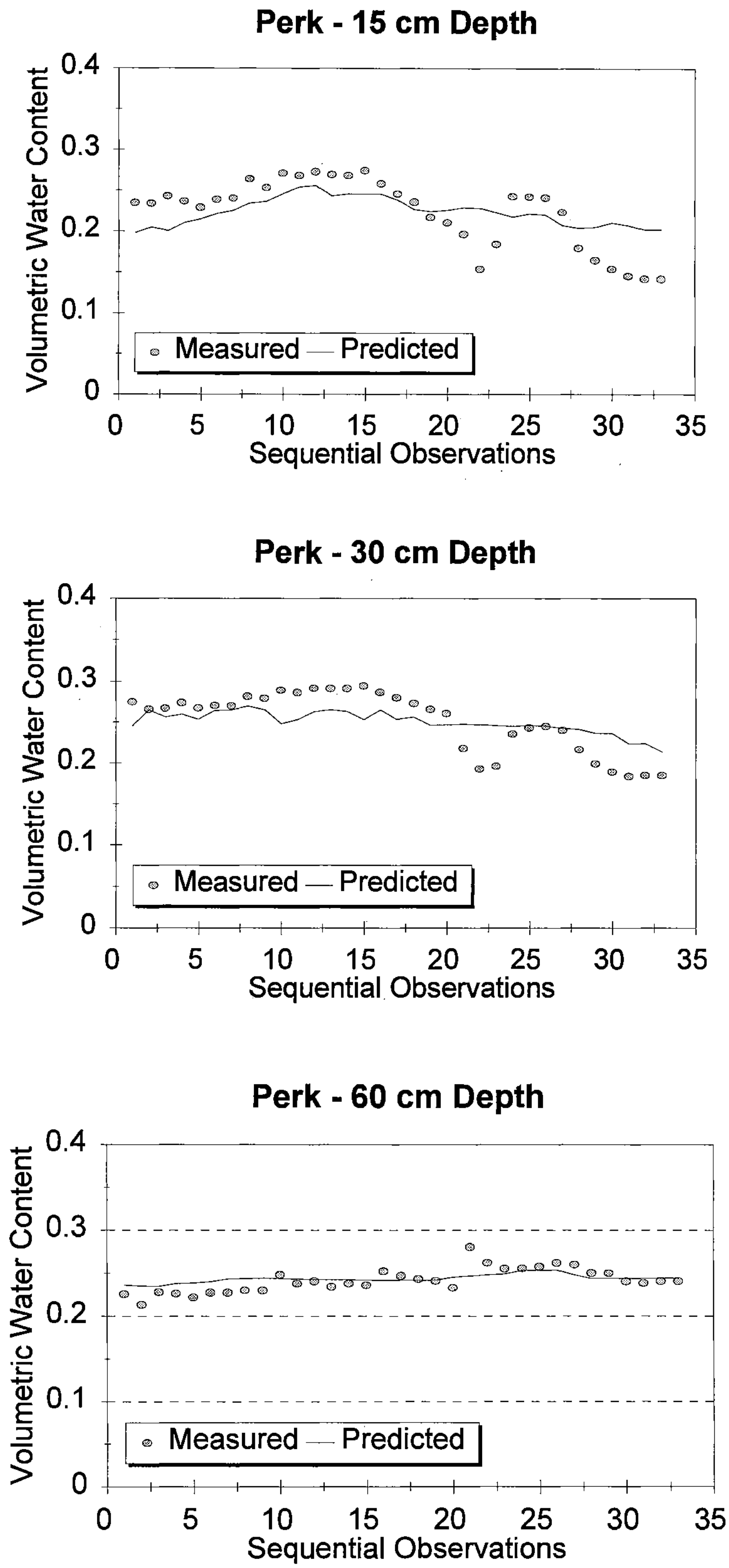

Figure 6.9. Perkins Networks Tested with Perkins Test Data.

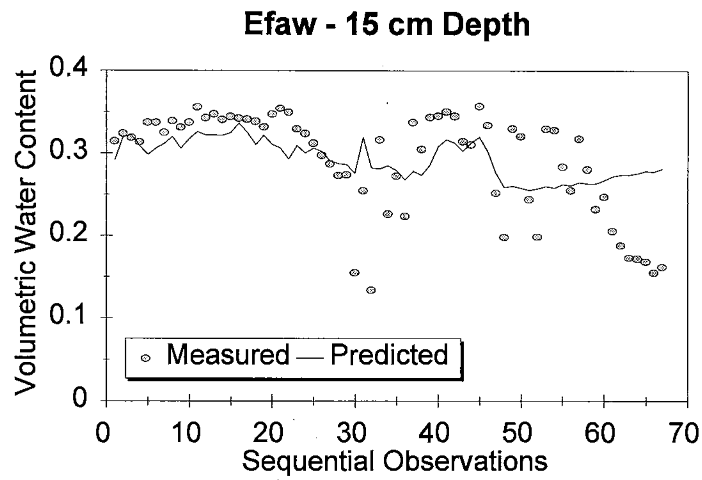

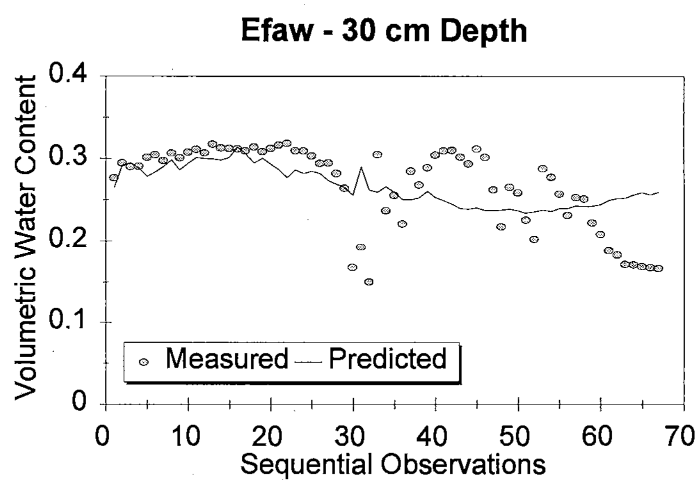

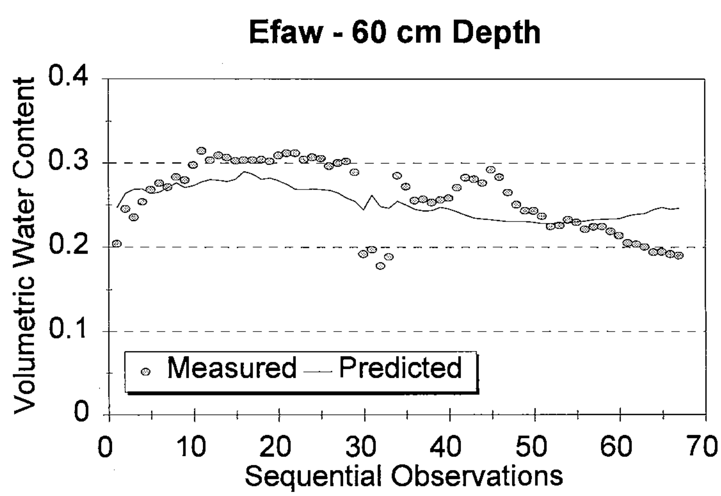

Figure 6.10. Efaw Networks Tested with Efaw Test Data.

Final Network Development

Since the networks seemed to be having difficulty in predicting extremes and the error values were higher than desired, it was concluded that there was not enough training data and that the input vectors and transfer function required adjustment. From the previous network analysis, it was determined that using four temperatures around the desired depth (two on each side - case 2) produced a better result than using only two temperatures (case 1). Also, since thermocouples are very inexpensive and quite reliable, providing two additional ones was viewed as a very minute product expense, definitely worth the performance change. Therefore, four cases, rather than the previous five, were designed for each depth (with the 120 cm depth only using two surrounding temperatures) at each of the two training locations. Another change related to the rainfall, air temperature and solar radiation data. Rather than using values for the previous 24 hours, it was decided that the network might benefit with more history, so cumulative rainfall was used for the previous 72 hours and air temperature and solar radiation were averaged over a three day period. The training moisture data was the same as before with the average value of the four tubes at a particular depth being used.

To adjust for the lack of training data, daily soil water values were interpolated using the measured data. In doing this, the training data set increased quite substantially allowing the network to learn faster and better. All of the soil moisture data from both sites was used for interpolation so that large data sets were obtained (approximately 547 days for Efaw and 365 days for Perkins). So that the entire span of the seasons could be taken into consideration for the training, every other soil moisture data point was extracted and used as the training data. The testing of these networks was performed using the remaining interpolated data values and also using an uninterpolated data set. This procedure did not bias the network results because the neural network is learning based on individual daily inputs and training data (current temperatures and previous 12 hours and soil water content). The network is not estimating predictions based on previous predictions. Also during training, an epoch size is chosen for which the neural network will update its error (change the weights to reduce error). For example, if the epoch size is set to 5, then the network will randomly select 5 of the training vectors out of the complete set and then update the error. Therefore, the actual order of the input vectors is not important.

The Delta Rule was once again used as the learning rule with this network configuration. The transfer function was changed from sigmoid to hyperbolic tangent. The hyperbolic tangent transfer function is similar to the sigmoid transfer function in shape (s-shaped). However, its output range is -1 to +1, as opposed to the sigmoid range of 0 to 1. Because the output of the transfer function is used as a multiplier in the weight update equation, a range of 0 to 1 means a smaller multiplier when the summation is a low value, and a higher multiplier for higher summations. This could lead to a bias to learning higher desired outputs (approaching 1). The hyperbolic tangent gives equal weight to low and high end values.

A MinMax table was used to set the network ranges. Problems often result from presenting data to a backpropagation network as raw values, rather than in values that have been suitably scaled to the neuro-dynamic functions being used. For example, a backpropagation network often uses sigmoid or hyperbolic transfer functions, which respond in a nearly linear fashion to summation between about -2 to +2. If a user presents a backpropagation network with input values such as 10,000, then even with small weights in the network, the summations will be huge and the sigmoids will become saturated. When saturated, the derivative of the sigmoid (or hyperbolic tangent) is close to zero at large (either positive or negative) summation values. Since the derivative is a multiplier in the weight update equation, learning stops for processing elements with such large summation values.

NeuralWare uses a pre-processing facility which computes the lows and highs of each data field for all the input data files to be used with a given network. These lows and highs are stored in a table called a MinMax table. The user then decides what ranges the input and output should be scaled to for presentation to the network. The proper scale is then computed and offset for each data field. Real world values are then scaled to network ranges for presentation to the network. After the network has produced a network scaled result, the result is de-scaled to real world units. The following MinMax table was used:

	Parameter	Units	Min	Max
Input	Soil Temperature	°C	-10.0	40.0
	Rainfall	mm	0.0	20.0
	Air Temperature	°C	-20.0	40.0
	Solar Radiation	W/m^2	0.0	100.0
Output	Soil Water Content	-	0.0	.40

Table 6.4. MinMax Table for Neural Network Input Parameters.

The learning coefficients used were the default values in the package and the threshold convergence (tolerance) was set to 0.01. Each network was trained for approximately 20,000 iterations and stopped when the convergence value was met or when the system became stable.

The root mean square error results for both Efaw and Perkins can be seen in Table 6.5. The average error for the Efaw networks (using uninterpolated test data) is 0.0307. The average error for the Perkins networks is 0.0260. Once again, when the models were tested using data from a different location, the results were rather poor, with the RMS error ranging 6 to 10%. It can be seen that the addition of the extra variables (air temperature, solar radiation, and rainfall) did not have much of an impact on the overall result. The solar radiation and rainfall sensors tend to be expensive and without the purchase or maintenance of them, the cost of the final product could be reduced substantially. Therefore, it was concluded that the additional input data did not help with the overall predictions of the soil water content. Therefore, the remainder of the network improvements and analysis considered only soil temperatures as inputs.

The measured and predicted soil water contents are plotted for both locations and 4 depths in Figures 6.11 through 6.18. These plots represent network predictions using soil temperatures only (case 2). The top plot on each page show the measured data points along with the predicted model (solid line). The bottom plot is the measured versus predicted in which case a perfect fit would fall on the diagonal line. The neural network model predictions are much better for this series of networks, although it still seems improvements could be made. The model follows the basic trend of the measured moisture data and seems to be capable of picking up on more of the extremes than in the

		Independent Verification from Same Location		Independent Verification from Alternate Location	
Depth (cm)	Network	Efaw RMSE	Perkins RMSE	Efaw RMSE	Perkins RMSE
15	2	.0392	.0302	.0778	.1038
	3	.0356	.0302	.0851	.1103
	4	.0349	.0309	.0762	.1069
	5	.0354	.0283	.0751	.1092
30	2	.0344	.0224	.0378	.0616
	3	.0318	.0224	.0348	.0659
	4	.0312	.0225	.0336	.0633
	5	.0284	.0220	.0326	.0620
60	2	.0282	.0098	.0390	.0589
	3	.0258	.0095	.0404	.0581
	4	.0271	.0092	.0375	.0595
	5	.0213	.0100	0.406	.0591
120	1	.0311	.0176	.0513	.0737
	3	.0312	.0189	.0513	.0710
	4	.0304	.0147	.0528	.0787
	5	.0249	.0136	.0524	.0813

Table 6.5. Root Mean Square Error Analysis for the Improved Networks and Depths.

previous runs. Once again, the Efaw data is more erratic than the Perkins data, covering a larger soil water content range. The Efaw plots also have more data points, again due to the date of startup. It should also be pointed out that the changes in soil moisture

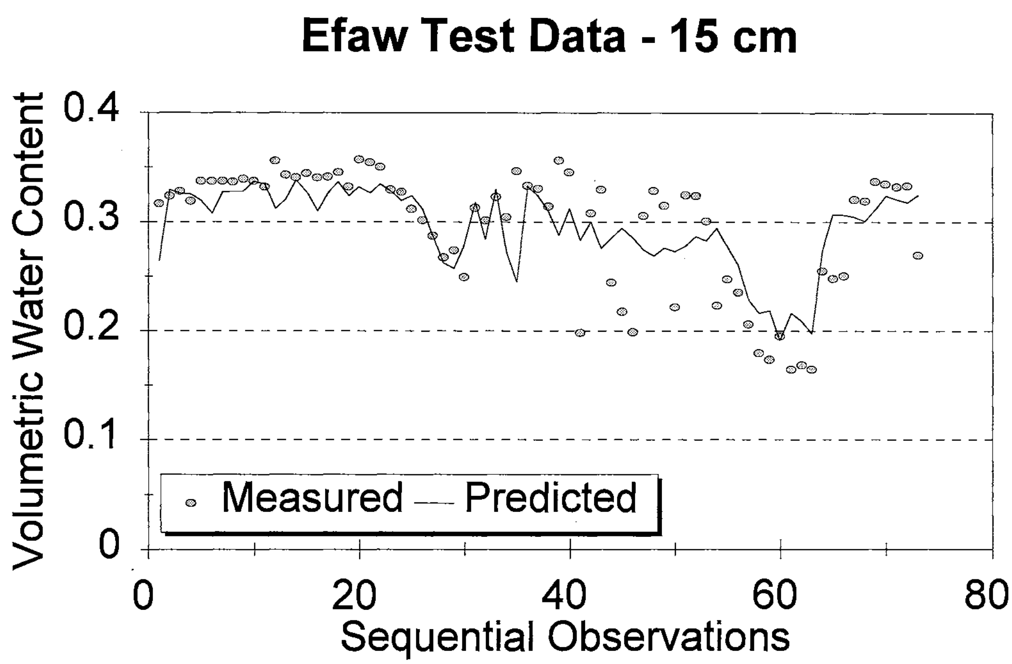

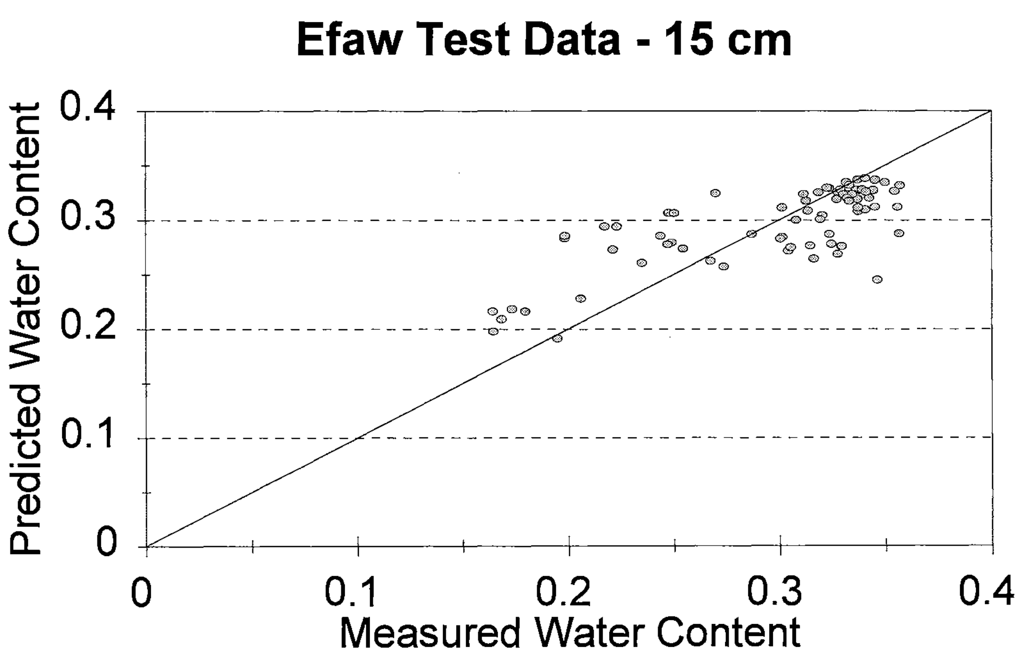

Figure 6.11. Predicted and Measured Values Using Efaw-Trained Network (15 cm).

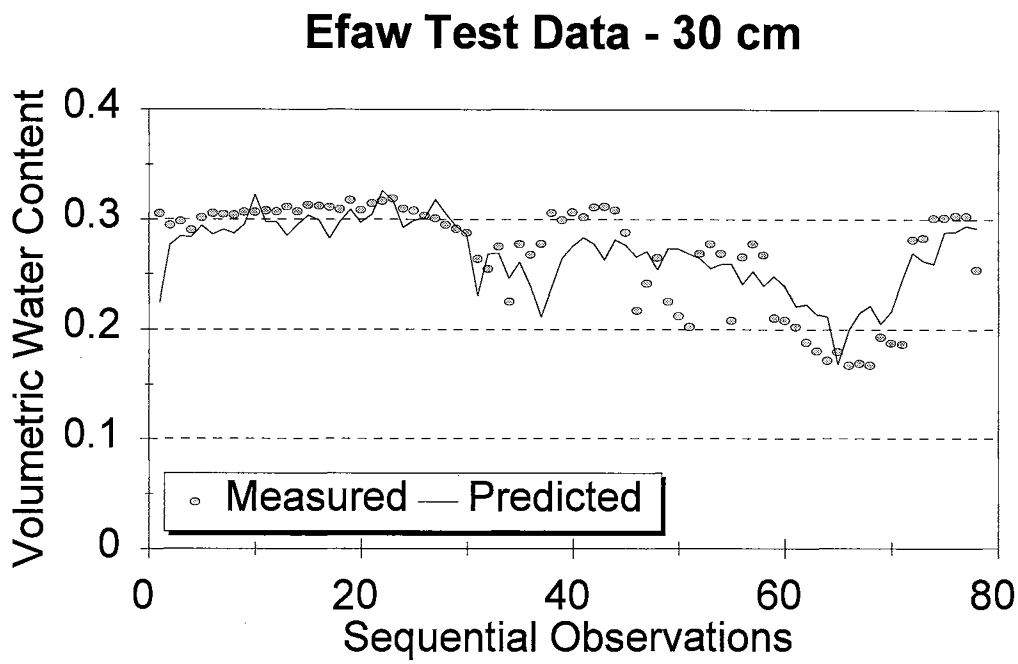

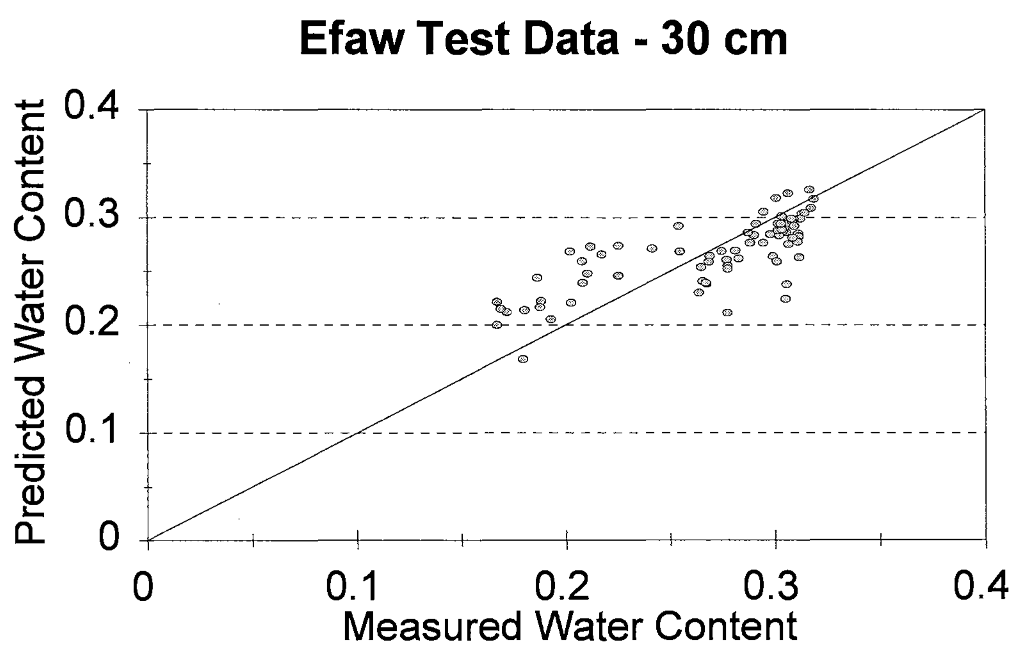

Figure 6.12. Predicted and Measured Values Using Efaw-Trained Network (30 cm).

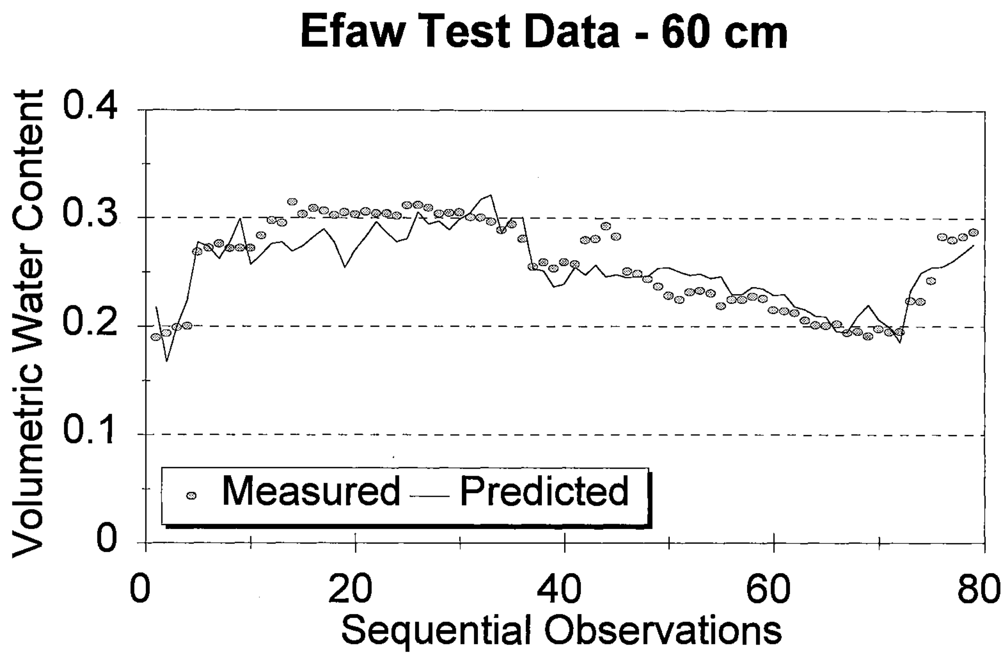

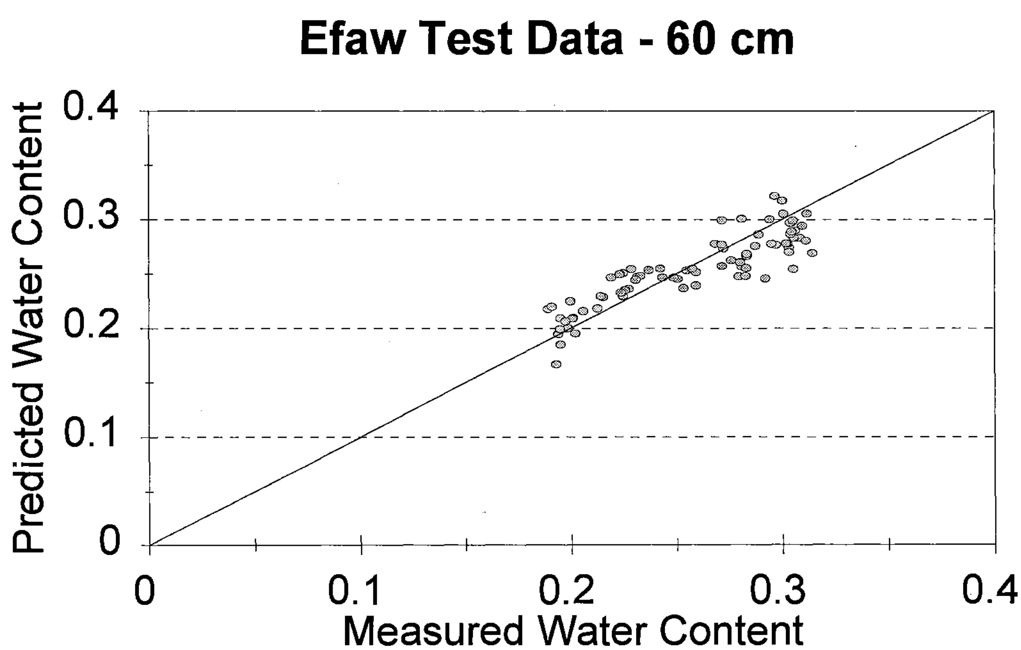

Figure 6.13. Predicted and Measured Values Using Efaw-Trained Network (60 cm).

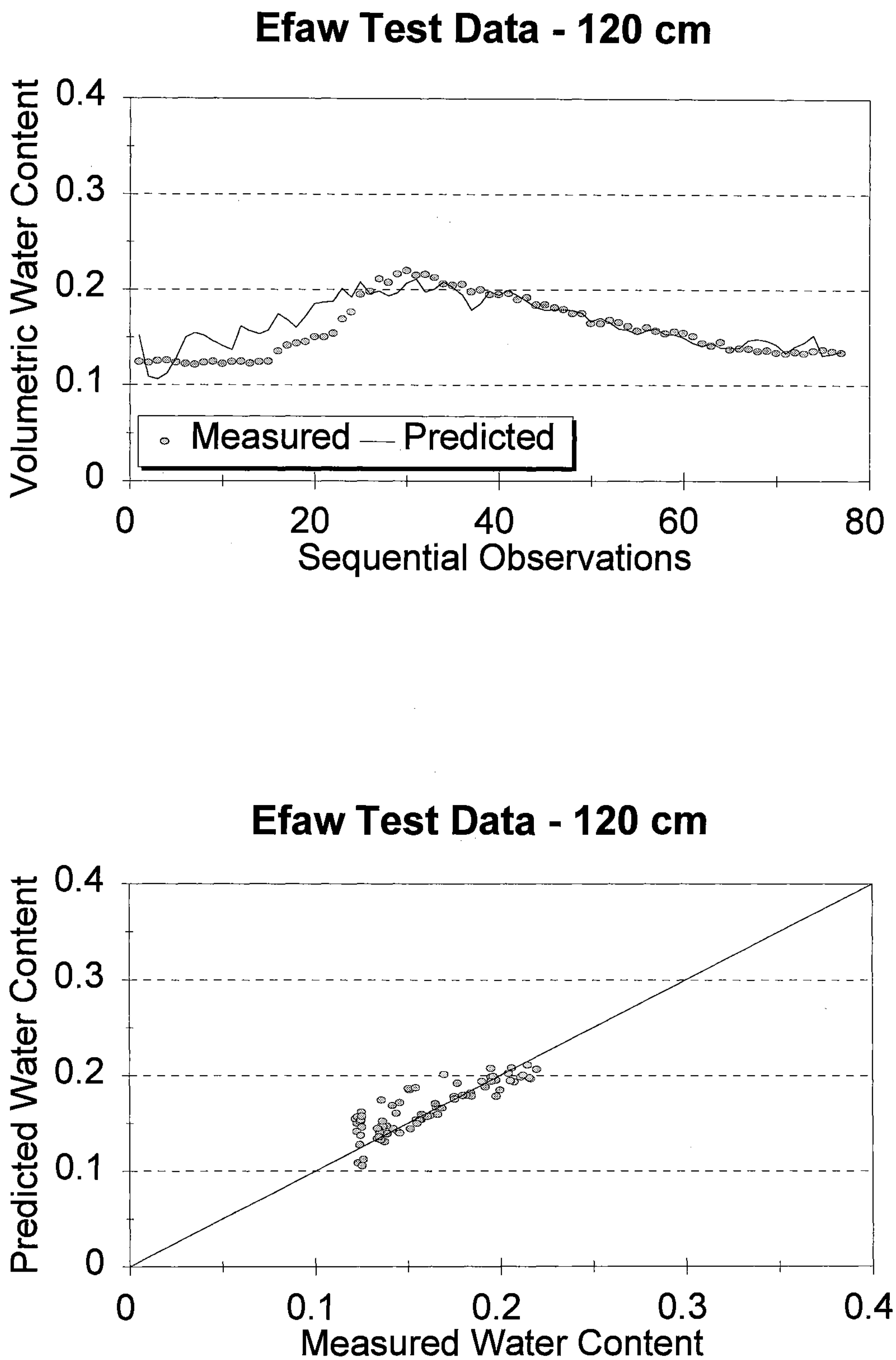

Figure 6.14. Predicted and Measured Values Using Efaw-Trained Network (120 cm).

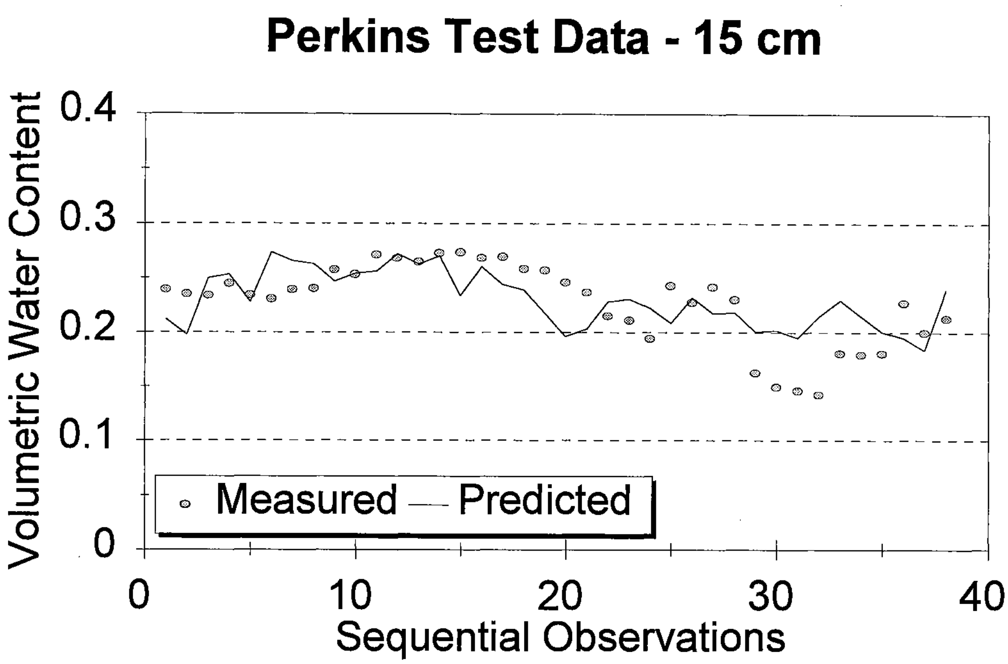

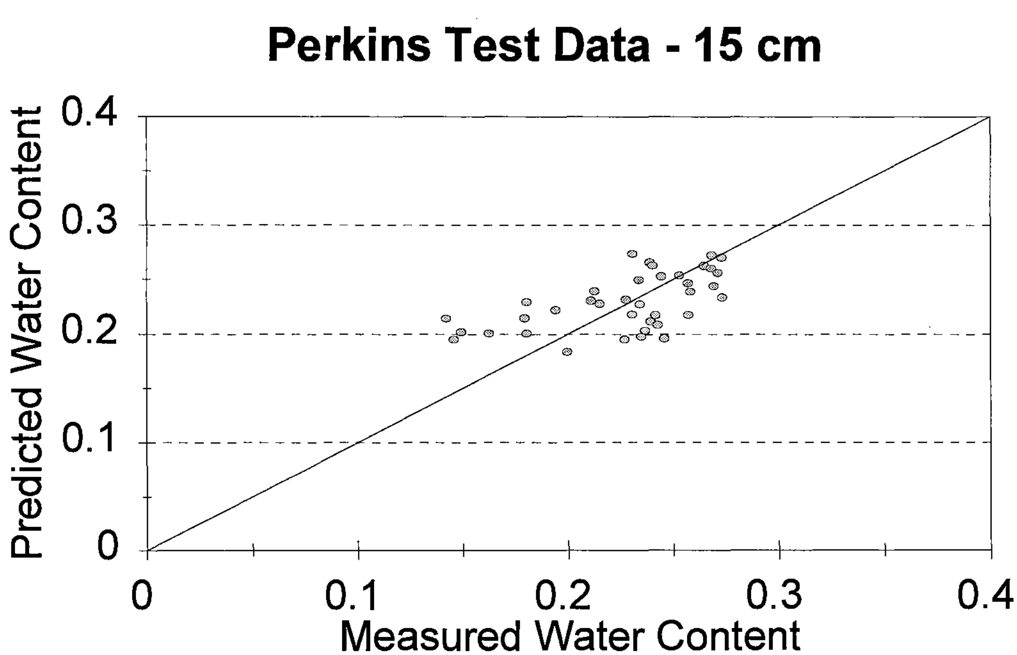

Figure 6.15. Predicted and Measured Values Using Perk-Trained Network (15 cm).

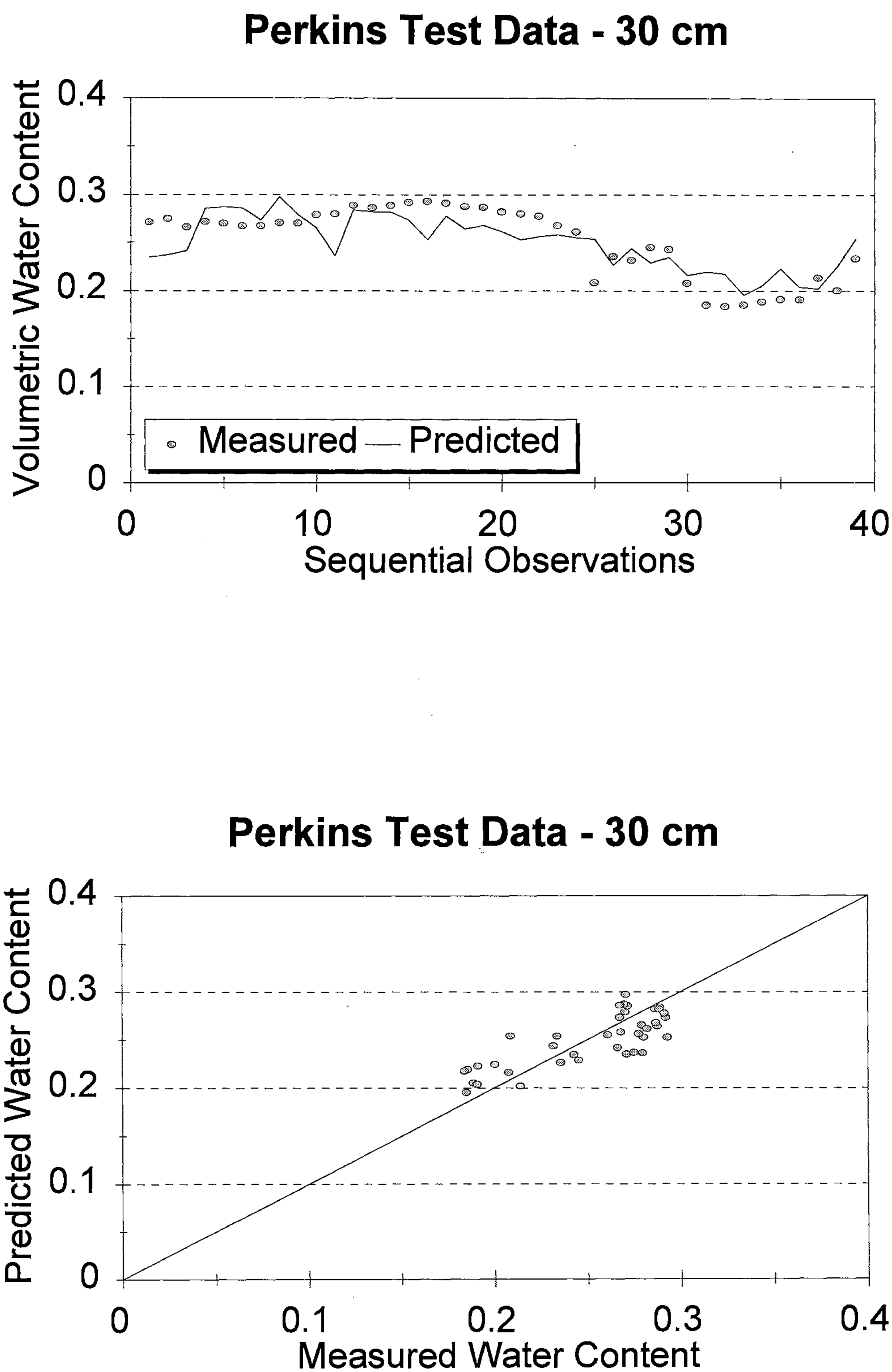

Figure 6.16. Predicted and Measured Values Using Perk-Trained Network (30 cm).

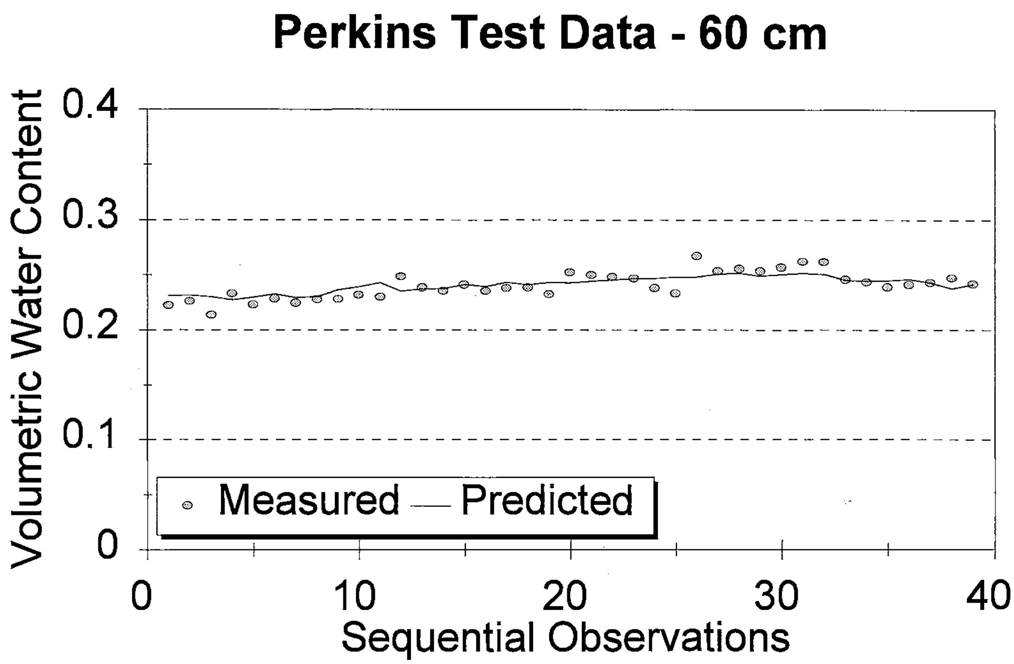

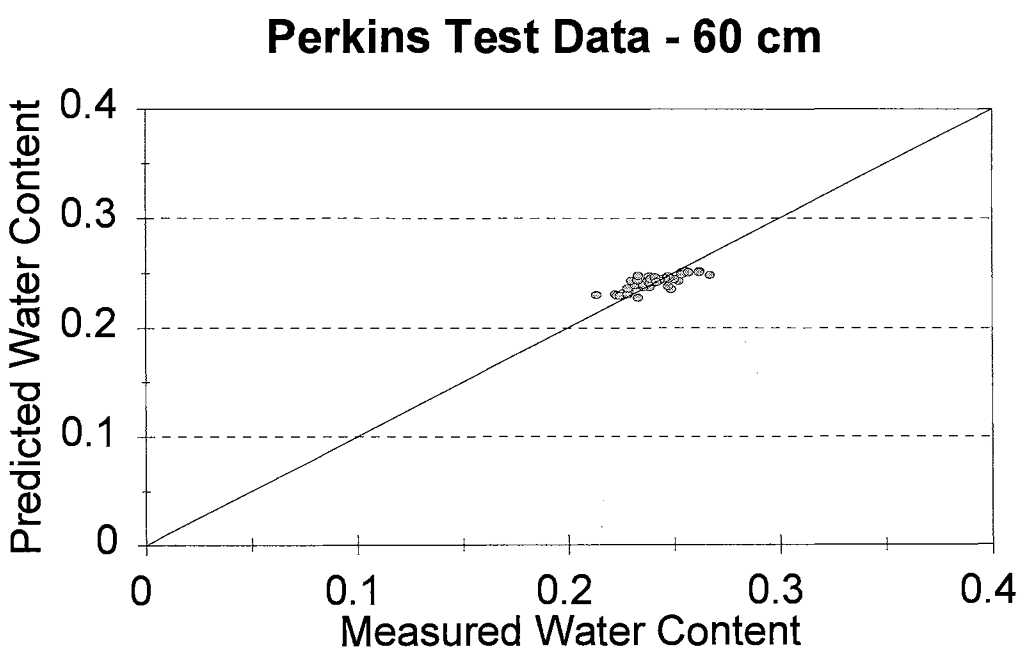

Figure 6.17. Predicted and Measured Values Using Perk-Trained Network (60 cm).

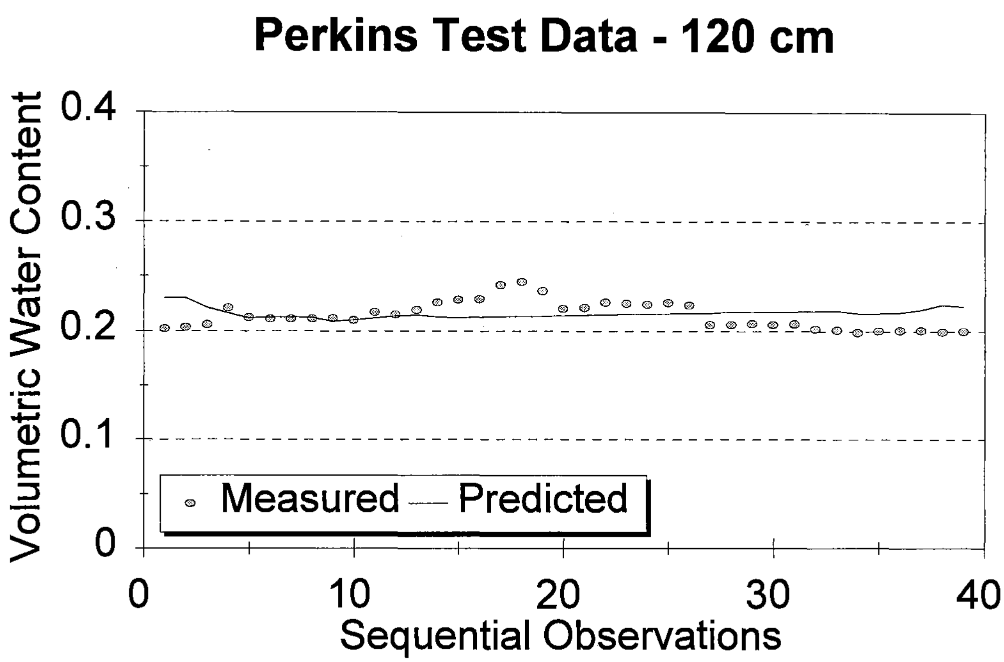

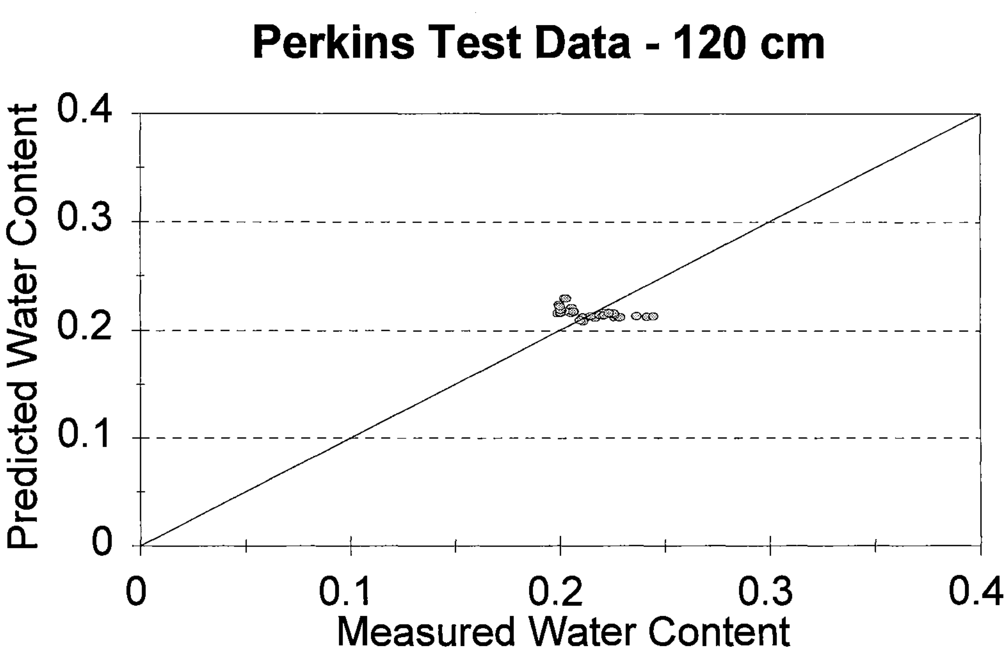

Figure 6.18. Predicted and Measured Values Using Perk-Trained Network (120 cm).

content decrease with depth which is to be expected.

Once it was determined that the individual location models seemed to be working when trained with the interpolated data, a combined model was developed. The training data for the two sites were combined into one file. The network was designed exactly as before except the training set was larger. The trained network was then tested also using combined test data. The root mean square error results fell in between the values for the two individual models. Plots of the test data (measured) versus the neural network predicted results for the combined model for the four depths can be seen Figures 6.19 through 6.22. As before, the model was trained using interpolated soil moisture data and tested using only measured data (uninterpolated) which was not used in the training session. A simple regression analysis of predicted water content on measured water content was performed on the combined model which is summarized in the following table.

Depth (cm)	Standard Error	Correlation Coeff (r^2)
15	.0267	0.661
30	.0216	0.545
60	.0178	0.610
120	.0206	0.560

Table 6.6. Regression Analysis Results of Combined Network.

The combined model worked well but it was trained with the same types of data that it was tested with. Ideally, the neural network model could use test data from other sites and predict accurately without actually having that soil type used in the training.

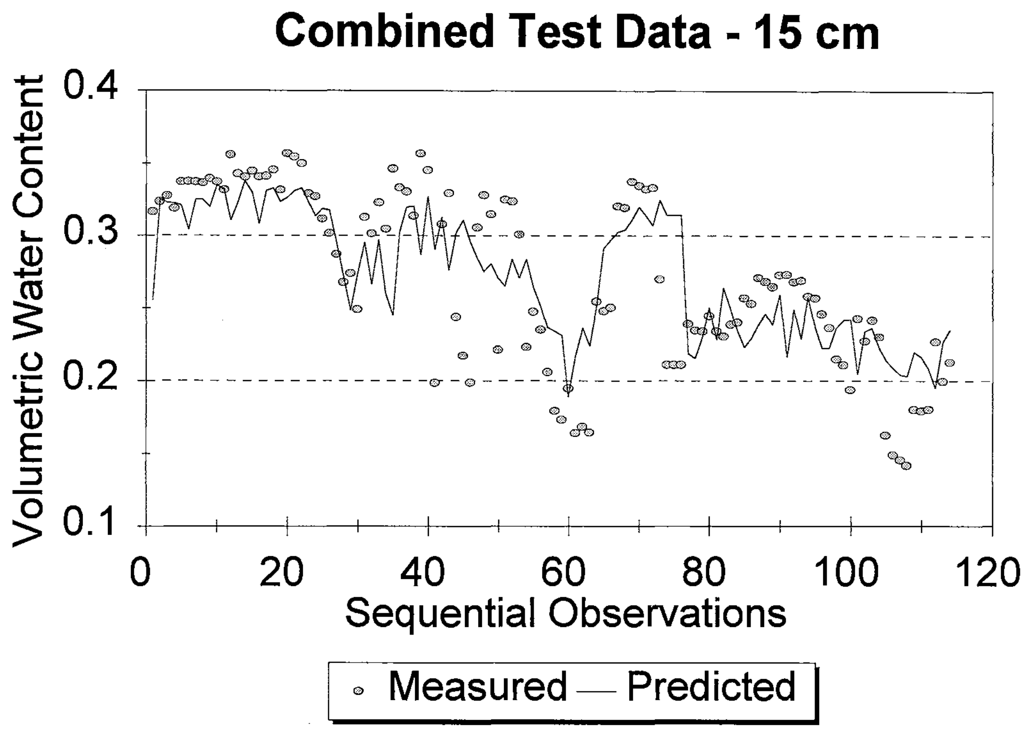

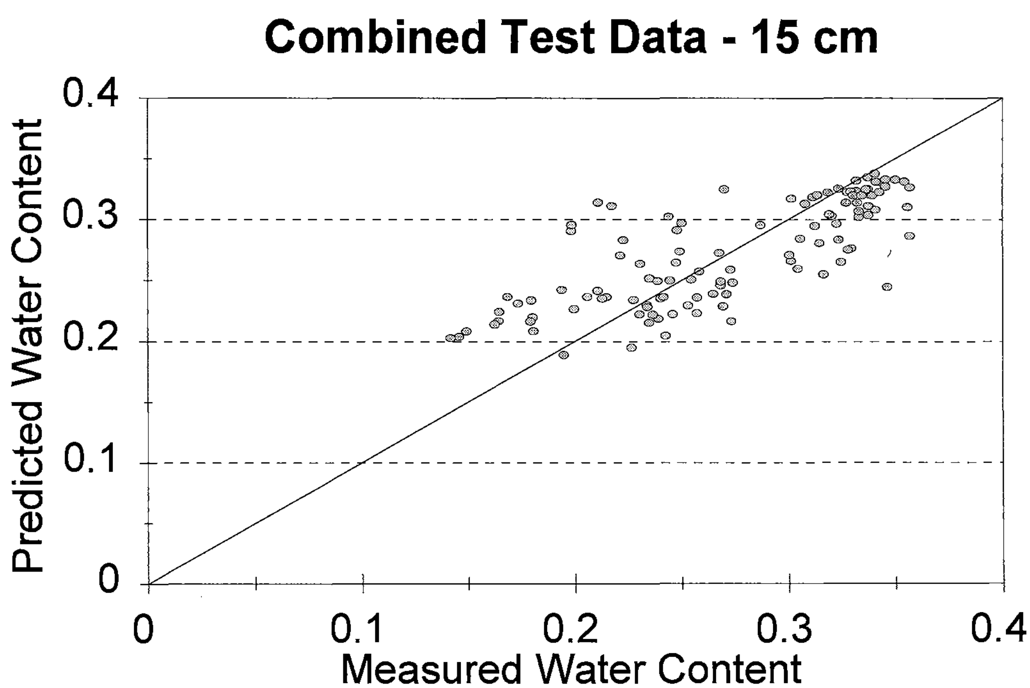

Figure 6.19. Measured and Predicted Values of Combined Model (15 cm).

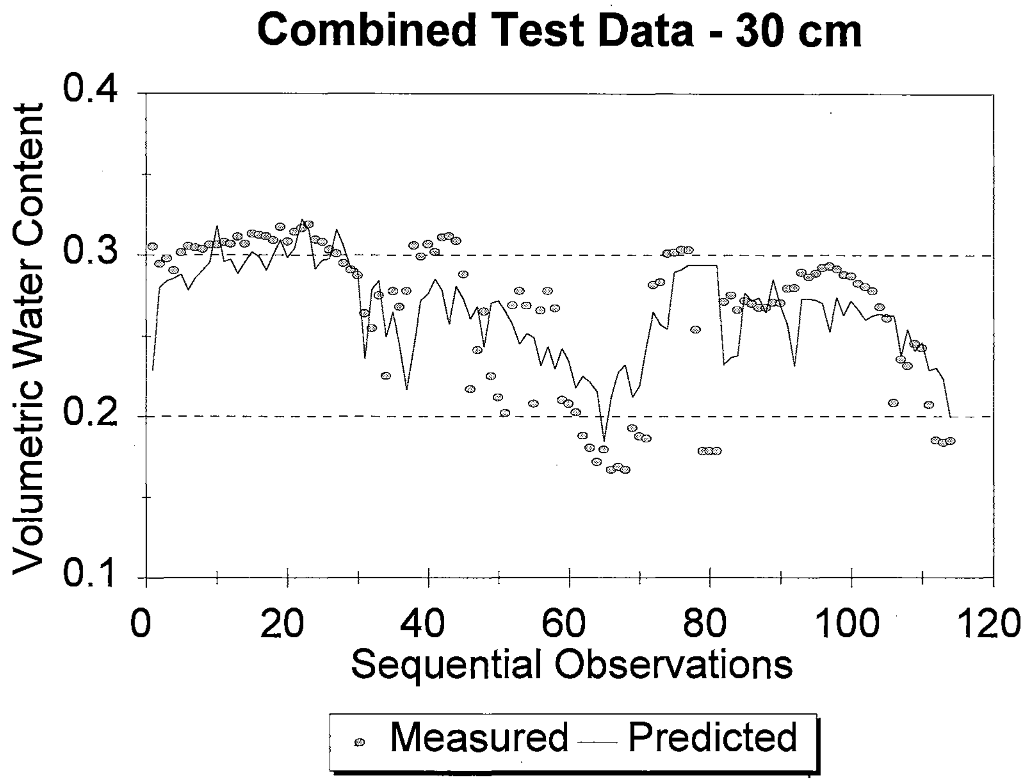

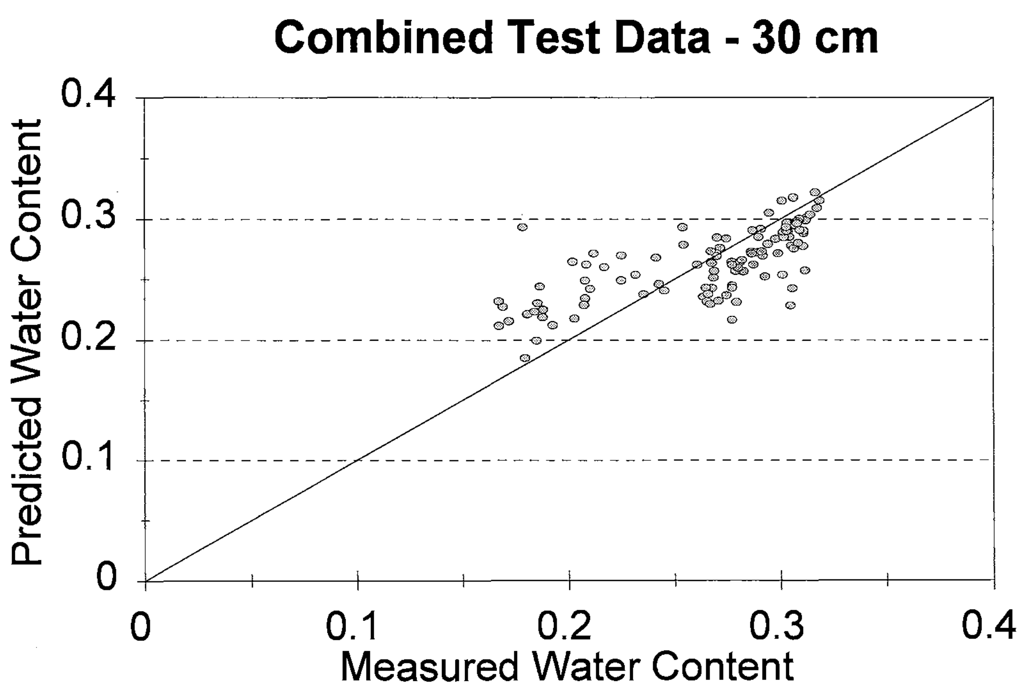

Figure 6.20. Measured and Predicted Values of Combined Model (30 cm).

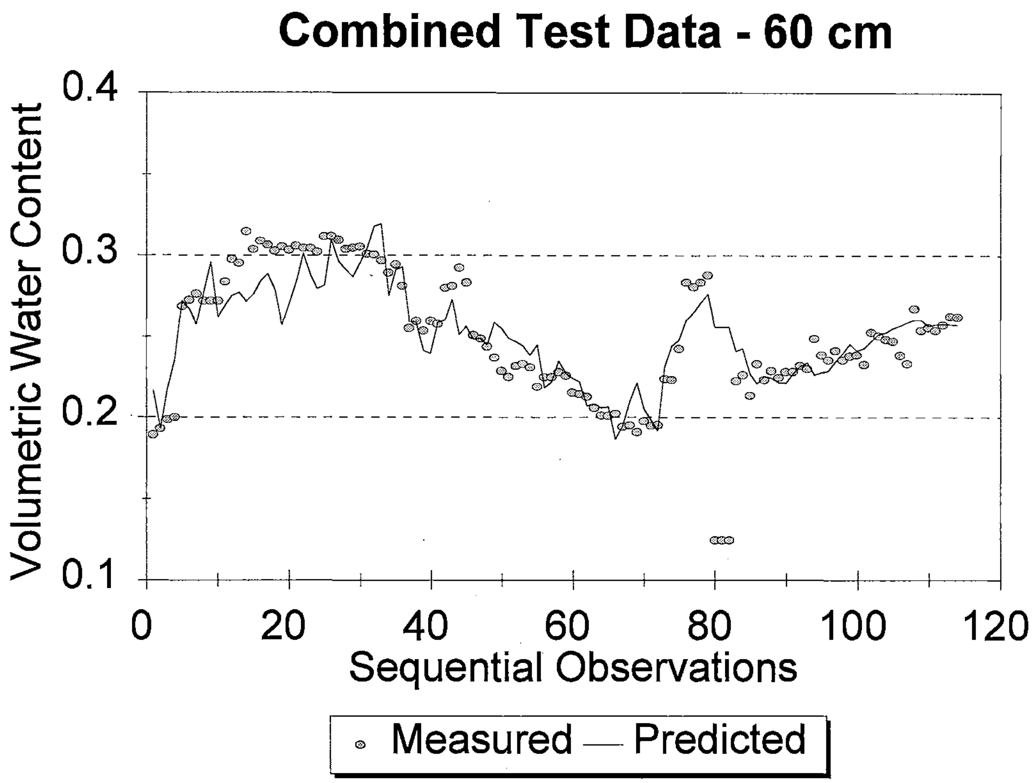

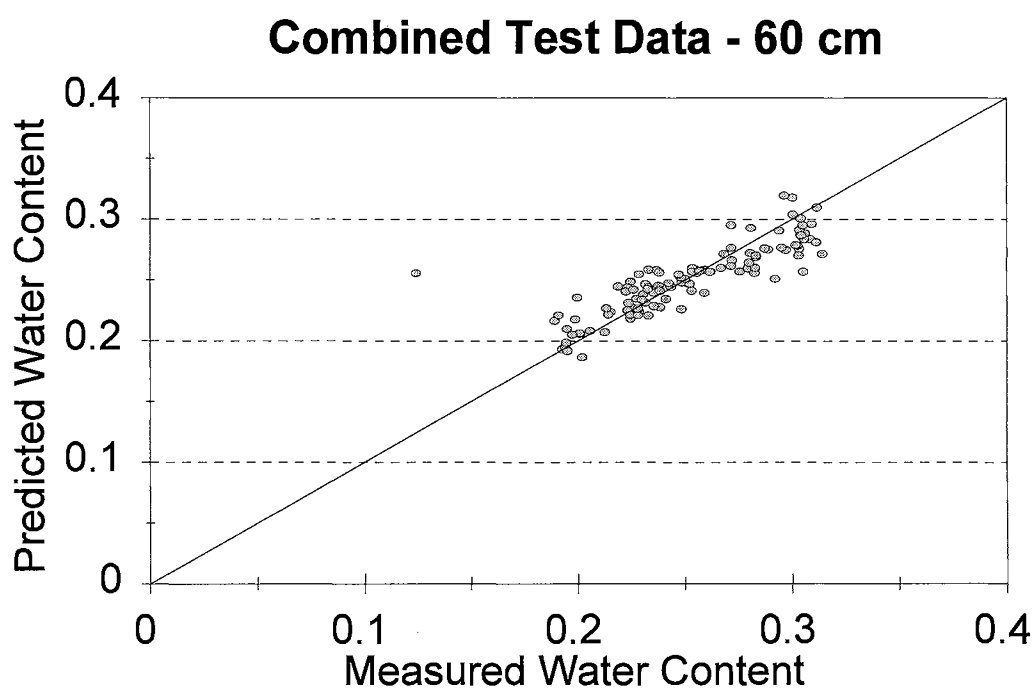

Figure 6.21. Measured and Predicted Values of Combined Model (60 cm).

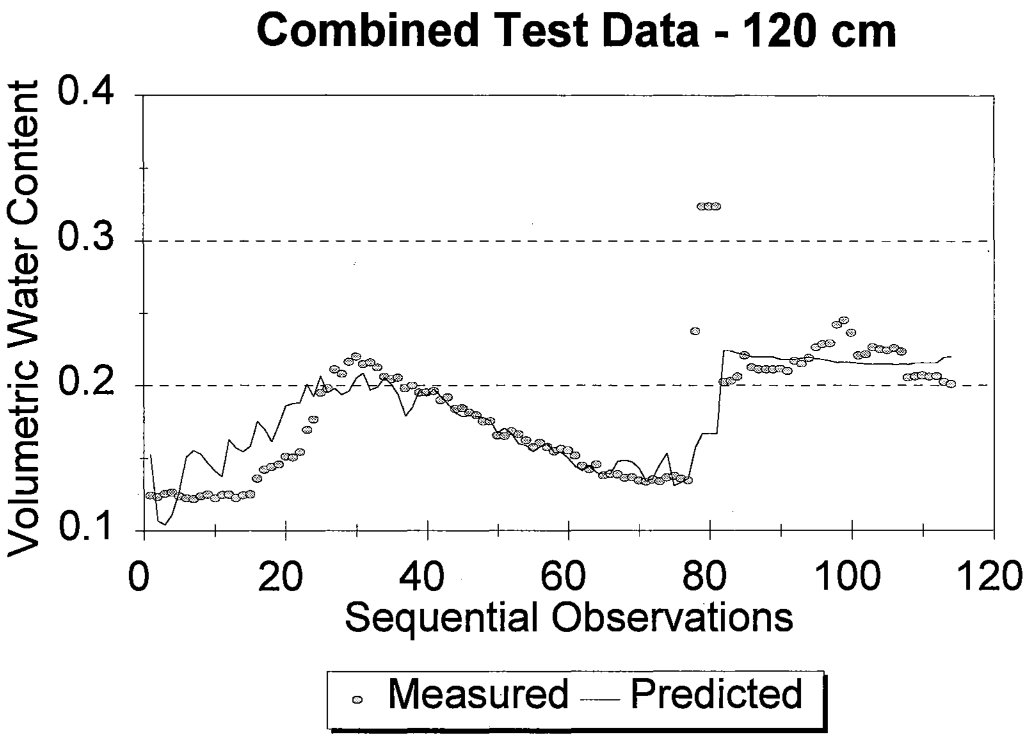

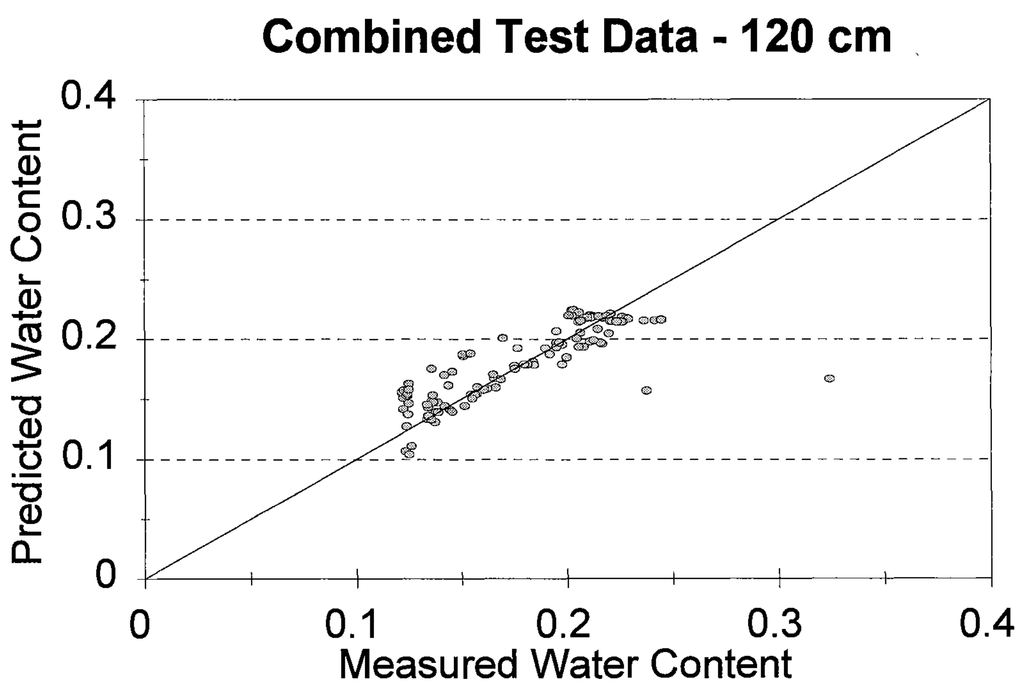

Figure 6.22. Measured and Predicted Values of Combined Model (120 cm).

Thermocouple Probe Installation Comparison

One other test was performed using the neural network. With the completion of this project it would be desired that a field-deployable instrument could be made available for measuring soil water content. With this in mind, the installation of the thermocouple probes should be convenient and the readings consistent among the various probes. Therefore, a test was conducted to determine if the performance of the neural network was affected by the use of only one temperature probe instead of three. The same training and test data were used, but the number of temperature inputs was reduced form 24 to 8 because rather than using all three probes, each one was used separately. The results of the probe test can be seen in Table 6.7.

Probe 1 is the east probe, probe 2 is in the center and probe 3 is the west probe. The difference between the individual probe results is insignificant. The most important factor when installing the probes was to make sure that there was good contact between the thermocouples and the soil. These results show that if the basic installation procedure is followed from Chapter 5, there should be minimal problems regardless of soil type. It should also be noted that the network predicts quite well with the use of only one probe. This preliminary analysis indicates that at a commercial level, probably only one temperature probe would need to be used (if interested in a small area). For the network optimization for this project, it was decided to use all three probes because the data was available and it could strengthen the relationships.

Depth (cm)	Probe	Combined RMSE	Perkins RMSE	Efaw RMSE
15	1	.0372	.0281	.0387
	2	.0370	.0271	.0400
	3	.0381	.0286	.0387
30	1	.0321	.0247	.0310
	2	.0331	.0229	.0318
	3	.0326	.0224	.0314
60	1	.0300	.0135	.0287
	2	.0298	.0138	.0296
	3	.0293	.0138	.0297
120	1	.0307	.0174	.0324
	2	.0315	.0171	.0319
	3	.0310	.0174	.0320

Table 6.7. Root Mean Square Error Analysis for the Individual Probes.

Network Optimization

Since it was shown that once the training set was large enough, soil water content could be predicted with an average RMS error of about 3% using soil temperatures only, it was decided to develop the network into a more universal model and optimize it as much as possible. Only the "combined" model was used for further development. At this point in time, the Efaw station had been collecting data for approximately 20 months and the Perkins station had been collecting data for 14 months. Therefore, it was decided that the training set was now large enough to train solely using measured data and no interpolated data. This would eliminate questions pertaining to the truth of the training set. Once again, all of the data were combined and every other datum was used for training while the rest were used for testing so that all seasonal effects could be accounted for.

Since data from both locations were combined into a single training set, it was decided to add one extra input processing element to the input layer which would be characteristic of the soil type. This input value is called the soil coefficient value and a value of 0 was chosen for Efaw and a value of 1 was chosen for Perkins. These values were arbitrarily selected to be representations of soil type. The values of 0 and 1 were chosen because of the normalization process used to make the activation function of the neural network valid. The rest of the network configuration was identical to the previous network with the exception of some of the learning coefficient values and changes from the default values of NeuralWare. Once again, the MinMax table was used. The following values were used:

	Parameter	Units	Min	Max
Input	Soil Temperature	°C	-10.0	40.0
	Soil Coefficient	-	0.0	1.0
Output	Soil Water Content	-	0.0	.40

Table 6.8. MinMax Table for Final Network Input Parameters.

The input network ranges were set from -5.0 to 5.0 while the output ranges were set from -0.01 to 0.01. Network range refers to the desired range of values required at the input and output buffers of the network. As data is read in, it will be scaled and offset so as to be within these low and high values. For each item of data input to an input buffer processing element, the input start column is used to calculate which entry in the MinMax table should be used as the source range. This range is used to derive a scale/offset mapping.

The input layer consisted of 25 processing elements for depths 15, 30 and 60 cm - 24 temperatures (two above and below desired depth, twice a day, on three probes) and one soil coefficient, and 13 processing elements for the 120 cm depth (12 temperature and one soil coefficient). The hidden layer again had 5 processing elements and the output layer had one element corresponding to soil water content. Each layer of the network has learning coefficient information. The coefficient information for each layer and depth can be seen in Appendix D.

The model was then trained using a convergence threshold of 0.001. The system was set to 100,000 iterations but was considered "trained" once the RMS error had stabilized and not changed for several hundred iterations. Once this "final" model was trained to the best of its capability, the processing element coefficients and weights were saved and stored. All of the processing element information for the entire network including transfer function values, summation values and corresponding weights can be seen in Appendix E.

Since the neural network model was developed on a SUN workstation, it is desirable to have the code in a form which is transportable and can be used on PC based systems. A C program was written which can use the input files and the stored weight files of the final network to estimate the soil water content without having to run it on a SUN or use the NeuralWare package. This makes the application much more universal. A printout of the C code can be seen in Appendix F.

This network was then tested for all four depths using Efaw and Perkins test data. It was also tested using Hyd data for 15 and 30 cm depths. The complete testing results and the validation of this "final" model using the Hyd data will be discussed in the next chapter.

Multiple Variable Linear Regression

A knowledge of statistics is excellent preparation for appreciating the power and flexibility of neural networks. In statistics, one must often make assumptions about the data, and must sometimes limit the analysis to a certain number of possible interactions. From a practical point of view, neural networks are basically "non-parametric", although in theory they are thought of as being parameterized by their weights. In addition, more terms can be examined for interaction by a neural network, since the network will place its emphasis on those inputs that help to predict the output. By allowing more data to be analyzed at the same time, more complex and subtle input interactions are possible.

After the "final" neural network was developed, the same parameters were used in a multiple variable linear regression analysis to use as a comparison. Since the neural network model only used soil temperatures, that is all that was considered in the linear regression analysis. The same data which was used as training data for the neural network was used to develop a linear regression equation while the test data was used to determine how well the equation worked as a predictor. The regression analysis was performed for moisture contents at depths of 15 and 30 cm.

The training data was combined using both Efaw and Perkins data so that a "combined" model could be developed to use as comparison with the "combined" final neural network model. The temperatures were averaged for the three thermocouple probes at depths of 5, 10, 20, 25, 40, and 50 cm. T_5, T_{10}, T_{20}, and T_{25} were used for the 15 cm depth soil water content prediction while T_{10}, T_{20}, T_{40}, and T_{50} were used for the 30 cm depth moisture prediction. The regression training data consisted of the temperatures taken at 2 a.m. and 2 p.m. as was used for the neural network. Three regressions were performed for each desired depth. The first regression consisted of using the raw temperatures at the 4 depths surrounding the moisture location at two times resulting in 8 variables. A multiple variable linear regression was performed using these eight temperatures as the independent variables and moisture content as the dependent variable. The equations for the 15 and 30 depths are given below:

$$\begin{aligned}\theta_{15} = {} & .298-.036T_{10a}+.198T_{20a}-.002T_{5a}-.174T_{25a} \\ & +.004T_{10p}-.007T_{20p}-.007T_{5p}+.023T_{25p}\end{aligned} \tag{6.3}$$

and

$$\begin{aligned}\theta_{30} = {} & .292+.045T_{20a}-.092T_{40a}-.022T_{10a}+.054T_{50a}-.088T_{20p} \\ & +.277T_{40p}+.016T_{10p}-.192T_{50p}\end{aligned} \tag{6.4}$$

The multiple linear equation models were then used with the test data to determine how well they could predict moisture content. The testing procedures and results will be discussed in the following chapter.

Although the input values into the neural network were individual temperatures, they were selected so that a change in temperature could be represented within the network. The neural network has the capability of using the individual temperatures as inputs, but with the learning weights on the connections, it can relate the variables in a number of ways. In Chapter 3, it was shown that the use of the changes in temperatures (ΔT) with time and depth are quite important and with the format of the input temperature into the neural network, it was possible for these relationships to be considered. The change in temperature with depth is important because of the basic heat flow equation concepts and the change in temperature with time is the basis for the diurnal heat fluctuation in the soil resulting in the sinusoidal curve. With these concepts in mind, a multivariate linear regression was performed on ΔT with time and ΔT with depth. Once again, the depths of 15 and 30 cm were used. Rather than 8 individual temperatures, the number of variables was reduced to four. For the change in temperature with time, the four depths surrounding the desired location were used, with the difference in temperature between 2 a.m. and 2 p.m. The linear regression analysis resulted in the following equation for 15 and 30 cm depths, respectively:

$$\theta_{15} = .277+.004T_{10p-a}-.003T_{20p-a}-.006T_{5p-a}+.011_{25p-a} \tag{6.5}$$

$$\theta_{30} = .241-.069T_{20p-a}+.156T_{40p-a}+.017T_{10p-a}-.079T_{50p-a} \tag{6.6}$$

As before, the model equations were used on the test data which had been organized into changes in temperature with time and a predicted soil water content was calculated.

Finally, an analysis was performed for the temperature change with depth for the two given times. For the 15 cm depth, the differences were taken between 10 and 20 cm, and 5 and 25 cm. For the 30 cm depth, the differences were taken between 20 and 40 cm, and 10 and 50 cm. The multivariate analysis resulted in the following equations:

$$\theta_{15} = .276 + .035T_{10\text{-}20a} - .003T_{5\text{-}25a} + .003T_{10\text{-}20p} - .007T_{5\text{-}25p} \tag{6.7}$$

$$\theta_{30} = .243 - .036T_{20\text{-}40a} + .034T_{10\text{-}50a} - .025T_{20\text{-}40p} + .001T_{10\text{-}50p} \tag{6.8}$$

Once again, the test results will be presented along with the neural network comparison in Chapter 7.

CHAPTER 7

MODEL VALIDATION

The goal of this research is to develop a sensor system which uses a neural network model to estimate water content using soil temperatures. Although there was extensive preliminary analysis before the final model could be fully developed, it is necessary to test the overall performance of the model using measured field data.

The final model was tested with data from three sites -- Efaw, Perkins (Perk) and Hydraulics Lab (Hyd). Although the final model was developed using training data from both Efaw and Perkins, the test data which was used had not previously been presented to the system. A soil coefficient value was calculated for the Hyd data set (not used in the model development) using the neural network model. As mentioned in the Field Procedure Chapter, the Hyd data collection was a scaled down version of that at the other two sites, with only enough temperatures collected for predictions of soil water content at depths of 15 and 30 cm.

Soil Coefficient Values

Each site was tested individually using the final model. As mentioned previously, each site also had a corresponding soil coefficient value which was used as an input. Efaw was given a value of 0 and Perkins a value of 1. Since the Hyd data was totally independent of the model development, a soil coefficient value had to be determined. Since it had a bulk density between the Efaw and Perkins values and the texture results (% sand, % silt and % clay) fell between the two also, the soil coefficient should fall somewhere between 0 and 1. The Hyd test data were run through the neural network for varying soil coefficient values from 0 to 1 by increments of 0.05 for both depths (15 and 30 cm). The soil coefficient value which corresponded to the minimum RMSE was the one which was selected. The results can be seen in Table 7.1.

The smallest root mean square error value was at a soil coefficient of 0.15 for both depths. Therefore, this was the value chosen as the representative coefficient for the Hyd data. A similar procedure could be used to develop soil coefficients for various soil types ranging from sand to clay. For now, it is suggested that if the soil has a relatively high content of clay, a soil coefficient between 0 and 0.5 be used, whereas if the soil is more on the sandy side, a value from 0.5 to 1.0 be used. This procedure would give the user an approximate initial value which could be altered as randomly gathered soil water content values are collected and compared to the neural network predictions to keep the system in "check".

Model Testing

The final model was tested using data from the three individual sites. The test data was formatted in the same manner as the training data, using 24 temperatures and a soil coefficient value for depths of 15, 30 and 60 cm, and 12 temperatures and a soil coefficient value for the 120 cm depth. All four depths were evaluated at the Efaw and Perkins sites, while only the 15 and 30 cm depths were examined at the Hyd site. These

Soil Coefficient Value	15 cm Depth RMSE	30 cm Depth RMSE
0.00	.0206	.0211
0.05	.0199	.0197
0.10	.0152	.0142
0.15	.0143	.0125
0.20	.0179	.0138
0.25	.0204	.0192
0.30	.0249	.0218
0.35	.0261	.0228
0.40	.0291	.0241
0.45	.0328	.0257
0.50	.0335	.0274
0.55	.0342	.0292
0.60	.0349	.0311
0.65	.0356	.0330
0.70	.0363	.0349
0.75	.0370	.0368
0.80	.0377	.0386
0.85	.0383	.0402
0.90	.0390	.0418
0.95	.0396	.0432
1.00	.0402	.0445

Table 7.1 Hyd Data Soil Coefficient Values.

inputs were run through the model and produced an output of predicted moisture content. The predicted moisture contents were then compared to moisture contents which were measured in the field on the same day as the temperature data used in the test set.

A root mean square error analysis was performed for each test set. There were a total of 10 test sets -- four depths each at Efaw and Perkins and two depths at Hyd. The Efaw and Perkins test sets consisted of 158 measured soil water content values (March 1992 - July 1993), while the Hyd test data had 60 values (April 1993 - July 1993). The predicted versus measured water contents were plotted for each test set, along with the residuals. A regression analysis was performed for each set, resulting in a correlation coefficient (r^2). The mean error and the standard deviation of the error were also calculated to help summarize the results.

Efaw

The graphical results for the Efaw test data can be seen in Figures 7.1-7.8. Figures 7.1, 7.3, 7.5, and 7.7 are the predicted and measured value plots for each depth. Figures 7.2, 7.4, 7.6, and 7.8 are the residual plots for each depth. It can be seen from the plots that for Efaw, the neural network model predicted quite well for all depths. This indicates that the network has learned the functional relationship between the input variables and the target output.

Two residual plots were done for each depth. The first plot shows the residuals versus the measured water content and the second plot is a time sequence of the residuals. For these residual plots, an overall impression of a horizontal band of residuals is regarded as satisfactory. For the depths of 15, 30, and 60 cm, the residual versus measured water content values appear to slant down across the plot, having more positive residual values for lower moisture contents and lower residual values for higher moisture contents. It could be concluded that there is some type of linear effect in the measured data which has not been removed, or else the neural network is not capturing the extremes. For the time sequence plots there seems to be a slight sinusoidal trend, especially for the 60 and 120 cm depths. This trend may be related to the natural cyclic behavior of the measured data which was not captured by the neural network model.

Perkins

The results of the Perkins test data were quite similar to those for Efaw, with the neural network generally predicting values very close to the measured soil water content values (Figures 7.9-7.16). As with the Efaw test data, the model had a slight tendency to predict higher for lower moisture contents and a little low for the higher moisture contents. This can be seen by looking at the residual versus measured water content plots. The measured moisture data have less variation as the depth increases which is expected as there is much less influence from surface activity and action in the root zone. The various depth models follow this trend well. The model seems to perform a little better for the Efaw data than the Perkins data. This could possibly be explained by the fact that the training set used to develop the final model consisted of more training data from the Efaw site.

Hyd

The Hyd data, collected from April through July of 1993, was the final set tested with this model. The graphical results can be seen in Figures 7.17-7.20. The model predictions follow the measured values but seem to vary more than the measured values.

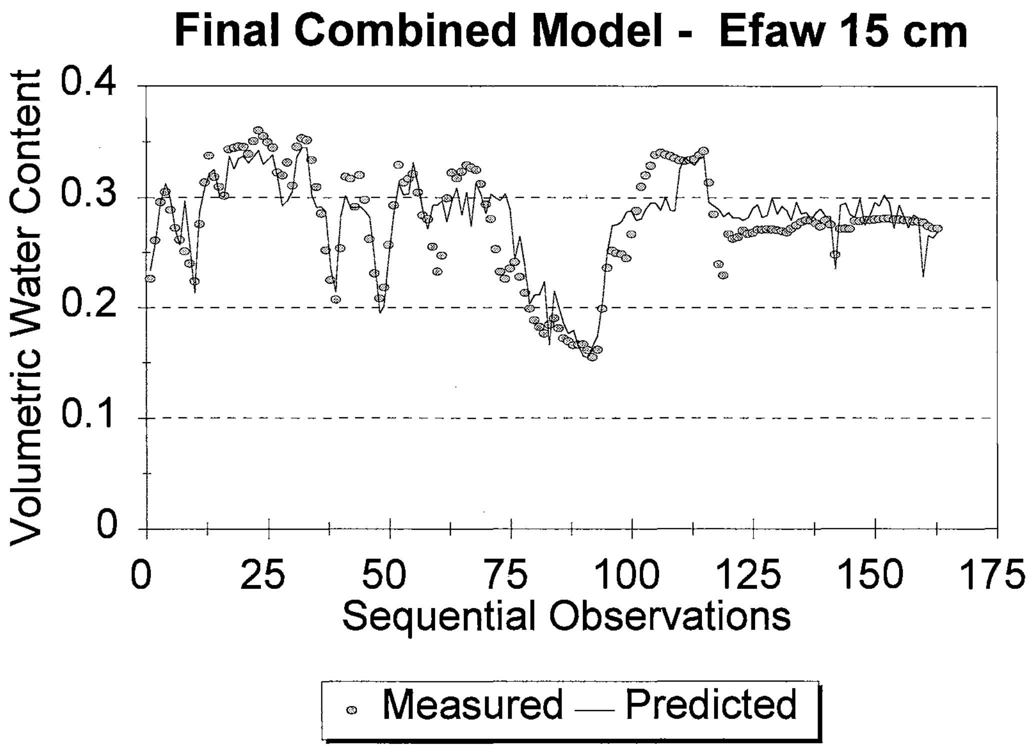

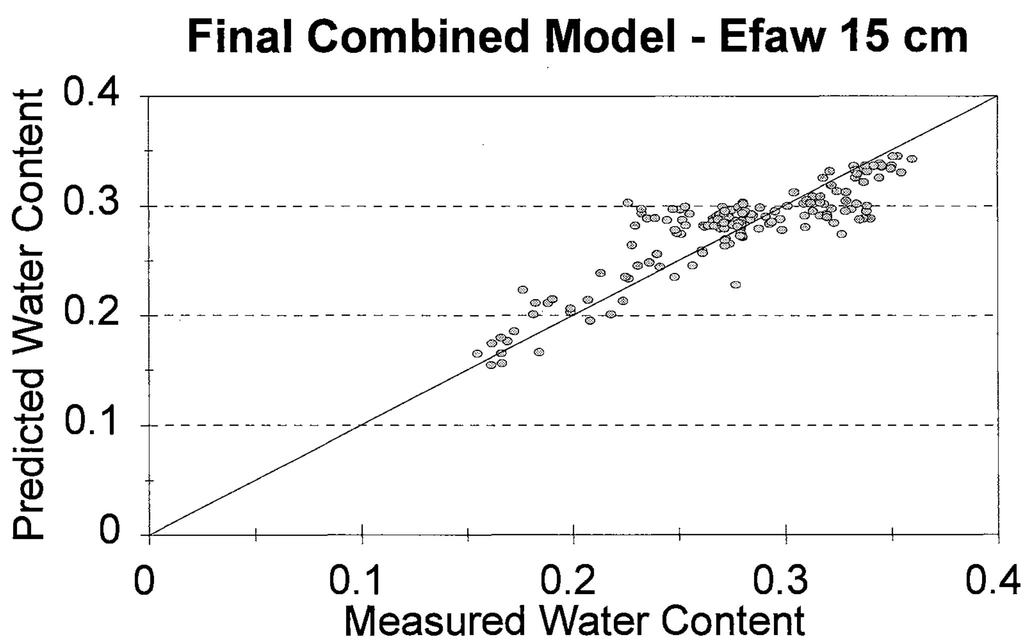

Figure 7.1. Measured and Predicted Test Results for Efaw (15 cm).

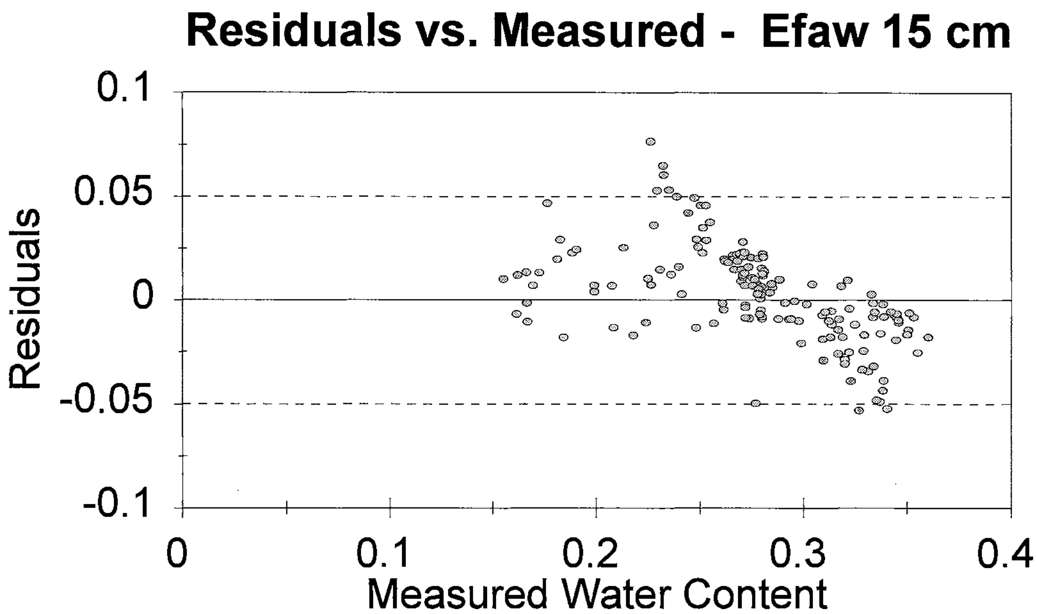

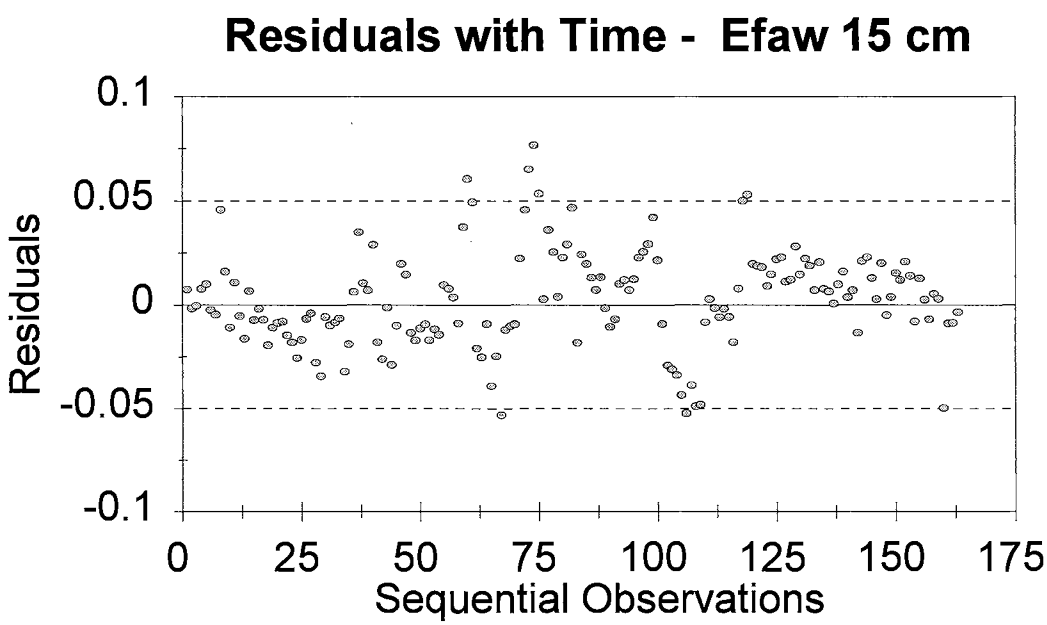

Figure 7.2. Residual Plots for Efaw (15 cm).

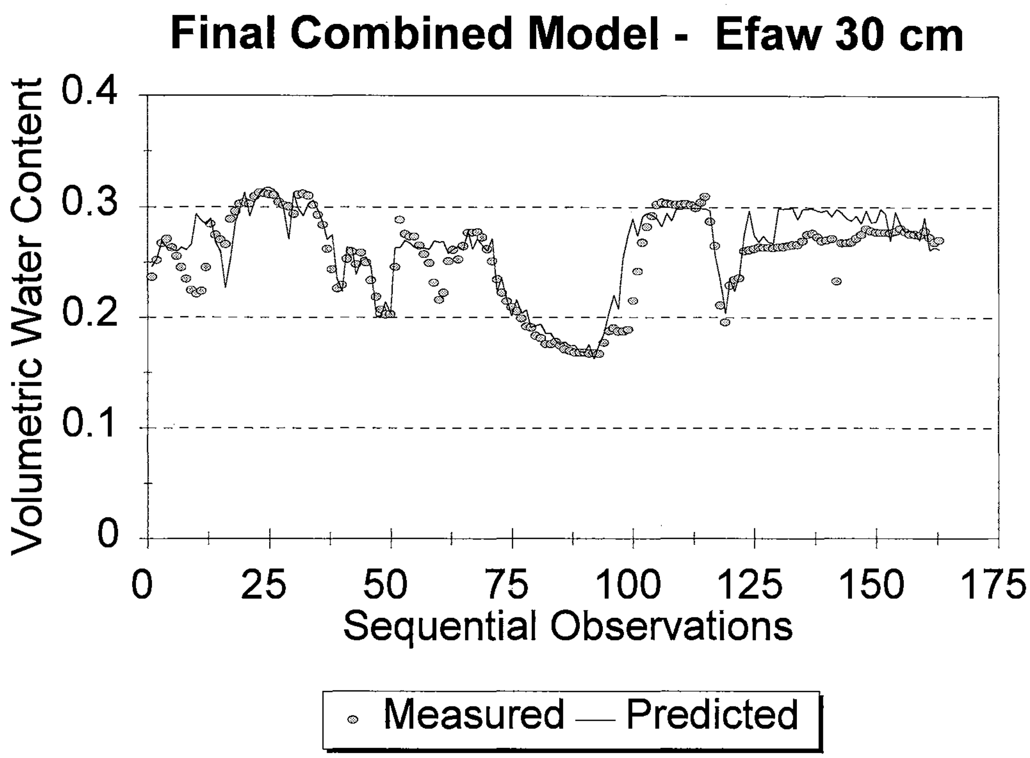

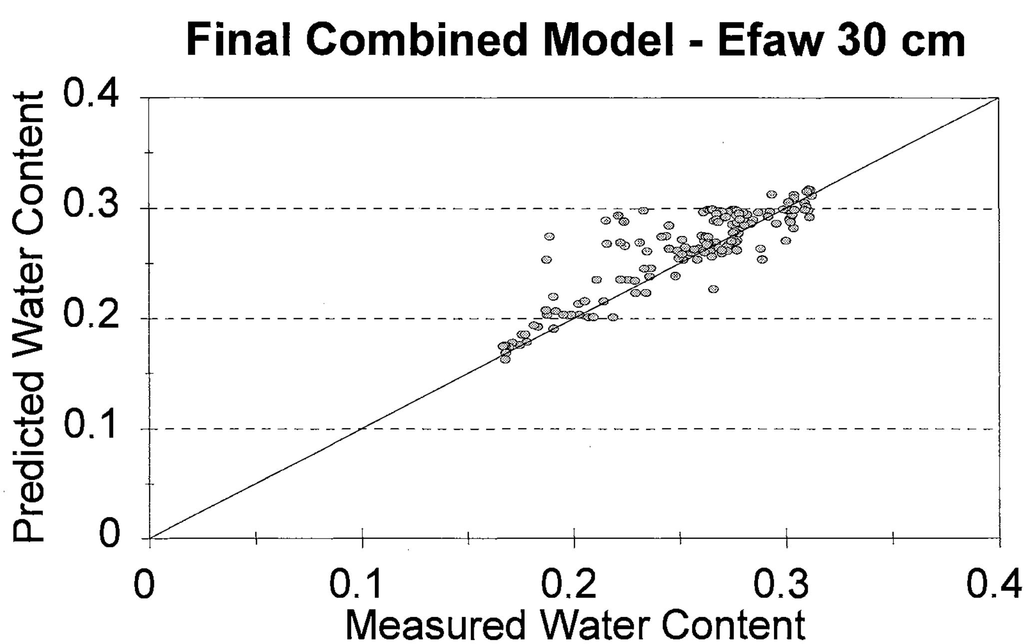

Figure 7.3. Measured and Predicted Test Results for Efaw (30 cm).

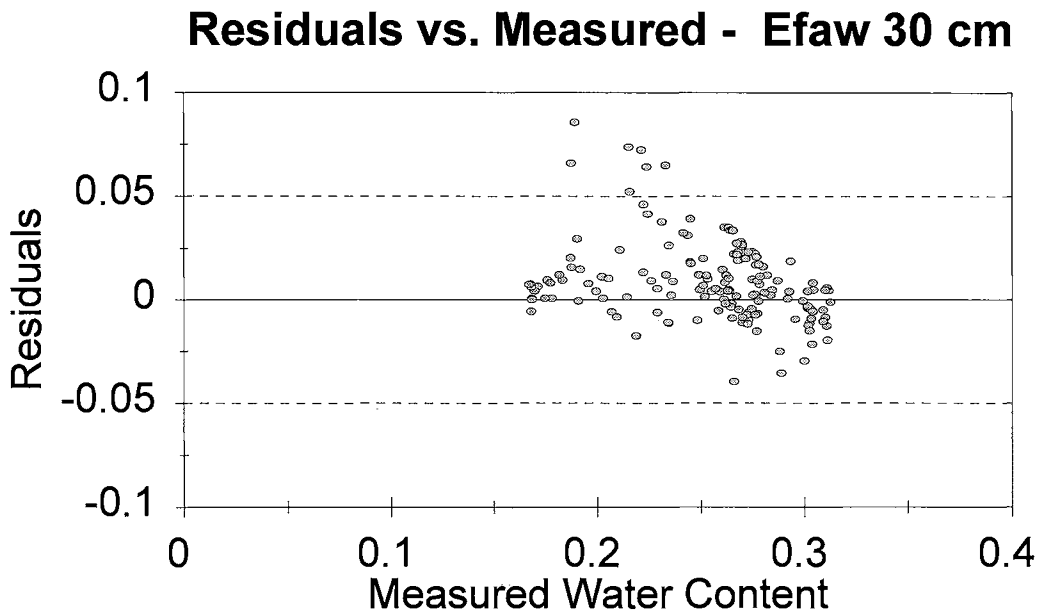

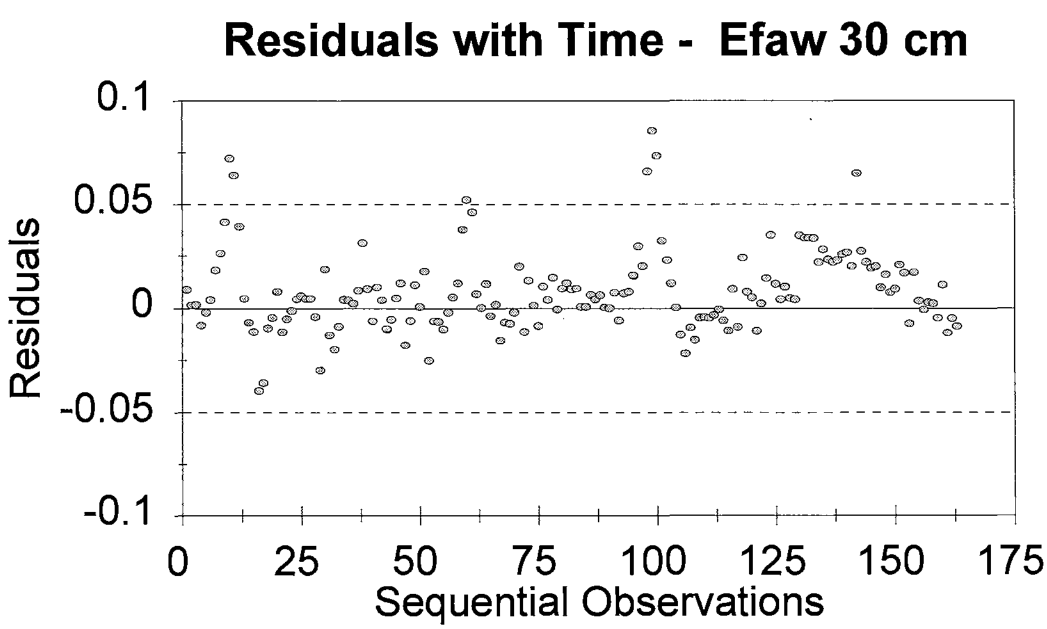

Figure 7.4. Residual Plots for Efaw (30 cm).

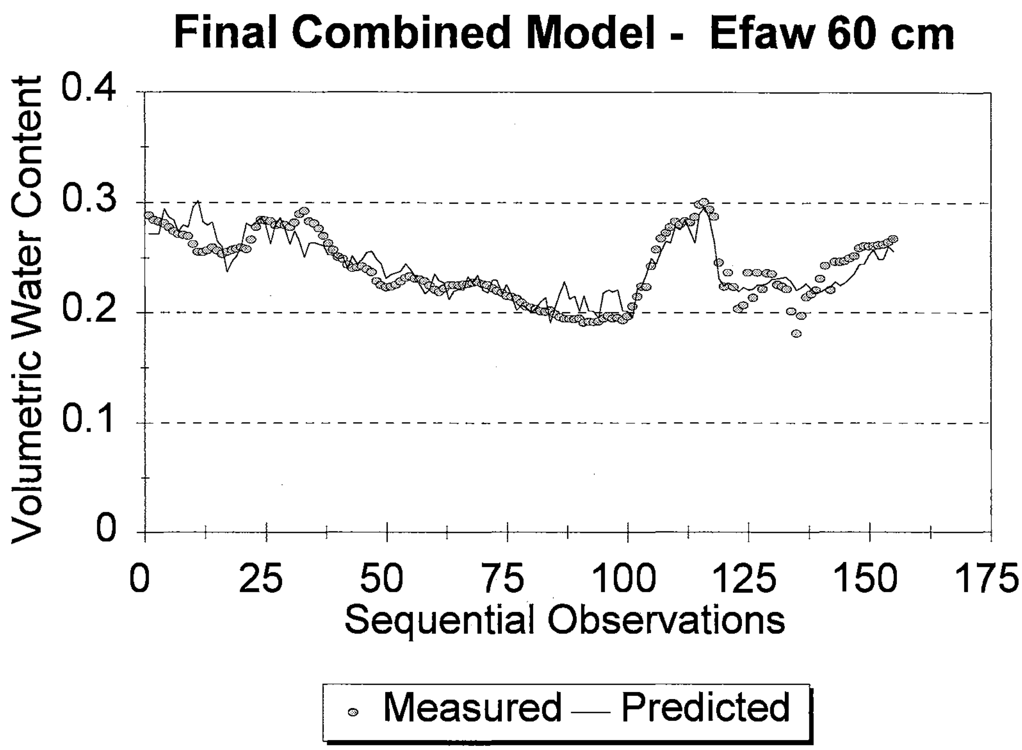

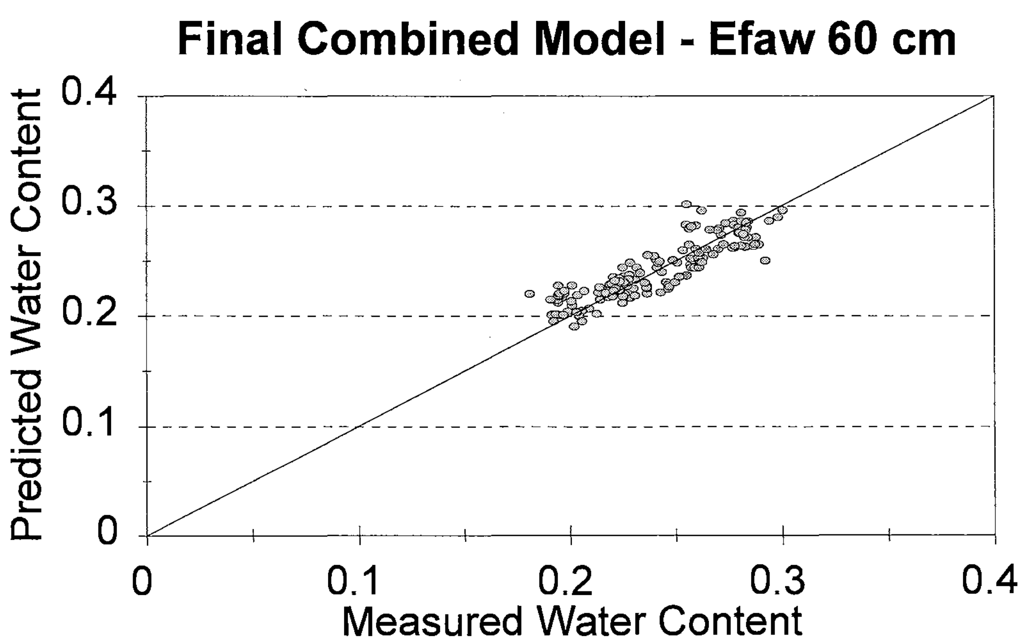

Figure 7.5. Measured and Predicted Test Results for Efaw (60 cm).

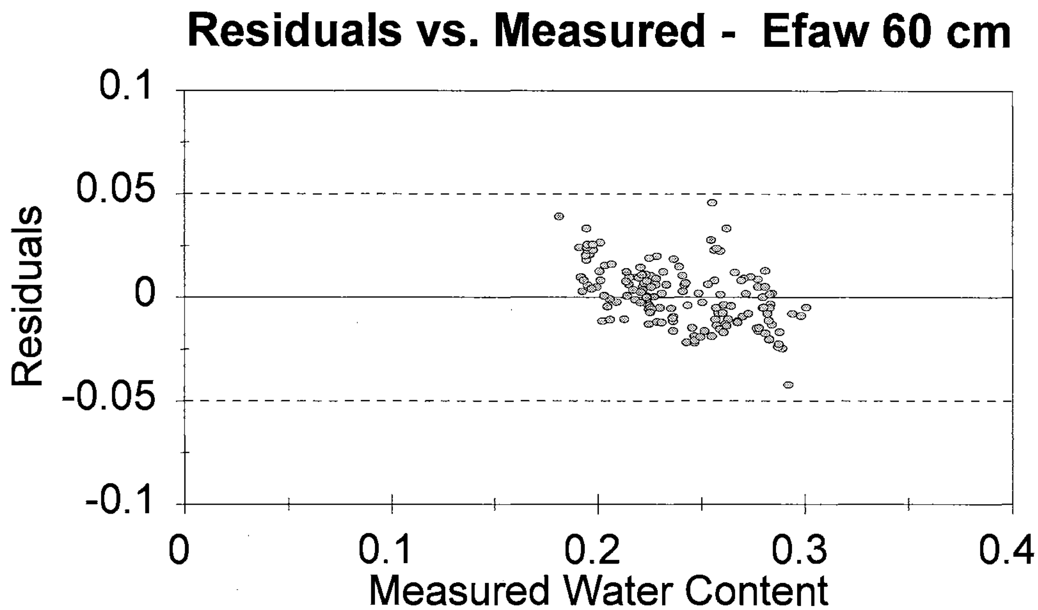

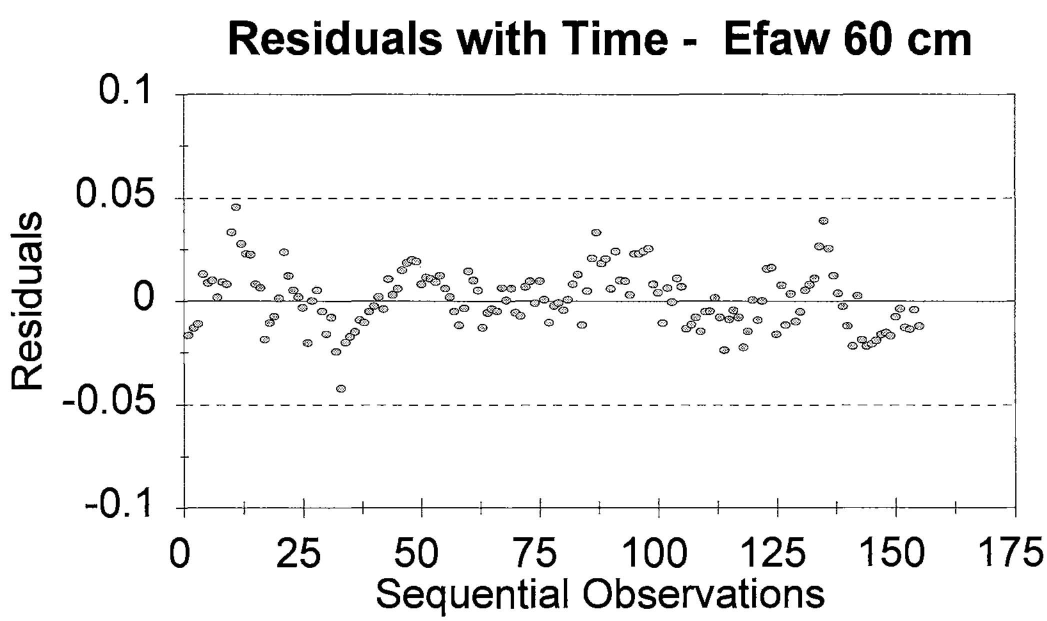

Figure 7.6. Residual Plots for Efaw (60 cm).

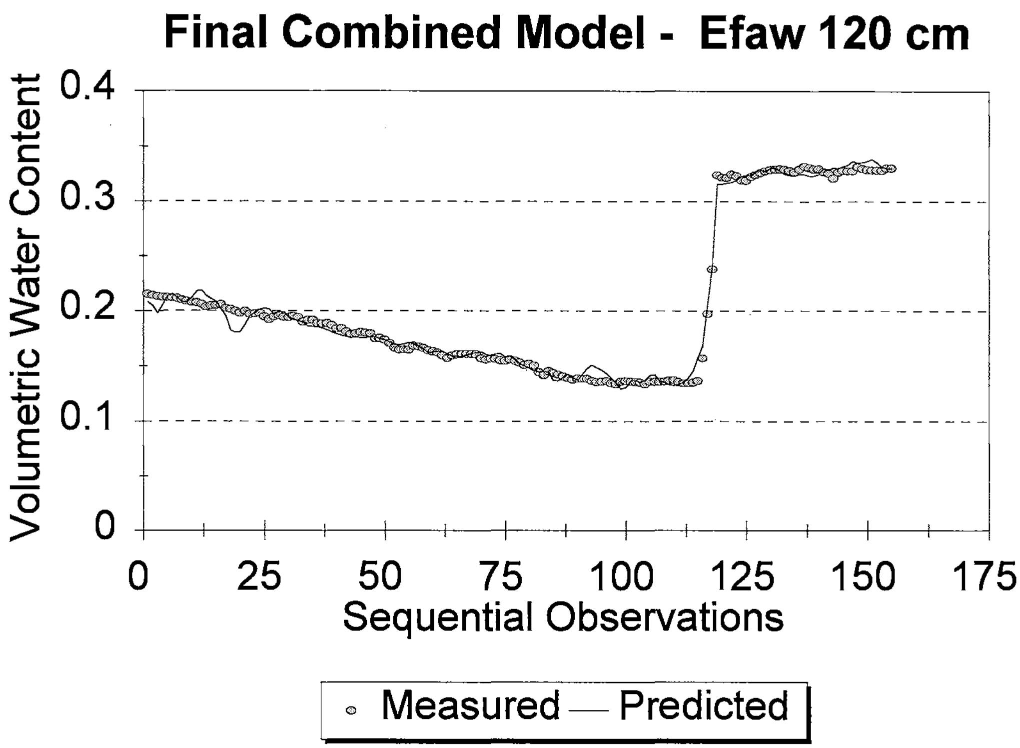

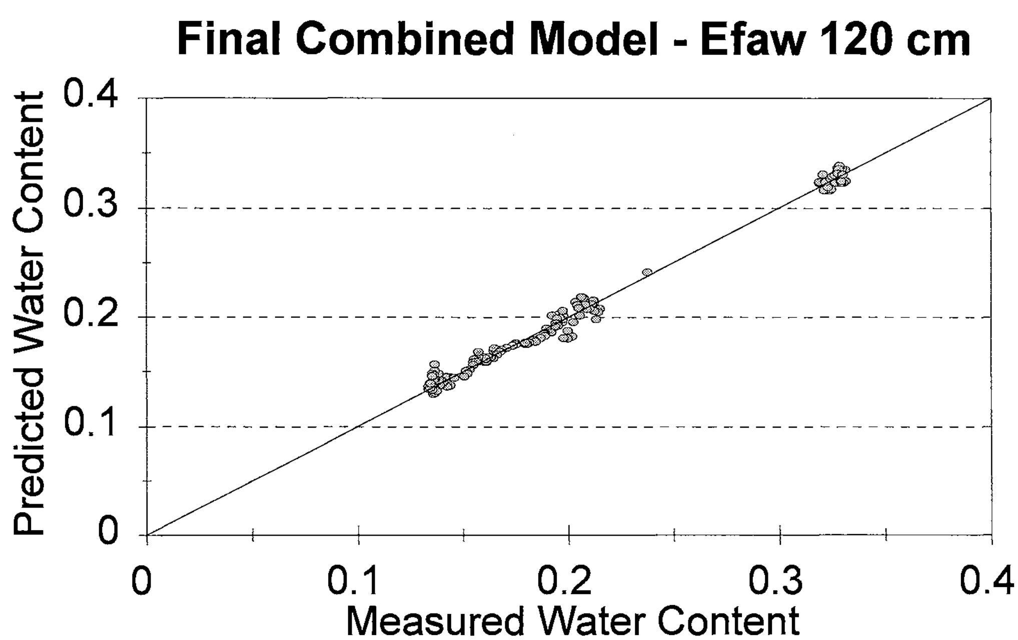

Figure 7.7. Measured and Predicted Test Results for Efaw (120 cm).

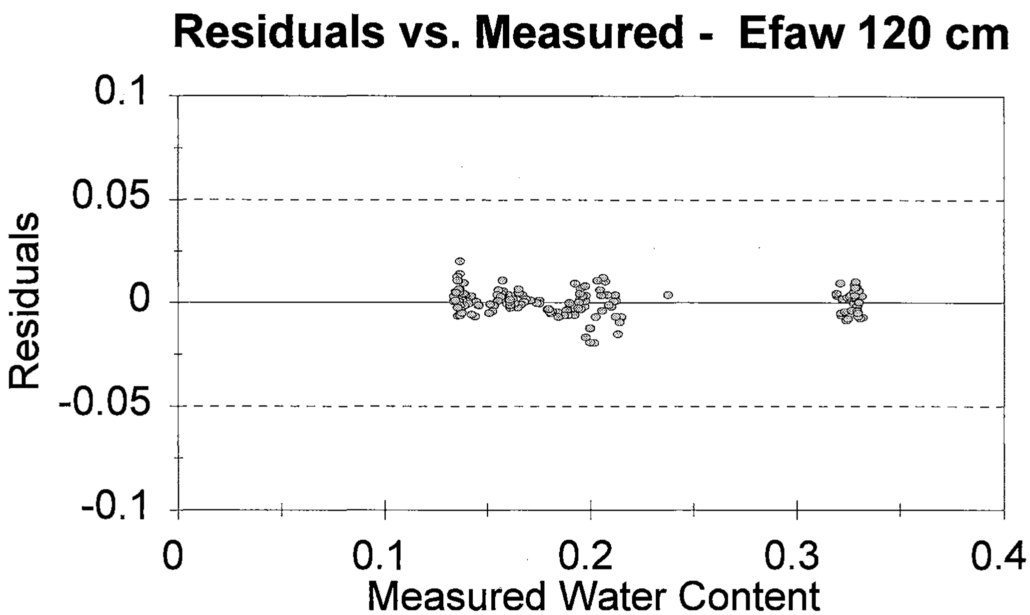

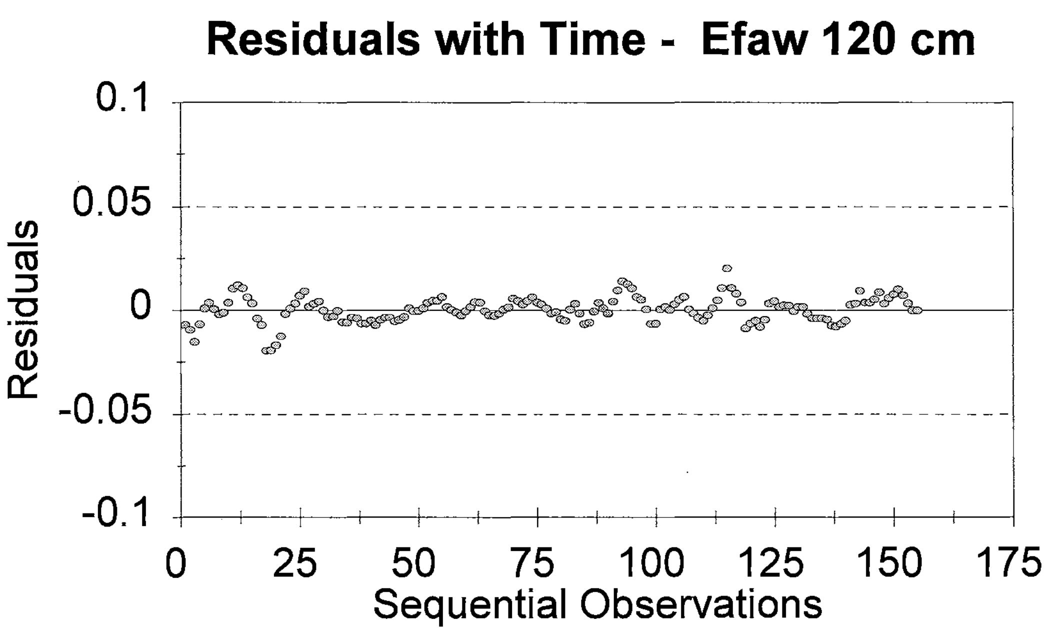

Figure 7.8. Residual Plots for Efaw (120 cm).

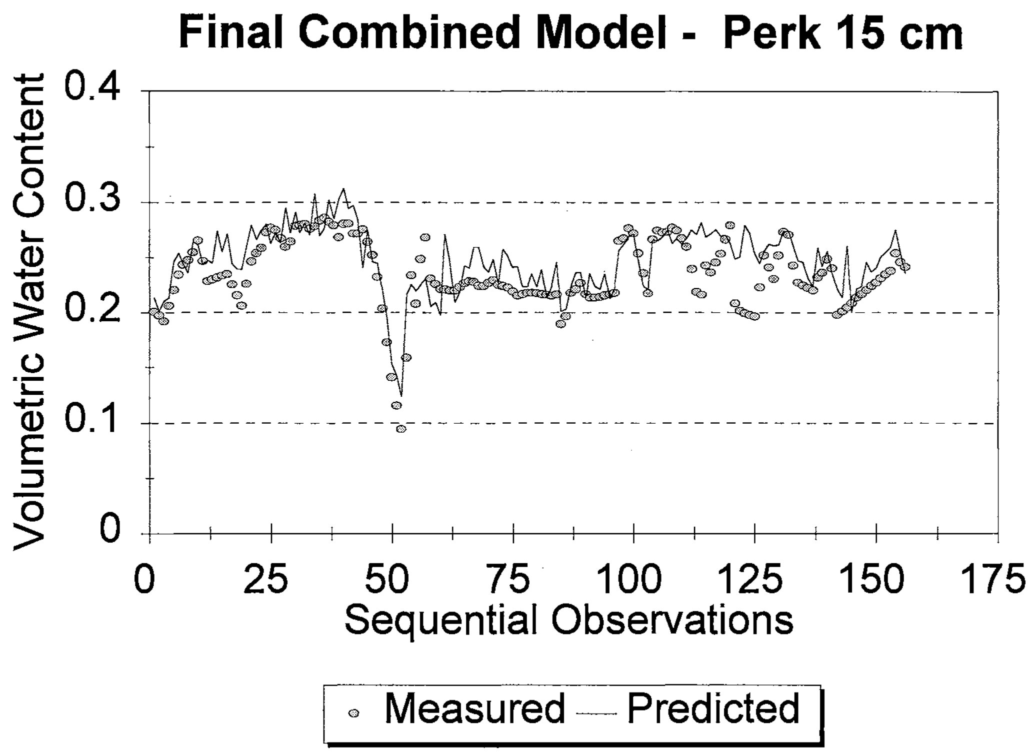

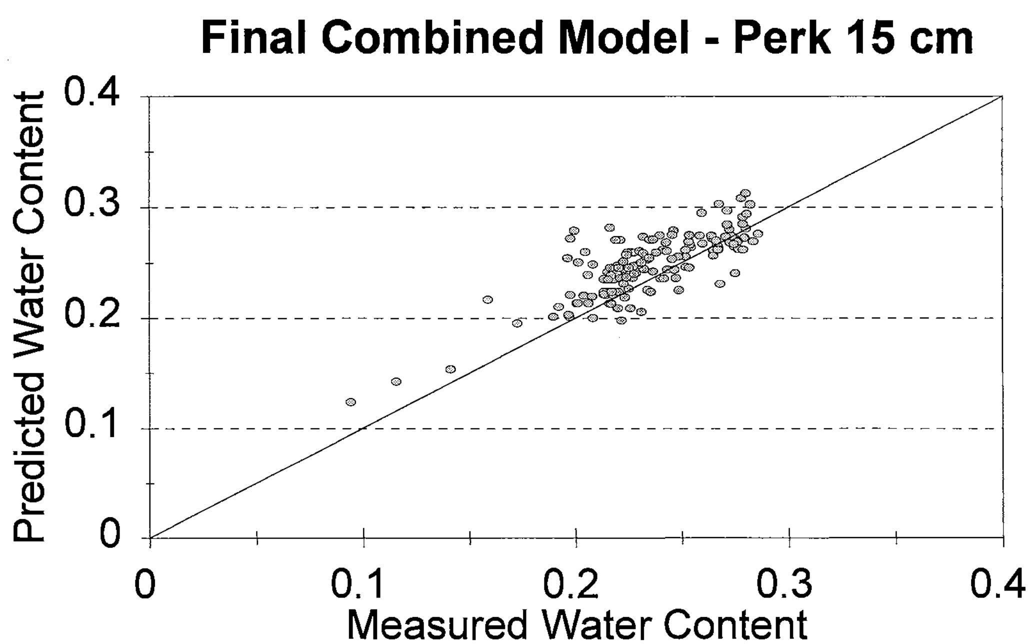

Figure 7.9. Measured and Predicted Test Results for Perkins (15 cm).

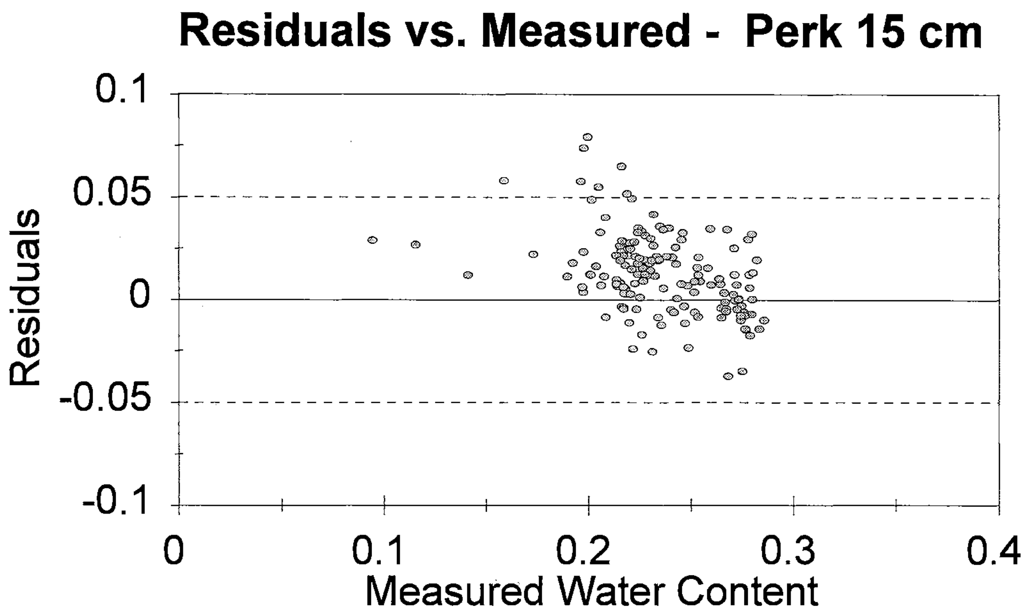

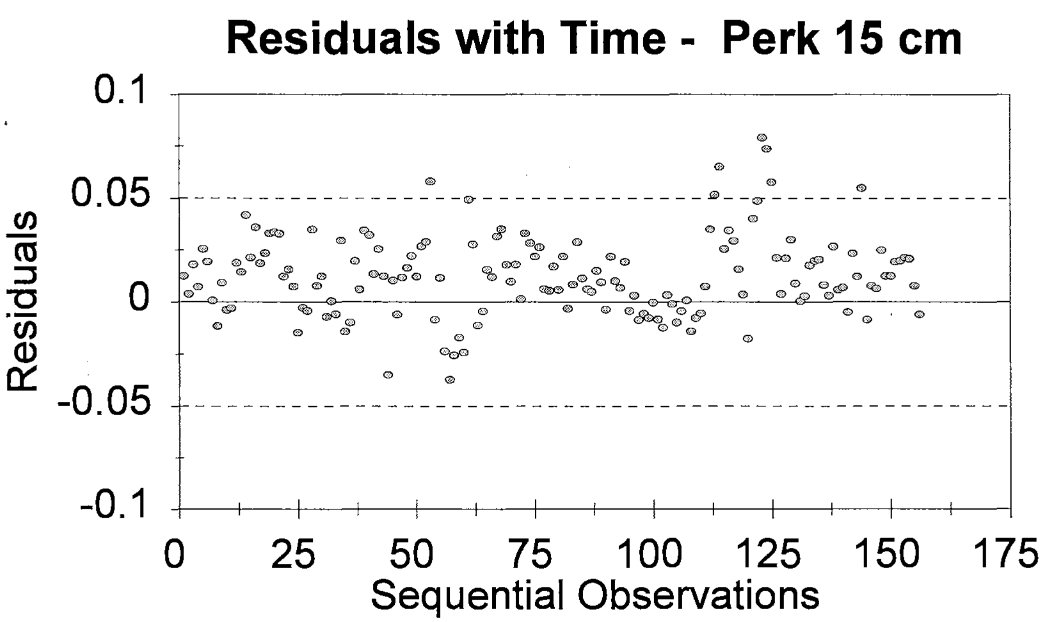

Figure 7.10. Residual Plots for Perkins (15 cm).

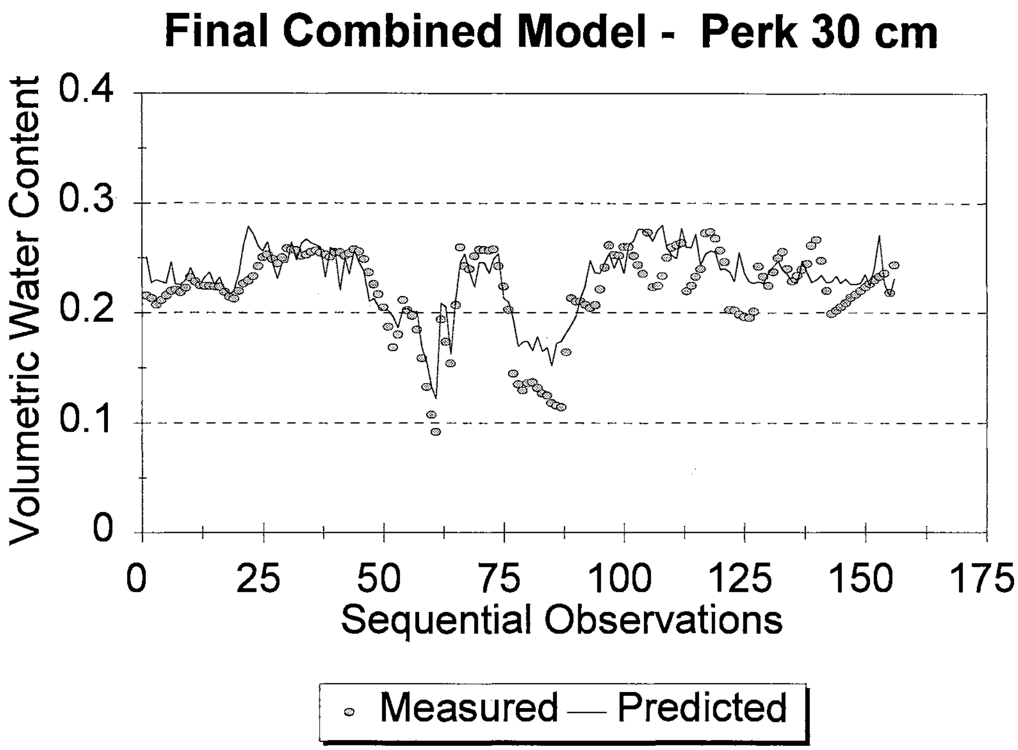

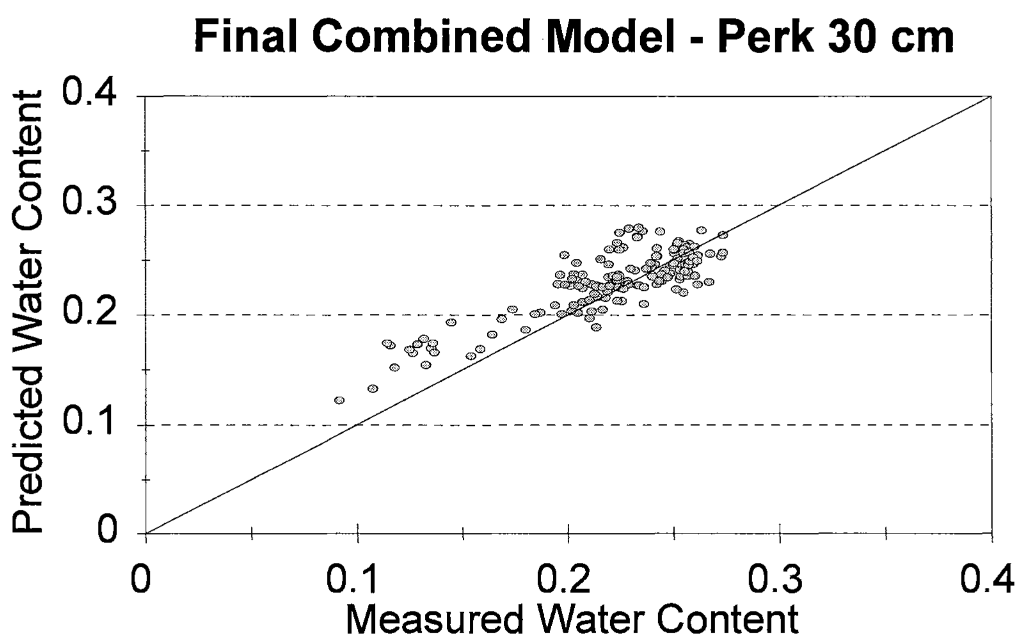

Figure 7.11. Measured and Predicted Test Results for Perkins (30 cm).

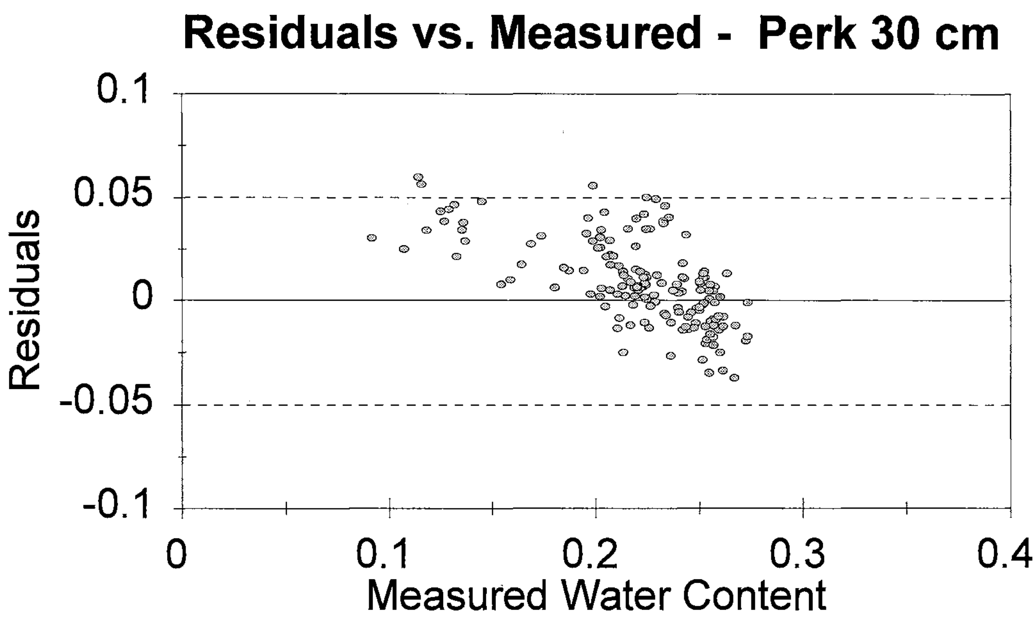

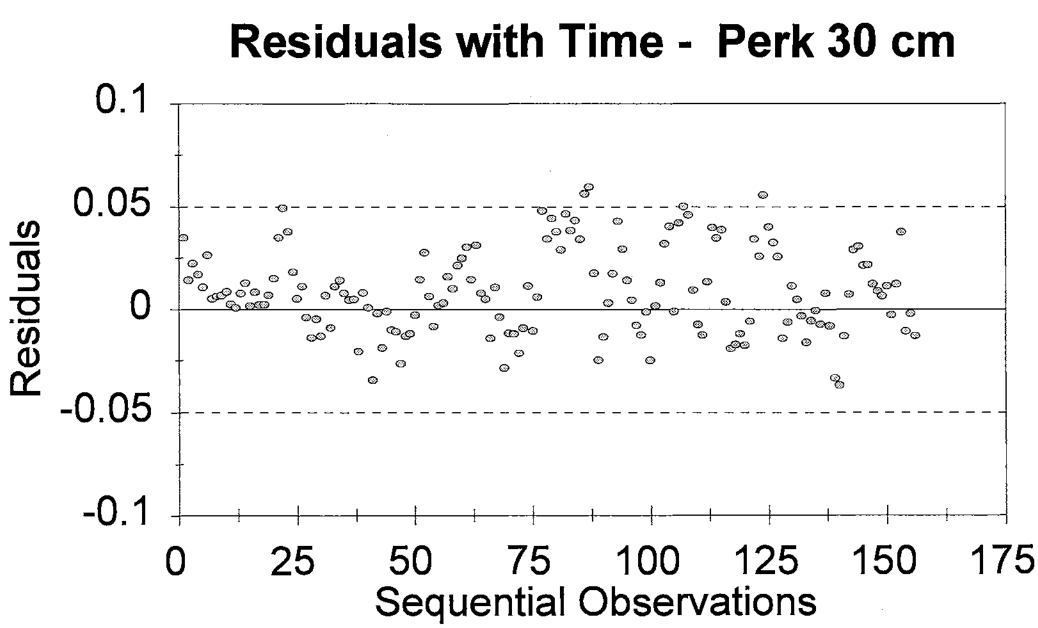

Figure 7.12. Residual Plots for Perkins (30 cm).

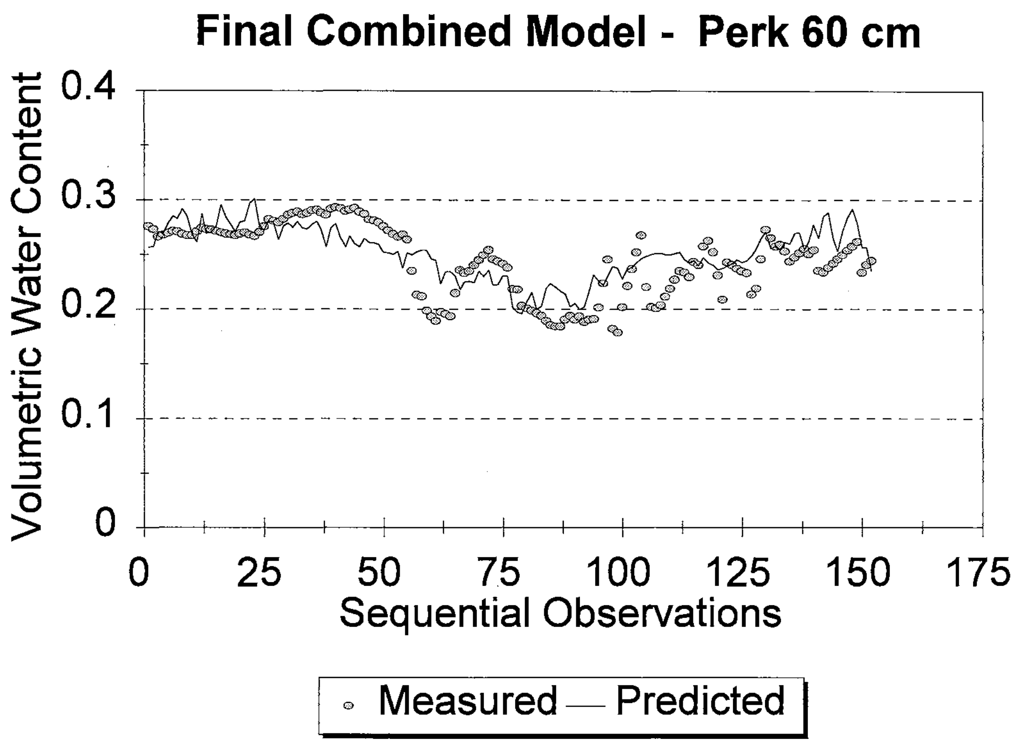

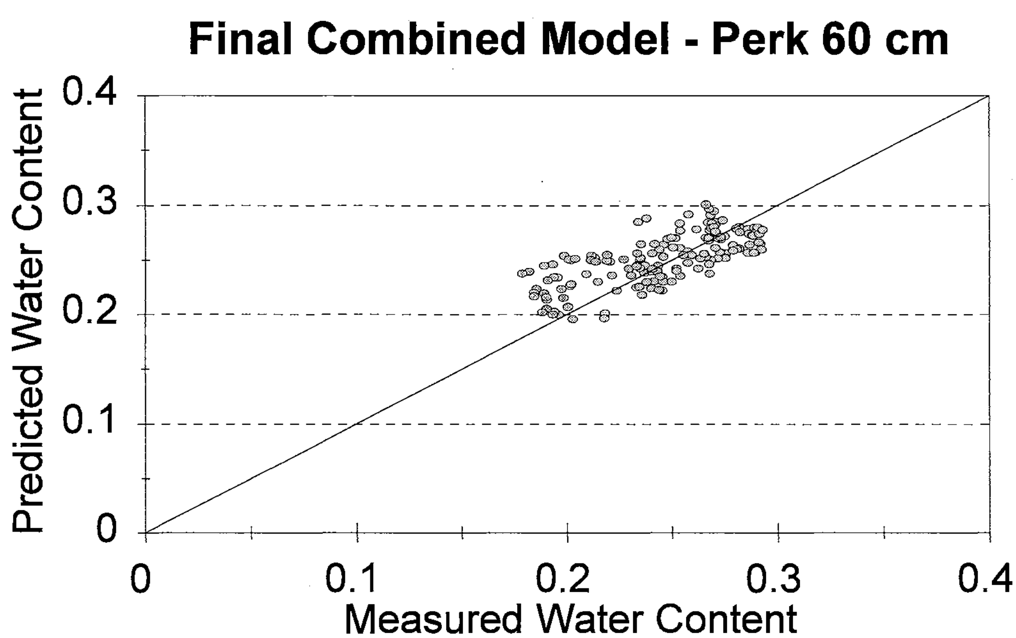

Figure 7.13. Measured and Predicted Test Results for Perkins (60 cm).

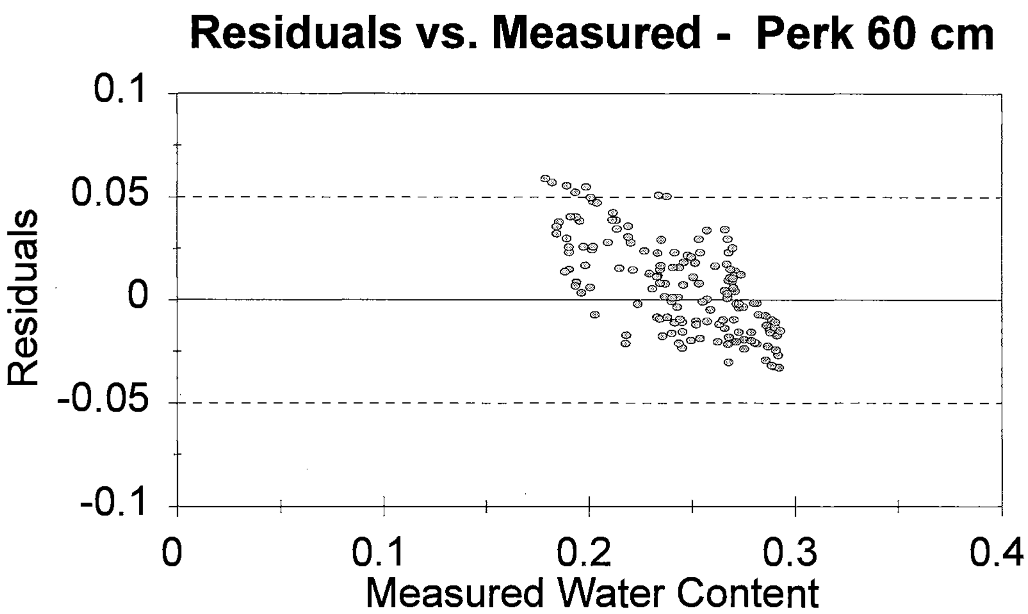

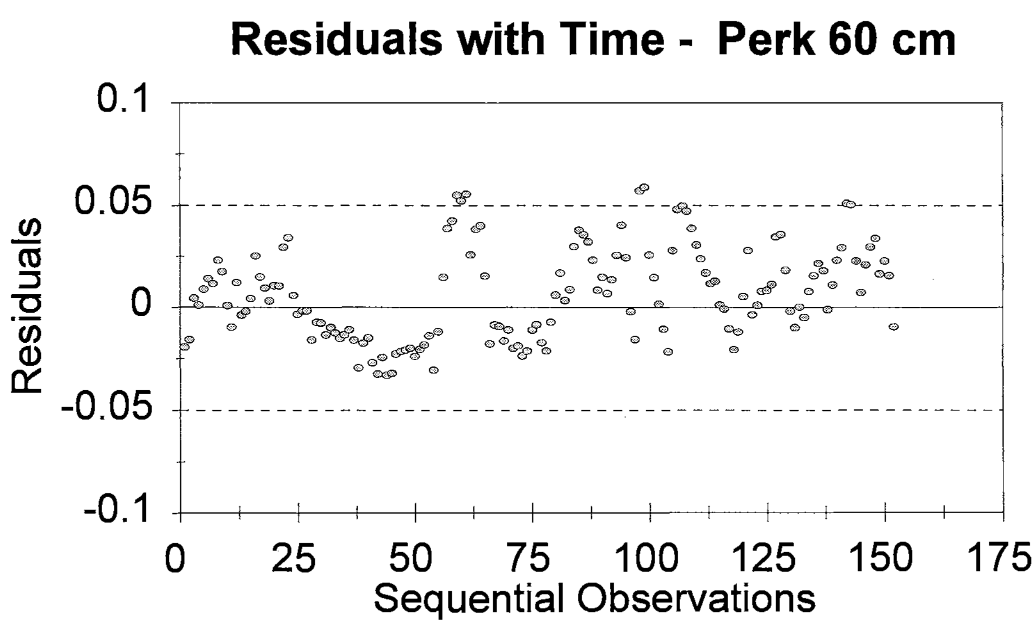

Figure 7.14. Residual Plots for Perkins (60 cm).

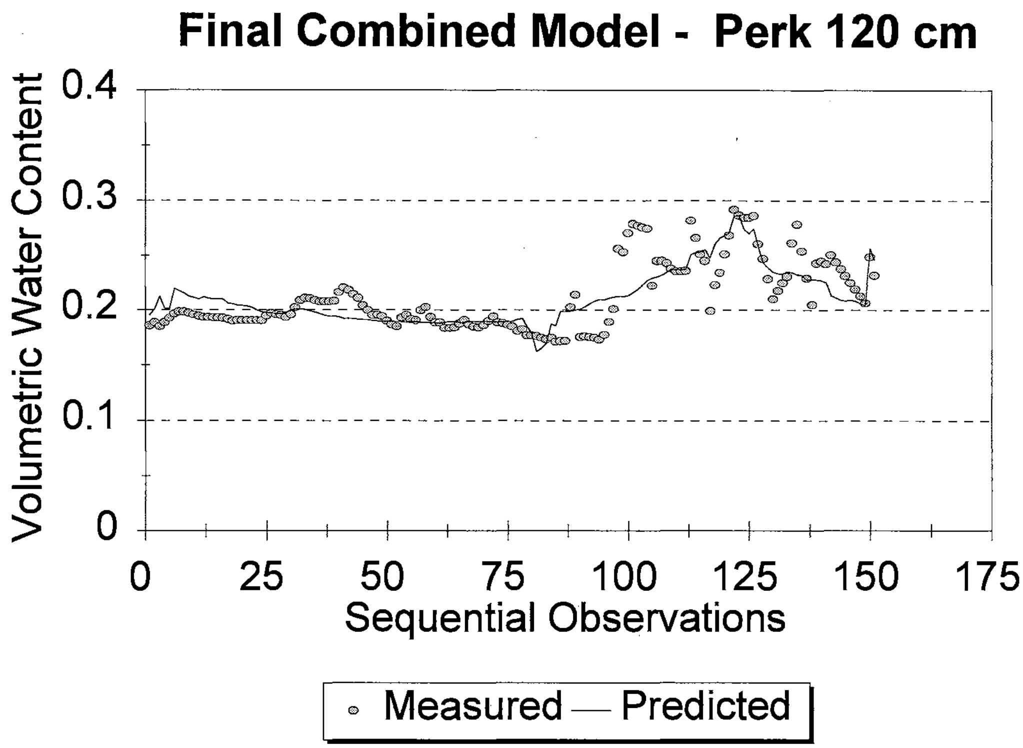

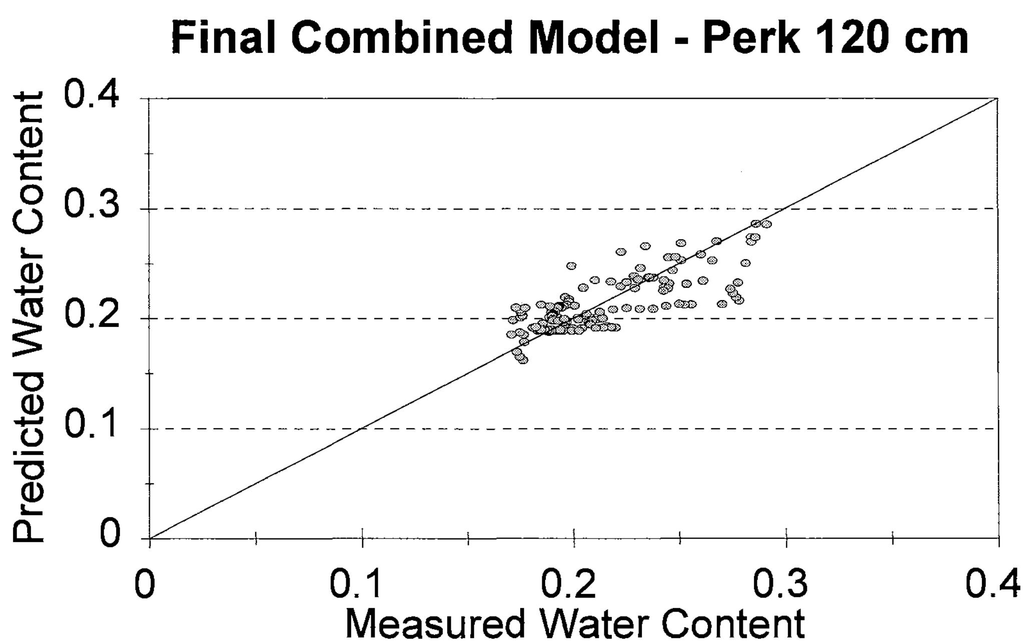

Figure 7.15. Measured and Predicted Test Results for Perkins (120 cm).

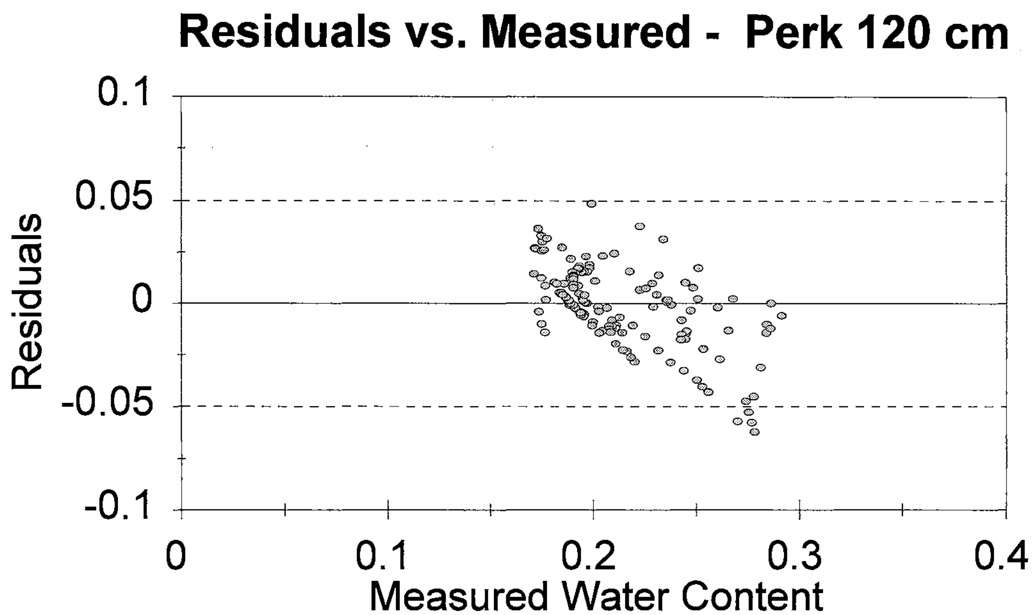

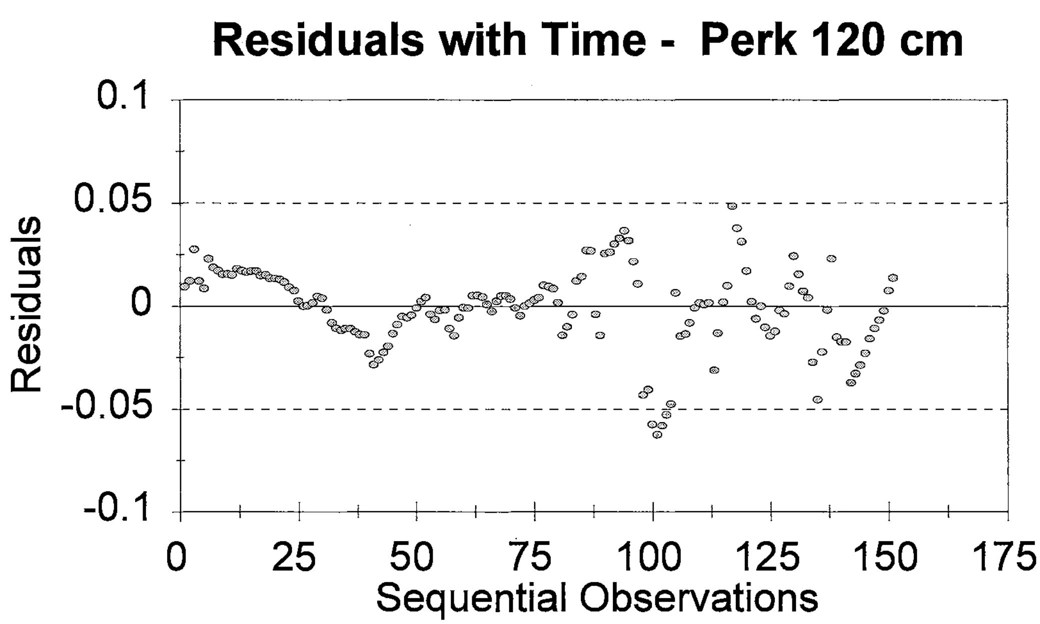

Figure 7.16. Residual Plots for Perkins (120 cm).

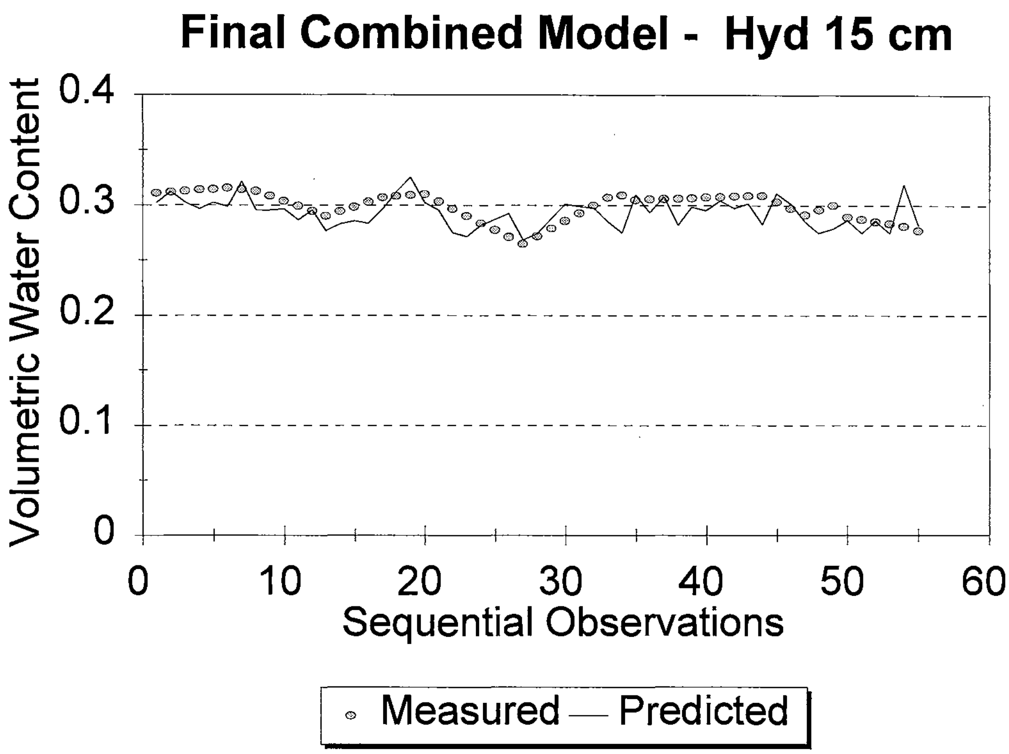

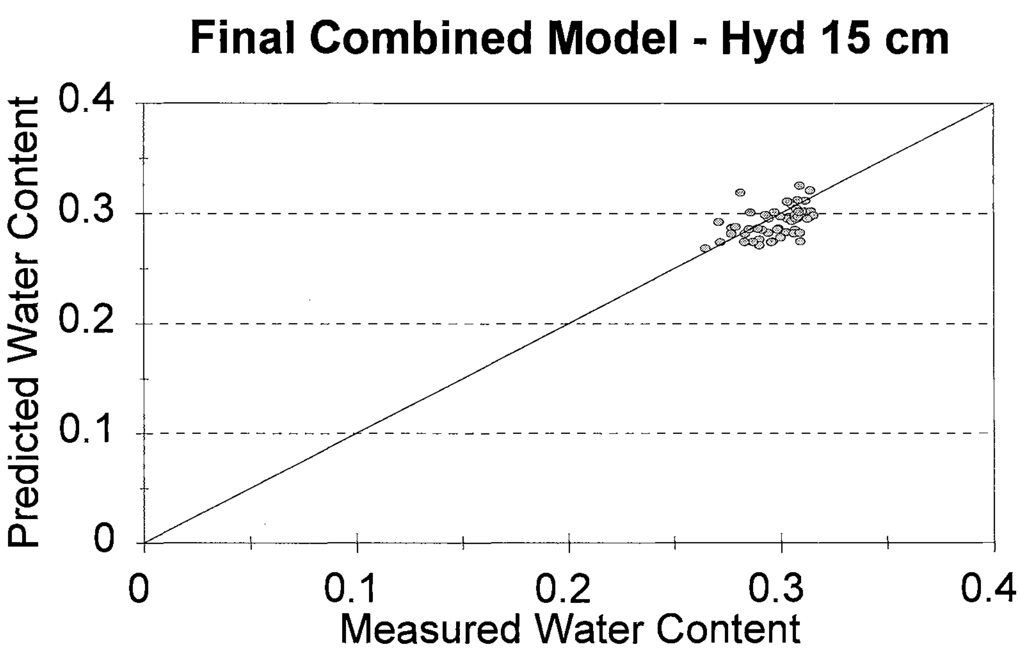

Figure 7.17. Measured and Predicted Test Results for Hyd (15 cm).

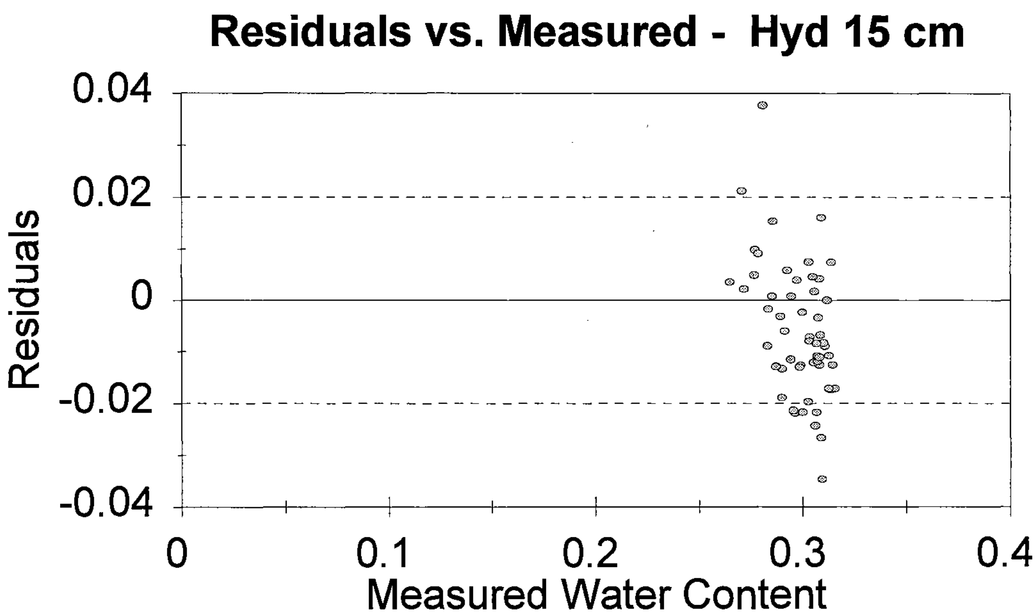

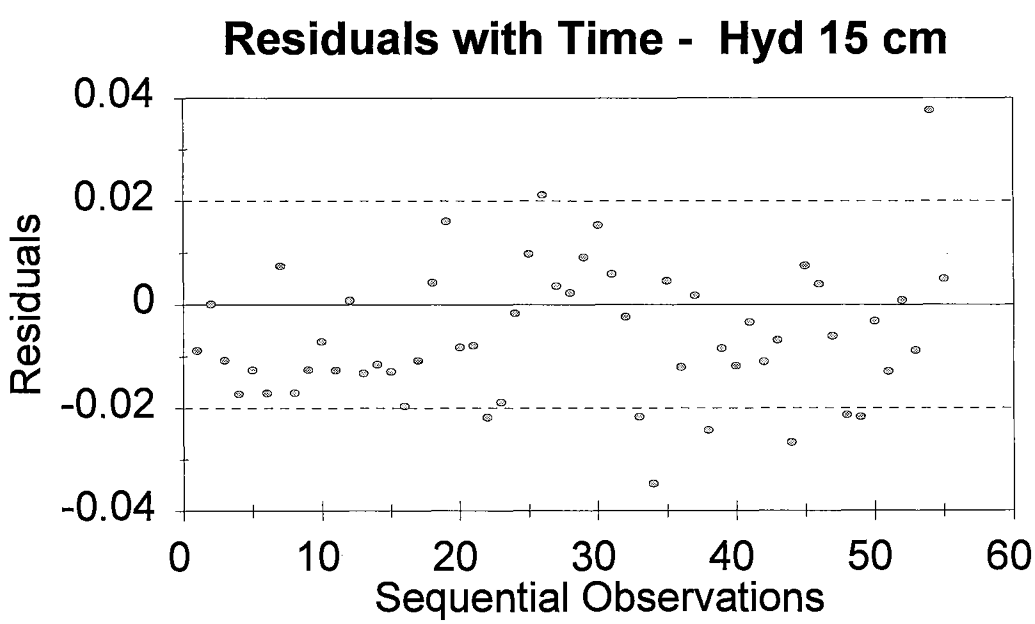

Figure 7.18. Residual Plots for Hyd (15 cm).

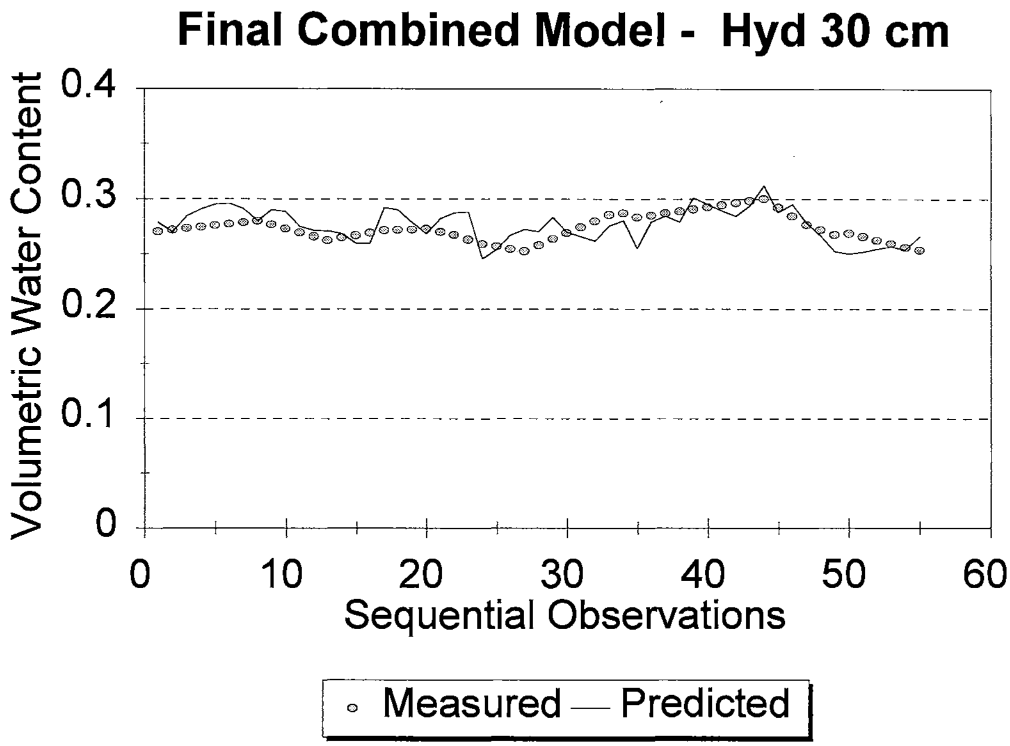

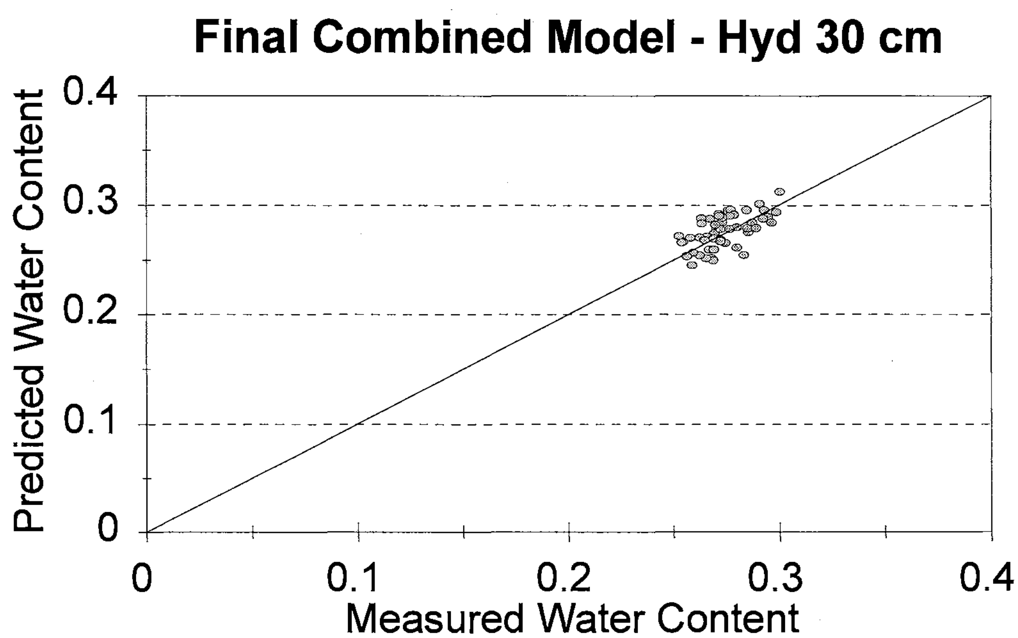

Figure 7.19. Measured and Predicted Test Results for Hyd (30 cm).

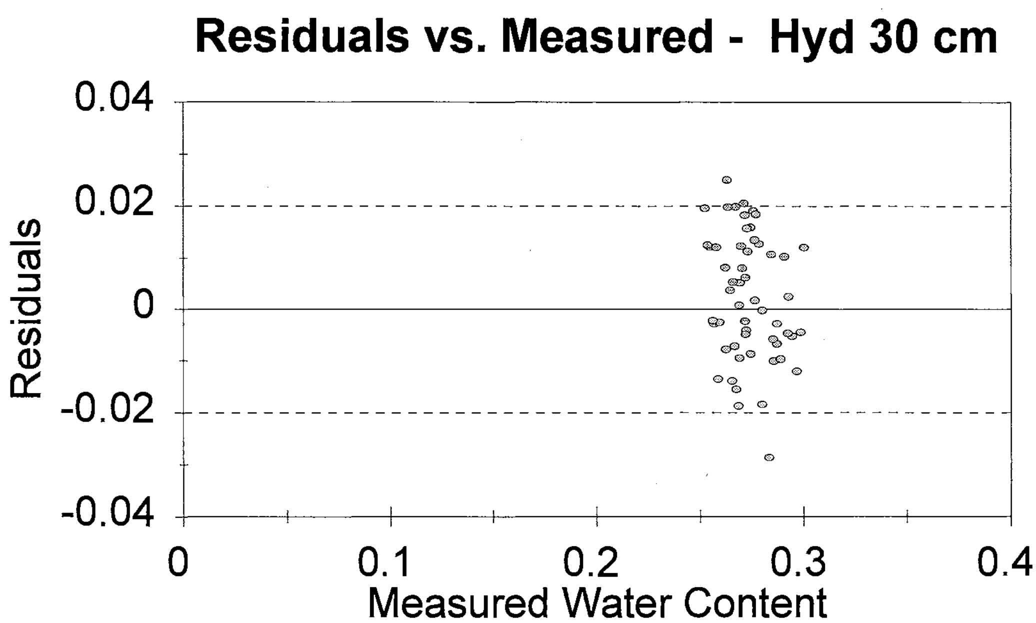

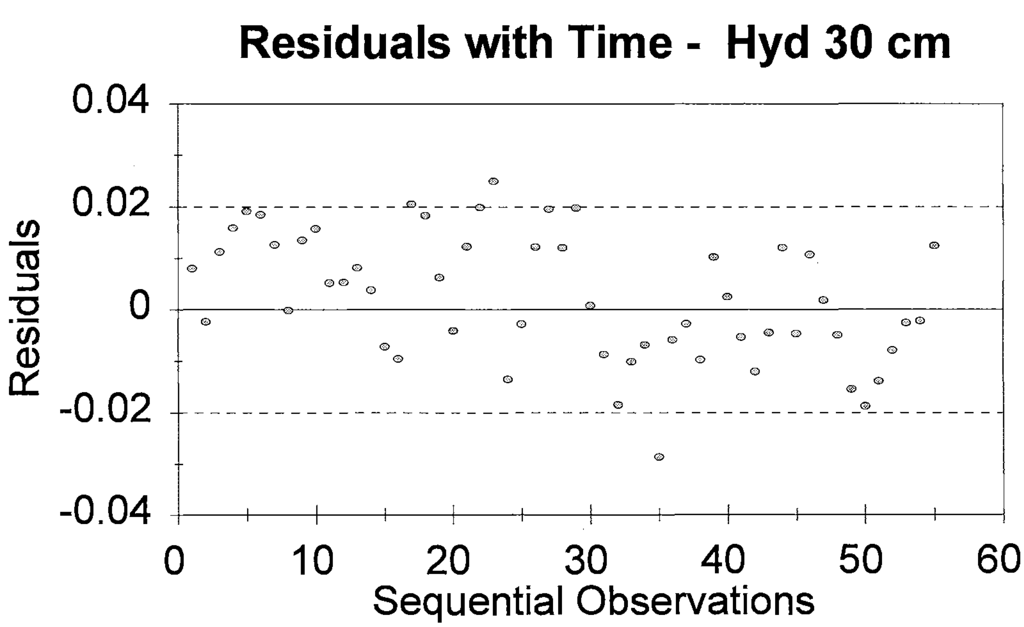

Figure 7.20. Residual Plots for Hyd (30 cm).

For the predicted versus measured plots, the data points closely grouped along the equality line but it can be seen that the span of the moisture contents is limited. The residual plots for both depths show that the lower water contents were overpredicted and the higher water contents were underpredicted. The residuals with time plots appear to be scattered randomly about zero, which is desired.

General

The overall performance of the neural network model was good. All of the general trends in the soil water content for the various locations were predicted well. The statistical results can be seen in Table 7.2.

The largest root mean square error is 0.0234 for all locations and depths. It can be seen that the RMSE values and the standard deviation of the errors are extremely close in value. This occurs when the mean of the errors is close to zero. The RMSE values are a comparison of the predicted to the measured values while the standard deviation of the error is a comparison of the residuals with the mean of the residuals. The correlation coefficient values are the best (closest to 1.0) for the Efaw data and the worst for the Hyd data. This can be partially explained by the fact that there is very little variation in the measured Hyd data, meaning that absolute errors have to be very small to achieve a high r^2.

Frequency distributions of the error for the various sites can be seen in Figures 7.21 - 7.25. For the most part, these plots tend to approach a normal distribution. Table 7.3 gives the percent of time which the neural network could predict within an error less than 3%, 2%, and 1% volumetric moisture content.

	15 cm	30 cm	60 cm	120 cm
EFAW				
RMSE	.0233	.0212	.0143	.0061
r^2	.778	.775	.779	.993
Std.Dev.(Error)	.0231	.0195	.0142	.0061
Mean Error	.0029	.0084	.0013	.0004
PERKINS				
RMSE	.0231	.0226	.0234	.0194
r^2	.632	.719	.519	.613
Std.Dev.(Error)	.0193	.0206	.0223	.0194
Mean Error	.0127	.0092	.0069	-.0008
HYD				
RMSE	.0143	.0125	NA	NA
r^2	.452	.481	NA	NA
Std.Dev.(Error)	.0130	.0122	NA	NA
Mean Error	-.0058	.0024	NA	NA

Figure 7.2. Statistics of Neural Network Results.

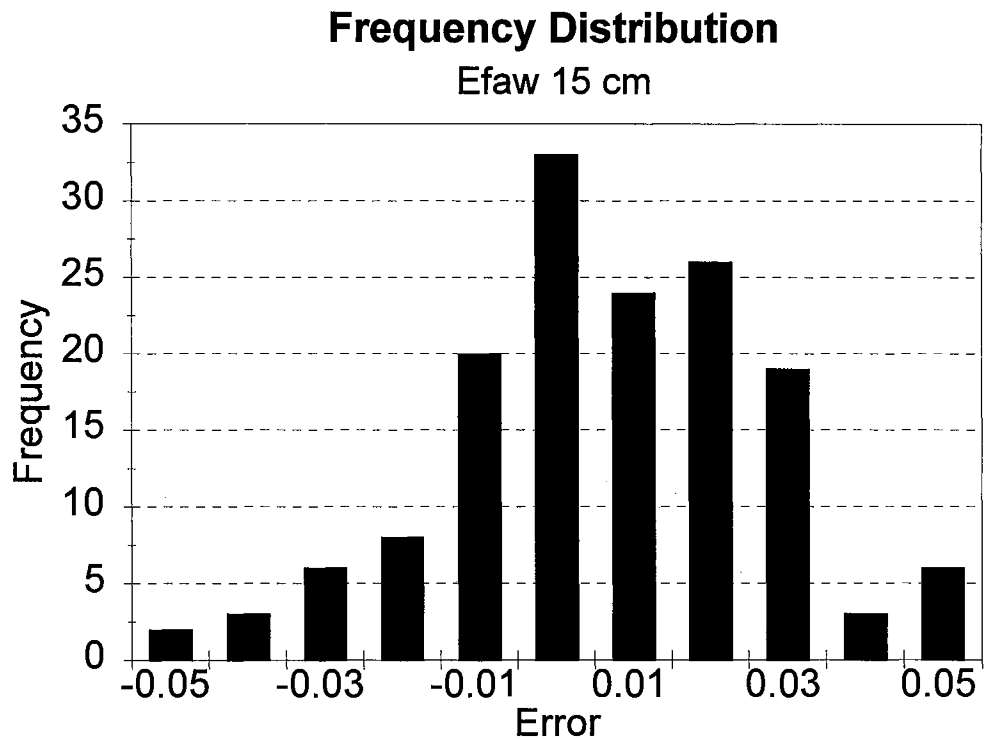

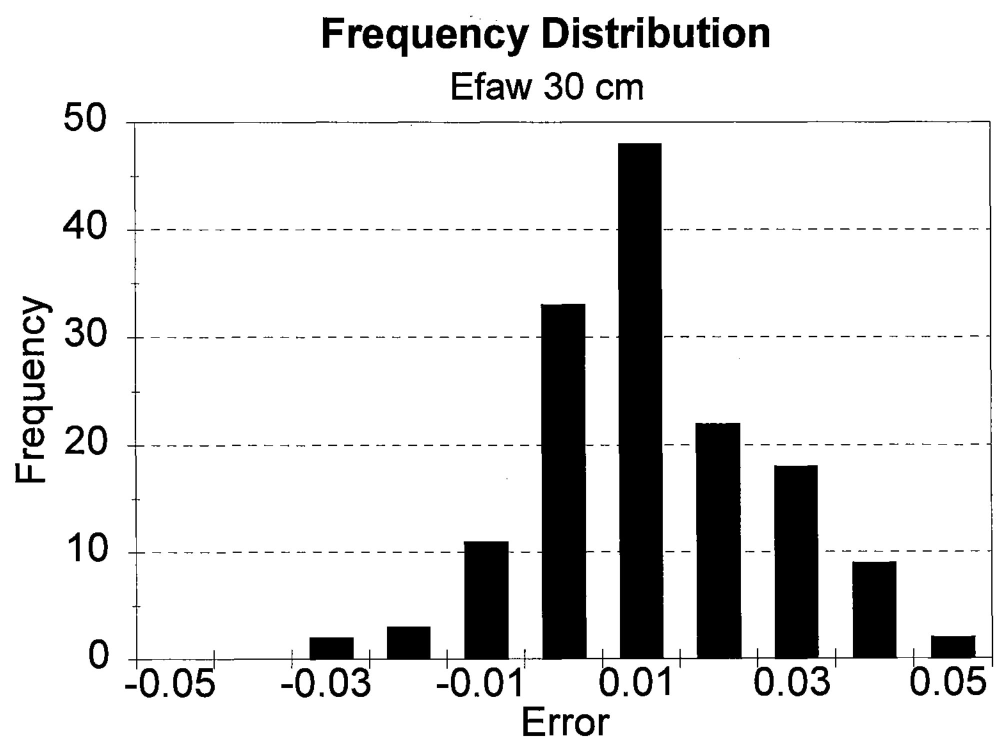

Figure 7.21. Frequency Distribution of Error for Efaw at 15 and 30 cm.

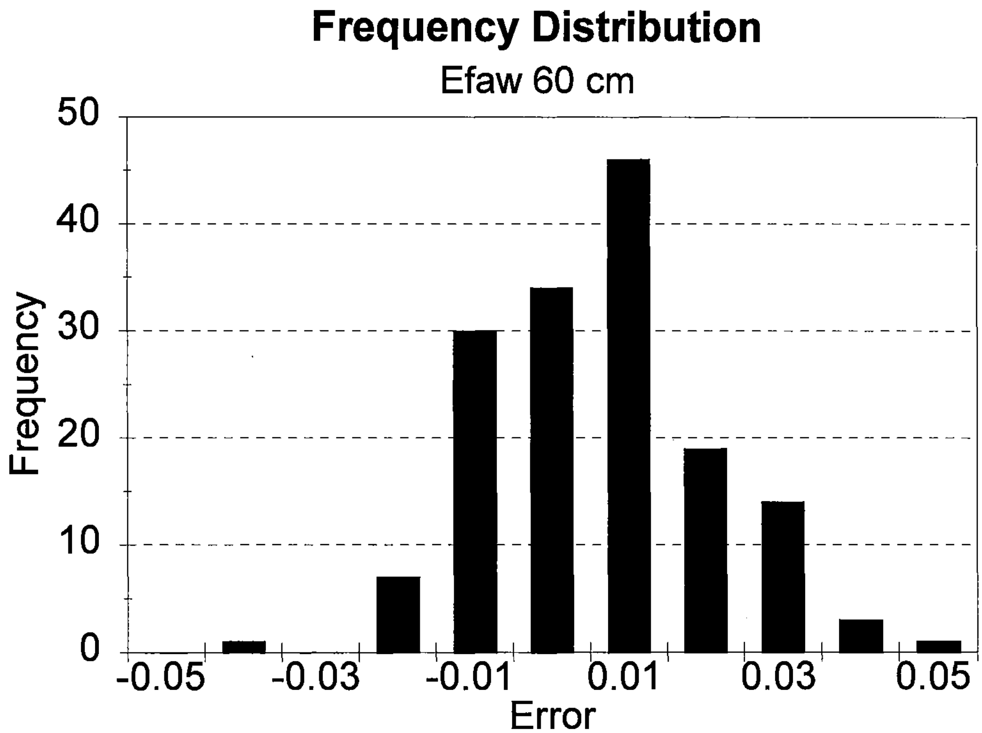

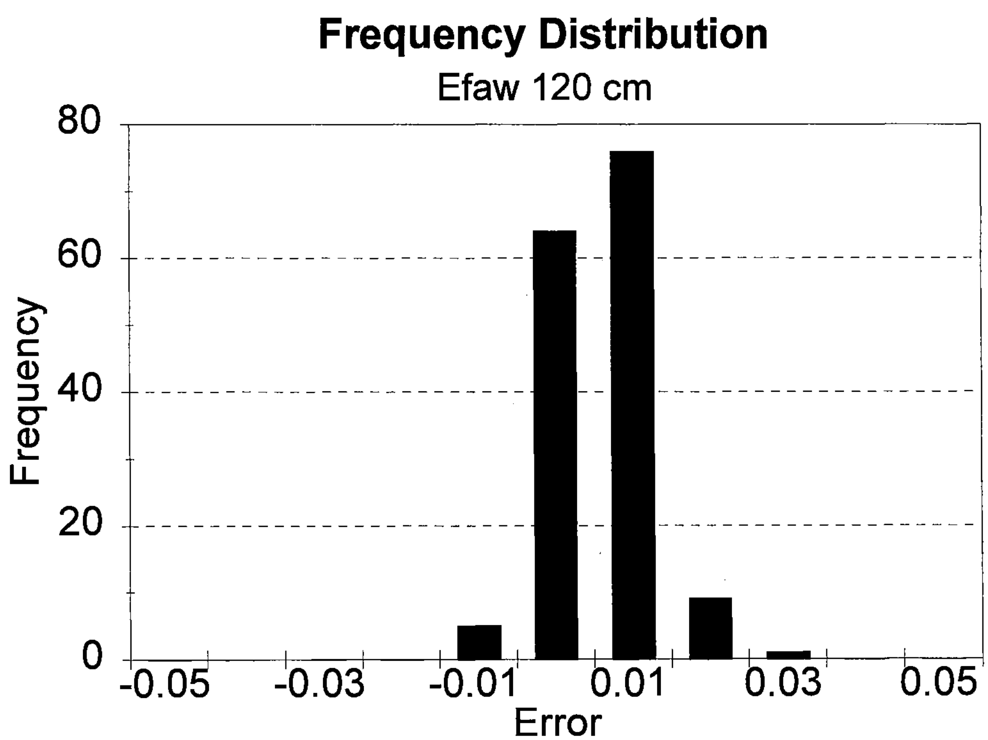

Figure 7.22. Frequency Distribution of Error for Efaw at 60 and 120 cm.

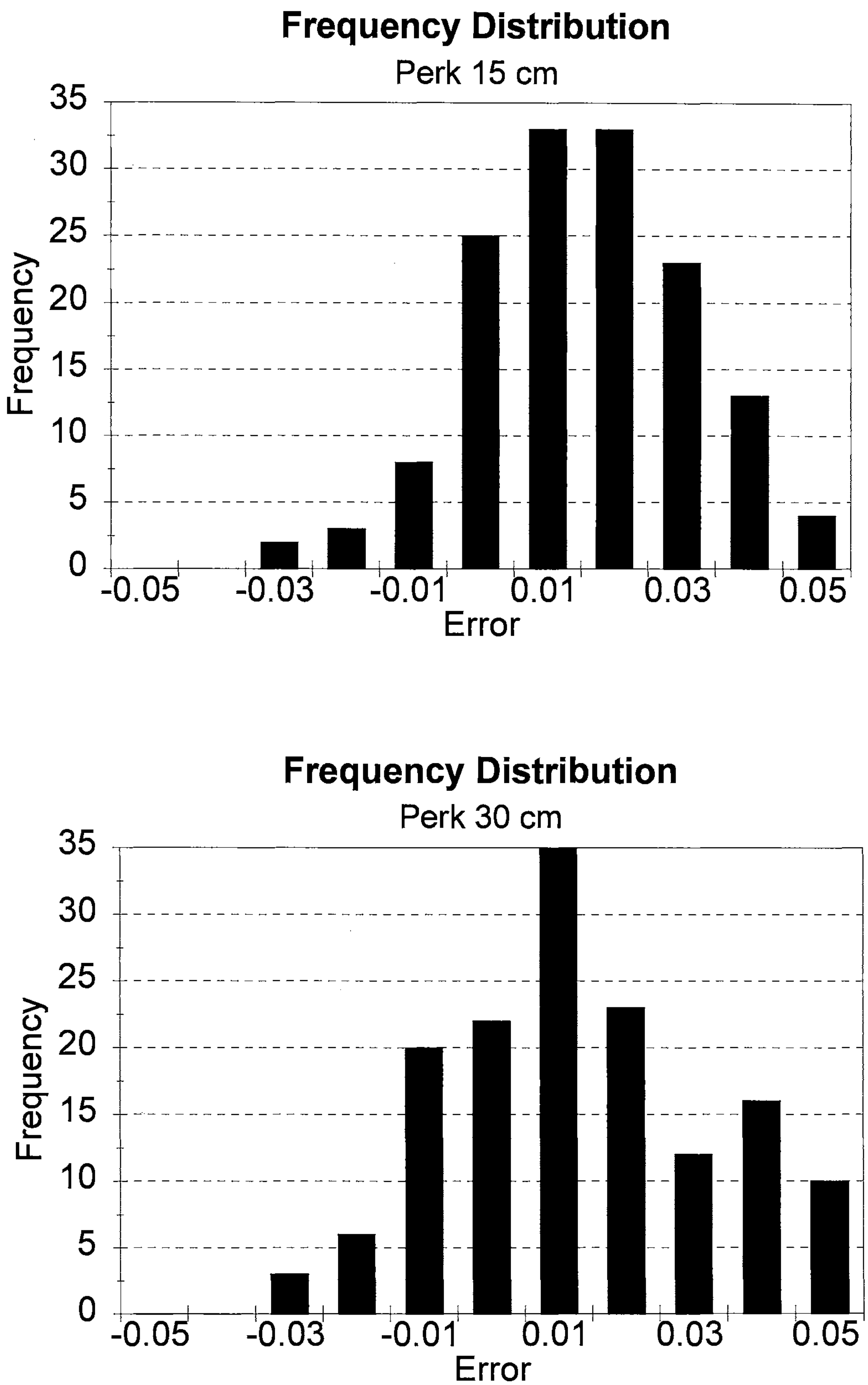

Figure 7.23. Frequency Distribution of Error for Perkins at 15 and 30 cm.

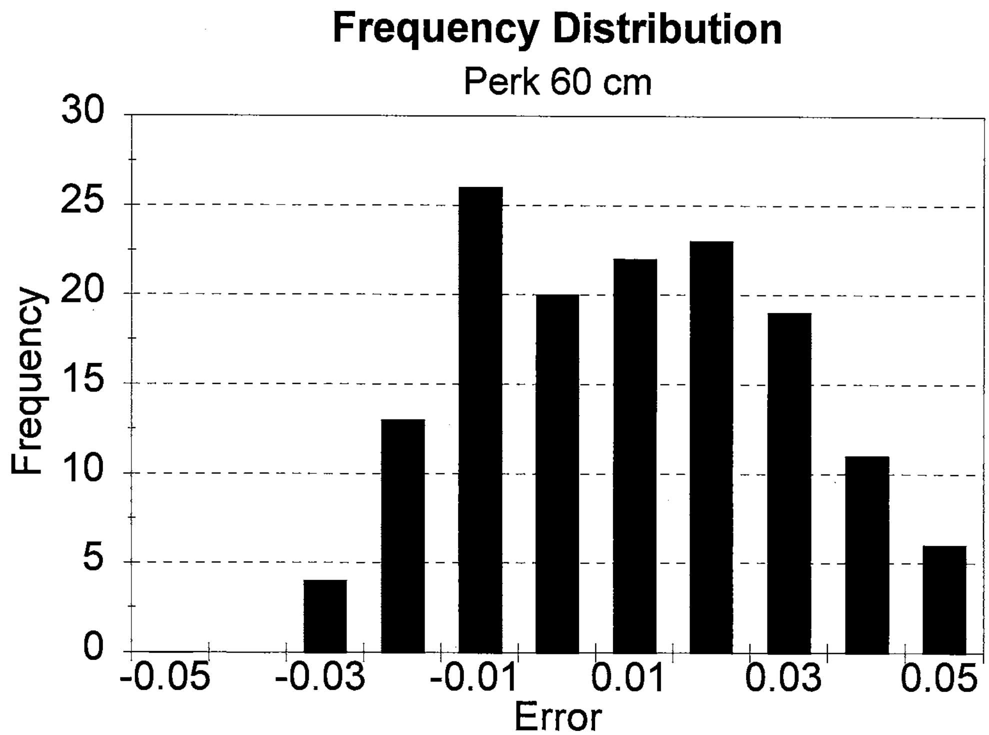

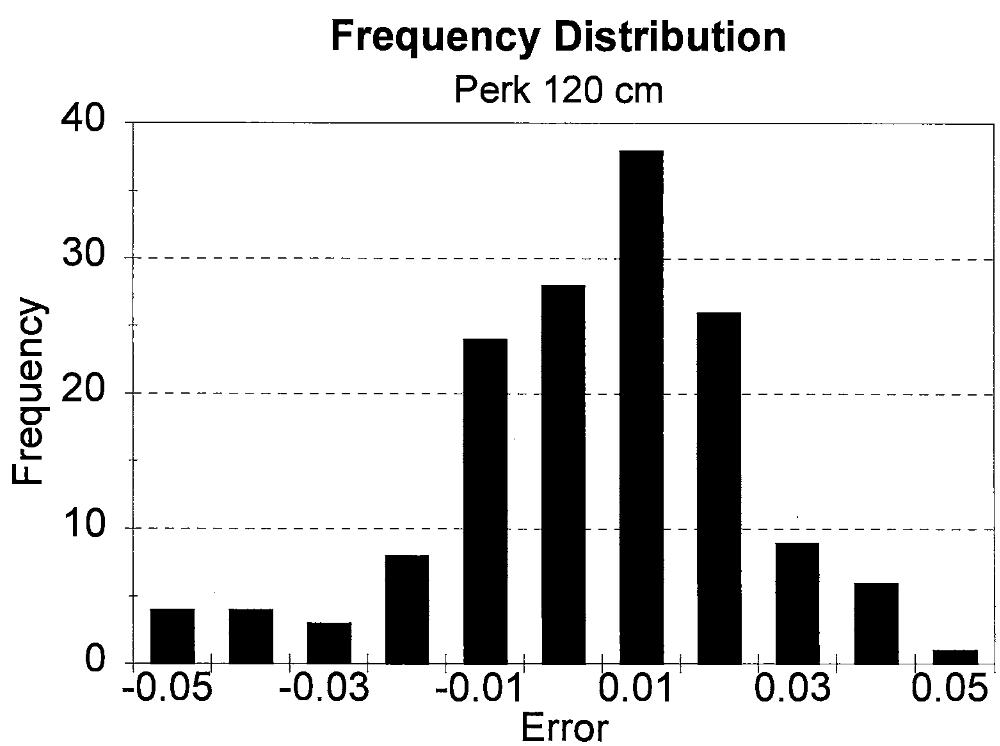

Figure 7.24. Frequency Distribution of Error for Perkins at 60 and 120 cm.

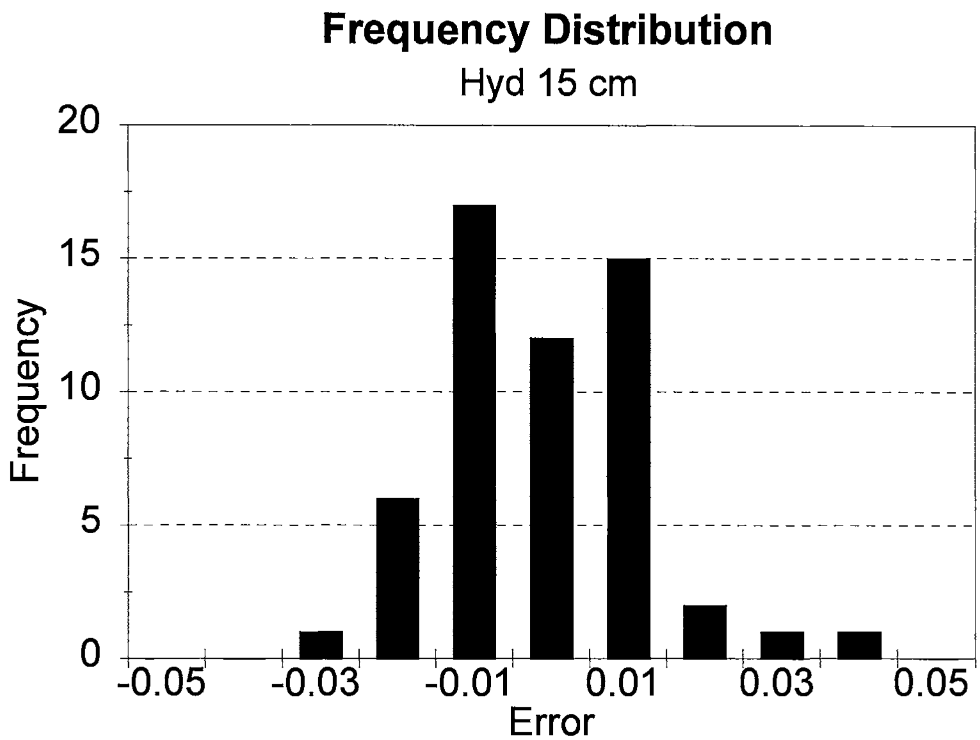

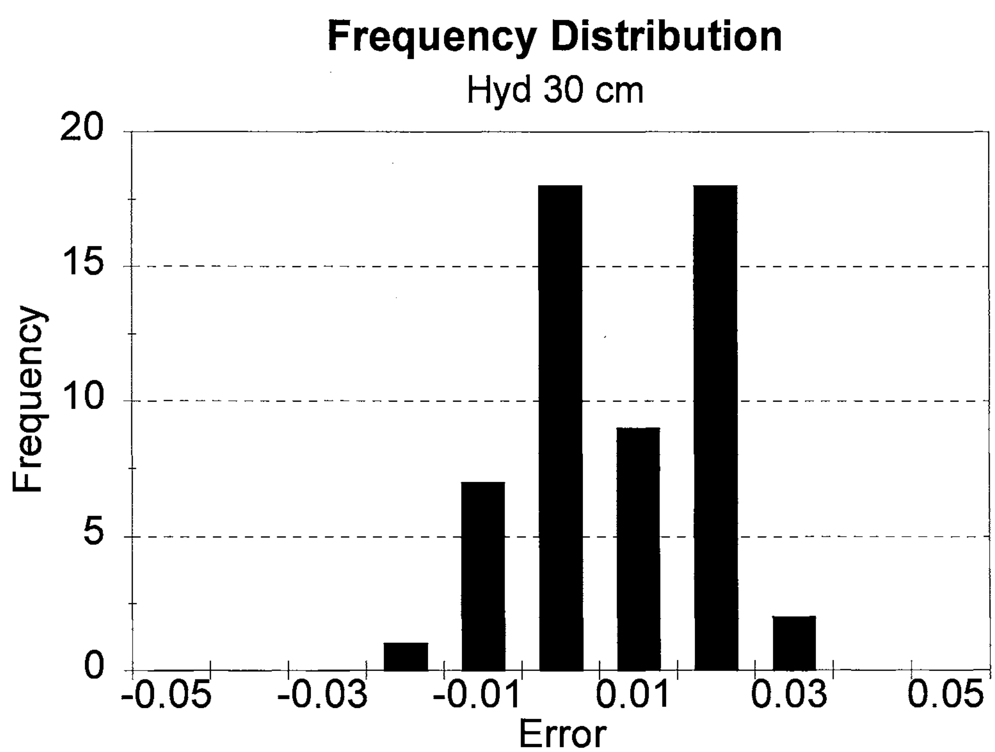

Figure 7.25. Frequency Distribution of Error for Hyd at 15 and 30 cm.

Location and Depth	< 3% Error	< 2% Error	< 1% Error
EFAW			
15 cm	84%	66%	37%
30 cm	87%	74%	54%
60 cm	97%	84%	90%
120 cm	100%	99%	90%
PERKINS			
15 cm	83%	66%	39%
30 cm	76%	67%	39%
60 cm	82%	61%	29%
120 cm	88%	77%	44%
HYD			
15 cm	96%	84%	49%
30 cm	100%	95%	49%

Table 7.3. Network Prediction Capabilities for Various Error Values.

When observing the residual versus time plots, there seem to be cyclic patterns in the residuals. Therefore, a spectral analysis using a Fourier transform was performed. SYSTAT was used to accomplish this task. Periodograms were graphed which are plots of the square of magnitude versus frequency. By analyzing these plots, it can be determined if there is a cycle or cycles (primary peaks in the plot) and the frequency at which that cycle is occurring. This testing procedure was performed on all threes sites for all the depths. The periodograms for the residuals showed that for some depths there appeared to be cyclic activity but there was no consistency through the depths for the specific locations. Other plots showed that there may be several cycles occurring, but once again, nothing which could be carried through the various depths.

After reviewing these residual Fourier plots, it was questioned whether the neural network model was somehow producing cyclic type predictions, causing the residuals to look cyclic. To answer this question, the Fourier analysis was performed on the measured soil water data to determine if it was cyclic or not. Once again, these tests proved inconclusive since for a few depths and locations there seemed to be some periodic behavior while at other depths it was random. Since soil water content is based on many interactions, most of which are unpredictable and random, it was concluded from this series of tests that the soil water content measurements were non-cyclic except for the obvious rainfall wetting and drying curves which occur randomly. From this analysis, it was concluded that the neural network was not always able to model the extremes, resulting in cyclic patterns in the residuals. The results and plots of the Fourier analysis can be seen in Appendix G.

Repeatability of Measured Soil Water Content

Throughout this entire project, the measured soil water content values which were gathered using a neutron probe were considered to be "true" values which were used both for training and testing of the neural network model. When comparing predicted data to measured data, it must be kept in mind that the measured values are not actually the "true" values but values estimated by a neutron moisture gauge. The random error is an estimate of soil moisture using the neutron method arises from three components. The heterogeneity of soil water content distribution over the site under study is the major source and is termed the location component (Hewlett et al., 1964). The random error in the detector electronics and that associated with the random decay process in the fast neutron source contributes the instrument error which is usually small compared to the location error. The third component of random error is that associated with the calibration equation (Greacen, 1981).

The neutron probe used in this research is calibrated on a regular basis using the protocol developed by the Agronomy Department at Oklahoma State University. Initially, two neutron moisture gauges were field calibrated and taken back to the laboratory and used as "truth". Several barrels, each containing various compounds with different moisture contents, were measured with the field calibrated probes. Remaining neutron probes were then calibrated using the barrels and the values produced by the field calibrated units. These calibration procedures have been performed for approximately 10 years and each neutron probe is recalibrated yearly. Therefore, the error due to calibration is minimized (Stone, 1993).

If calibration errors are ignored, the variance of measured soil water is the sum of the variance due to the measuring error of the technique involved and the variance due to the innate variability of the soil itself. A test was performed to evaluate the technique and the repeatability of the particular neutron probe used in this research. Since this research has been ongoing for approximately two years, and several different individuals have collected neutron soil water readings, technique should be checked.

The testing procedure involved placing the neutron gauge on the access tube and taking a standard count (reading with the probe secured in the gauge body). The soil water content is calculated based on a ratio of a measured count to the standard count. For this reason, measurements made with the instrument can be no more accurate than the accuracy of the standard count (Troxler, Inc., 1983). Once the standard count was noted, a measured count at a depth of 30 cm was determined. The instrument was then turned off and removed from the access tube. This exact procedure was repeated 20 times at the same location and depth.

The results from the neutron probe test can be seen in Table 7.4. The soil water content values were calculated using the ratio of the measured count to the standard count and a calibration equation. The standard deviations for the standard count, measured count, ratio and soil water content are 5.25, 7.35, 0.0057, and 0.0032, respectively. This small value for the standard deviation of the soil water content indicates that when using the same neutron moisture gauge, the measured values are quite consistent. Therefore, the use of the neutron moisture gauge to collect soil water content values proved to be a reliable selection.

Multiple Variable Linear Regression Results

The test data sets which were used for the multiple variable linear regression were the same sets as used in the neural network predictions for Efaw and Perkins except rather than using the three individual probe temperatures, the temperatures were averaged as with the training data. The testing sets corresponded to the individual temperatures, change in temperature with time, and change in temperature with depth, as discussed previously. The same soil temperature depths were used which resulted in predictions at 15 and 30 cm. A predicted value of soil water content was calculated using this test temperature data and the multivariable linear equations determined in Chapter 6. The

	Standard Count	Measured Count	Ratio	θ
	1354	546	.4032	.2115
	1349	544	.4033	.2115
	1345	554	.4119	.2163
	1342	557	.4151	.2181
	1347	549	.4076	.2139
	1344	542	.4033	.2115
	1352	557	.4120	.2164
	1346	545	.4049	.2124
	1350	540	.4000	.2096
	1358	566	.4168	.2191
	1361	542	.3982	.2086
	1353	553	.4087	.2145
	1360	538	.3956	.2071
	1353	546	.4035	.2116
	1351	552	.4086	.2145
	1350	549	.4067	.2134
	1348	555	.4117	.2162
	1352	538	.3979	.2085
	1349	546	.4047	.2123
	1358	555	.4087	.2145
Average	1351	549	.4061	.2131
Std. Dev.	5.25	7.35	.0057	.0032

Table 7.4. Neutron Moisture Gauge Readings.

predicted values were then compared to the measured values and a simple regression analysis was performed. Plots of predicted and measured values for the 15 cm depth can be seen in Figures 7.26 through 7.31 for Efaw and Perkins for each of the three scenarios. The plots for the 30 cm depth are very similar to those for the 15 cm depth. It appears that the measured and predicted values did not correlate very well. All of the plots show that the linear regression model tends to predict the average and does not follow the measured data well at all. The predicted versus measured plots are basically a horizontal line which indicates that the model is predicting nearly a constant value regardless of the measured moisture content. The correlation coefficients can be seen in the following table:

	15 cm Depth		30 cm Depth	
	r^2 Efaw	r^2 Perkins	r^2 Efaw	r^2 Perkins
8 Indiv. Temps	.034	.038	.021	.107
ΔT with Time	.025	.027	.135	.009
ΔT with Depth	.068	.018	.039	.001

Table 7.5. Correlation Coefficients of Multivariate Linear Regression.

The correlation values are extremely low stating that the linear regression model is not predicting the measured water contents at all. This linear regression test proves that the neural network model was much more capable at estimating the soil water content values. The neural network was able to use the input temperature data and process a relationship which predicted soil water content accurately.

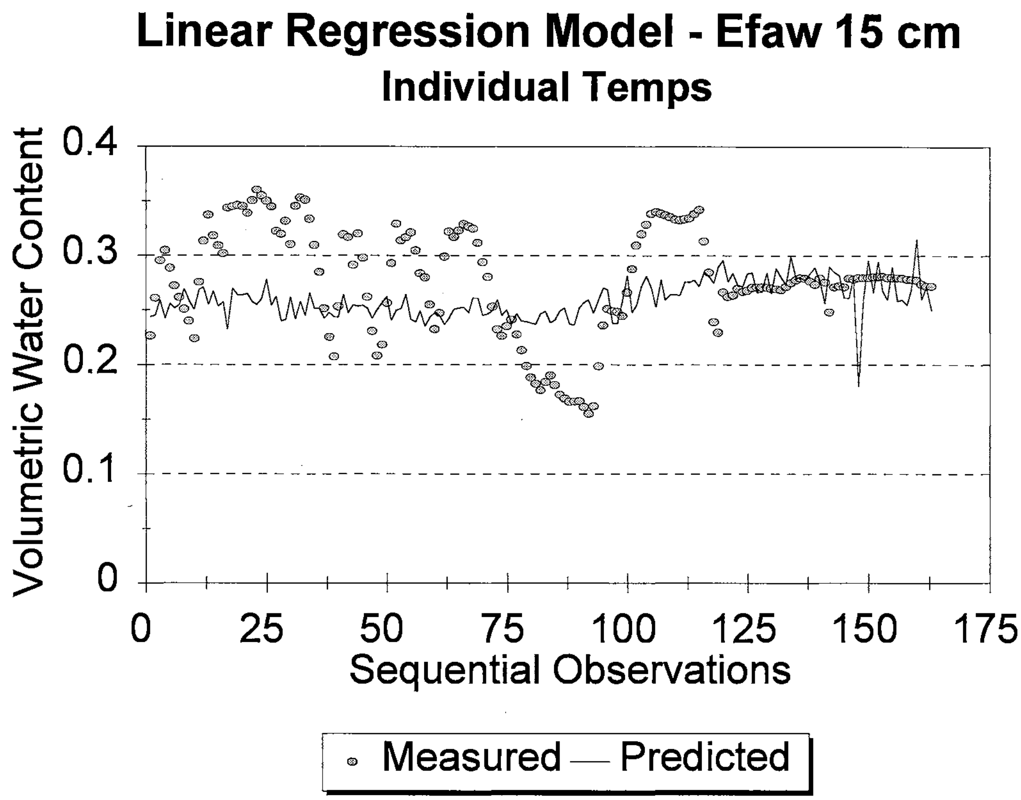

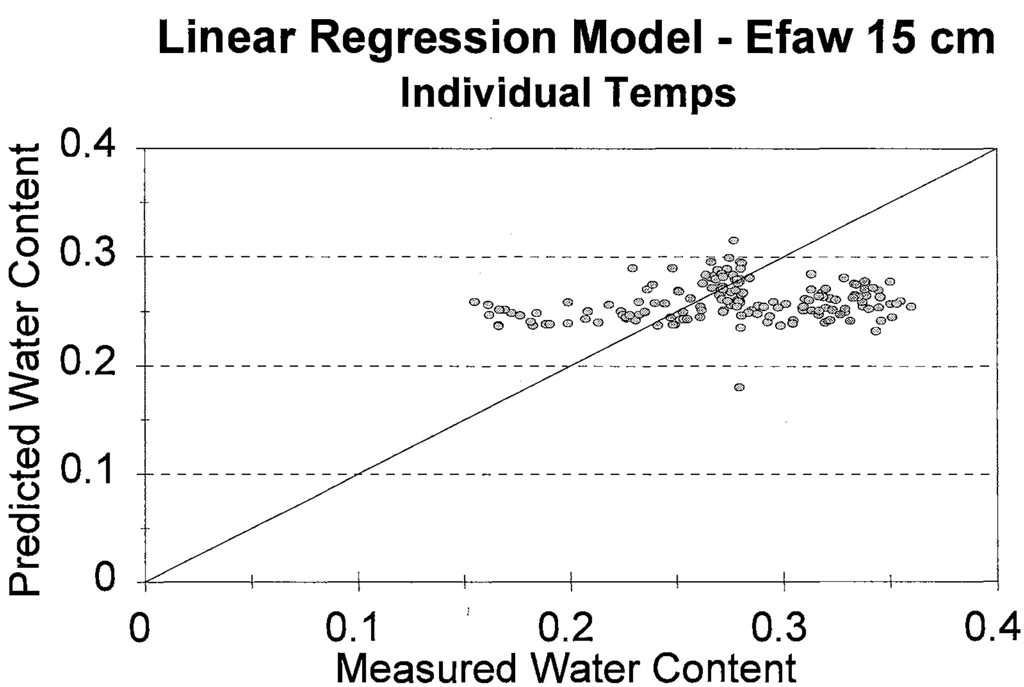

Figure 7.26. Individual Temperatures Test Results for Efaw (15 cm).

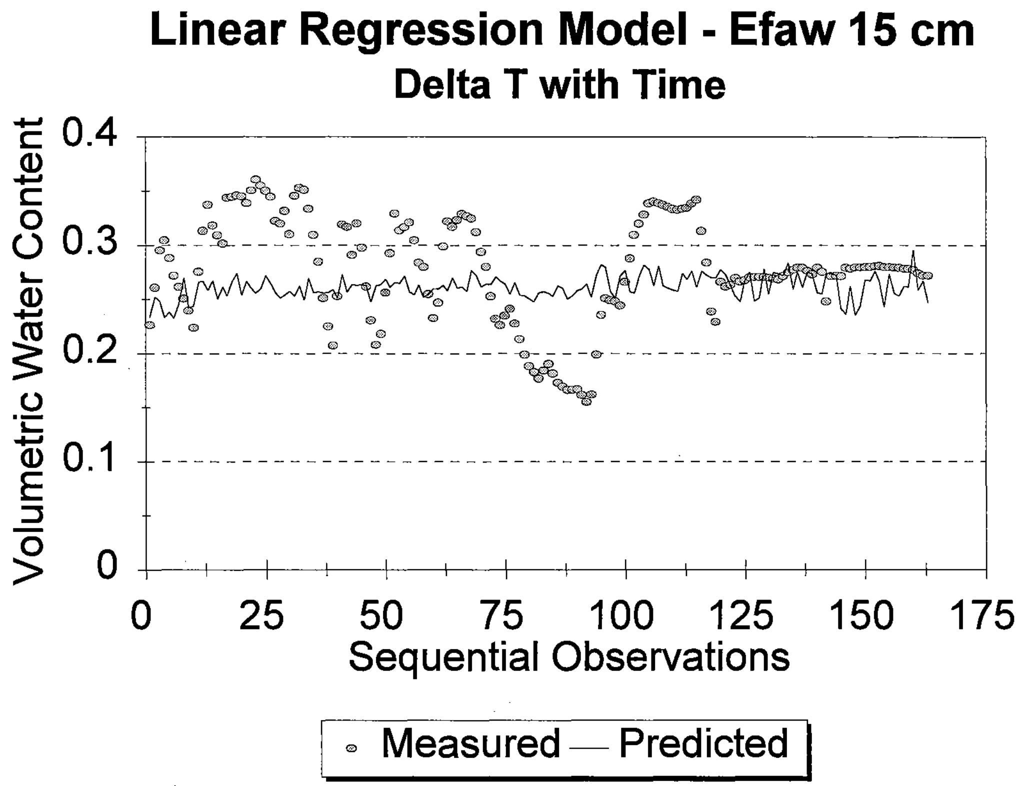

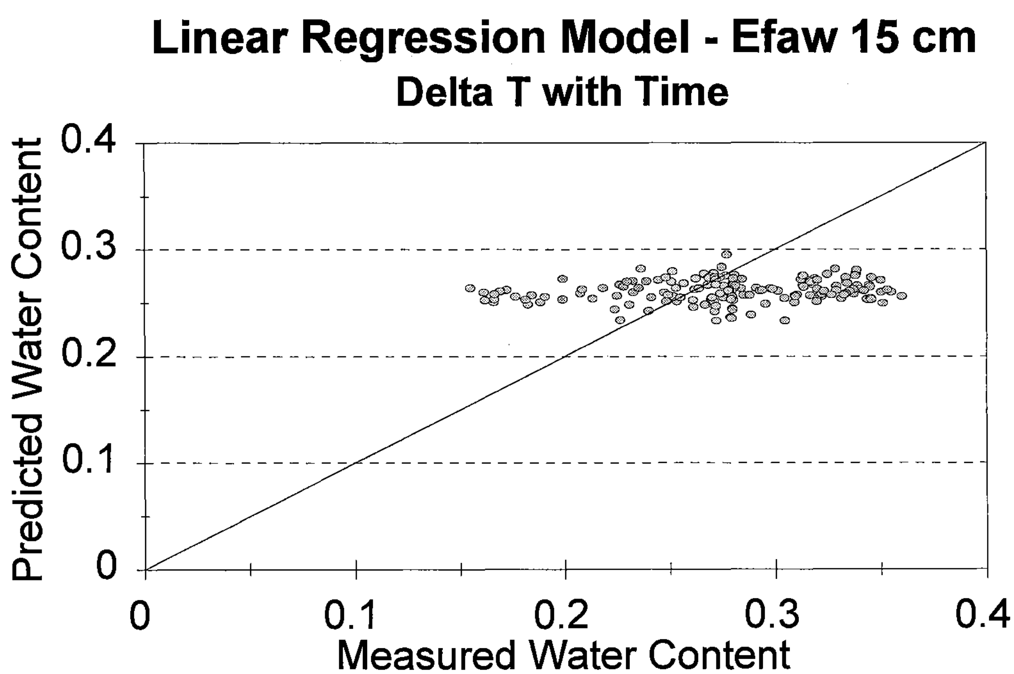

Figure 7.27. ΔT with Time Test Results for Efaw (15 cm).

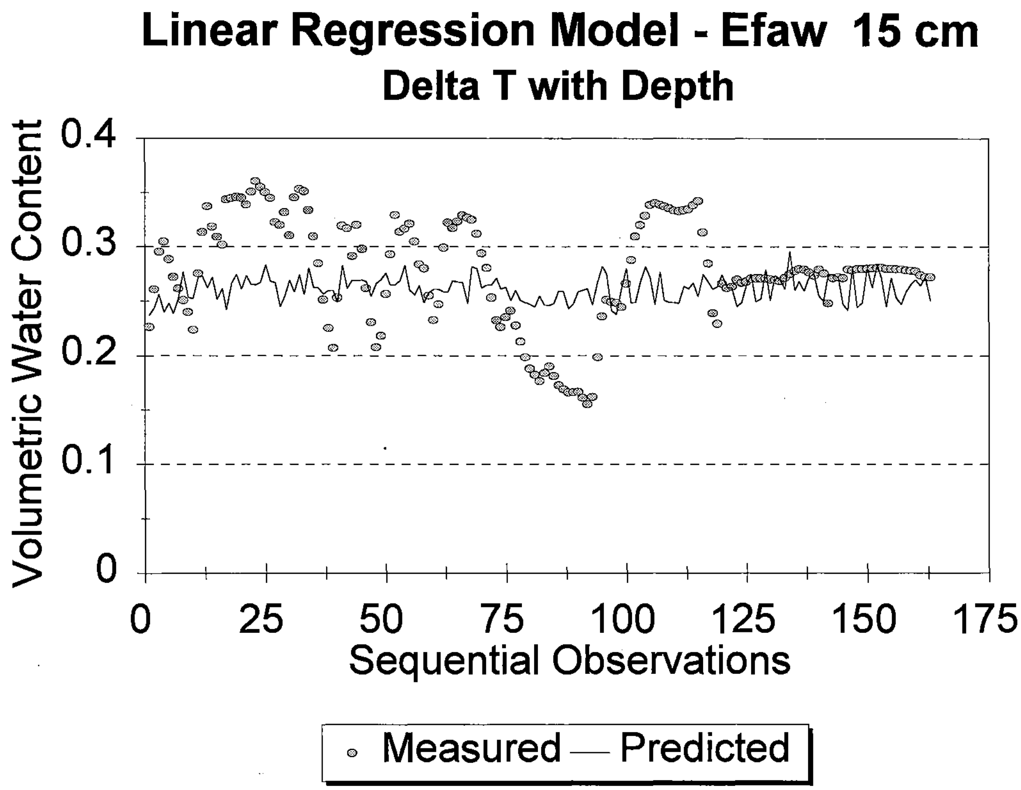

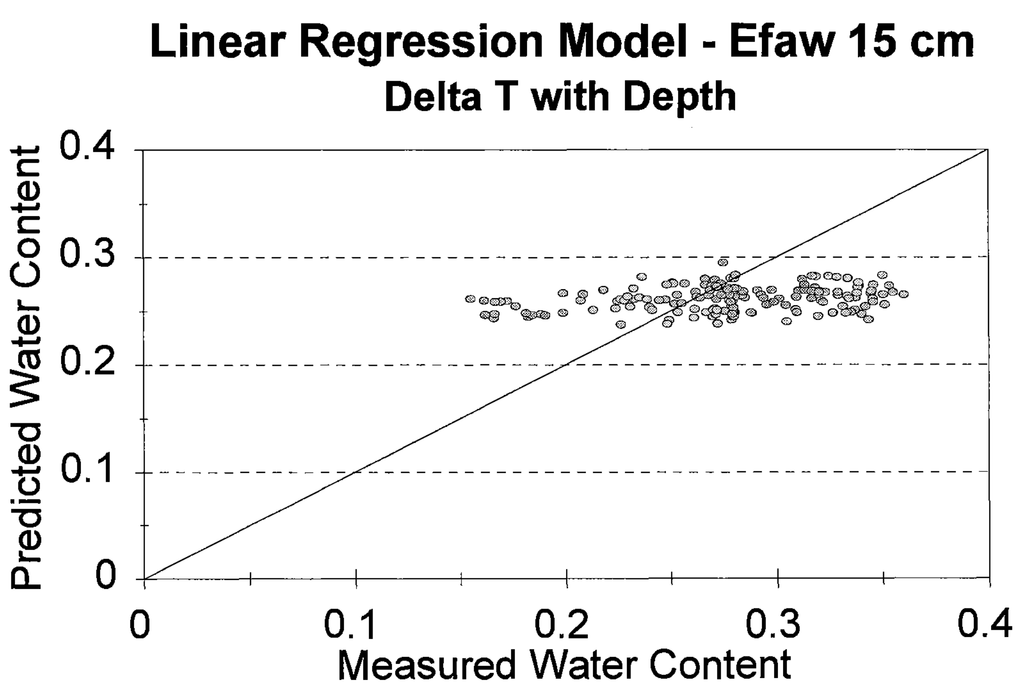

Figure 7.28. ΔT with Depth Test Results for Efaw (15 cm).

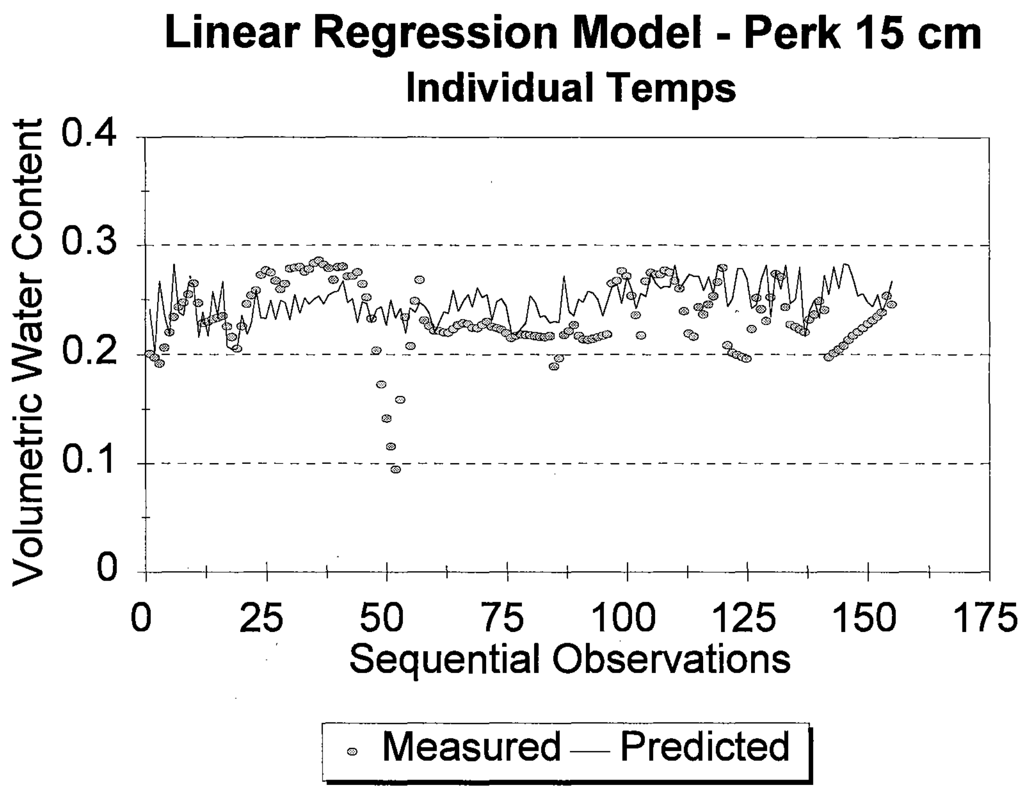

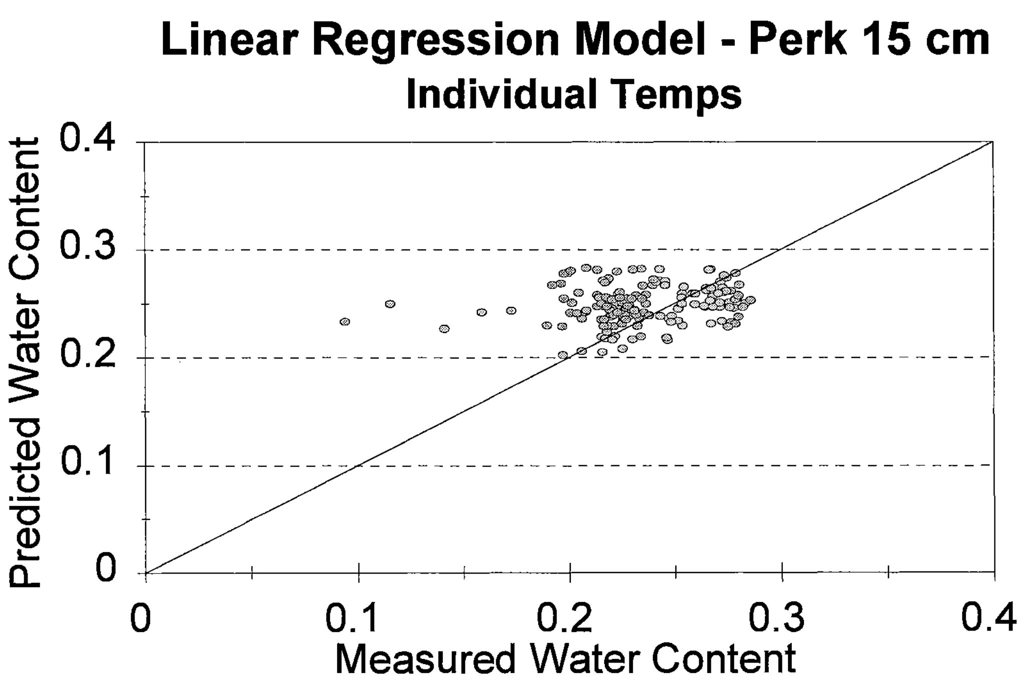

Figure 7.29. Individual Temperatures Test Results for Perkins (15 cm).

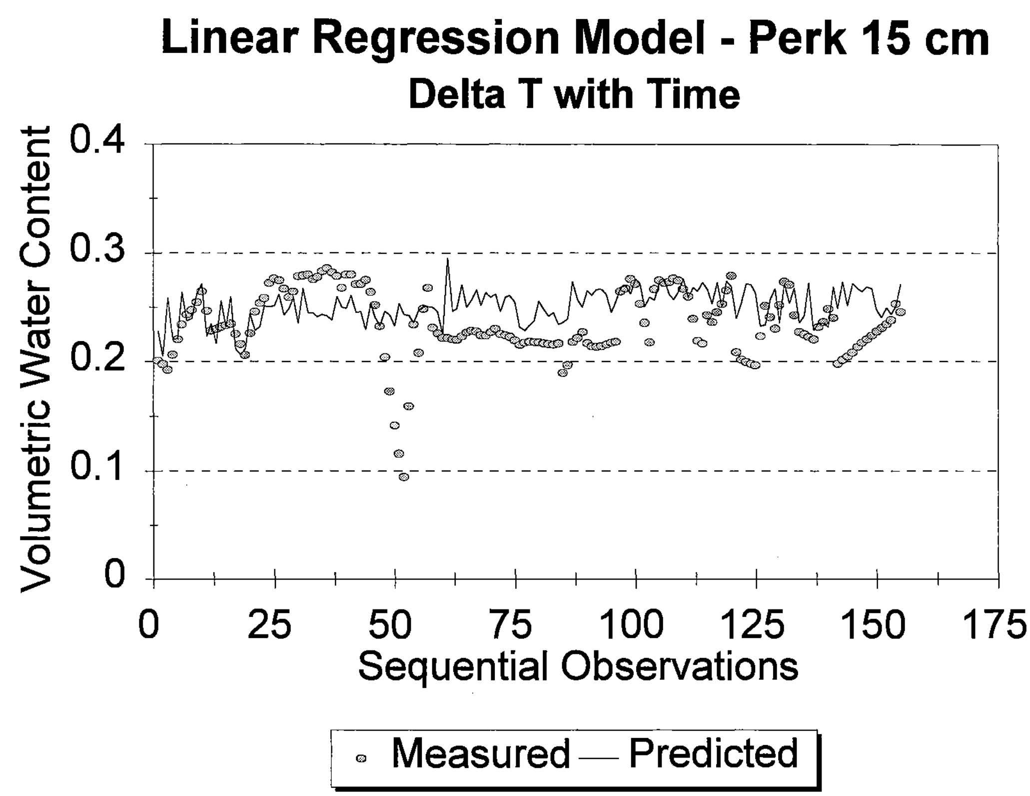

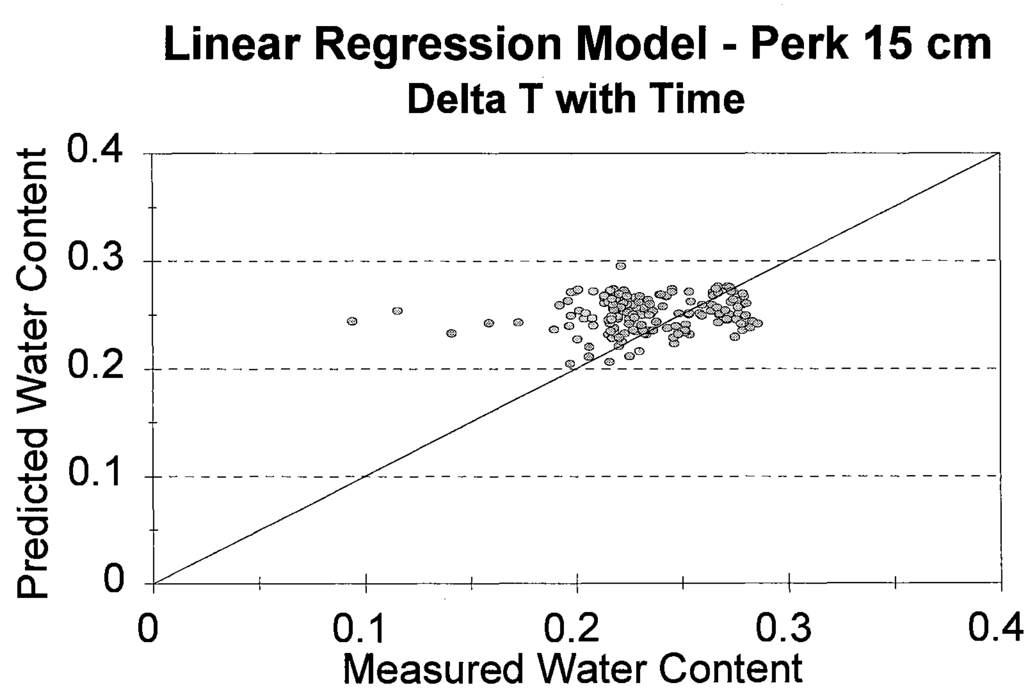

Figure 7.30. ΔT with Time Test Results for Perkins (15 cm).

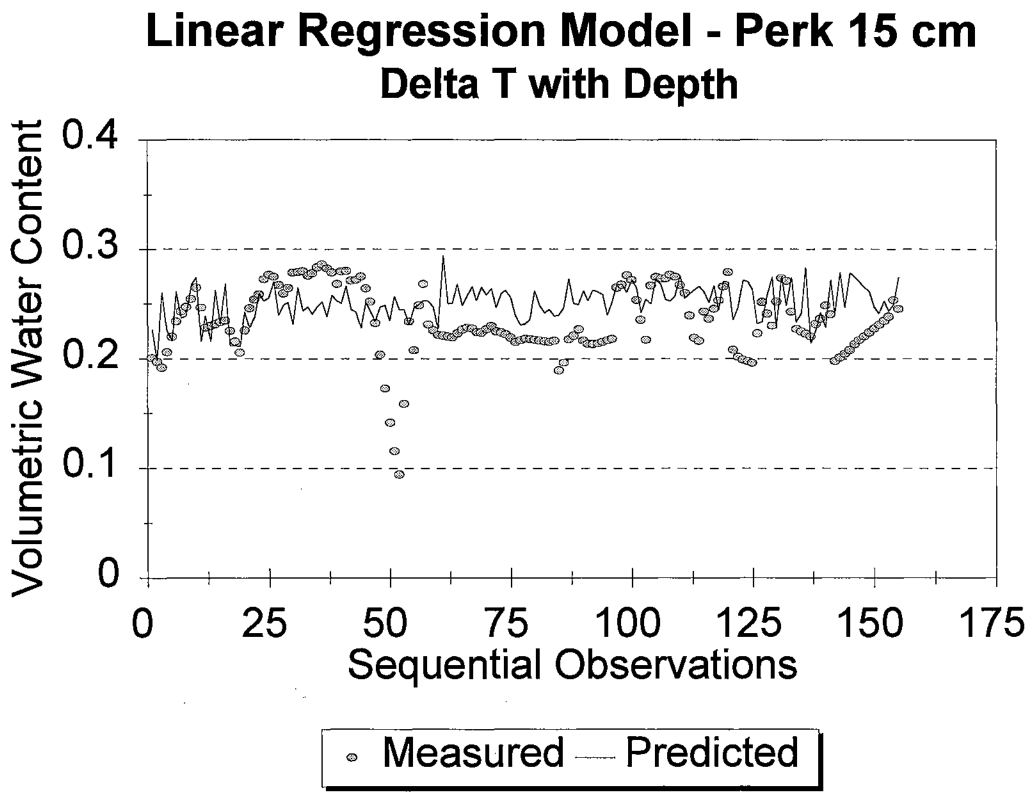

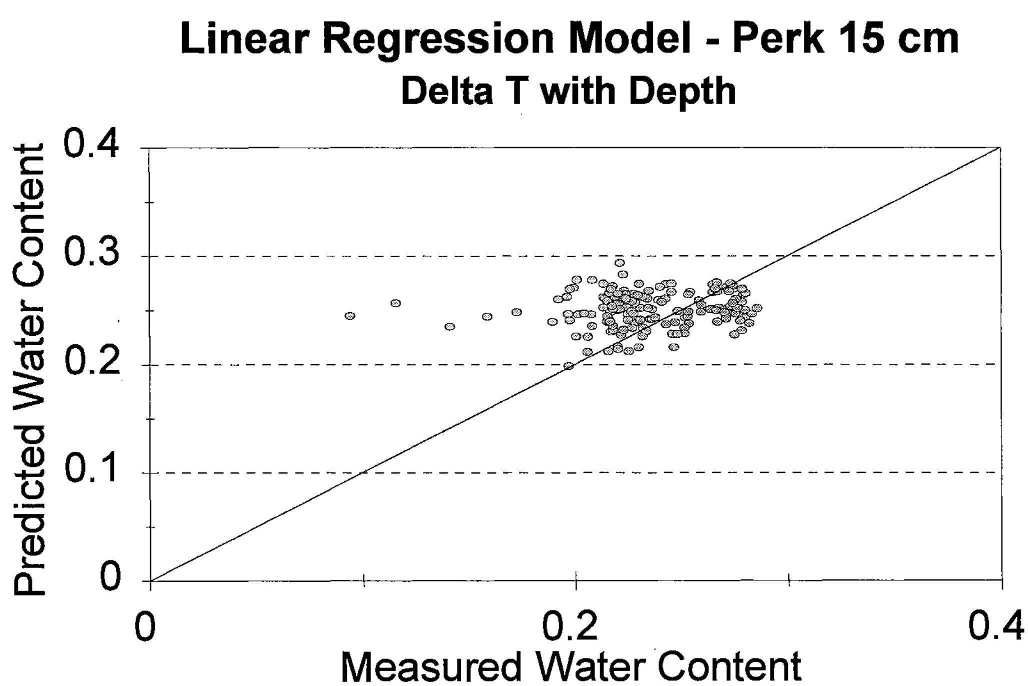

Figure 7.31. ΔT with Depth Test Results for Perkins (15 cm).

CHAPTER 8

SUMMARY, CONCLUSIONS AND RECOMMENDATIONS

Summary and Conclusions

Knowledge of soil water content is an important consideration in many applications. Not only is it an important factor affecting the growth of plants, but numerous other soil properties such as consistency, plasticity, strength, and trafficability depend very strongly upon water content. The need to determine the amount of soil water arises frequently in agronomic, ecological, hydrological, biological, and engineering studies. There are direct and indirect methods to measure soil moisture, but no universally recognized standard method of measurement.

The overall objective of this research was to develop a system which can measure soil water content accurately and inexpensively based on soil thermal properties, mainly temperature. A neural network model which uses field data was developed to estimate soil water content at various depths and locations. The use of a neural network was selected for this project because of the uncertain, non-linear interrelationships between soil water content and soil thermal properties. If soil temperatures are measured at various depths, then a relationship between temperature and soil moisture can be developed, but not without knowing the soil's thermal diffusivity or conductivity and bulk density. None of these properties is easily measured. One reason for using a neural network is to circumvent measurement of these "unknowns".

Since the model was to be developed using field data as inputs, two automated stations at sites near Stillwater, Oklahoma were deployed for monitoring soil and weather data. The soil types at these two sites were Easpur clay loam and Teller sandy loam. The data collected at each site included: air temperature, solar radiation, rainfall, soil temperature and soil water content. There were three soil temperature probes at each site. Each probe measured temperature at 14 depths ranging from the surface to 150 cm. All of the weather and soil instrumentation was controlled by a datalogger which read each sensor every 60 seconds and then recorded hourly averages. The soil moisture data were collected two to three times a week using a neutron moisture gauge. A third site, which was a scaled down version of the other two, was later set up to collect test data. The soil at this site was an Ashport loam. The measurements made at this site included soil temperatures to a depth of 50 cm, air temperature and soil water content.

Initial data analysis was performed on the soil thermal properties. Bulk densities were determined using the core samples gathered when the neutron access tubes were placed at the sites. Thermal diffusivity values were calculated using a numerical method which relates soil temperatures at various depths to thermal diffusivity. Finally, thermal conductivity was determined for various moisture contents using specific heat values and the calculated thermal diffusivity values.

With the preliminary analysis, it was determined that for this particular data, soil water content was not having a large impact on the calculated thermal properties. Direct relationships could not be found with the field data. The progression of the development of the neural network model occurred in several stages. The neural network selected consisted of a backpropagation paradigm. The development and testing of the neural network application was performed using workstation. Various input combinations were used as training data until an optimal neural network was designed. The final network used only soil temperatures and a soil coefficient value (dependent on soil type) to estimate soil water content. The soil water content values were determined at depths of 15, 30, 60 and 120 cm. The neural network was trained using temperatures surrounding these depths and measured soil moisture values from the two initial site locations. Once trained to a desired tolerance, the network model was tested using independent data from each of the three sites.

The overall performance of the neural network model was good. All of the general trends in soil water content for the three sites were predicted well. The largest RMS error for all locations and depths was 2.34% volumetric moisture content. The correlation coefficient (r^2) values ranged from 0.452 to 0.993. A residual analysis was performed which reflected that the mean of the errors was very close to zero, which resulted in a standard deviation of the errors very close to the RMSE values. The model had a tendency to underpredict higher moisture content values and overpredict the lower moisture values. A multiple variable linear regression analysis was also performed on the same data as used in the neural network. The multivariate regression predicted soil water contents quite poorly yielding average values regardless of the trends of the measured water content. The neural network is in a form (compilable C code) which is easily transportable and can estimate soil water contents given the easily measured soil temperature inputs, once the soil coefficient for the specific site is calibrated.

Recommendations

The research in this dissertation presents the development and testing of a soil moisture system which uses soil temperatures and a neural network. The results have been promising for this to be developed into a complete self-calibrating soil moisture system. The possible directions for future research may be described as follows:

1. Increase the number of test sites (in a similar manner to the Hyd test site) so that a data base can be developed which has a wide range of soil types with corresponding soil coefficient values. The user could then match their particular soil type with one in the data base to obtain an initial estimate of the soil coefficient.

2. Investigate the possibility of using soil texture information to estimate soil coefficient values.

3. Develop software which links the collection of soil temperatures directly to the neural network, thereby producing an instantaneous output.

4. Develop software to adjust the soil coefficient values based on field feedback. The user could make periodic measurements of soil water content and compare these values to those predicted by the network. If the two values vary from one another, the software could adjust the soil coefficient value until the measured and estimated values match.

5. Develop an integrated system with spatially distributed sensors. Such a system would be useful in irrigation and other applications.

REFERENCES

Ackley, D.H., G.E. Hinton, and T.J. Sejnowski. 1985. A learning algorithm for Boltzmann machines. Cognitive Science. 9:147-169.

Aitchison, G.D., P.F. Butler, and C.G. Gurr. 1950. Techniques associated with the use of gypsum block soil moisture meters. Austr. J. Appl. Sci. 2:57-77.

Anderson, M.G. and T.P. Burt. 1977. Automatic monitoring of soil moisture conditions in a hill slope spur and hollow. J. Hydrol. 33(1/2):27-36.

Armstrong, C.F., J.T. Ligon, and S.J. Thomson. 1985. Calibration of Watermark model 200 soil moisture sensor. ASAE Technical Paper 85-2077. ASAE, St. Joseph, MI.

Arnold, G.J., M.L. Stone, and R.L. Elliott. 1992. Design of a dielectric based soil moisture sensor. ASAE Technical Paper 92-3001. ASAE, St. Joseph, MI.

Arsenault, H.H. and B. Macukow. 1989. Neural network model for fast learning and retrieval. Optical Engineering 28(5):506-512.

Bailey, D.L. and D.M. Thompson. 1990. Developing neural network applications. AI Expert. 9:31-36.

Beroza, M., K.R. Hill, and K.H. Norris. 1968. Determination of reflectance of pesticide spots on thin-layer chromatograms using fiber optics. Analytical Chemistry 40(11):1608-1613.

Birth, G.S. 1967. A fiber optics reflectance attachment. Agricultural Engineering 48(8):448-449.

Bloodworth, M.E. and J. B. Page. 1957. Use of thermistors for the measurement of soil moisture and temperature. Soil Sci. Soc. Amer. Proc. 21:11-15.

Bolt, G.H. 1976. Soil physics terminology. Bull. Int. Soc. Soil Sci. 49:26-36.

Bolte, J.P. 1989. Applications of neural networks in agriculture. ASAE Technical Paper 89-7591, ASAE, St. Joseph, MI.

Bottcher, A.B. and L.W. Miller. 1982. Automatic tensiometer scanner for rapid measurements. Trans. Am. Soc. Agric. Eng. 25(5):1338-1342.

Bouyoucos, G.J. 1955. Electrical resistance methods as finally perfected for making continuous measurement of soil moisture content under field conditions. Michigan Quarterly Bulletin. 37(1):132-149.

Bowers, S.A. and R.J. Hanks. 1965. Reflection of radiant energy from soils. Soil Sci. 100(2):130-138.

Bowers, S.A. and S.J. Smith. 1972. Spectrophotometric determination of soil water content. Soil Sci. Soc. of Am. Proc. 36(6):978-980.

Bowers, S.A., S.J. Smith, H.D. Fisher, and G.E. Miller. 1975. Soil water measurement with an inexpensive spectrophotometer. Soil Sci. Soc. of Am. Proc. 39(3):391-393.

Brown, R.W. and D.L. Bartos. 1982. A calibration model for screen-cage peltier thermocouple psychrometers. Intermountain Forest and Range Experiment Station, Res. Pap. INT-193, Odgen, UT 84401.

Campbell, G.S. 1985. Soil Physics with Basic - Transport Models for Soil-Plant Systems. Elsevier Science Publishers, New York, New York.

Cardon, G.E., C.J. Phene, and D.A. Clark. 1993. Soil matric potential sensor calibration:physical equipment and statistical data processing methods. Applied Engineering in Agriculture. 9(2):213-219.

Carslaw, H.S. and J.C. Jaeger. 1959. Conduction of Heat in Solids. Osvord University Press, London.

Caudill, M. 1991. Avoiding the great backpropagation trap. AI Expert. 6:29-35.

Christensen, D.A. and J.W. Hummel. 1985. A real-time soil moisture content sensor. ASAE Technical Paper 85-1589. ASAE, St. Joseph, MI.

Cochran, P.H., L. Boersma, and C.T. Youngberg. 1967. Thermal properties of a pumice soil. Soil Sci. Soc. Amer. Proc. 31:454-459.

Collins, E., S. Ghosh, and C. Scofield. 1988. An application of a multiple neural network learning system to emulation of mortgage underwriting judgements. IEEE International Conference on Neural Networks, II:459-466.

Conrad, V. and L.W. Pollak. 1950. Methods in climatology. Harvard Univ. Press, Cambridge, Mass.

Cottrell, G.W., P. Munro, and D. Zipser. 1987. Learning internal representations from gray-scale images: An example of extensional programming. In Proc. 9th Annual Conference of the Cognitive Science Society. 461-473.

Curcio, J.A. and C.C. Petty. 1951. The near infrared absorption spectrum of liquid water. Jour. Opt. Soc. of Am. 41(5):302-304.

Dalal, R.C. and R.J. Henry. 1985. Simultaneous determination of moisture, organic carbon and total nitrogen in soils by near infrared reflectance spectrophotometry. Soil Sci. Soc. of Am. Proc.

Daniel, K.E., J.M. Hamilton, and R.E. Olson. 1981. Suitability of thermocouple psychrometers for studying moisture movement in unsaturated soils. American Society for Testing Materials, Permeability and Groundwater Contaminant Transport, ASTM STP 746:84-100.

Dayhoff, J.E. 1990. Neural Network Architectures. Van Nostrand Reinhold, New York, NY. 58-73.

Dean, T.J., J.P. Bell, and A.J.B. Baty. 1987. Soil moisture measurement by an improved capacitance technique, part I. Sensor design and performance. Journal of Hydrology, 93:79-90.

de Vries, D.A. 1952. The thermal conductivity of soil. Meded. Landbouwhogeschool, Wageningen.

de Vries, D.A. 1963. Thermal properties of soils. In Physics of Plant Environment. North-Holland Publishing Co., Amsterdam.

de Vries, D.A. 1975. Heat transfer in soils. In Heat and Mass Transfer in the Biosphere. 5-28. Scripta Book Co., Washington, D.C.

de Vries, D.A. and A.J. Peck. 1968. On the cylindrical probe method of measuring thermal conductivity with special reference to soils. Aust. J. Phys. 11:255-271.

Draper, N.R. and H. Smith. 1966. Applied regression analysis. John Wiley and Sons, Inc., New York.

Enfield, G. and C.V. Gillaspy. 1980. Pressure transducer for remote data acquisition. Trans. Am. Soc. Agric. Eng. 23(5):1195-1196.

England, C.B. 1965. Changes in fiber-glass soil moisture-electrical resistance elements in long-term installations. Soil Sci. Soc. Am. Proc. 29(2):229-231.

Fukushima, K. 1987. A neural network model for selective attention in visual pattern recognition and associative recall. Applied Optics 26(23):4985-4992.

Gardner, R. 1955. Relation of temperature to moisture tension of soil. Soil Sci. 79:257-267.

Gemant, A. 1952. How to compute thermal soil conductivities. Heating, Piping, and Air conditioning. 24(1):122-123.

Greacen, E.L. 1981. Soil water assessment by the neuton method. CSIRO. East Melbourne, Victoria, Austrailia.

Groenevelt, P.H. and G.H. Bolt. 1969. Non-equilibrium thermodynamics of the soil-water system. J. Hydrol. 7:358-388.

HNC Incorporated. 1991. HNC Neurosoftware. HNC, Inc. San Diego, CA.

Hansen, G. 1993. Personal Interview. USDA Hydraulics Laboratory. Stillwater, OK 74074.

Herkelrath, W.N., S.P. Hamburg, and F. Murphy. 1991. Automatic, real-time monitoring os soil moisture in a remote field area with time domain reflectometry. Water Resources Research. 27(5):857-864.

Hewlett, J.D., J.E. Douglas, and J.L. Cutter. 1964. Instrumental ans soil moisture variance using the neutron scattering method. Soil Sci. 97:19-24.

Hillel, D. 1980. Fundamentals of Soil Physics. Academic Press, Inc. Orlando, Florida. 128-132.

Hillman, D. 1991. Knowledge based. AI Expert 12:46-53.

Holmes, J.W. 1956. Calibration and field use of the neutron scattering method of measuring soil water content. Aust. J. Appl. Sci. 7:45-58.

Horton, R., P.J. Wierenga and D.R. Nielsen. 1983. Evaluation of methods for determining the apparent thermal diffusivity of soil near the surface. Soil Sci. Soc. Am. J. 47:25-31.

Hunt, G.R. and J.W. Salisbury. 1970. Visible and near-infrared spectra of minerals and rocks: I. Silicate minerals. Modern Geology 1:283-300.

Jackel, L.D., Howard, R.E., Denker, Hubbard, and S.A. Sola. 1987. Building a hierarchy with neural networks: an example-image vector quantization. Applied Optics. 26(23):5081-5084.

Jackson, R.D. and S.A. Taylor. 1965. Heat Transfer. In Methods of Soil Analysis. Monograph No. 9. 349-360. Am. Soc. Agron., Madison, WI.

Johansen, O. 1975. Thermal conductivity of soils. Ph.D. Thesis. Trondheim, Norway.

Johnston, L.N. 1942. Water permeable jacketed thermal radiators as indicators of field capacity and permanent wilting percentage in soils. Soil Sci. 54:123-126.

Jury, W.A. 1973. Simultaneous transport of heat and moisture through a medium sand. Ph.D. Thesis, Univ. of Wisconsin, Madison, WI.

Jury, W.A. and E.E. Miller. 1974. Measurement of the transport coefficients for coupled flow of heat and moisture in a medium sand. Soil Sci. Soc. Am. Proc. 38:551-557.

Jury, W.A., W.R. Gardner, and W.H. Gardner. 1991. Soil Physics. John Wiley and Sons, Inc. New York.

Kano, Y., W.F. McClure, and R.W. Skaggs. 1985. A near-infrared soil moisture meter. Trans. of the ASAE. 28:1853-1855.

Kersten, M.S. 1949. Thermal Properties of Soils, Bulletin 28, Engineering Experiment Station, University of Minnesota, Minneapolis, MN.

Lapedes, A. and R. Farber. 1987. Non-linear signal processing using neural networks: Prediction and system modeling. Los Alamos National Laboratory Report LA-UR-87-2662.

Lettau, H. 1954. Improved models of thermal diffusion in the soil. Trans. Am. Geophys. Union 35:121-132.

Long, F.L. 1982. A new solid state device for reading tensiometers. Soil Sci. 133(2):131-132.

Long, F.L. and M.G. Huck. 1980. An automated system for measuring soil water potential gradients in a rhizotron soil profile. Soil Sci. 129(5):305-310.

Malicki, M.A. and R.J. Hanks. 1989. Interfacial contribution to two-electrode soil moisture sensor readings. Irrigation Science. 10:41-54.

Merrill, S.K. and L.L. Rawlins. 1972. Field measurements of soil water potential with thermocouple psychrometers. Soil Sci. 113(2):102-109.

Misra, A. 1992. Relationship of porosity and elastic properties for consolidated granular aggregates. In Microstructural Characterization in Constitutive Models for Metals and Soils. ASME Press, New York, 81-94.

Misra, A., B.R. Becker, and B.A. Fricke. 1993. Prediction methods for soil thermal conductivity. From Snethen.

Morrison, R.D. 1983. Ground Water Monitoring Technology. Procedures, Equipment and Applications. Timco Mfg., Inc. Prairie du Sac, WI 53578.

Neprin, S.V. and A.F. Chudnovskii. 1967. Physics of the soil. Israel Program for Scientific Translations. Keter Press, Jerusalem.

NeuralWare, Incorporated. 1991. Neural Computing. NeuralWorks Professional II/PLUS and NeuralWorks Explorer. NeuralWare, Inc. Pittsburgh, PA.

Pawlicki, T.F., D. Lee, J.J. Hull, and S.N. Srihari. 1988. Neural network models and their application to handwritten digit recognition. IEEE International Conference on Neural Networks, II:63-70.

Patten, H.E. 1909. Heat transference in soils. Bulletin 59. U.S. Department of Agriculture Bureau of Soils, Washington, D.C.

Peterson. J.B. and M.F. Baumgardner. 1981. Use of spectral data to estimate the relationship between soil moisture tensions and their corresponding reflectances. Purdue Unoversity Water Resources Research Center. Tech. Report 143.

Phene, C.J., G.J. Hoffman, and S.L. Rawlins. 1971. Measuring soil matric potential in situ by sensing heat dissipation within a porous body: I. Theory and sensor calibration. Soil Sci. Soc. Am. Proc. 35(1):27-33.

Phene, C.J., D.A. Clarck, G.E. Cardon and R.M. Mead. 1992. The soil matric potential sensor. Research and applications. In Advances in Measurement of Soil Properties: Bringing Theory into Practice, eds. G.C. Topp, W.D. Reynolds and R.E. Green. SSSA Special Publication 30. Madison WI: Soil Sci. Soc. Am.

Price, R.R., X. Huang, and L.D. Gaultney. 1990. Development of a soil moisture sensor. ASAE Technical Paper 90-3555. ASAE, St. Joseph, MI.

Reid, W.P. 1988. An introduction to machine learning with neural networks. Proceedings of the Oklahoma Symposium on Artificial Intelligence. Norman, Oklahoma. 429-439.

Richtmeyer, R.D. and K.W. Morton. 1967. Difference methods for initial value problems. Interscience Publishers, New York.

Rigney, M.R. and G.A. Kranzler. 1989. Seedling classification performance of a neural network. ASAE Technical Paper 89-7523. ASAE, St. Joseph, MI.

Roeser, W.F. 1940. Thermoelectric thermometry. J. Appl. Phys. 11:388-407.

Salomone, L.A., W.D. Kovacs, D. William. 1984. Thermal resistivity of soils. Journal of Geotechnical Engineering. ASCE, 110(3):375-389.

Salomone, L.A. and J.I. Marlow. 1989. Soil rock classification according to thermal conductivity. EPRI CU-6482. Electric Power Research Institute, Palo Alto, CA.

Schwartz, T.J. 1989. Yes, Virginia, there are neural network applications. IEEE Expert, 4(3):77-78.

Seemann, J. 1979. Measuring technology. In J. Agrometeorology. Springer-Verlag, Berlin. 40-45.

Selig, E.T. and S. Mansukhani. 1975. Relationship of soil moisture to the dielectric property. J. of Geotech. Eng. Div. 770-775.

Servick, G.W. 1972. Investigations on the adaptation of the MC-300A soil moisture meter and cells to solid waste studies. An independent study report, Civil and Environmental Engineering, University of Wisconsin.

Shackleford, J.B. 1989. Neural data structures: programming with neurons. Hewlett-Packard Journal 40(3):69-78.

Shaw, B. and L.D. Baver. 1939. An electrothermal method for following moisture changes of the soil in situ. Soil Sci. Soc. Amer. Proc. 4:78-83.

Shea, P.M. and V. Lin. 1988. Detection of explosive in checked airline baggage using an artificial neural system. Science Applications International Corporation, Santa Clara, CA.

Singh, S.R. and B.K. Sinha. 1977. Soil thermal diffusivity determination from overspecification of boundary data. Soil Sci. Soc. Am. J. 41:831-834.

Skagges, R.W., and E. M. Smith. 1967. Apparent thermal conductivity of soil as related to soil porosity. ASAE Technical Paper 67-114. ASAE, St. Joseph, MI.

Stone, J.F. 1993. Personal interview. Oklahoma State University, Stillwater, OK.

Thai, C.N. and R.L. Shewfelt. 1990. Modeling sensory color quality: neural networks vs statistical regression. ASAE Technical Paper 90-6038. ASAE, St. Joseph, MI.

Topp, G.C., J.L. Davis and A.P. Annan. 1980. Electromagnetic determination of soil water content: by measurements in coaxial transmission lines. Water Resources Research, 16(3):574-582.

Troxler Electronics Laboratory Incorporated. 1983. 3300 Model Depth Moisture Gauge Instruction Manual. Troxler International, LTD. Research Triangle Park, N.C.

van Bavel, C.H.M. 1963. Neutron scattering measurements of soil moisture:development and current status. Proc. Int. Symp. Humidity Moisture, Washington, D.C. 171-184.

van Rooyen, M. and H.F. Winterkorn. 1957.Structural and textural influences on thermal conductivity of soils. Highway Research Board Proceedings. 39:576-621.

van Wesenbeeck, I.J., and R.G. Kachanoski. 1988. Spatial and temporal distribution of soil water in the tilled layer under a corn crop. Soil Sci. Soc. of Am. J. 52:363-368.

van Wijk, W.R. (ed). 1963. Physics of plant environment. North-Holland Publishing Co., Amsterdam.

Waite, T. and H. Hardenbergh. 1989. Neural nets. Programmer's Journal 7.3:13-20.

Weibe, H.H., R.W. Brown, and J. Baker. 1977. Temperature gradient effects on in situ hygrometer measurements of water potential. Agron. J. 69(6):933-939.

Weibe, H.H. and R. Brown. 1979. Temperature gradient effects on in situ hygrometric measurements of soil water potential. II. Water Movement. Agron. J. 71(3):397-401.

Wieland, A. and R. Leighton. 1989. Geometric analysis of neural network capabilities. IERR. First International Conference on Neural Networks. III:385-392.

Wierenga, P.J. and C.T. de Wit. 1970. Simulation of heat transfer in soils. Soil Sci. Soc. Am. Proc. 34:845-848.

Wierenga, P.J., R.M. Hagan, and D.R. Nielsen. 1969. Soil temperature profiles during infiltration and redistribution of warm or cold irrigation water. Water Resources Res. 9:95-99.

Wong D.K. H. and A. Ho. 1987. An evaluation of a thermal conductivity sensor for the measurement of soil suction. Report, Dept. of Civil Engineering, Univ. of Saskatchewan, Saskatoon, Saskatchewan, Canada.

Woodside, W., and J.B. Cliffe. 1959. Heat and moisture transfer in closed systems of two granular materials. Soil Sci. 87:75-82.

Zeidenberg, M. 1987. Modeling the brain. Byte 12:238-246.

Zhuang, X. and B.A. Engel. 1990. Classification of multispectral remote sensing data using neural networks vs statistical methods. ASAE Technical Paper 90-7552. ASAE, St. Joseph, MI.

APPENDICES

APPENDIX A

CAMPBELL SCIENTIFIC DATALOGGER PROGRAM

CAMPBELL SCIENTIFIC DATA LOGGER (CR10) PROGRAM

01:00	
01:60.000	Scan Rate (sec)
01:P11	Thermocouple Reference Temperature (Thermistor)
01:01	Reps
02:01	Input Channel
03:03	Excitation Channel
04:0001	Intermediate Storage Location
05:1.0000	Multiplier (Centigrade)
06:0.0000	Offset (Voltage)
02:P01	Single Ended Voltage (Net Radiometer)
01:01	Reps
02:04	Range (250 mV slow)
03:02	Input Channel
04:0002	Intermediate Storage Location
05:13.5 (13.7)	Multiplier (W/m^2)
06:0.0000	Offset
03:P01	Single Ended Voltage (Pyranometer)
01:01	Reps
02:03	Range (25 mV slow)
03:06	Input Channel
04:0003	Intermediate Storage Location
05:11.389 (10.081)	Multiplier (W/m^2)
06:0.0000	Offset
04:P01	Single Ended Voltage (Heat Flux Plate 1)
01:01	Reps
02:02	Range (7.5 mV slow)
03:07	Input Channel
04:0004	Intermediate Storage Location
05:43.8 (37.9)	Multiplier (W/m^2)
06:0.0000	Offset
05:P01	Single Ended Voltage (Heat Flux Plate 2)
01:01	Reps
02:02	Range (7.5 mV slow)
03:08	Input Channel
04:0005	Intermediate Storage Location
05:42.9 (37.0)	Multiplier (W/m^2)
06:0.0000	Offset
06:P01	Single Ended Voltage (Heat Flux Plate 3)
01:01	Reps
02:02	Range (7.5 mV slow)
03:09	Input Channel
04:0006	Intermediate Storage Location
05:42.9 (39.2)	Multiplier (W/m^2)

06:0.0000	Offset
07:P01	Single Ended Voltage (Heat Flux Plate 4)
01:01	Reps
02:02	Range (7.5 mV slow)
03:10	Input Channel
04:0007	Intermediate Storage Location
05:43.2 (43.5)	Multiplier (W/m^2)
06:0.0000	Offset
08:P01	Single Ended Voltage (Heat Flux Plate 5)
01:01	Reps
02:02	Range (7.5 mV slow)
03:11	Input Channel
04:0008	Intermediate Storage Location
05:44.1 (42.1)	Multiplier (W/m^2)
06:0.0000	Offset
09:P01	Single Ended Voltage (Heat Flux Plate 6)
01:01	Reps
02:02	Range (7.5 mV slow)
03:12	Input Channel
04:0009	Intermediate Storage Location
05:42.8 (42.5)	Multiplier (W/m^2)
06:0.0000	Offset
10:P03	Pulse Count (Anemometer)
01:01	Reps
02:01	Pulse Input Channel
03:12	Configuration (Switch Closure - discard long counts
04:0010	Intermediate Storage Location
05:.01333	Multiplier (m/s - 60 sec interval)
06:.44700	Offset (m/s)
11:P03	Pulse Count (Rain Gauge)
01:01	Reps
02:02	Pulse Input Channel
03:02	Configuration (Switch Closure)
04:0011	Intermediate Storage Location
05:.25400	Multiplier (mm)
06:0.0000	Offset
12:P86	Do
01:41	Set Port 1 High (Activates multiplexer)
13:P87	Loop (Repeats reading of probe thermocouples)
01:0000	Delay
02:0014	Count (Repititions-# of thermocouple sets)
14:P86	Do
01:72	Pulse Port 2 (Steps multiplexer to next H set)
15:P90	Loop Index
01:03	Step 3 (Reads 3 thermocouples per loop)

16:P13	Single Ended (Thermocouple)
01:03	Reps
02:01	Range (2.5 mV slow)
03:03	Input Channel
04:01	Thermocouple Type (Cu/Co)
05:0001	Reference Location
06:0012--	Intermediate Storage Location (Indexed - input 12C)
07:1.0000	Multiplier (Centigrade)
08:0.0000	Offset
17:P95	End Loop
18:P86	Do
01:72	Pulse Port 2 (Steps multiplexer to next H set)
19:P13	Single Ended (Thermocouple - air)
01:01	Reps
02:01	Range (2.5 mV slow)
03:03	Input Channel
04:01	Thermocouple Type (Cu/Co)
05:0001	Reference Location
06:0054	Intermediate Storage Location
07:1.0000	Multiplier (Centigrade)
08:0.0000	Offset
20:P86	Do
01:51	Set Port 1 Low (Deactivates Muliplexer)
21:P10	Battery Voltage
01:0055	Intermediate Storage Location
22:P92	If Time
01:0.0000	Delay
02:0060	Interval (min)
03:10	Set Output Flag
23:P77	Real Time
01:0110	Option (Jday, Hour, Min)
24:P71	Average
01:55	Reps
02:0001	Location (Beginning with Location 1)

APPENDIX B

THERMAL DIFFUSIVITY PROGRAM

```
/*****************************************************************
  Goal:   calculate alpha value
  Input: original data file efaw.all
  Output: transformed data file - merge.dat
  Usage: cc alpha.c
        a.out
*****************************************************************/
#include <stdio.h>
#include <stdlib.h>
#define MAX_LENGTH 58
#define  MAX  24

#define pos1 5
#define pos2 7
#define pos3 8            /* defind temp pos. correspoding to mois at 15cm*/

#define DZ 10            /* Delta z */
#define DT 3600          /* Delta t */

main()
{


 int i,n=0,julia,jdate,nnjdate,time;
 char ch;
 float onehour[MAX_LENGTH+1],moist;
 float d_alpha, alpha[MAX+1],t1,old_t1,t2,old_t2,t3,old_t3, p_t, pp_z;
 FILE  *ifp,*ifp1,*ifp2,*ofp;


 if((ifp=fopen("/home/neusun/mason/efaw/efaw.all","r"))==NULL){
    printf(" Can't open efaw.all\n");
    exit(1);
   }

 if((ofp=fopen("temps.dat","w"))==NULL){
    printf(" Can't open temps.dat\n");
    exit(1);
   }

 while(!feof(ifp)){
   for(i=1;i<=58;i++){
     ch='a';
     while((ch>'9')||(ch<'0')&&!feof(ifp))
       ch=fgetc(ifp);
```

```
    if(feof(ifp)==0) fgetc(ifp);
    if(feof(ifp)==0) fscanf(ifp,"%f",&onehour[i]);
   }

/* check data */
  if (onehour[6]<0.0)  onehour[6]=0.0;
  if(onehour[6]>120)  printf(" Too high radi on %3.0f: %3.2f\n"
                        ,onehour[2],onehour[6]);

  if (onehour[14]<0.0) onehour[14]= 0.0;
  if (onehour[14]>100.0) printf("Too high RainFall on %3.0f :%3.2f\n"
                    ,onehour[2], onehour[14]);

  if  (onehour[57]<-20.0) printf("Air temperature too low on %3.0f : %3.2f\n"
                    ,onehour[2], onehour[57]);
  if  (onehour[57]>50.0) printf("Air temperature too   high on %3.0f: %3.2f\n"
                    , onehour[2],onehour[57]);

  for(i= 15;i<=28;i++)
      if (onehour[i]<-20.0||onehour[i]>60.0)
        onehour[i] = (onehour[i+14] + onehour[i+28])/2;

  for(i= 29;i<=42;i++)
      if (onehour[i]<-20.0 || onehour[i] > 60.0)
        onehour[i] = (onehour[i-14] + onehour[i+14])/2;

  for(i=43;i<=56;i++)
      if (onehour[i]<-20.0 || onehour[i] > 60.0)
        onehour[i] = (onehour[i-14] + onehour[i-28])/2;


                              /* print julia date and time */
 fprintf(ofp," %3.0f %3.0f",onehour[2],onehour[3]/100);

 t1=t2=t3=0.0;  /* initialize t1 --- coresponding soil temp at 10 cm
                 initialize t2 --- coresponding soil temp at 20 cm
                 initialize t3 --- coresponding soil temp at 30 cm */
 for(i=1;i<=3;i++)
     t1 = t1 + onehour[14*i+pos1];
 fprintf(ofp," %3.6f ", t1/3);
                       /* print out average temp over 3 probe at 10 cm */

 for(i=1;i<=3;i++)
     t2 = t2 + onehour[14*i+pos2];
 fprintf(ofp," %3.6f ", t2/3);
```

```
                    /* print out average temp over 3 probe at 20 cm */

  for(i=1;i<=3;i++)
      t3 = t3 + onehour[14*i+pos3];
  fprintf(ofp," %3.6f ", t3/3);
                    /* print out average temp over 3 probe at 30 cm */

  fprintf(ofp,"\n");
 }

 fclose(ifp);
 fclose(ofp);

/************** merge ********************************/

 if((ifp1=fopen("mois2.dat","r"))==NULL){
    printf(" Can't open mois1.dat\n");
    exit(1);
   }

 if((ifp2=fopen("temps.dat","r"))==NULL){
    printf(" Can't open temps.dat\n");
    exit(1);
   }

 if((ofp=fopen("merge.dat","a"))==NULL){
    printf(" Can't open merge.dat\n");
    exit(1);
   }

 while(!feof(ifp1)){
   fscanf(ifp1," %d %f",&jdate,&moist);
   if(jdate==22) break;
   while(!feof(ifp2)&&!(nnjdate==jdate&&time==0))
     fscanf(ifp2," %d %d %f %f %f",&nnjdate,&time,&t1,&t2,&t3);

   if(nnjdate==jdate&&time==0){
     n=0;
     do{
       old_t2=t2;    old_t1=t1;    old_t3=t3;
       fscanf(ifp2," %d %d %f %f %f",&nnjdate,&time,&t1,&t2,&t3);
       p_t=(t2-old_t2)/DT;
       pp_z = (old_t1 - old_t2*2 + old_t3) / (DZ*DZ);
       alpha[n] = p_t / pp_z ;
                                  /* use the formula to calculate alpha */
```

```
    n++;
   }while(!feof(ifp2)&&nnjdate==jdate);

  printf(" nnjdate = %d    n= %d", nnjdate,n);
  if(feof(ifp2)){
     printf("   ---- ---- Data integratial problem \n");
     fclose(ifp2);
     if((ifp2=fopen("temps.dat","r"))==NULL){
       printf(" Can't open temps.dat\n");
       exit(1);
      }
     continue;
    }
  if(n<23) continue;
  d_alpha=0.0;
  for(i=0;i<MAX;i++)
    d_alpha = d_alpha + alpha[i];
  d_alpha = d_alpha / (n-1) ;

  printf("    alpha: %2.5f\n",d_alpha);
  fprintf(ofp," %d  %3.5f  ",nnjdate, d_alpha);
  fprintf(ofp," %1.6f\n",moist);
  printf("  check:  %4.3f \n", 2.0*d_alpha*DT/(DZ*DZ));
                              /* double check if any error */
  }

 else{
   fclose(ifp2);
   if((ifp2=fopen("temps.dat","r"))==NULL){
     printf(" Can't open temps.dat\n");
     exit(1);
    }
   }
 }

fclose(ifp1);
fclose(ifp2);
fclose(ofp);


}
```

APPENDIX C

EXAMPLE RAW DATA COLLECTED FROM DATALOGGER

01+0122.	02+0078.	03+1500.	04+09.34	05+167.5	06+28.69	07+27.52	08+15.96
09+15.81	10+13.04	11+15.92	12+10.36	13+1.407	14+0.000	15+6.699	16+07.97
17+6.395	18+6.185	19+6.238	20+6.268	21+6.333	22+6.619	23+6.819	24+6.963
25+07.18	26+07.45	27+07.97	28+08.40	29+07.07	30+08.67	31+6.457	32+6.227
33+6.161	34+6.225	35+6.289	36+6.440	37+6.779	38+07.01	39+07.32	40+07.68
41+08.07	42+08.42	43+08.54	44+6.877	45+6.417	46+6.285	47+6.238	48+6.216
49+6.303	50+6.555	51+6.971	52+07.18	53+07.28	54+07.62	55+08.04	56+08.38
57+09.22	58+13.72						
01+0122.	02+0078.	03+1600.	04+10.18	05+097.7	06+18.52	07+23.06	08+17.61
09+13.66	10+15.15	11+14.45	12+12.41	13+2.027	14+0.000	15+07.01	16+08.17
17+6.517	18+6.260	19+6.245	20+6.255	21+6.260	22+6.542	23+6.751	24+6.940
25+07.16	26+07.45	27+07.86	28+08.29	29+07.38	30+08.70	31+6.689	32+6.377
33+6.272	34+6.237	35+6.281	36+6.425	37+6.745	38+6.994	39+07.22	40+07.58
41+07.98	42+08.39	43+08.70	44+07.20	45+6.597	46+6.388	47+6.293	48+6.245
49+6.313	50+6.553	51+6.870	52+07.08	53+07.18	54+07.59	55+07.97	56+08.34
57+09.02	58+10.11						
01+0122.	02+0078.	03+1700.	04+10.01	05+69.82	06+13.75	07+15.67	08+14.00
09+09.42	10+12.52	11+09.94	12+10.16	13+2.485	14+0.000	15+07.06	16+07.97
17+6.677	18+6.383	19+6.313	20+6.297	21+6.306	22+6.522	23+6.739	24+6.954
25+07.15	26+07.45	27+07.84	28+08.25	29+07.53	30+08.45	31+6.915	32+6.573
33+6.372	34+6.314	35+6.331	36+6.443	37+6.734	38+6.988	39+07.19	40+07.53
41+07.96	42+08.35	43+08.43	44+07.37	45+6.852	46+6.554	47+6.410	48+6.341
49+6.347	50+6.563	51+6.819	52+07.01	53+07.14	54+07.53	55+07.93	56+08.31
57+08.78	58+13.36						
01+0122.	02+0078.	03+1800.	04+09.41	05+18.85	06+4.915	07+08.35	08+09.76
09+4.974	10+09.04	11+5.795	12+07.51	13+2.028	14+0.000	15+07.04	16+07.61
17+6.732	18+6.449	19+6.350	20+6.311	21+6.307	22+6.480	23+6.687	24+6.918
25+07.10	26+07.42	27+07.78	28+08.19	29+07.48	30+07.96	31+07.03	32+6.711
33+6.486	34+6.395	35+6.381	36+6.459	37+6.719	38+6.978	39+07.14	40+07.49
41+07.92	42+08.33	43+07.98	44+07.39	45+6.973	46+6.677	47+6.516	48+6.436
49+6.402	50+6.585	51+6.779	52+6.965	53+07.10	54+07.49	55+07.90	56+08.28
57+08.21	58+13.43						
01+0122.	02+0078.	03+1900.	04+08.80	05+5.104	06+2.273	07+4.727	08+6.265
09+2.648	10+5.828	11+3.394	12+5.091	13+1.818	14+0.000	15+6.993	16+07.34
17+6.769	18+6.513	19+6.413	20+6.354	21+6.335	22+6.470	23+6.663	24+6.885
25+07.07	26+07.39	27+07.77	28+08.17	29+07.39	30+07.64	31+07.08	32+6.811
33+6.598	34+6.488	35+6.449	36+6.472	37+6.700	38+6.955	39+07.12	40+07.47
41+07.91	42+08.32	43+07.64	44+07.32	45+07.01	46+6.770	47+6.615	48+6.511
49+6.449	50+6.592	51+6.772	52+6.953	53+07.08	54+07.48	55+07.89	56+08.28
57+07.95	58+13.08						
01+0122.	02+0078.	03+2000.	04+08.26	05-4.323	06+0.255	07+1.960	08+3.760
09+0.994	10+3.589	11+1.617	12+3.297	13+1.302	14+0.000	15+6.915	16+07.10
17+6.756	18+6.547	19+6.458	20+6.394	21+6.368	22+6.471	23+6.645	24+6.866
25+07.05	26+07.37	27+07.74	28+08.15	29+07.27	30+07.36	31+07.06	32+6.860
33+6.675	34+6.568	35+6.513	36+6.498	37+6.699	38+6.941	39+07.10	40+07.45
41+07.89	42+08.30	43+07.35	44+07.22	45+07.01	46+6.817	47+6.681	48+6.580
49+6.502	50+6.609	51+6.763	52+6.933	53+07.06	54+07.47	55+07.88	56+08.27
57+07.58	58+12.73						
01+0122.	02+0078.	03+2100.	04+07.85	05-5.311	06-0.050	07+0.506	08+1.993
09+0.112	10+1.937	11+0.559	12+1.897	13+1.600	14+0.000	15+6.848	16+6.937
17+6.743	18+6.570	19+6.503	20+6.438	21+6.403	22+6.488	23+6.641	24+6.851
25+07.04	26+07.35	27+07.74	28+08.14	29+07.15	30+07.15	31+07.04	32+6.884
33+6.730	34+6.636	35+6.579	36+6.529	37+6.703	38+6.934	39+07.10	40+07.45

41+07.89 42+08.29 43+07.15 44+07.12 45+6.984 46+6.843 47+6.730 48+6.636
49+6.555 50+6.635 51+6.773 52+6.941 53+07.06 54+07.47 55+07.88 56+08.25
57+07.37 58+12.52
01+0122. 02+0078. 03+2200. 04+07.54 05-5.104 06-0.055 07+0.081 08+1.062
09-0.169 10+1.006 11+0.170 12+1.098 13+1.332 14+0.000 15+6.785 16+6.836
17+6.722 18+6.581 19+6.533 20+6.478 21+6.439 22+6.510 23+6.644 24+6.840
25+07.02 26+07.34 27+07.73 28+08.13 29+07.06 30+07.03 31+6.990 32+6.878
33+6.756 34+6.678 35+6.623 36+6.559 37+6.712 38+6.924 39+07.09 40+07.44
41+07.87 42+08.28 43+07.03 44+07.03 45+6.940 46+6.845 47+6.758 48+6.672
49+6.597 50+6.655 51+6.783 52+6.937 53+07.06 54+07.46 55+07.87 56+08.25
57+07.15 58+12.45
01+0122. 02+0078. 03+2300. 04+07.20 05-2.936 06-0.050 07-0.030 08+0.540
09-0.253 10+0.505 11+0.060 12+0.620 13+1.559 14+0.000 15+6.732 16+6.760
17+6.689 18+6.577 19+6.548 20+6.501 21+6.466 22+6.521 23+6.643 24+6.833
25+07.01 26+07.33 27+07.71 28+08.12 29+6.976 30+6.925 31+6.939 32+6.861
33+6.761 34+6.699 35+6.651 36+6.585 37+6.716 38+6.919 39+07.08 40+07.42
41+07.86 42+08.27 43+6.933 44+6.961 45+6.889 46+6.827 47+6.763 48+6.692
49+6.620 50+6.671 51+6.782 52+6.927 53+07.04 54+07.44 55+07.85 56+08.24
57+6.610 58+12.38
01+0122. 02+0079. 03+0000. 04+6.844 05-2.685 06-0.061 07-0.364 08+0.178
09-0.479 10+0.154 11-0.091 12+0.291 13+1.392 14+0.000 15+6.695 16+6.701
17+6.667 18+6.574 19+6.558 20+6.523 21+6.491 22+6.542 23+6.648 24+6.824
25+6.998 26+07.30 27+07.70 28+08.12 29+6.917 30+6.841 31+6.898 32+6.846
33+6.765 34+6.722 35+6.681 36+6.611 37+6.722 38+6.919 39+07.07 40+07.41
41+07.85 42+08.27 43+6.860 44+6.910 45+6.855 46+6.814 47+6.770 48+6.704
49+6.643 50+6.689 51+6.792 52+6.928 53+07.03 54+07.42 55+07.84 56+08.24
57+6.396 58+12.29
01+0122. 02+0079. 03+0100. 04+6.628 05-2.582 06-0.051 07-0.653 08-0.089
09-0.666 10-0.095 11-0.327 12+0.028 13+1.660 14+0.000 15+6.657 16+6.652
17+6.646 18+6.559 19+6.560 20+6.530 21+6.505 22+6.558 23+6.652 24+6.817
25+6.971 26+07.29 27+07.70 28+08.12 29+6.857 30+6.769 31+6.861 32+6.824
33+6.763 34+6.733 35+6.701 36+6.631 37+6.738 38+6.909 39+07.05 40+07.40
41+07.84 42+08.26 43+6.803 44+6.862 45+6.828 46+6.804 47+6.772 48+6.716
49+6.662 50+6.708 51+6.806 52+6.922 53+07.02 54+07.42 55+07.84 56+08.24
57+6.271 58+12.39
01+0122. 02+0079. 03+0200. 04+6.386 05-1.785 06-0.054 07-1.217 08-0.518
09-1.047 10-0.479 11-0.662 12-0.183 13+1.982 14+0.000 15+6.617 16+6.597
17+6.616 18+6.549 19+6.557 20+6.538 21+6.519 22+6.570 23+6.648 24+6.797
25+6.962 26+07.27 27+07.69 28+08.11 29+6.784 30+6.663 31+6.806 32+6.783
33+6.739 34+6.721 35+6.698 36+6.642 37+6.734 38+6.901 39+07.05 40+07.39
41+07.83 42+08.26 43+6.718 44+6.803 45+6.775 46+6.763 47+6.746 48+6.709
49+6.665 50+6.710 51+6.796 52+6.911 53+07.01 54+07.41 55+07.83 56+08.23
57+5.958 58+12.36
01+0122. 02+0079. 03+0300. 04+6.120 05-1.977 06-0.058 07-2.020 08-1.026
09-1.613 10-0.946 11-1.192 12-0.518 13+2.392 14+0.000 15+6.574 16+6.526
17+6.585 18+6.523 19+6.541 20+6.528 21+6.512 22+6.564 23+6.646 24+6.799
25+6.957 26+07.27 27+07.68 28+08.10 29+6.730 30+6.553 31+6.774 32+6.766
33+6.729 34+6.721 35+6.705 36+6.651 37+6.751 38+6.907 39+07.04 40+07.38
41+07.83 42+08.25 43+6.644 44+6.764 45+6.751 46+6.753 47+6.744 48+6.711
49+6.669 50+6.722 51+6.804 52+6.912 53+07.00 54+07.40 55+07.83 56+08.22
57+5.674 58+12.42
01+0122. 02+0079. 03+0400. 04+5.839 05-2.552 06-0.058 07-2.931 08-1.769
09-2.264 10-1.634 11-1.798 12-1.012 13+1.980 14+0.000 15+6.531 16+6.456

17+6.555 18+6.506 19+6.532 20+6.525 21+6.515 22+6.570 23+6.649 24+6.793
25+6.949 26+07.26 27+07.68 28+08.10 29+6.666 30+6.448 31+6.731 32+6.736
33+6.712 34+6.713 35+6.707 36+6.658 37+6.751 38+6.907 39+07.04 40+07.37
41+07.82 42+08.24 43+6.564 44+6.717 45+6.719 46+6.734 47+6.736 48+6.708
49+6.673 50+6.727 51+6.811 52+6.913 53+07.00 54+07.39 55+07.82 56+08.22
57+5.483 58+12.40
01+0122. 02+0079. 03+0500. 04+5.647 05-3.009 06-0.064 07-2.866 08-2.048
09-2.214 10-1.950 11-1.684 12-1.288 13+1.383 14+0.000 15+6.492 16+6.402
17+6.530 18+6.488 19+6.523 20+6.521 21+6.517 22+6.577 23+6.653 24+6.789
25+6.940 26+07.25 27+07.67 28+08.09 29+6.620 30+6.420 31+6.698 32+6.714
33+6.703 34+6.715 35+6.713 36+6.667 37+6.764 38+6.908 39+07.04 40+07.37
41+07.82 42+08.24 43+6.508 44+6.682 45+6.696 46+6.721 47+6.732 48+6.713
49+6.684 50+6.740 51+6.827 52+6.923 53+07.00 54+07.39 55+07.82 56+08.22
57+5.420 58+12.38
01+0122. 02+0079. 03+0600. 04+5.528 05-4.116 06-0.064 07-3.056 08-2.266
09-2.329 10-2.119 11-1.864 12-1.486 13+1.646 14+0.000 15+6.454 16+6.345
17+6.500 18+6.467 19+6.513 20+6.515 21+6.513 22+6.582 23+6.649 24+6.781
25+6.929 26+07.23 27+07.67 28+08.09 29+6.577 30+6.345 31+6.661 32+6.689
33+6.686 34+6.707 35+6.711 36+6.676 37+6.772 38+6.913 39+07.05 40+07.37
41+07.82 42+08.24 43+6.459 44+6.641 45+6.667 46+6.707 47+6.723 48+6.711
49+6.686 50+6.750 51+6.839 52+6.931 53+07.01 54+07.39 55+07.82 56+08.22
57+5.493 58+12.37
01+0122. 02+0079. 03+0700. 04+5.542 05-5.222 06-0.053 07-4.018 08-2.720
09-3.047 10-2.536 11-2.419 12-1.749 13+2.780 14+0.000 15+6.436 16+6.317
17+6.486 18+6.459 19+6.512 20+6.521 21+6.529 22+6.601 23+6.668 24+6.793
25+6.936 26+07.24 27+07.67 28+08.10 29+6.534 30+6.266 31+6.638 32+6.673
33+6.680 34+6.712 35+6.722 36+6.691 37+6.790 38+6.924 39+07.06 40+07.38
41+07.82 42+08.25 43+6.414 44+6.615 45+6.653 46+6.698 47+6.726 48+6.713
49+6.697 50+6.760 51+6.860 52+6.950 53+07.02 54+07.40 55+07.83 56+08.23
57+5.643 58+12.35
01+0122. 02+0079. 03+0800. 04+5.626 05-5.104 06+0.071 07-5.198 08-3.544
09-3.952 10-3.243 11-3.351 12-2.280 13+3.171 14+0.000 15+6.416 16+6.277
17+6.475 18+6.456 19+6.517 20+6.531 21+6.539 22+6.613 23+6.684 24+6.810
25+6.947 26+07.24 27+07.68 28+08.10 29+6.483 30+6.145 31+6.604 32+6.651
33+6.666 34+6.703 35+6.718 36+6.700 37+6.806 38+6.934 39+07.07 40+07.38
41+07.82 42+08.25 43+6.354 44+6.581 45+6.626 46+6.684 47+6.715 48+6.715
49+6.700 50+6.772 51+6.871 52+6.953 53+07.02 54+07.40 55+07.83 56+08.23
57+5.663 58+12.33
01+0122. 02+0079. 03+0900. 04+5.754 05+4.411 06+1.663 07-3.903 08-3.515
09-3.046 10-3.363 11-2.803 12-2.453 13+2.528 14+0.000 15+6.403 16+6.291
17+6.466 18+6.456 19+6.521 20+6.539 21+6.548 22+6.628 23+6.698 24+6.814
25+6.957 26+07.24 27+07.68 28+08.11 29+6.463 30+6.215 31+6.584 32+6.636
33+6.660 34+6.704 35+6.724 36+6.709 37+6.814 38+6.948 39+07.08 40+07.39
41+07.83 42+08.25 43+6.385 44+6.562 45+6.611 46+6.675 47+6.715 48+6.713
49+6.707 50+6.782 51+6.892 52+6.978 53+07.04 54+07.40 55+07.84 56+08.23
57+5.896 58+12.32
01+0122. 02+0079. 03+1000. 04+6.014 05+23.56 06+4.799 07-2.385 08-2.507
09-2.045 10-2.509 11-1.878 12-1.889 13+3.115 14+0.000 15+6.420 16+6.393
17+6.471 18+6.456 19+6.528 20+6.547 21+6.562 22+6.651 23+6.714 24+6.824
25+6.964 26+07.24 27+07.70 28+08.13 29+6.485 30+6.354 31+6.579 32+6.629
33+6.654 34+6.709 35+6.732 36+6.722 37+6.833 38+6.956 39+07.10 40+07.40
41+07.84 42+08.26 43+6.515 44+6.578 45+6.605 46+6.669 47+6.711 48+6.709
49+6.709 50+6.788 51+6.911 52+6.996 53+07.05 54+07.41 55+07.85 56+08.24

57+6.128 58+12.54
01+0122. 02+0079. 03+1100. 04+6.342 05+44.70 06+08.38 07-1.276 08-1.634
09-1.241 10-1.666 11-1.156 12-1.320 13+3.600 14+0.000 15+6.489 16+6.560
17+6.517 18+6.493 19+6.563 20+6.582 21+6.595 22+6.682 23+6.741 24+6.848
25+6.987 26+07.26 27+07.71 28+08.15 29+6.564 30+6.550 31+6.606 32+6.642
33+6.664 34+6.714 35+6.738 36+6.738 37+6.854 38+6.977 39+07.12 40+07.42
41+07.85 42+08.27 43+6.694 44+6.636 45+6.629 46+6.676 47+6.710 48+6.712
49+6.718 50+6.799 51+6.928 52+07.01 53+07.07 54+07.42 55+07.85 56+08.25
57+6.288 58+13.31
01+0122. 02+0079. 03+1200. 04+6.666 05+077.9 06+14.29 07+1.943 08-0.151
09+0.784 10-0.424 11+0.519 12-0.496 13+3.021 14+0.000 15+6.569 16+6.788
17+6.566 18+6.517 19+6.589 20+6.609 21+6.618 22+6.715 23+6.782 24+6.874
25+07.01 26+07.27 27+07.73 28+08.16 29+6.675 30+6.887 31+6.652 32+6.669
33+6.685 34+6.737 35+6.765 36+6.762 37+6.878 38+6.995 39+07.14 40+07.43
41+07.86 42+08.28 43+6.972 44+6.725 45+6.663 46+6.696 47+6.729 48+6.724
49+6.732 50+6.820 51+6.954 52+07.04 53+07.09 54+07.42 55+07.86 56+08.25
57+6.475 58+13.71
01+0122. 02+0079. 03+1300. 04+6.981 05+084.5 06+15.78 07+4.154 08+2.063
09+2.258 10+1.571 11+1.973 12+0.870 13+3.043 14+0.000 15+6.689 16+07.06
17+6.634 18+6.565 19+6.624 20+6.643 21+6.644 22+6.743 23+6.811 24+6.912
25+07.04 26+07.30 27+07.75 28+08.18 29+6.842 30+07.23 31+6.726 32+6.708
33+6.703 34+6.749 35+6.774 36+6.776 37+6.901 38+07.02 39+07.17 40+07.44
41+07.87 42+08.28 43+07.30 44+6.858 45+6.728 46+6.722 47+6.743 48+6.730
49+6.735 50+6.827 51+6.974 52+07.06 53+07.11 54+07.43 55+07.86 56+08.26
57+6.441 58+14.09
01+0122. 02+0079. 03+1400. 04+07.37 05+111.9 06+20.66 07+07.23 08+4.075
09+4.309 10+3.355 11+3.961 12+2.255 13+2.769 14+0.000 15+6.837 16+07.38
17+6.737 18+6.623 19+6.667 20+6.678 21+6.674 22+6.777 23+6.844 24+6.930
25+07.06 26+07.32 27+07.78 28+08.21 29+07.06 30+07.66 31+6.847 32+6.782
33+6.745 34+6.780 35+6.800 36+6.793 37+6.923 38+07.04 39+07.20 40+07.48
41+07.89 42+08.30 43+07.69 44+07.03 45+6.827 46+6.778 47+6.771 48+6.749
49+6.744 50+6.838 51+07.00 52+07.08 53+07.13 54+07.46 55+07.88 56+08.27
57+6.844 58+14.41
01+0122. 02+0079. 03+1500. 04+08.04 05+168.1 06+30.38 07+11.92 08+6.854
09+07.05 10+5.758 11+6.650 12+4.185 13+2.650 14+0.000 15+07.05 16+07.82
17+6.877 18+6.718 19+6.742 20+6.736 21+6.723 22+6.828 23+6.893 24+6.952
25+07.09 26+07.34 27+07.85 28+08.28 29+07.37 30+08.32 31+07.02 32+6.894
33+6.825 34+6.842 35+6.849 36+6.817 37+6.956 38+07.07 39+07.26 40+07.54
41+07.96 42+08.34 43+08.24 44+07.26 45+6.973 46+6.875 47+6.835 48+6.779
49+6.768 50+6.856 51+07.06 52+07.14 53+07.19 54+07.49 55+07.93 56+08.30
57+07.89 58+14.38
01+0122. 02+0079. 03+1600. 04+09.85 05+294.1 06+55.43 07+26.62 08+15.08
09+15.34 10+12.14 11+14.92 12+09.11 13+3.013 14+0.000 15+07.43 16+08.99
17+07.12 18+6.850 19+6.851 20+6.816 21+6.746 22+6.858 23+6.909 24+6.875
25+07.02 26+07.25 27+07.98 28+08.42 29+07.98 30+09.90 31+07.32 32+07.09
33+6.916 34+6.916 35+6.895 36+6.764 37+6.911 38+07.00 39+07.38 40+07.67
41+08.08 42+08.44 43+09.75 44+07.71 45+07.17 46+6.991 47+6.901 48+6.735
49+6.719 50+6.785 51+07.20 52+07.29 53+07.32 54+07.58 55+08.02 56+08.39
57+10.31 58+13.77

APPENDIX D

NEURAL NETWORK COEFFICIENT INFORMATION

Final Neural Network Configuration

Neural Network Model: Backpropagation

Learning Rule: Delta Rule

Transfer Function: Hyperbolic Tangent

Network Ranges: Input -5.0 to +5.0
Output -0.01 to 0.01

Learning Coefficients for 15 cm depth:

Output Layer	Learn Count	10000	30000	70000	150000	310000
	Coefficient 1	0.3	0.2	0	0	0
	Coefficient 2	0.15	0.05	0	0	0
	Coefficient 3	0.1	0.1	0	0	0
Hidden Layer	Learn Count	10000	30000	70000	150000	310000
	Coefficient 1	0.6	0.4	0	0	0
	Coefficient 2	0.2	0.1	0	0	0
	Coefficient 3	0.1	0.1	0	0	0
Input Layer	Learn Count	5000				
	Coefficient 1	0.9				
	Coefficient 2	0.6				
	Coefficient 3	0				

Learning Coefficients for 30 cm depth:

Output Layer	Learn Count	10000	30000	70000	150000	310000
	Coefficient 1	0.15	0.075	0	0	0
	Coefficient 2	0.4	0.2	0	0	0
	Coefficient 3	0.1	0.1	0	0	0
Hidden Layer	Learn Count	10000	30000	70000	150000	310000
	Coefficient 1	0.9	0.45	0	0	0
	Coefficient 2	0.4	0.2	0	0	0
	Coefficient 3	0.1	0.1	0	0	0
Input Layer	Learn Count	5000				
	Coefficient 1	0.9				
	Coefficient 2	0.6				
	Coefficient 3	0				

Final Neural Network Configuration

Neural Network Model: Backpropagation

Learning Rule: Delta Rule

Transfer Function: Hyperbolic Tangent

Network Ranges: Input -5.0 to +5.0
Output -0.01 to 0.01

Learning Coefficients for 60 cm depth:

Output Layer	Learn Count	10000	30000	70000	150000	310000
	Coefficient 1	0.15	0.075	0	0	0
	Coefficient 2	0.4	0.2	0	0	0
	Coefficient 3	0.1	0.1	0	0	0
Hidden Layer	Learn Count	10000	30000	70000	150000	310000
	Coefficient 1	0.3	0.15	0	0	0
	Coefficient 2	0.4	0.2	0	0	0
	Coefficient 3	0.1	0.1	0	0	0
Input Layer	Learn Count	5000				
	Coefficient 1	0.9				
	Coefficient 2	0.6				
	Coefficient 3	0				

Learning Coefficients for 120 cm depth:

Output Layer	Learn Count	10000	30000	70000	150000	310000
	Coefficient 1	0.15	0.075	0	0	0
	Coefficient 2	0.4	0.2	0	0	0
	Coefficient 3	0.1	0.1	0	0	0
Hidden Layer	Learn Count	10000	30000	70000	150000	310000
	Coefficient 1	0.3	0.15	0	0	0
	Coefficient 2	0.4	0.2	0	0	0
	Coefficient 3	0.1	0.1	0	0	0
Input Layer	Learn Count	5000				
	Coefficient 1	0.9				
	Coefficient 2	0.6				
	Coefficient 3	0				

APPENDIX E

PROCESSING ELEMENT INFORMATION
(Weights, Connections, Summations, Etc.)

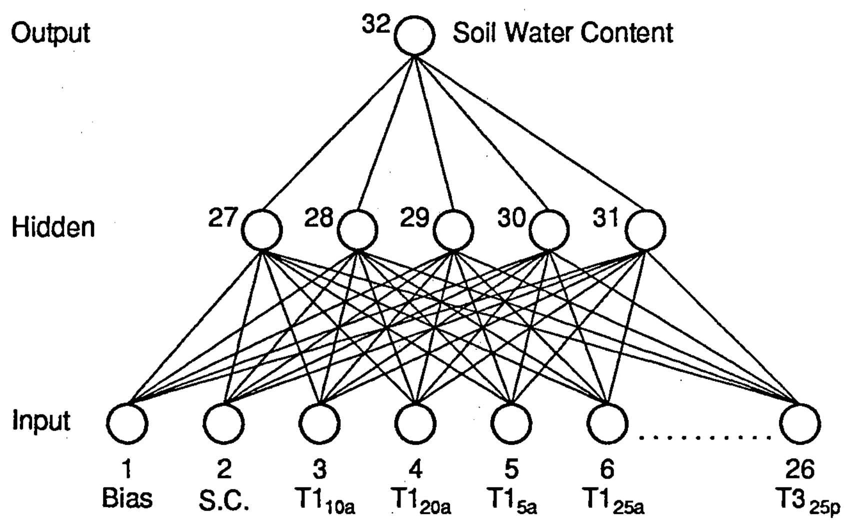

Neural Network Processing Elements and Connections

Depth=15 cm				Processing Element Information						
Bias			PE 2			PE 3			PE 4	
Sum	0		Sum	5		Sum	-4.247		Sum	-4.247
Transfer	1		Transfer	5		Transfer	-4.247		Transfer	-4.247
Output	1		Output	5		Output	-4.247		Output	-4.247
PE 5			PE 6			PE 7			PE 8	
Sum	-4.247		Sum	-4.247		Sum	-4.247		Sum	-4.247
Transfer	-4.247		Transfer	-4.247		Transfer	-4.247		Transfer	-4.247
Output	-4.247		Output	-4.247		Output	-4.247		Output	-4.247
PE 9			PE 10			PE 11			PE 12	
Sum	-4.247		Sum	-4.247		Sum	-4.247		Sum	-4.247
Transfer	-4.247		Transfer	-4.247		Transfer	-4.247		Transfer	-4.247
Output	-4.247		Output	-4.247		Output	-4.247		Output	-4.247
PE 13			PE 14			PE 15			PE 16	
Sum	-4.247		Sum	-4.247		Sum	-4.247		Sum	-4.247
Transfer	-4.247		Transfer	-4.247		Transfer	-4.247		Transfer	-4.247
Output	-4.247		Output	-4.247		Output	-4.247		Output	-4.247
PE 17			PE 18			PE 19			PE 20	
Sum	-4.247		Sum	-4.247		Sum	-4.247		Sum	-4.247
Transfer	-4.247		Transfer	-4.247		Transfer	-4.247		Transfer	-4.247
Output	-4.247		Output	-4.247		Output	-4.247		Output	-4.247
PE 21			PE 22			PE 23			PE 24	
Sum	-4.247		Sum	-4.247		Sum	-4.247		Sum	-4.247
Transfer	-4.247		Transfer	-4.247		Transfer	-4.247		Transfer	-4.247
Output	-4.247		Output	-4.247		Output	-4.247		Output	-4.247
PE 25			PE 26			PE 27			PE 28	
Sum	-4.247		Sum	-4.247		Sum	4.666		Sum	-7.243
Transfer	-4.247		Transfer	-4.247		Transfer	1		Transfer	-1
Output	-4.247		Output	-4.247		Output	1		Output	-1
PE 29			PE 30			PE 31			Output	
Sum	0.064		Sum	-0.087		Sum	5.92		Sum	0.003
Transfer	0.064		Transfer	-0.087		Transfer	1		Transfer	0.003
Output	0.064		Output	-0.087		Output	1		Output	0.003

Depth=15 cm							
PE 27			PE 28			PE 29	
Connection	Weight		Connection	Weight		Connection	Weight
bias	1.3140		bias	-0.9227		bias	0.0369
2	0.3447		2	-0.2217		2	0.0064
3	-1.5356		3	-1.9521		3	0.3385
4	-2.3618		4	-1.5278		4	0.5621
5	1.9600		5	0.1156		5	0.3501
6	1.4432		6	-0.2037		6	-0.3273
7	-0.4086		7	-2.0918		7	-0.2056
8	1.4710		8	0.5056		8	0.3738
9	-1.8366		9	1.9292		9	0.2535
10	-1.9437		10	-0.9049		10	-0.0635
11	1.2373		11	-0.7106		11	-0.4703
12	1.7703		12	0.3898		12	-0.1780
13	-0.8213		13	-0.5464		13	-0.0871
14	1.2025		14	2.0876		14	0.0449
15	-0.4967		15	-0.3142		15	0.8275
16	-1.5773		16	0.6355		16	0.6509
17	0.9979		17	-1.7210		17	0.4653
18	1.2154		18	0.0907		18	-0.7549
19	-0.0202		19	-1.4430		19	-0.1331
20	0.5766		20	1.2531		20	-0.4405
21	0.0858		21	-0.7796		21	0.4450
22	-1.2640		22	1.4012		22	-0.0775
23	-0.4302		23	1.0069		23	-0.4235
24	0.5627		24	1.4462		24	-0.6636
25	0.2316		25	0.4734		25	-0.0515
26	-0.4418		26	2.0786		26	-0.4340
PE 30			PE 31			Output	
Connection	Weight		Connection	Weight		Connection	Weight
bias	-0.0672		bias	0.8975		bias	0.0055
2	-0.0143		2	0.1553		27	-0.0034
3	-0.4555		3	-1.9528		28	-0.0053
4	-0.1175		4	-1.3089		29	-0.0020
5	0.1170		5	0.3238		30	0.0033
6	-0.0769		6	-0.2023		31	-0.0038
7	0.0721		7	-0.6029			
8	0.1598		8	1.4827			
9	-0.0987		9	1.0391			
10	-0.4964		10	-1.8021			
11	0.1667		11	0.5083			
12	0.2486		12	-0.1033			
13	-0.0227		13	0.5991			
14	0.1755		14	2.2727			
15	-0.4743		15	0.0841			
16	0.0330		16	0.5687			
17	-0.3082		17	-2.4206			
18	0.4312		18	-1.2344			
19	0.2064		19	-0.6181			
20	0.3286		20	0.6988			
21	-0.0373		21	0.0481			
22	-0.2482		22	0.2862			
23	0.0695		23	1.0036			
24	0.2059		24	-0.5959			
25	0.0054		25	-0.0136			
26	0.1038		26	0.9399			

Depth=30 cm				Processing Element Information						
Bias			PE 2			PE 3			PE 4	
Sum	0		Sum	7.2		Sum	0.428		Sum	0.071
Transfer	1		Transfer	7.2		Transfer	0.428		Transfer	0.071
Output	1		Output	7.2		Output	0.428		Output	0.071
PE 5			PE 6			PE 7			PE 8	
Sum	0.644		Sum	0.283		Sum	0.796		Sum	0.368
Transfer	0.644		Transfer	0.283		Transfer	0.796		Transfer	0.368
Output	0.644		Output	0.283		Output	0.796		Output	0.368
PE 9			PE 10			PE 11			PE 12	
Sum	0.428		Sum	-0.167		Sum	0.599		Sum	0.019
Transfer	0.428		Transfer	-0.167		Transfer	0.599		Transfer	0.019
Output	0.428		Output	-0.167		Output	0.599		Output	0.019
PE 13			PE 14			PE 15			PE 16	
Sum	0.785		Sum	0.1		Sum	0.331		Sum	0.011
Transfer	0.785		Transfer	0.1		Transfer	0.331		Transfer	0.011
Output	0.785		Output	0.1		Output	0.331		Output	0.011
PE 17			PE 18			PE 19			PE 20	
Sum	0.454		Sum	0.134		Sum	0.644		Sum	0.231
Transfer	0.454		Transfer	0.134		Transfer	0.644		Transfer	0.231
Output	0.454		Output	0.134		Output	0.644		Output	0.231
PE 21			PE 22			PE 23			PE 24	
Sum	0.841		Sum	-0.13		Sum	1.053		Sum	0
Transfer	0.841		Transfer	-0.13		Transfer	1.053		Transfer	0
Output	0.841		Output	-0.13		Output	1.053		Output	0
PE 25			PE 26			PE 27			PE 28	
Sum	1.302		Sum	0.082		Sum	2.305		Sum	0.263
Transfer	1.302		Transfer	0.082		Transfer	0.98		Transfer	0.257
Output	1.302		Output	0.082		Output	0.98		Output	0.257
PE 29			PE 30			PE 31			Output	
Sum	0.025		Sum	1.397		Sum	-4.999		Sum	0.106
Transfer	0.025		Transfer	0.885		Transfer	-1		Transfer	0.106
Output	0.025		Output	0.885		Output	-1		Output	0.106

Depth=30 cm							
PE 27			PE 28			PE 29	
Connection	Weight		Connection	Weight		Connection	Weight
bias	0.2990		bias	-1.3673		bias	-0.7761
2	-0.0495		2	0.0327		2	0.0719
3	0.3811		3	0.0194		3	-0.0534
4	-0.4441		4	-0.1573		4	-0.2101
5	0.4295		5	-0.0011		5	-0.0701
6	-0.1362		6	-0.0086		6	-0.0510
7	0.1643		7	-0.0290		7	-0.1012
8	-0.2438		8	-0.0414		8	-0.1334
9	0.3294		9	0.2239		9	0.1028
10	-0.6450		10	-0.1105		10	-0.2508
11	0.3583		11	0.1255		11	0.2052
12	-0.1214		12	-0.1525		12	-0.3520
13	0.2416		13	0.1303		13	0.2009
14	-0.8898		14	-0.3993		14	-0.2368
15	0.2406		15	0.4728		15	0.0197
16	-0.3788		16	0.1907		16	-0.0540
17	0.3244		17	0.5669		17	0.2042
18	-0.0630		18	0.2660		18	0.0680
19	0.1405		19	0.4200		19	0.1045
20	-0.1110		20	0.3650		20	-0.0251
21	0.3910		21	0.2612		21	0.0321
22	-0.6545		22	0.0656		22	-0.2294
23	0.4700		23	0.1138		23	0.0506
24	-0.4707		24	0.2002		24	-0.2214
25	0.2078		25	0.0562		25	-0.0600
26	-0.8426		26	-0.2492		26	-0.3271
PE 30			PE 31			Output	
Connection	Weight		Connection	Weight		Connection	Weight
bias	-0.6196		bias	0.2059		bias	0.0888
2	0.1368		2	-0.3474		27	0.0685
3	0.0503		3	-0.1533		28	0.0839
4	-0.1183		4	-0.1339		29	0.0476
5	-0.0460		5	-0.1663		30	-0.0764
6	-0.1375		6	-0.2021		31	0.0051
7	0.0241		7	-0.2617			
8	-0.2184		8	-0.0394			
9	0.2179		9	-0.4162			
10	-0.1839		10	-0.1247			
11	0.1487		11	-0.4520			
12	-0.1675		12	-0.0554			
13	0.1891		13	-0.3005			
14	-0.0762		14	-0.0285			
15	0.1862		15	-0.1902			
16	-0.0926		16	-0.0743			
17	0.0330		17	-0.3015			
18	-0.0007		18	-0.1752			
19	0.0921		19	0.3495			
20	-0.0965		20	-0.1945			
21	0.2933		21	-0.3072			
22	-0.1808		22	-0.1843			
23	0.1013		23	-0.3873			
24	-0.1995		24	-0.0983			
25	0.2467		25	-0.3212			
26	-0.1564		26	-0.1588			

Depth=60 cm				Processing Element Information			
Bias		PE 2		PE 3		PE 4	
Sum	0	Sum	-1	Sum	-0.336	Sum	-0.347
Transfer	1	Transfer	-1	Transfer	-0.336	Transfer	-0.347
Output	1	Output	-1	Output	-0.336	Output	-0.347
PE 5		PE 6		PE 7		PE 8	
Sum	-0.318	Sum	-0.336	Sum	-0.325	Sum	-0.343
Transfer	-0.318	Transfer	-0.336	Transfer	-0.325	Transfer	-0.343
Output	-0.318	Output	-0.336	Output	-0.325	Output	-0.343
PE 9		PE 10		PE 11		PE 12	
Sum	-0.317	Sum	-0.354	Sum	-0.29	Sum	-0.347
Transfer	-0.317	Transfer	-0.354	Transfer	-0.29	Transfer	-0.347
Output	-0.317	Output	-0.354	Output	-0.29	Output	-0.347
PE 13		PE 14		PE 15		PE 16	
Sum	-0.304	Sum	-0.348	Sum	0.329	Sum	-0.337
Transfer	-0.304	Transfer	-0.348	Transfer	-0.329	Transfer	-0.337
Output	-0.304	Output	-0.348	Output	-0.329	Output	-0.337
PE 17		PE 18		PE 19		PE 20	
Sum	-0.313	Sum	-0.319	Sum	-0.313	Sum	-0.326
Transfer	-0.313	Transfer	-0.319	Transfer	-0.313	Transfer	-0.326
Output	-0.313	Output	-0.319	Output	-0.313	Output	-0.326
PE 21		PE 22		PE 23		PE 24	
Sum	-0.333	Sum	-0.347	Sum	-0.322	Sum	-0.329
Transfer	-0.333	Transfer	-0.347	Transfer	-0.322	Transfer	-0.329
Output	-0.333	Output	-0.347	Output	-0.322	Output	-0.329
PE 25		PE 26		PE 27		PE 28	
Sum	-0.326	Sum	-0.332	Sum	-0.009	Sum	0.091
Transfer	-0.326	Transfer	-0.332	Transfer	-0.009	Transfer	0.091
Output	-0.326	Output	-0.332	Output	-0.009	Output	0.091
PE 29		PE 30		PE 31		Output	
Sum	-0.052	Sum	-1.179	Sum	0.713	Sum	0.228
Transfer	-0.052	Transfer	-0.827	Transfer	0.612	Transfer	0.224
Output	-0.052	Output	-0.827	Output	0.612	Output	0.224

Depth=60 cm							
PE 27			PE 28			PE 29	
Connection	Weight		Connection	Weight		Connection	Weight
bias	0.0005		bias	-0.458		bias	0.5035
2	0.0015		2	-0.088		2	0.0512
3	0.0503		3	-0.090		3	0.0129
4	0.1053		4	-0.221		4	0.2782
5	-0.0721		5	0.104		5	-0.0018
6	-0.0329		6	-0.236		6	0.1798
7	0.0767		7	-0.097		7	0.0223
8	0.0695		8	-0.251		8	0.2191
9	0.0759		9	0.193		9	-0.1424
10	0.0434		10	-0.242		10	0.3025
11	0.0284		11	0.227		11	-0.2940
12	-0.0583		12	-0.260		12	0.3690
13	0.0915		13	0.257		13	-0.2805
14	0.0819		14	-0.339		14	0.2217
15	0.0147		15	-0.016		15	-0.0272
16	-0.0829		16	-0.135		16	0.2351
17	-0.0913		17	0.097		17	-0.0368
18	0.0445		18	-0.182		18	0.1625
19	-0.0652		19	0.050		19	0.0073
20	-0.0190		20	-0.066		20	0.2075
21	-0.0309		21	0.173		21	-0.3300
22	0.0060		22	-0.271		22	0.3223
23	-0.0183		23	0.278		23	-0.1790
24	-0.0640		24	-0.235		24	0.3732
25	-0.0538		25	0.274		25	-0.3439
26	-0.0824		26	-0.253		26	0.1690
PE 30			PE 31			Output	
bias	0.1516		bias	0.396		bias	0.0404
2	0.1543		2	-0.031		27	0.0068
3	-0.1023		3	-0.285		28	-0.2913
4	0.2704		4	0.136		29	0.3335
5	-0.2003		5	-0.523		30	-0.5229
6	0.1416		6	0.002		31	-0.3289
7	0.1637		7	-0.084			
8	0.2731		8	0.081			
9	-0.3461		9	-0.693			
10	0.6864		10	0.750			
11	-0.4629		11	-0.794			
12	0.6123		12	0.675			
13	-0.2477		13	-0.653			
14	0.7881		14	0.582			
15	-0.1048		15	-0.339			
16	0.2129		16	0.104			
17	-0.2047		17	-0.512			
18	0.3078		18	-0.073			
19	0.2929		19	0.074			
20	0.2499		20	0.267			
21	-0.2541		21	-0.471			
22	0.5830		22	0.523			
23	-0.2938		23	-0.808			
24	0.5392		24	0.654			
25	-0.2270		25	-0.506			
26	0.6155		26	0.631			

Depth=120 cm			Processing Element Information								
Bias			PE 2			PE 3			PE 4		
Sum	0		Sum	-1		Sum	-0.098		Sum	-0.084	
Transfer	1		Transfer	-1		Transfer	-0.098		Transfer	-0.084	
Output	1		Output	-1		Output	-0.098		Output	-0.084	
PE 5			PE 6			PE 7			PE 8		
Sum	-0.091		Sum	-0.079		Sum	-0.09		Sum	-0.076	
Transfer	-0.091		Transfer	-0.079		Transfer	-0.09		Transfer	-0.076	
Output	-0.091		Output	-0.079		Output	-0.09		Output	-0.076	
PE 9			PE 10			PE 11			PE 12		
Sum	-0.069		Sum	-0.051		Sum	-0.065		Sum	-0.05	
Transfer	-0.069		Transfer	-0.051		Transfer	-0.065		Transfer	-0.05	
Output	-0.069		Output	-0.051		Output	-0.065		Output	-0.05	
PE 13			PE 14			PE 15			PE 16		
Sum	-0.059		Sum	-0.044		Sum	0.673		Sum	1.381	
Transfer	-0.059		Transfer	-0.044		Transfer	0.587		Transfer	0.881	
Output	-0.059		Output	-0.044		Output	0.587		Output	0.881	
PE 17			PE 18			PE 19			PE 20		
Sum	0.433		Sum	-0.179		Sum	-0.062		Sum	1.046	
Transfer	0.408		Transfer	-0.177		Transfer	-0.062		Transfer	0.78	
Output	0.408		Output	-0.177		Output	-0.062		Output	0.78	

Depth=120 cm							
PE 15			PE 16			PE 17	
Connection	Weight		Connection	Weight		Connection	Weight
bias	-2.5744		bias	-0.4088		bias	0.405
2	-2.3817		2	-1.6257		2	-0.171
3	-0.4084		3	-0.0467		3	0.5718
4	-2.3485		4	-0.4625		4	-0.3708
5	-0.1526		5	0.0036		5	0.9261
6	-1.7379		6	-0.5616		6	-0.0413
7	-0.269		7	0.0848		7	0.4924
8	-2.1522		8	-0.7112		8	0.188
9	-0.4245		9	0.2365		9	0.0682
10	-2.1407		10	-0.318		10	-0.8539
11	0.0297		11	0.068		11	0.5616
12	-1.5514		12	-0.4812		12	-0.3828
13	0.1172		13	0.3575		13	0.1871
14	-1.8537		14	-0.4957		14	-0.2607
PE 18			PE 19			Output	
Connection			Connection	Weight		Connection	Weight
bias	-0.1014		bias	1.8978		bias	0.2585
2	0.0776		2	1.795		15	0.8689
3	0.0594		3	1.1933		16	0.5956
4	0.0266		4	-0.9999		17	-0.4412
5	0.0809		5	1.4055		18	-0.0423
6	0.0253		6	-1.2821		19	1.2017
7	-0.1079		7	1.1883			
8	0.0424		8	-1.2846			
9	-0.1046		9	1.2443			
10	0.0272		10	-1.0047			
11	0.0108		11	1.4245			
12	-0.0231		12	-1.0162			
13	-0.0476		13	1.2554			
14	-0.0326		14	-1.2103			

APPENDIX F

C CODE OF NEURAL NETWORK MODEL

/*This is a PC version for the final combined neural network model, which can estimate the same predicted water content values as when run with NeuralWare. The input file name is "test.nna" and the result is stored in a file called "test.nnr". The parameters extracted from the trained combined model by NeuralWare are included in the files named "weight.dat" and "cmimat.dat". These two files should be in the working directory when the program is run. This version can be supported by almost all C compilers since it is system independent.*/

```
#include <stdio.h>
#include <math.h>
#define numlayers 3

FILE *fp1,*fp2,*fp3,*fp4;
int layer, node, i, plant;
float tan_h();
float sum, out,minsum,maxsum;
int max[30],min[30];
float max_m,min_m;
float measured;
int numnodes[4];
        /* numnodes array contains number of nodes in each layer,  */
        /* including input layer.  */
float nodeout[4][26];
        /* nodeout array contains node outputs. */
        /* indices are [layer#][node#]. */
float weight[4][5][26] ;
        /* Array 'weight' contains node weights. */
        /* Indices are [layer#][node#][weight#]. */
        /* First weight for each node is the bias weight. */
        /* The other 3 are the weights on the inputs from the previous layer. */

int main()
{
  int i;
  float high,low,offset,scale;
  float high_o,low_o;
  fp1 = fopen("weight.dat","r");
  fp2 = fopen("test.nna","r");
  if ((fp3 = fopen("test.nnr","w")) == NULL)
    printf("file open error\n");

  numnodes[0] = 25;
  numnodes[1] = 5;
  numnodes[2] = 1;
  high = 5.0;
```

```
  low = -5.0;
  high_o = 0.01;
  low_o = -0.01;
/* Following section defines neural network inputs. */
   input_weight();
   input_mintable();
   while(!feof(fp2))
   {
       input_test();
       for (i = 0; i < 25; i++)
       {
          scale = (high - low) / (max[i] - min[i]);
          offset = (max[i] * low - min[i] * high) / (max[i] - min[i]);
          nodeout[0][i] = nodeout[0][i] * scale + offset;
       }

/* Following section passes inputs through network. */
   for (layer = 1 ; layer < numlayers ; layer++)
   {
       for (node = 0 ; node < numnodes[layer] ; node++)
       {
          sum = 1.0 * weight[layer][node][0];   /* initialize sum with bias */
          for (i = 1 ; i <=  numnodes[layer-1] ; i++)
             sum = sum + nodeout[layer-1][i-1] * weight[layer][node][i];
          nodeout[layer][node] = tan_h(sum);
/*       printf("nodeout = %f \n",nodeout[layer][node]);*/
                      /* nodeout[layer][node] = tanh(sum); */
       }
   }
/* Following section scales output. */
   scale = (0.4 - 0) / (high_o - low_o);
   offset = (0.01 * 0 - (-0.01) * 0.4) / (high_o - low_o);
   out = nodeout[2][0] * scale + offset;
/*   printf("out = %f\n",out);*/
   out_result();
   }
   fclose(fp1);
   fclose(fp2);
   fclose(fp3);



}
/*read weight data from weight file*/
input_weight()
```

```
{
   int i,j,k;

   for ( i = 1; i < numlayers; i++)
      for (j = 0; j < numnodes[i]; j++)
         for (k = 0; k <= numnodes[i-1]; k++)
            fscanf(fp1,"%f",&weight[i][j][k]);
}
/*input test data from test file*/
input_test()
{
   int i;

   for (i = 0; i < 25; i++)
      fscanf(fp2,"%f",&nodeout[0][i]);
   fscanf(fp2,"%f",&measured);
}
/*output test result to result file */
out_result()
{
   int i;

   fprintf(fp3,"          %f      %f\n",measured,out);
}
/* input min-max table */
input_mintable()
{

   int i;

   fp4 = fopen("cmimat.dat","r");
   for (i = 0; i < 25; i++)
      fscanf(fp4,"%d %d",&min[i],&max[i]);
   fscanf(fp4,"%f %f",&min_m,&max_m);
   fclose(fp4);
}
/* calculate hyper tangent */
float tan_h(x)
float x;
{
   float y;

   y = (exp(x) - exp(-x)) / (exp(x) + exp(-x));
   return(y);
}
```

APPENDIX G

FOURIER ANALYSIS PERIODOGRAMS

Efaw
SERIES IS TRANSFORMED
SERIES HAS BEEN TRUNCATED TO 128 NONMISSING CASES

FOURIER COMPONENTS OF RES15

INDEX	FREQUENCY	REAL	IMAGINARY	MAGNITUDE	PHASE	PERIODOGRAM
1	0.00000	-0.002	0.000	0.002	0.000	.668705E-03
2	0.00781	-0.002	0.003	0.004	-1.066	0.004
3	0.01563	0.004	-0.003	0.005	-0.622	0.007
4	0.02344	0.006	0.002	0.006	0.404	0.010
5	0.03125	.474050E-03	0.001	0.001	1.188	.411436E-03
6	0.03906	-.470628E-03	0.002	0.002	-1.376	0.002
7	0.04688	-0.006	0.002	0.007	-0.301	0.012
8	0.05469	0.002	-0.004	0.005	-1.141	0.006
9	0.06250	-0.002	.190733E-03	0.002	-0.120	.646298E-03
10	0.07031	0.003	-.144712E-03	0.003	-0.055	0.002
11	0.07813	-0.004	0.003	0.005	-0.715	0.007
12	0.08594	0.001	-0.003	0.004	-1.162	0.003
13	0.09375	-0.001	.361852E-03	0.002	-0.240	.592694E-03
14	0.10156	0.001	.482382E-03	0.002	0.324	.589186E-03
15	0.10938	0.002	0.001	0.002	0.676	0.001

SERIES IS TRANSFORMED
PLOT OF RES15
NUMBER OF CASES = 128
MEAN OF SERIES = .482415E-05
STANDARD DEVIATION OF SERIES = .880413E-05

SEQUENCE PLOT OF SERIES

CASE VALUE .265787E-08 .461923E-04

CASE	VALUE
1	.261213E-05
2	.139324E-04
3	.259180E-04
4	.381847E-04
5	.160717E-05
6	.593467E-05
7	.461923E-04
8	.241215E-04
9	.252460E-05
10	.685853E-05
11	.279578E-04
12	.131719E-04
13	.231521E-05
14	.230151E-05
15	.494408E-05

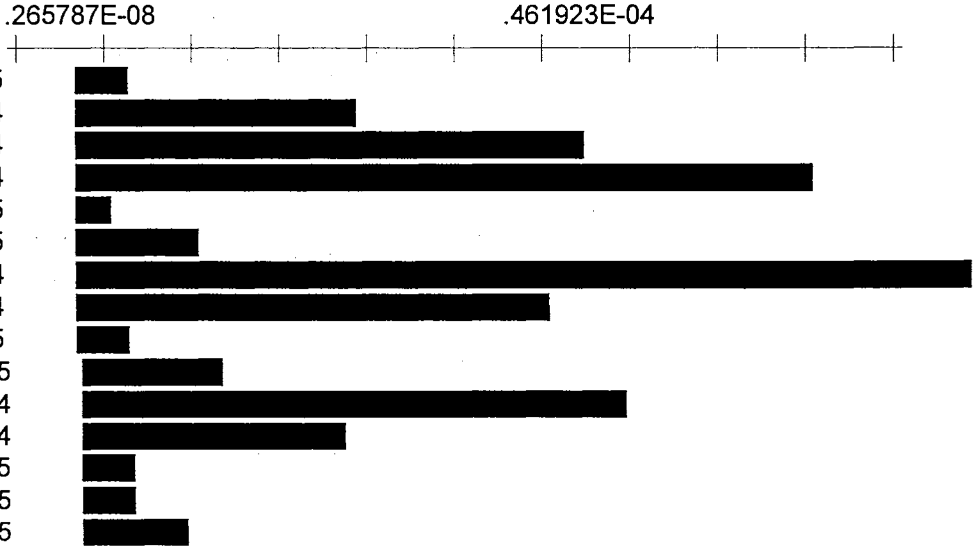

Efaw

FOURIER COMPONENTS OF RES30

INDEX	FREQUENCY	REAL	IMAGINARY	MAGNITUDE	PHASE	PERIODOGRAM
1	0.00000	-0.003	0.000	0.003	0.000	0.002
2	0.00781	.441160E-03	0.002	0.002	1.393	0.002
3	0.01563	.279491E-03	-.435237E-03	.517249E-03	-1.000	.684918E-04
4	0.02344	0.001	-0.004	0.004	-1.221	0.004
5	0.03125	0.004	-0.001	0.004	-0.317	0.004
6	0.03906	-.209900E-03	.321539E-04	.212349E-03	-0.152	.115435E-04
7	0.04688	-0.004	0.002	0.004	-0.565	0.005
8	0.05469	-0.003	-0.004	0.005	0.903	0.007
9	0.06250	-0.001	.646749E-04	0.001	-0.045	.526970E-03
10	0.07031	.216098E-04	0.002	0.002	1.562	0.002
11	0.07813	-0.002	0.006	0.006	-1.225	0.009
12	0.08594	.593993E-03	.531030E-03	.796756E-03	0.729	.162514E-03
13	0.09375	-.193519E-03	.192270E-04	.194472E-03	-0.099	.968176E-05
14	0.10156	0.004	0.001	0.004	0.252	0.004
15	0.10938	.795281E-03	.885845E-03	0.001	0.839	.362802E-03

SERIES IS TRANSFORMED
PLOT OF RES30
NUMBER OF CASES = 128
MEAN OF SERIES = .312696E-05
STANDARD DEVIATION OF SERIES = .670098E-05

SEQUENCE PLOT OF SERIES

CASE VALUE .330426E-07 .369967E-04

CASE	VALUE
1	.706913E-05
2	.620182E-05
3	.267546E-06
4	.153806E-04
5	.155341E-04
6	.450919E-07
7	.183523E-04
8	.289002E-04
9	.205848E-05
10	.624906E-05
11	.369967E-04
12	.634820E-06
13	.378194E-07
14	.162629E-04
15	.141719E-05

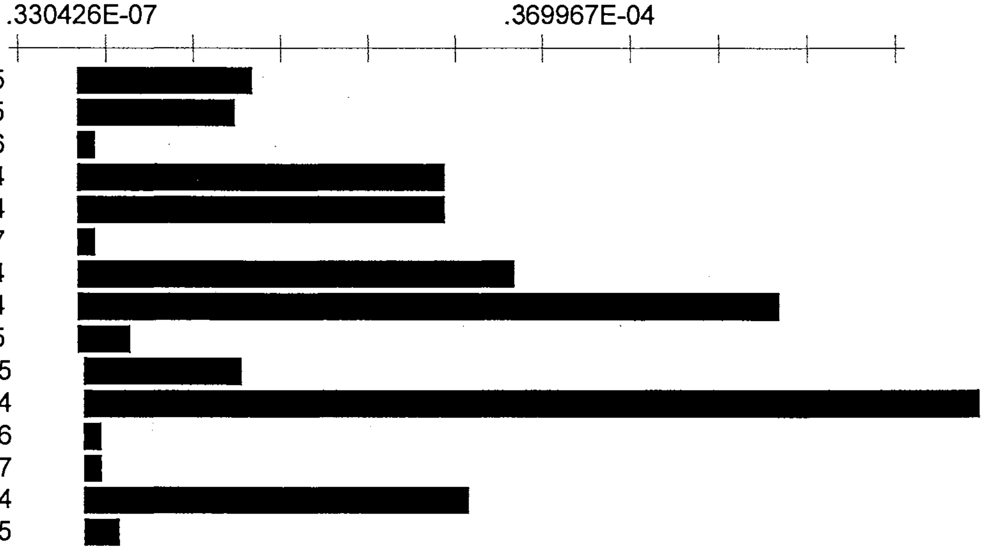

Efaw

FOURIER COMPONENTS OF RES60

INDEX	FREQUENCY	REAL	IMAGINARY	MAGNITUDE	PHASE	PERIODOGRAM
1	0.00000	0.001	0.000	0.001	0.000	.262252E-03
2	0.00781	-.809876E-03	0.001	0.001	-0.951	.497546E-03
3	0.01563	.268072E-03	-0.002	0.002	-1.441	0.001
4	0.02344	0.002	-0.005	0.006	-1.176	0.008
5	0.03125	-0.001	-.139468E-03	0.001	0.100	.503474E-03
6	0.03906	-.708563E-03	0.002	0.002	-1.187	.917016E-03
7	0.04688	-.200147E-03	-0.001	0.001	1.415	.424558E-03
8	0.05469	-0.002	.167626E-03	0.002	-0.103	.676104E-03
9	0.06250	-0.002	.859423E-03	0.002	-0.472	.913683E-03
10	0.07031	-.479172E-03	0.002	0.002	-1.267	.657134E-03
11	0.07813	-.500324E-03	0.002	0.002	-1.316	0.001
12	0.08594	.373294E-04	-.316922E-03	.319113E-03	-1.454	.260693E-04
13	0.09375	.318304E-03	.149141E-03	.351512E-03	0.438	.316316E-04
14	0.10156	.400283E-03	-.122819E-03	.418702E-03	-0.298	.448797E-04
15	0.10938	-.458957E-03	-0.002	0.002	1.289	.696817E-03

SERIES IS TRANSFORMED
PLOT OF RES60
NUMBER OF CASES = 128
MEAN OF SERIES = .146368E-05
STANDARD DEVIATION OF SERIES = .389508E-05

SEQUENCE PLOT OF SERIES

CASE	VALUE
1	.102442E-05
2	.194354E-05
3	.426057E-05
4	.310555E-04
5	.196669E-05
6	.358209E-05
7	.165843E-05
8	.264103E-05
9	.356907E-05
10	.256693E-05
11	.392965E-05
12	.101833E-06
13	.123561E-06
14	.175311E-06
15	.272194E-05

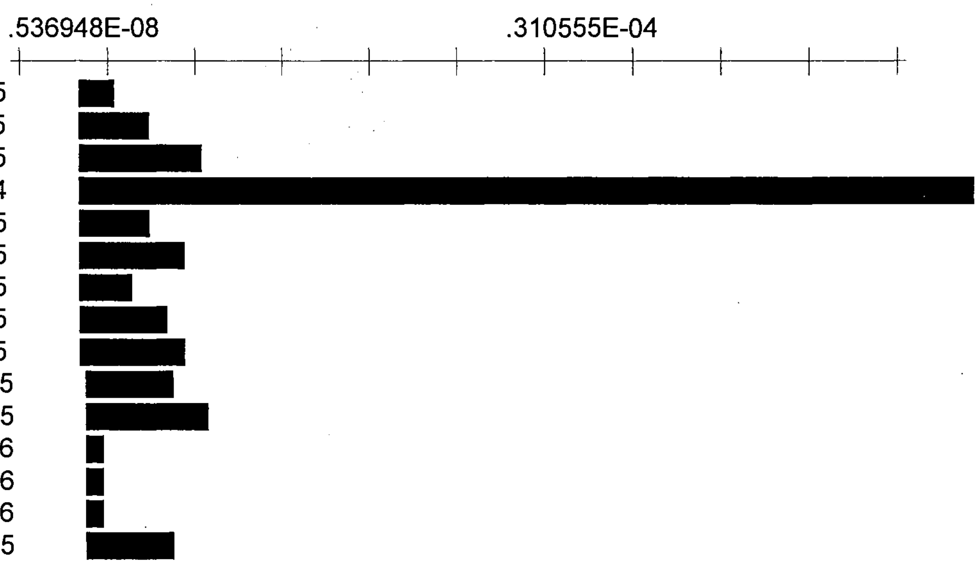

Efaw
FOURIER COMPONENTS OF RES120

INDEX	FREQUENCY	REAL	IMAGINARY	MAGNITUDE	PHASE	PERIODOGRAM
1	0.00000	-.185667E-03	0.000	.185667E-03	0.000	.882494E-05
2	0.00781	-.255616E-03	0.001	0.001	-1.354	.360035E-03
3	0.01563	.116420E-03	.150497E-03	.190271E-03	0.912	.926798E-05
4	0.02344	-.499948E-03	-.371010E-03	.622573E-03	0.638	.992247E-04
5	0.03125	.127638E-03	.292259E-03	.318915E-03	1.159	.260369E-04
6	0.03906	-.233952E-03	-.272419E-03	.359091E-03	0.861	.330102E-04
7	0.04688	-0.001	-0.002	0.002	0.847	0.001
8	0.05469	-.339496E-03	-.567267E-04	.344203E-03	0.166	.303298E-04
9	0.06250	-.629447E-03	0.001	0.001	-1.018	.367552E-03
10	0.07031	.189762E-03	0.001	0.001	1.390	.284836E-03
11	0.07813	0.001	.635682E-03	0.001	0.463	.519341E-03
12	0.08594	0.001	.496614E-03	0.001	0.384	.449535E-03
13	0.09375	-.977106E-04	.898593E-03	.903890E-03	-1.462	.209156E-03
14	0.10156	-0.001	-.265172E-03	0.001	0.216	.391267E-03
15	0.10938	-.950841E-03	.177221E-04	.951006E-03	-0.019	.231530E-03

SERIES IS TRANSFORMED
PLOT OF RES120
NUMBER OF CASES = 128
MEAN OF SERIES = .300999E-06
STANDARD DEVIATION OF SERIES = .702756E-06

SEQUENCE PLOT OF SERIES

CASE VALUE .903864E-10 .452123E-05

CASE	VALUE
1	.344724E-07
2	.140639E-05
3	.362031E-07
4	.387597E-06
5	.101707E-06
6	.128946E-06
7	.452123E-05
8	.118476E-06
9	.143575E-05
10	.111264E-05
11	.202868E-05
12	.175600E-05
13	.817017E-06
14	.152839E-05
15	.904412E-06

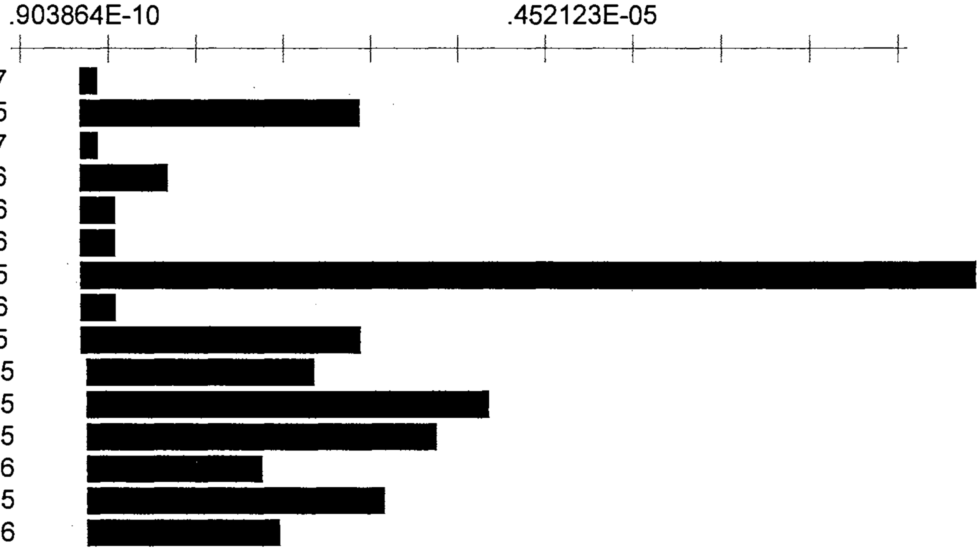

Perk
SERIES IS TRANSFORMED
SERIES HAS BEEN TRUNCATED TO 128 NONMISSING CASES

FOURIER COMPONENTS OF RES15

INDEX	FREQUENCY	REAL	IMAGINARY	MAGNITUDE	PHASE	PERIODOGRAM
1	0.00000	-0.002	0.000	0.002	0.000	.668705E-03
2	0.00781	-0.002	0.003	0.004	-1.066	0.004
3	0.01563	0.004	-0.003	0.005	-0.622	0.007
4	0.02344	0.006	0.002	0.006	0.404	0.010
5	0.03125	.474050E-03	0.001	0.001	1.188	.411436E-03
6	0.03906	-.470628E-03	0.002	0.002	-1.376	0.002
7	0.04688	-0.006	0.002	0.007	-0.301	0.012
8	0.05469	0.002	-0.004	0.005	-1.141	0.006
9	0.06250	-0.002	.190733E-03	0.002	-0.120	.646298E-03
10	0.07031	0.003	-.144712E-03	0.003	-0.055	0.002
11	0.07813	-0.004	0.003	0.005	-0.715	0.007
12	0.08594	0.001	-0.003	0.004	-1.162	0.003
13	0.09375	-0.001	.361852E-03	0.002	-0.240	.592694E-03
14	0.10156	0.001	.482382E-03	0.002	0.324	.589186E-03
15	0.10938	0.002	0.001	0.002	0.676	0.001

SERIES IS TRANSFORMED
PLOT OF RES15
NUMBER OF CASES = 128
MEAN OF SERIES = .482415E-05
STANDARD DEVIATION OF SERIES = .880413E-05

SEQUENCE PLOT OF SERIES

CASE VALUE .265787E-08 .461923E-04

CASE	VALUE
1	.261213E-05
2	.139324E-04
3	.259180E-04
4	.381847E-04
5	.160717E-05
6	.593467E-05
7	.461923E-04
8	.241215E-04
9	.252460E-05
10	.685853E-05
11	.279578E-04
12	.131719E-04
13	.231521E-05
14	.230151E-05
15	.494408E-05

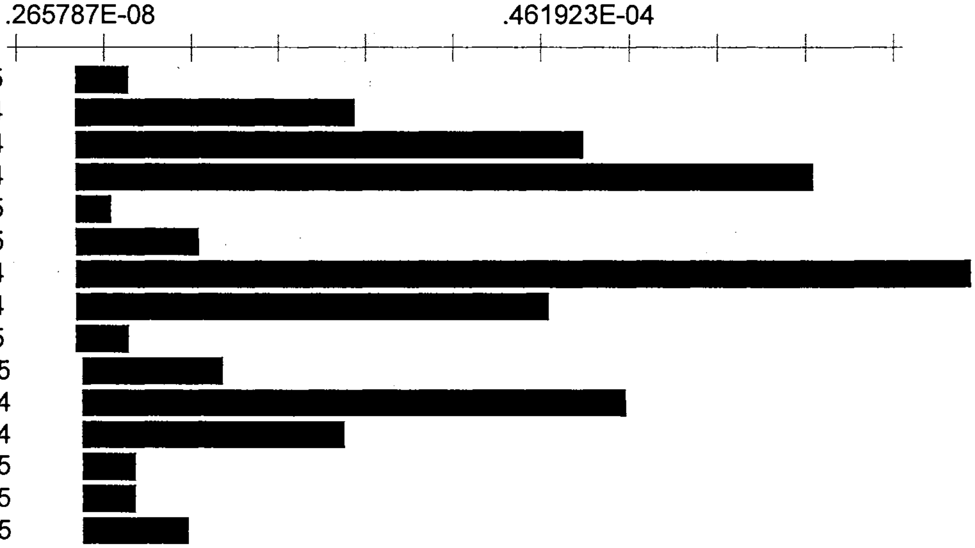

Perk

FOURIER COMPONENTS OF RES30

INDEX	FREQUENCY	REAL	IMAGINARY	MAGNITUDE	PHASE	PERIODOGRAM
1	0.00000	0.001	0.000	0.001	0.000	.455374E-03
2	0.00781	0.002	0.004	0.004	1.196	0.005
3	0.01563	.819604E-03	-0.003	0.003	-1.284	0.002
4	0.02344	.454980E-03	.147386E-03	.478256E-03	0.313	.585546E-04
5	0.03125	-0.002	0.003	0.003	-1.010	0.003
6	0.03906	0.003	-0.004	0.005	-0.936	0.007
7	0.04688	0.003	0.004	0.005	0.897	0.007
8	0.05469	0.001	-.502737E-03	0.001	-0.376	.479388E-03
9	0.06250	.984652E-03	.793900E-03	0.001	0.679	.409553E-03
10	0.07031	-0.003	.153055E-03	0.003	-0.048	0.003
11	0.07813	-.397230E-03	0.002	0.002	-1.313	.619540E-03
12	0.08594	0.001	0.002	0.002	0.989	.889079E-03
13	0.09375	-.210085E-03	0.003	0.003	-1.488	0.002
14	0.10156	-0.003	-0.001	0.003	0.345	0.003
15	0.10938	-0.003	-0.003	0.004	0.758	0.005

SERIES IS TRANSFORMED
PLOT OF RES30
NUMBER OF CASES = 128
MEAN OF SERIES = .345241E-05
STANDARD DEVIATION OF SERIES = .575468E-05

SEQUENCE PLOT OF SERIES

CASE VALUE .671506E-08 .261758E-04

CASE	VALUE
1	.177881E-05
2	.191822E-04
3	.838172E-05
4	.228729E-06
5	.120975E-04
6	.254468E-04
7	.261758E-04
8	.187261E-05
9	.159982E-05
10	.102634E-04
11	.242008E-05
12	.347297E-05
13	.652949E-05
14	.120944E-04
15	.201857E-04

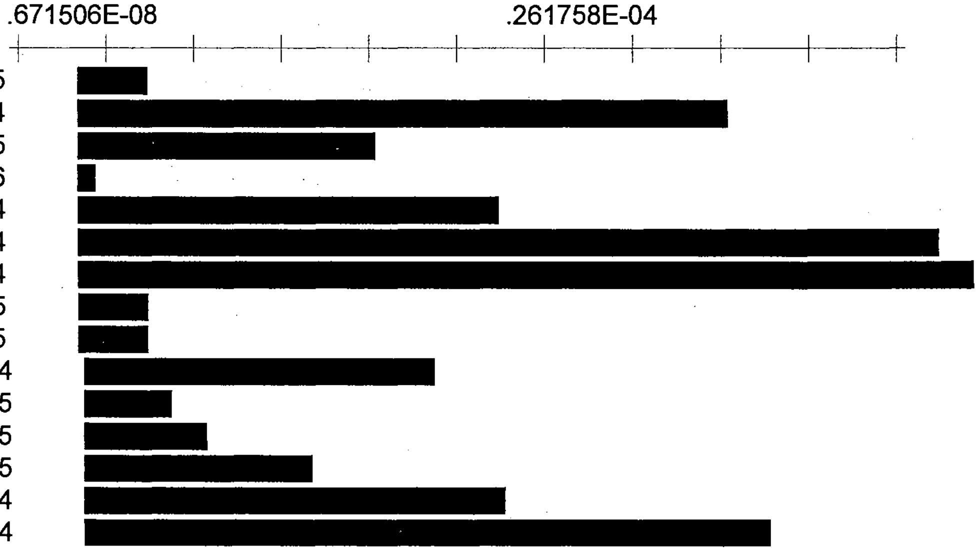

Perk

FOURIER COMPONENTS OF RES60

INDEX	FREQUENCY	REAL	IMAGINARY	MAGNITUDE	PHASE	PERIODOGRAM
1	0.00000	-0.002	0.000	0.002	0.000	.886609E-03
2	0.00781	0.002	0.006	0.007	1.204	0.012
3	0.01563	.494636E-03	-0.001	0.001	-1.201	.479142E-03
4	0.02344	-0.004	-0.005	0.007	0.863	0.011
5	0.03125	0.002	0.004	0.005	1.230	0.006
6	0.03906	-.865091E-03	-0.005	0.005	1.392	0.006
7	0.04688	0.004	0.003	0.005	0.774	0.006
8	0.05469	.940406E-03	-0.002	0.002	-1.028	.847653E-03
9	0.06250	-.126592E-04	0.002	0.002	-1.565	0.001
10	0.07031	-.698390E-03	.242360E-03	.739248E-03	-0.334	.139901E-03
11	0.07813	-0.004	0.002	0.004	-0.424	0.005
12	0.08594	.564869E-03	-0.002	0.002	-1.244	.792148E-03
13	0.09375	.487918E-04	.823803E-04	.957453E-04	1.036	.234679E-05
14	0.10156	.827193E-03	0.001	0.002	1.034	.670143E-03
15	0.10938	-.959269E-03	.746779E-03	0.001	-0.661	.378336E-03

SERIES IS TRANSFORMED
PLOT OF RES60
NUMBER OF CASES = 128
MEAN OF SERIES = .409669E-05
STANDARD DEVIATION OF SERIES = .898873E-05

SEQUENCE PLOT OF SERIES

CASE	VALUE
1	.346332E-05
2	.455942E-04
3	.187165E-05
4	.425583E-04
5	.221897E-04
6	.235737E-04
7	.243162E-04
8	.331115E-05
9	.463679E-05
10	.546487E-06
11	.197826E-04
12	.309433E-05
13	.916716E-08
14	.261775E-05
15	.147788E-05

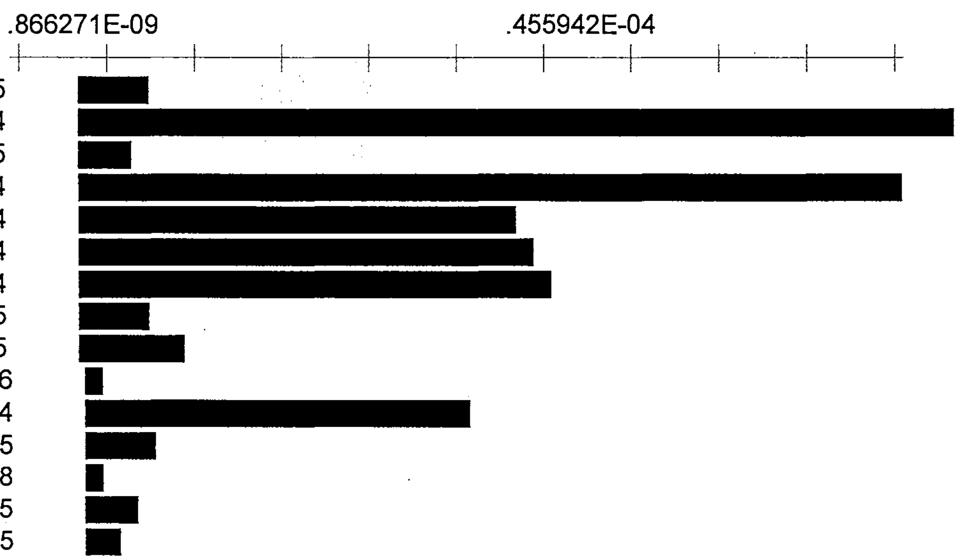

Perk

FOURIER COMPONENTS OF RES120

INDEX	FREQUENCY	REAL	IMAGINARY	MAGNITUDE	PHASE	PERIODOGRAM
1	0.00000	0.001	0.000	0.001	0.000	.493935E-03
2	0.00781	0.002	-.128720E-03	0.002	-0.060	0.001
3	0.01563	0.004	-0.005	0.006	-0.972	0.010
4	0.02344	0.001	-.319421E-03	0.001	-0.236	.476030E-03
5	0.03125	-0.002	0.004	0.005	-1.132	0.005
6	0.03906	-0.004	-.519640E-03	0.004	0.135	0.004
7	0.04688	-0.001	-0.005	0.005	1.335	0.006
8	0.05469	0.002	-.324698E-03	0.002	-0.189	.766299E-03
9	0.06250	.404664E-03	0.001	0.001	1.236	.388081E-03
10	0.07031	-0.003	-0.002	0.003	0.550	0.003
11	0.07813	.261474E-03	-0.003	0.003	-1.483	0.002
12	0.08594	0.003	-0.002	0.004	-0.713	0.003
13	0.09375	0.002	0.001	0.003	0.508	0.002
14	0.10156	-.310238E-03	0.002	0.002	-1.375	.652947E-03
15	0.10938	.102865E-03	-.690730E-03	.698348E-03	-1.423	.124849E-03

SERIES IS TRANSFORMED
PLOT OF RES120
NUMBER OF CASES = 128
MEAN OF SERIES = .282841E-05
STANDARD DEVIATION OF SERIES = .665848E-05

SEQUENCE PLOT OF SERIES

CASE VALUE .237954E-08 .406008E-04

CASE	VALUE
1	.192944E-05
2	.459315E-05
3	.406008E-04
4	.185949E-05
5	.212457E-04
6	.148659E-04
7	.227395E-04
8	.299336E-05
9	.151594E-05
10	.121632E-04
11	.884649E-05
12	.123772E-04
13	.682890E-05
14	.255057E-05
15	.487689E-06

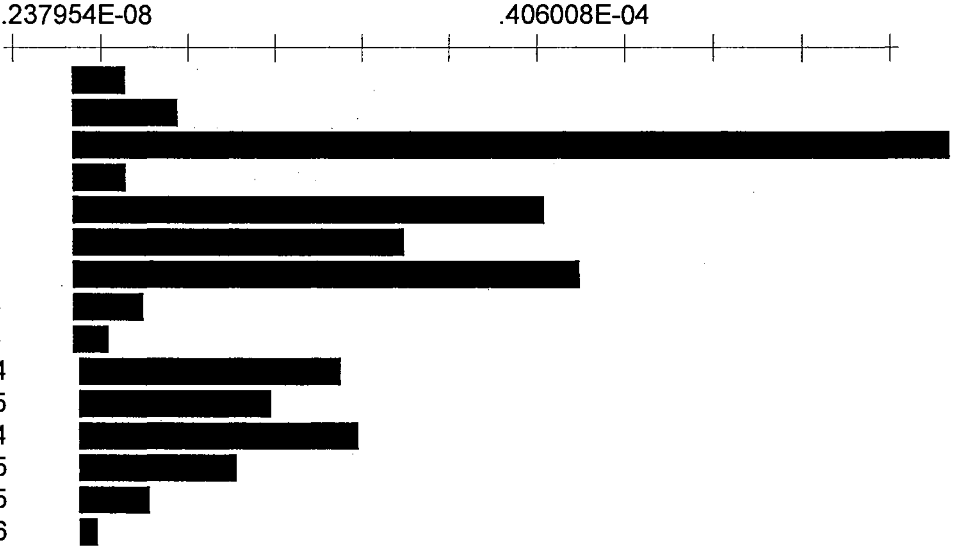

SERIES IS TRANSFORMED
SERIES HAS BEEN TRUNCATED TO 32 NONMISSING CASES
HYD
FOURIER COMPONENTS OF RES15

INDEX	FREQUENCY	REAL	IMAGINARY	MAGNITUDE	PHASE	PERIODOGRAM
1	0.00000	0.001	0.000	0.001	0.000	.922100E-04
2	0.03125	0.002	0.004	0.004	1.108	0.001
3	0.06250	-.320288E-03	0.002	0.002	-1.439	.381454E-03
4	0.09375	-0.002	0.002	0.002	-0.733	.388128E-03
5	0.12500	.849514E-03	-0.002	0.002	-1.177	.314294E-03
6	0.15625	0.001	0.003	0.003	1.252	.715178E-03
7	0.18750	-0.002	-0.001	0.002	0.745	.270271E-03
8	0.21875	-.293762E-03	-0.002	0.002	1.393	.177099E-03
9	0.25000	-.775094E-03	-0.001	0.002	1.081	.173439E-03
10	0.28125	.637093E-03	.438807E-03	.773589E-03	0.603	.383001E-04
11	0.31250	-.377505E-03	.671153E-04	.383425E-03	-0.176	.940893E-05
12	0.34375	.931568E-03	.965713E-04	.936560E-03	0.103	.561373E-04
13	0.37500	-.707889E-03	-0.001	0.001	1.008	.112522E-03
14	0.40625	-0.001	-0.001	0.002	0.606	.204511E-03
15	0.43750	.913726E-04	0.002	0.002	1.521	.218587E-03
16	0.46875	-.323955E-03	.455489E-03	.558942E-03	-0.953	.199947E-04
17	0.50000	.338594E-03	0.000	.338594E-03	0.000	.733733E-05

SERIES IS TRANSFORMED

PLOT OF RES15
NUMBER OF CASES = 32
MEAN OF SERIES = .404534E-05
STANDARD DEVIATION OF SERIES = .410977E-05

SEQUENCE PLOT OF SERIES

CASE	VALUE
1	.144078E-05
2	.158334E-04
3	.596022E-05
4	.606450E-05
5	.491084E-05
6	.111747E-04
7	.422298E-05
8	.276717E-05
9	.270998E-05
10	.598440E-06
11	.147015E-06
12	.877145E-06
13	.175816E-05
14	.319548E-05
15	.341542E-05

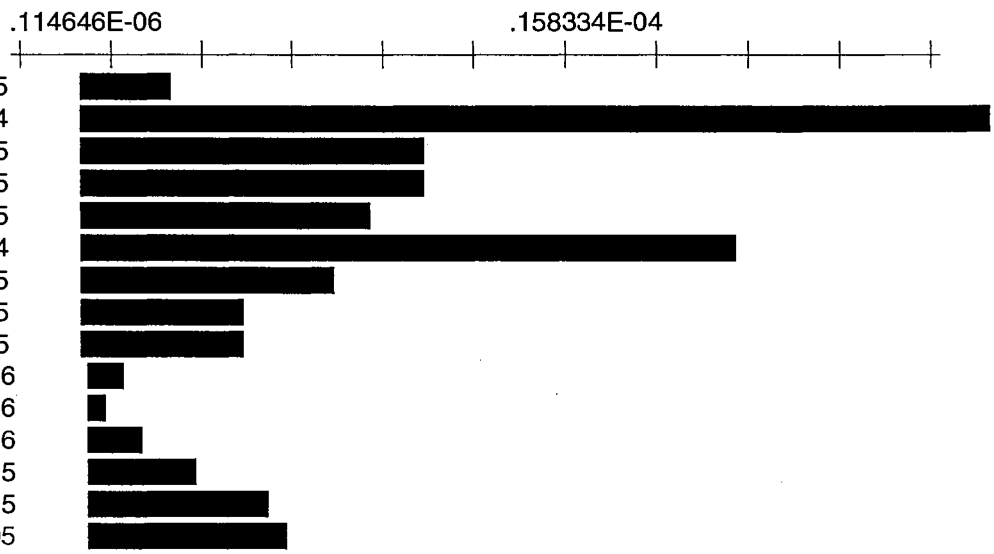

Hyd

FOURIER COMPONENTS OF RES30

INDEX	FREQUENCY	REAL	IMAGINARY	MAGNITUDE	PHASE	PERIODOGRAM
1	0.00000	0.005	0.000	0.005	0.000	0.002
2	0.03125	-.168476E-03	-.341684E-03	.380962E-03	1.113	.928843E-05
3	0.06250	-0.002	-0.002	0.003	0.776	.509692E-03
4	0.09375	-0.002	.974331E-04	0.002	-0.048	.261279E-03
5	0.12500	-0.002	-0.002	0.003	0.797	.618535E-03
6	0.15625	-0.002	-0.002	0.002	0.777	.294471E-03
7	0.18750	0.003	-.644893E-03	0.003	-0.233	.500450E-03
8	0.21875	-.746624E-03	0.002	0.002	-1.256	.371513E-03
9	0.25000	0.001	-0.003	0.003	-1.235	.688006E-03
10	0.28125	.523215E-03	.111377E-03	.534938E-03	0.210	.183142E-04
11	0.31250	0.001	0.001	0.002	0.832	.164053E-03
12	0.34375	-.351758E-04	.746907E-03	.747735E-03	-1.524	.357829E-04
13	0.37500	.917050E-03	-.949226E-03	0.001	-0.803	.111489E-03
14	0.40625	.382148E-03	-.123161E-03	.401505E-03	-0.312	.103172E-04
15	0.43750	.437226E-03	.284821E-03	.521814E-03	0.577	.174265E-04

SERIES IS TRANSFORMED
PLOT OF RES30
NUMBER OF CASES = 32
MEAN OF SERIES = .462113E-05
STANDARD DEVIATION OF SERIES = .514781E-05

SEQUENCE PLOT OF SERIES

CASE VALUE .145132E-06 .253082E-04

CASE	VALUE
1	.253082E-04
2	.145132E-06
3	.796394E-05
4	.408248E-05
5	.966461E-05
6	.460110E-05
7	.781953E-05
8	.580489E-05
9	.107501E-04
10	.286159E-06
11	.256333E-05
12	.559107E-06
13	.174201E-05
14	.161206E-06
15	.272290E-06

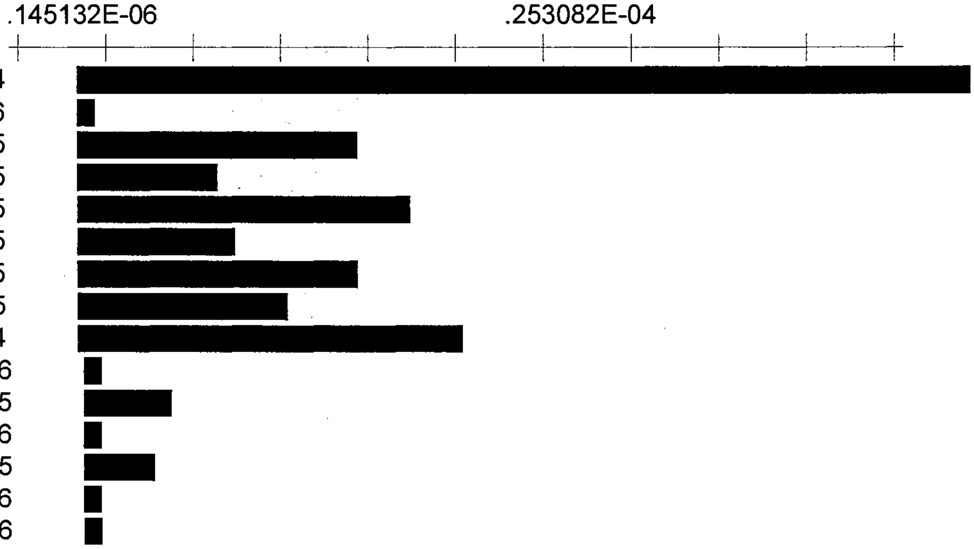

SERIES IS TRANSFORMED
SERIES HAS BEEN TRUNCATED TO 128 NONMISSING CASES
EFAW

FOURIER COMPONENTS OF MEAS15

INDEX	FREQUENCY	REAL	IMAGINARY	MAGNITUDE	PHASE	PERIODOGRAM
1	0.00000	.456927E-03	0.000	.456927E-03	0.000	.534483E-04
2	0.00781	0.011	-0.017	0.020	-0.983	0.103
3	0.01563	.154073E-03	0.010	0.010	1.555	0.024
4	0.02344	-0.025	0.002	0.025	-0.060	0.166
5	0.03125	.376040E-03	-0.004	0.004	-1.485	0.005
6	0.03906	0.004	.227315E-03	0.004	0.059	0.004
7	0.04688	0.004	-0.001	0.004	-0.261	0.004
8	0.05469	.701993E-03	0.003	0.003	1.300	0.002
9	0.06250	0.004	-0.002	0.004	-0.538	0.005
10	0.07031	0.002	0.003	0.004	0.956	0.004
11	0.07813	.849870E-03	-0.005	0.005	-1.391	0.006
12	0.08594	-0.005	0.004	0.006	-0.659	0.010
13	0.09375	0.006	.334424E-03	0.006	0.054	0.010
14	0.10156	-0.005	-0.005	0.008	0.774	0.014
15	0.10938	-0.006	-0.001	0.006	0.188	0.009

SERIES IS TRANSFORMED
PLOT OF MEAS15
NUMBER OF CASES = 128
MEAN OF SERIES = .234960E-04
STANDARD DEVIATION OF SERIES = .940240E-04

SEQUENCE PLOT OF SERIES

CASE VALUE .610105E-08 .649261E-03

CASE	VALUE
1	.208782E-06
2	.401100E-03
3	.941009E-04
4	.649261E-03
5	.194359E-04
6	.146295E-04
7	.150502E-04
8	.688758E-05
9	.188035E-04
10	.140560E-04
11	.224840E-04
12	.390163E-04
13	.390183E-04
14	.564038E-04
15	.350806E-04

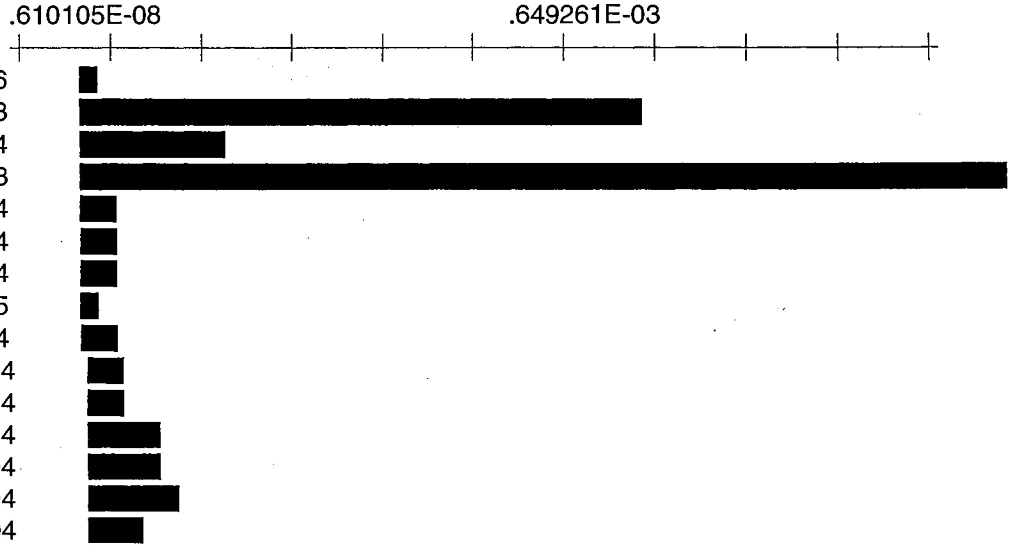

EFAW

FOURIER COMPONENTS OF MEAS30

INDEX	FREQUENCY	REAL	IMAGINARY	MAGNITUDE	PHASE	PERIODOGRAM
1	0.00000	-0.004	0.000	0.004	0.000	0.004
2	0.00781	0.011	-0.015	0.019	-0.906	0.088
3	0.01563	.459133E-04	0.007	0.007	1.565	0.014
4	0.02344	-0.018	0.005	0.019	-0.288	0.093
5	0.03125	.758637E-03	-0.002	0.003	-1.271	0.002
6	0.03906	0.004	-0.003	0.005	-0.622	0.007
7	0.04688	0.005	-0.001	0.005	-0.293	0.007
8	0.05469	0.004	0.004	0.006	0.878	0.008
9	0.06250	0.002	-0.002	0.003	-0.896	0.002
10	0.07031	0.001	0.002	0.002	0.950	0.001
11	0.07813	0.001	-0.003	0.003	-1.154	0.002
12	0.08594	-0.002	0.004	0.005	-1.116	0.006
13	0.09375	0.001	.418864E-03	0.001	0.341	.402641E-03
14	0.10156	-0.005	-0.003	0.006	0.506	0.008
15	0.10938	-0.003	-.932994E-04	0.003	0.031	0.002

SERIES IS TRANSFORMED
PLOT OF MEAS30
NUMBER OF CASES = 128
MEAN OF SERIES = .152899E-04
STANDARD DEVIATION OF SERIES = .617229E-04

SEQUENCE PLOT OF SERIES

CASE VALUE .118308E-08 .364699E-03

CASE	VALUE
1	.137042E-04
2	.343999E-03
3	.560551E-04
4	.364699E-03
5	.659416E-05
6	.285796E-04
7	.254156E-04
8	.308542E-04
9	.678225E-05
10	.502025E-05
11	.773003E-05
12	.227203E-04
13	.157282E-05
14	.305569E-04
15	.930634E-05

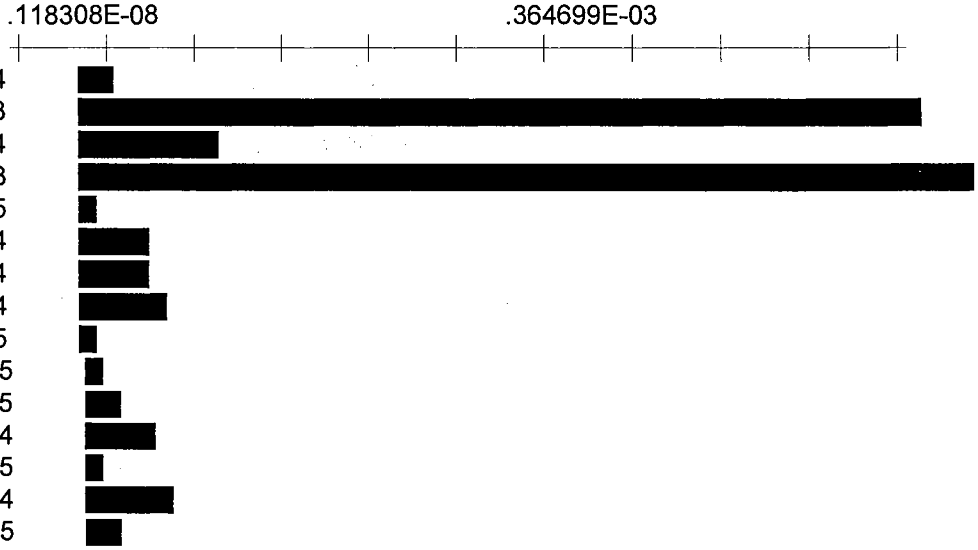

EFAW

FOURIER COMPONENTS OF MEAS60

INDEX	FREQUENCY	REAL	IMAGINARY	MAGNITUDE	PHASE	PERIODOGRAM
1	0.00000	.618429E-03	0.000	.618429E-03	0.000	.979083E-04
2	0.00781	0.012	-0.011	0.017	-0.760	0.071
3	0.01563	-.315972E-03	0.004	0.004	-1.483	0.003
4	0.02344	-0.006	0.006	0.009	-0.778	0.019
5	0.03125	-0.002	-0.003	0.004	1.092	0.003
6	0.03906	-.507330E-03	-0.007	0.007	1.495	0.011
7	0.04688	.679630E-03	-0.005	0.005	-1.444	0.007
8	0.05469	0.002	-0.002	0.003	-0.866	0.002
9	0.06250	0.001	-0.002	0.002	-1.067	0.001
10	0.07031	0.001	-0.001	0.002	-0.847	.725264E-03
11	0.07813	.998063E-03	-0.001	0.002	-0.911	.678888E-03
12	0.08594	0.002	.514784E-04	0.002	0.025	0.001
13	0.09375	0.002	-.491880E-03	0.002	-0.290	.755542E-03
14	0.10156	-.582543E-03	.344181E-03	.676621E-03	-0.534	.117201E-03
15	0.10938	-.390618E-03	.610585E-03	.724842E-03	-1.002	.134501E-03

SERIES IS TRANSFORMED
PLOT OF MEAS60
NUMBER OF CASES = 128
MEAN OF SERIES = .773674E-05
STANDARD DEVIATION OF SERIES = .357399E-04

SEQUENCE PLOT OF SERIES

CASE	VALUE
1	.382454E-06
2	.276971E-03
3	.130575E-04
4	.741790E-04
5	.125319E-04
6	.449022E-04
7	.290801E-04
8	.973335E-05
9	.563261E-05
10	.283306E-05
11	.265191E-05
12	.407653E-05
13	.295134E-05
14	.457816E-06
15	.525396E-06

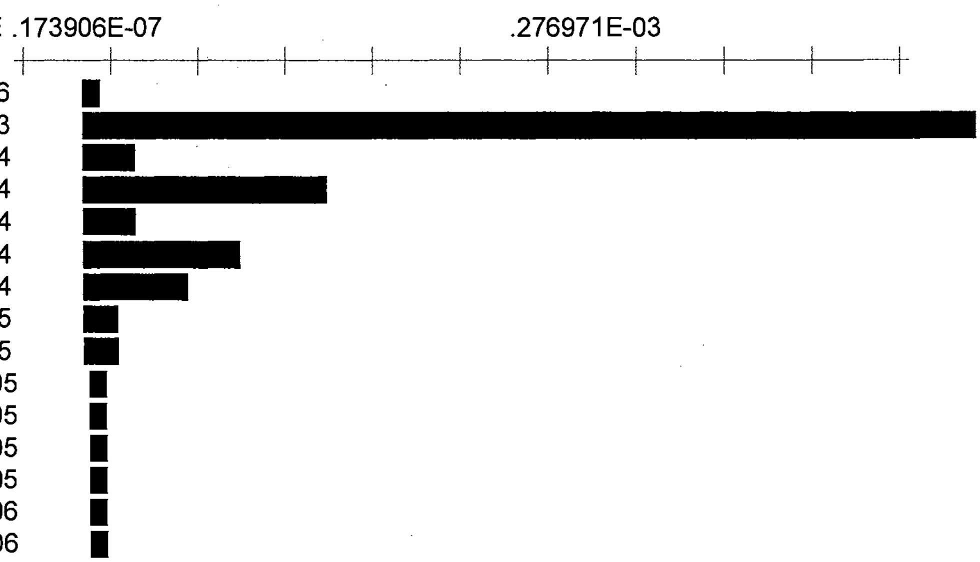

EFAW
FOURIER COMPONENTS OF MEAS120

INDEX	FREQUENCY	REAL	IMAGINARY	MAGNITUDE	PHASE	PERIODOGRAM
1	0.00000	-0.026	0.000	0.026	0.000	0.167
2	0.00781	0.019	-0.011	0.022	-0.540	0.120
3	0.01563	0.014	0.002	0.014	0.146	0.051
4	0.02344	0.010	0.008	0.012	0.691	0.040
5	0.03125	0.005	0.008	0.010	0.988	0.024
6	0.03906	0.002	0.009	0.009	1.393	0.021
7	0.04688	-0.002	0.007	0.008	-1.360	0.015
8	0.05469	-0.003	0.005	0.006	-1.017	0.010
9	0.06250	-0.004	0.003	0.005	-0.685	0.006
10	0.07031	-0.003	.641152E-03	0.003	-0.202	0.003
11	0.07813	-0.002	-.524266E-03	0.002	0.248	0.001
12	0.08594	-.485891E-03	-.631509E-03	.796802E-03	0.915	.162533E-03
13	0.09375	.436061E-03	-.772129E-03	.886754E-03	-1.057	.201301E-03
14	0.10156	0.001	.697177E-03	0.001	0.507	.526893E-03
15	0.10938	0.001	0.001	0.002	0.631	.756314E-03

SERIES IS TRANSFORMED
PLOT OF MEAS120
NUMBER OF CASES = 128
MEAN OF SERIES = .235317E-04
STANDARD DEVIATION OF SERIES = .868893E-04

SEQUENCE PLOT OF SERIES

CASE	VALUE
1	.654197E-03
2	.469151E-03
3	.198251E-03
4	.155054E-03
5	.956673E-04
6	.810181E-04
7	.578355E-04
8	.373959E-04
9	.218834E-04
10	.102110E-04
11	.455877E-05
12	.634894E-06
13	.786332E-06
14	.205817E-05
15	.295435E-05

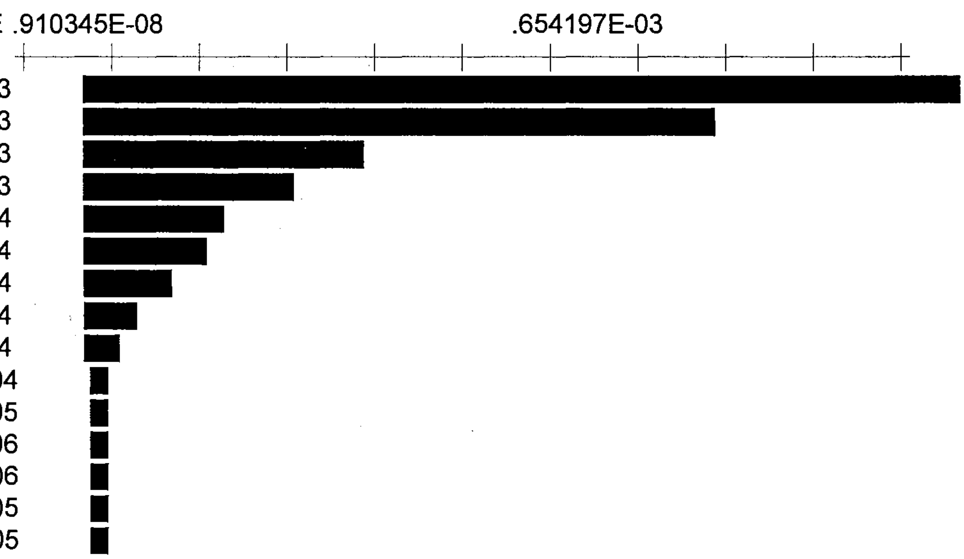

PERK
SERIES IS TRANSFORMED
SERIES HAS BEEN TRUNCATED TO 128 NONMISSING CASES

FOURIER COMPONENTS OF MEAS15

INDEX	FREQUENCY	REAL	IMAGINARY	MAGNITUDE	PHASE	PERIODOGRAM
1	0.00000	.934553E-03	0.000	.934553E-03	0.000	.223588E-03
2	0.00781	0.005	-0.004	0.007	-0.663	0.011
3	0.01563	-0.010	0.002	0.010	-0.159	0.026
4	0.02344	-0.006	0.006	0.008	-0.790	0.018
5	0.03125	0.005	-0.006	0.008	-0.847	0.016
6	0.03906	-0.004	-0.003	0.005	0.728	0.006
7	0.04688	.555067E-03	0.003	0.003	1.385	0.002
8	0.05469	-0.001	-0.005	0.005	1.275	0.007
9	0.06250	-0.006	0.002	0.006	-0.384	0.009
10	0.07031	0.003	0.001	0.003	0.478	0.002
11	0.07813	-0.003	-0.002	0.004	0.534	0.004
12	0.08594	0.002	0.003	0.004	0.978	0.003
13	0.09375	0.004	-0.004	0.006	-0.693	0.009
14	0.10156	.310743E-03	0.003	0.004	1.482	0.003
15	0.10938	0.002	0.004	0.005	1.145	0.006

SERIES IS TRANSFORMED
PLOT OF MEAS15
NUMBER OF CASES = 128
MEAN OF SERIES = .854228E-05
STANDARD DEVIATION OF SERIES = .184893E-04

SEQUENCE PLOT OF SERIES

CASE VALUE .400665E-08 .103458E-03

CASE	VALUE
1	.873389E-06
2	.425538E-04
3	.103458E-03
4	.689728E-04
5	.639696E-04
6	.219956E-04
7	.902694E-05
8	.256742E-04
9	.367776E-04
10	.851712E-05
11	.141601E-04
12	.133029E-04
13	.334943E-04
14	.122698E-04
15	.229697E-04

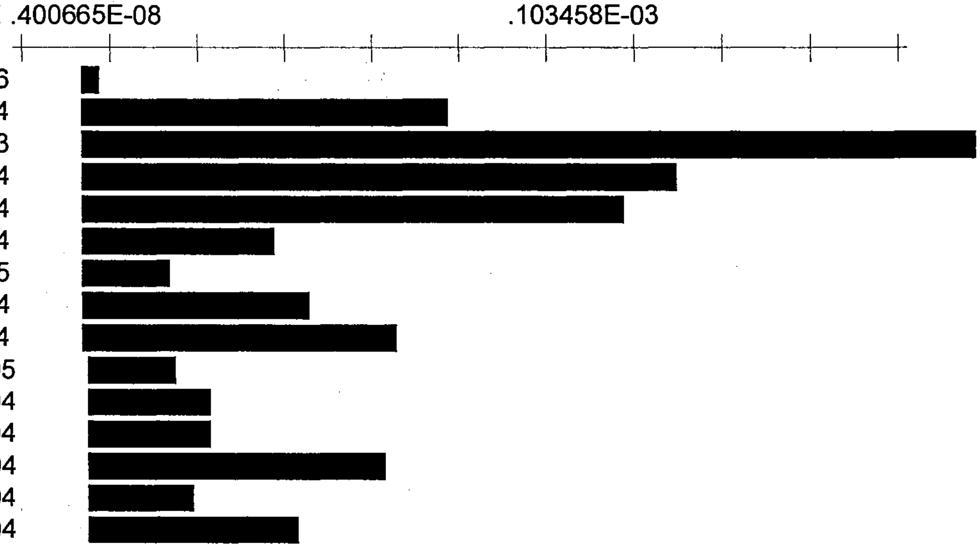

PERK

FOURIER COMPONENTS OF MEAS30

INDEX	FREQUENCY	REAL	IMAGINARY	MAGNITUDE	PHASE	PERIODOGRAM
1	0.00000	-0.002	0.000	0.002	0.000	.806480E-03
2	0.00781	0.010	-0.006	0.012	-0.514	0.037
3	0.01563	-0.008	0.008	0.012	-0.781	0.035
4	0.02344	-0.007	0.005	0.009	-0.588	0.019
5	0.03125	0.006	-0.010	0.012	-1.039	0.037
6	0.03906	-0.003	0.010	0.011	-1.268	0.030
7	0.04688	-0.004	-0.009	0.009	1.171	0.023
8	0.05469	.390885E-03	0.002	0.002	1.378	0.001
9	0.06250	-0.003	-0.003	0.004	0.802	0.004
10	0.07031	0.002	0.001	0.002	0.475	0.001
11	0.07813	.609372E-03	-0.002	0.002	-1.316	0.001
12	0.08594	.261530E-03	0.001	0.001	1.349	.362296E-03
13	0.09375	0.003	-0.003	0.004	-0.792	0.004
14	0.10156	.554577E-03	-.546821E-03	.778825E-03	-0.778	.155282E-03
15	0.10938	0.004	0.003	0.005	0.597	0.007

SERIES IS TRANSFORMED
PLOT OF MEAS30
NUMBER OF CASES = 128
MEAN OF SERIES = .134835E-04
STANDARD DEVIATION OF SERIES = .348873E-04

SEQUENCE PLOT OF SERIES

CASE	VALUE
1	.315031E-05
2	.145006E-03
3	.138428E-03
4	.746766E-04
5	.144049E-03
6	.115339E-03
7	.902155E-04
8	.415738E-05
9	.156818E-04
10	.526388E-05
11	.585609E-05
12	.141522E-05
13	.154879E-04
14	.606568E-06
15	.260225E-04

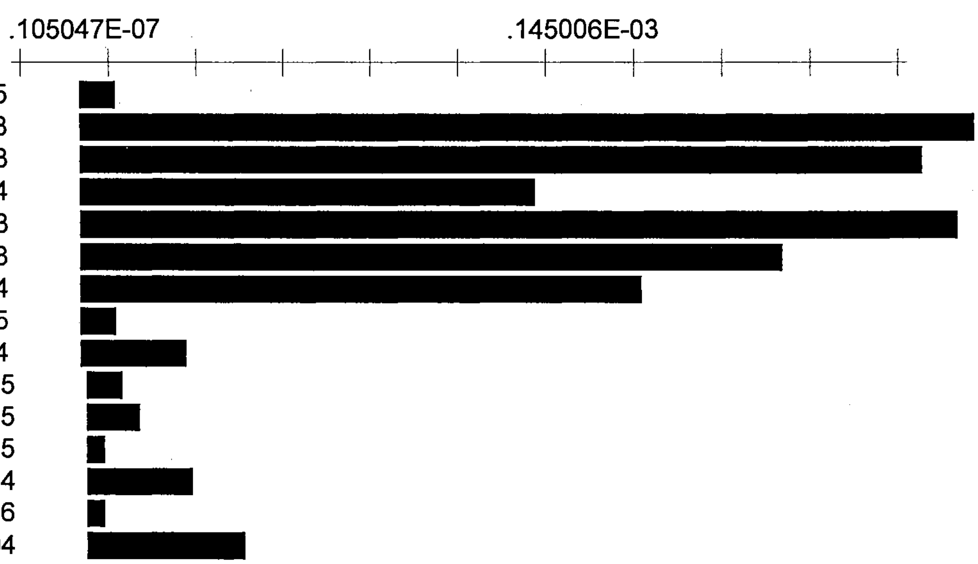

PERK

FOURIER COMPONENTS OF MEAS60

INDEX	FREQUENCY	REAL	IMAGINARY	MAGNITUDE	PHASE	PERIODOGRAM
1	0.00000	-.986112E-03	0.000	.986112E-03	0.000	.248939E-03
2	0.00781	0.006	-0.019	0.020	-1.271	0.106
3	0.01563	-0.002	0.003	0.003	-0.909	0.003
4	0.02344	0.001	0.003	0.003	1.086	0.002
5	0.03125	-0.002	-0.007	0.007	1.355	0.013
6	0.03906	0.002	0.004	0.004	1.146	0.004
7	0.04688	-0.003	-0.004	0.005	0.910	0.007
8	0.05469	-.158014E-03	0.001	0.001	-1.419	.279342E-03
9	0.06250	-.759816E-03	-0.003	0.004	1.353	0.003
10	0.07031	0.001	-.617558E-03	0.001	-0.435	.550304E-03
11	0.07813	0.002	-0.001	0.002	-0.648	0.001
12	0.08594	.317836E-04	.679338E-03	.680081E-03	1.524	.118403E-03
13	0.09375	.137596E-03	.363558E-03	.388725E-03	1.209	.386834E-04
14	0.10156	-0.002	-0.001	0.002	0.552	.996338E-03
15	0.10938	.410204E-03	-0.001	0.001	-1.276	.508622E-03

SERIES IS TRANSFORMED
PLOT OF MEAS60
NUMBER OF CASES = 128
MEAN OF SERIES = .935182E-05
STANDARD DEVIATION OF SERIES = .515760E-04

SEQUENCE PLOT OF SERIES

CASE	VALUE
1	.972417E-06
2	.414618E-03
3	.102063E-04
4	.975055E-05
5	.491449E-04
6	.154965E-04
7	.267256E-04
8	.109118E-05
9	.123876E-04
10	.214963E-05
11	.557490E-05
12	.462510E-06
13	.151107E-06
14	.389194E-05
15	.198681E-05

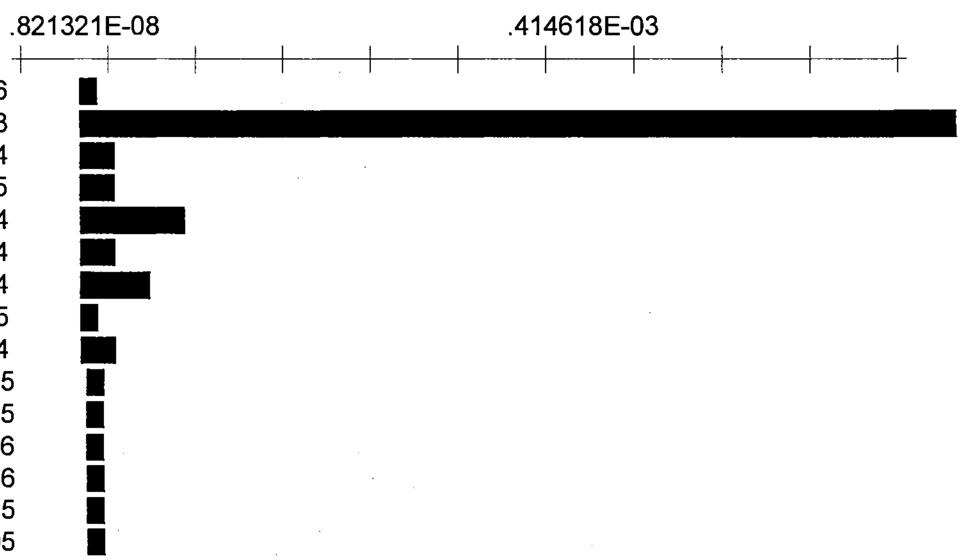

PERK

FOURIER COMPONENTS OF MEAS120

INDEX	FREQUENCY	REAL	IMAGINARY	MAGNITUDE	PHASE	PERIODOGRAM
1	0.00000	-0.004	0.000	0.004	0.000	0.004
2	0.00781	0.011	0.006	0.012	0.480	0.039
3	0.01563	-0.001	0.012	0.012	-1.481	0.038
4	0.02344	-0.002	0.004	0.004	-1.098	0.005
5	0.03125	0.002	-0.001	0.003	-0.542	0.002
6	0.03906	0.002	0.003	0.004	1.015	0.004
7	0.04688	-.424891E-03	0.006	0.006	-1.498	0.009
8	0.05469	-0.002	0.003	0.003	-0.924	0.003
9	0.06250	-0.002	.533902E-03	0.002	-0.244	0.001
10	0.07031	0.002	0.002	0.003	0.792	0.002
11	0.07813	-0.001	0.004	0.004	-1.307	0.005
12	0.08594	-0.004	0.003	0.005	-0.616	0.007
13	0.09375	-0.003	-.823572E-03	0.003	0.313	0.002
14	0.10156	-.733433E-03	-.573224E-03	.930865E-03	0.663	.221826E-03
15	0.10938	-0.001	.386806E-03	0.001	-0.315	.397834E-03

SERIES IS TRANSFORMED
PLOT OF MEAS120
NUMBER OF CASES = 128
MEAN OF SERIES = .773062E-05
STANDARD DEVIATION OF SERIES = .264516E-04

SEQUENCE PLOT OF SERIES

CASE VALUE .601169E-08 .153079E-03

CASE	VALUE
1	.160038E-04
2	.153079E-03
3	.147773E-03
4	.177601E-04
5	.826195E-05
6	.165049E-04
7	.343480E-04
8	.113917E-04
9	.487500E-05
10	.786625E-05
11	.190209E-04
12	.264708E-04
13	.716400E-05
14	.866509E-06
15	.155404E-05

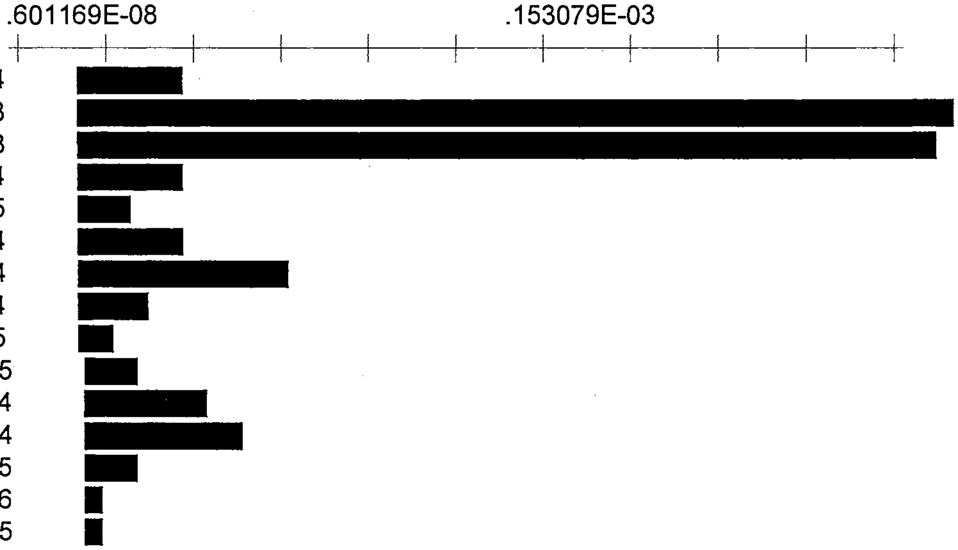

HYD

FOURIER COMPONENTS OF MEAS15

INDEX	FREQUENCY	REAL	IMAGINARY	MAGNITUDE	PHASE	PERIODOGRAM
1	0.00000	-.277732E-03	0.000	.277732E-03	0.000	.493663E-05
2	0.03125	-.266879E-03	-0.006	0.006	1.530	0.003
3	0.06250	0.004	-0.006	0.007	-1.012	0.003
4	0.09375	.599695E-03	0.002	0.002	1.243	.222453E-03
5	0.12500	.760434E-03	.437226E-03	.877170E-03	0.522	.492434E-04
6	0.15625	-.986619E-04	-.772201E-04	.125288E-03	0.664	.100461E-05
7	0.18750	-.983424E-04	-.749922E-04	.123673E-03	0.651	.978884E-06
8	0.21875	.400912E-03	-.578105E-03	.703516E-03	-0.964	.316758E-04
9	0.25000	.278125E-03	.701249E-04	.286829E-03	0.247	.526533E-05
10	0.28125	.203681E-03	.928770E-04	.223857E-03	0.428	.320716E-05
11	0.31250	.135406E-03	-.213972E-04	.137086E-03	-0.157	.120273E-05
12	0.34375	-.205150E-03	.148400E-05	.205156E-03	-0.007	.269369E-05
13	0.37500	.276064E-03	-.167023E-03	.322658E-03	-0.544	.666293E-05
14	0.40625	.163367E-03	-.301763E-04	.166131E-03	-0.183	.176636E-05
15	0.43750	.217293E-03	.518281E-04	.223388E-03	0.234	.319375E-05

SERIES IS TRANSFORMED
PLOT OF MEAS15
NUMBER OF CASES = 32
MEAN OF SERIES = .622468E-05
STANDARD DEVIATION OF SERIES = .156198E-04

SEQUENCE PLOT OF SERIES

CASE VALUE .152951E-07 .525074E-04

CASE	VALUE
1	.771348E-07
2	.418763E-04
3	.525074E-04
4	.347583E-05
5	.769427E-06
6	.156971E-07
7	.152951E-07
8	.494935E-06
9	.822708E-07
10	.501119E-07
11	.187927E-07
12	.420889E-07
13	.104108E-06
14	.275994E-07
15	.499024E-07

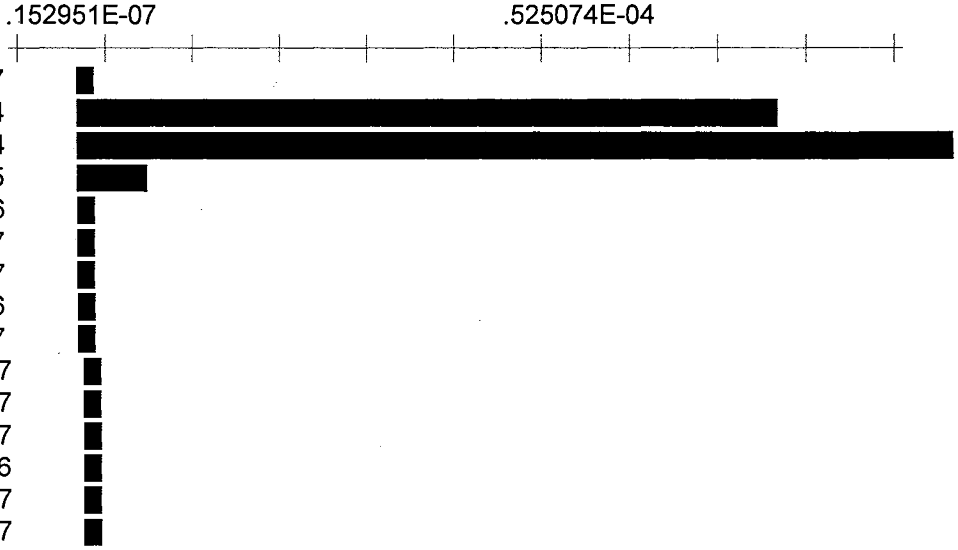

HYD

FOURIER COMPONENTS OF MEAS30

INDEX	FREQUENCY	REAL	IMAGINARY	MAGNITUDE	PHASE	PERIODOGRAM
1	0.00000	-0.005	0.000	0.005	0.000	0.001
2	0.03125	.908046E-03	-0.003	0.003	-1.289	.683647E-03
3	0.06250	0.002	-0.002	0.003	-0.918	.484023E-03
4	0.09375	.920158E-04	0.002	0.002	1.530	.330515E-03
5	0.12500	.328358E-03	0.001	0.001	1.262	.749218E-04
6	0.15625	-.250362E-03	.213885E-03	.329284E-03	-0.707	.693940E-05
7	0.18750	-.273059E-03	.342075E-03	.437694E-03	-0.897	.122609E-04
8	0.21875	-.191444E-03	.720739E-04	.204562E-03	-0.360	.267811E-05
9	0.25000	-.113033E-03	.297282E-03	.318045E-03	-1.207	.647379E-05
10	0.28125	-.235132E-04	.338402E-03	.339218E-03	-1.501	.736442E-05
11	0.31250	-.203000E-03	.142899E-03	.248252E-03	-0.613	.394426E-05
12	0.34375	-.408641E-03	.850896E-04	.417406E-03	-0.205	.111506E-04
13	0.37500	-.115482E-03	.382509E-04	.121652E-03	-0.320	.947153E-06
14	0.40625	-.177672E-03	.897268E-04	.199043E-03	-0.468	.253556E-05
15	0.43750	-.125611E-03	.943815E-04	.157118E-03	-0.644	.157991E-05

SERIES IS TRANSFORMED
PLOT OF MEAS30
NUMBER OF CASES = 32
MEAN OF SERIES = .232625E-05
STANDARD DEVIATION OF SERIES = .490667E-05

SEQUENCE PLOT OF SERIES

CASE	VALUE
1	.233379E-04
2	.106820E-04
3	.756286E-05
4	.516430E-05
5	.117065E-05
6	.108428E-06
7	.191576E-06
8	.418455E-07
9	.101153E-06
10	.115069E-06
11	.616291E-07
12	.174228E-06
13	.147993E-07
14	.396182E-07
15	.246861E-07

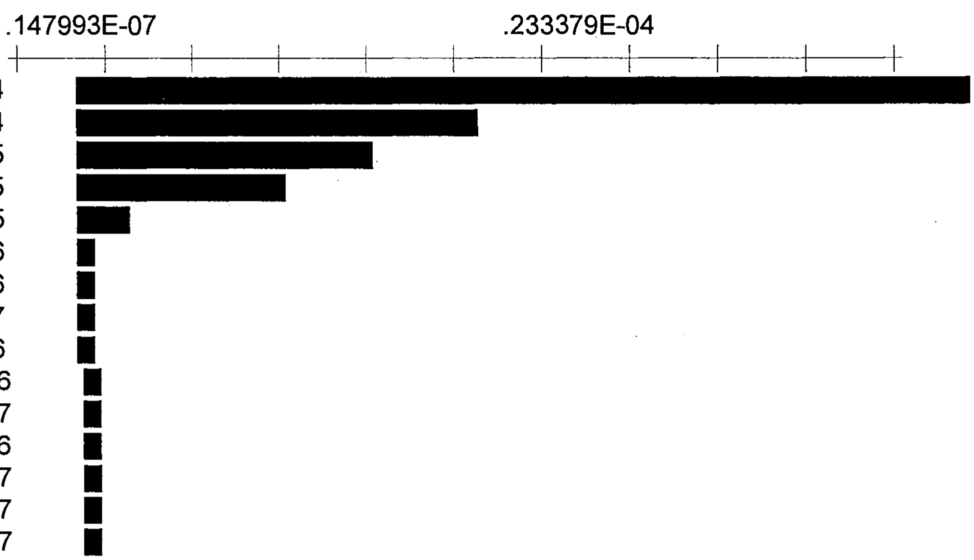

VITA

Christine Theresa Altendorf

Candidate for the Degree of

Doctor of Philosophy

Thesis: ESTIMATING SOIL WATER CONTENT USING SOIL TEMPERATURES AND A NEURAL NETWORK

Major Field: Biosystems and Agricultural Engineering

Biographical:

Personal Data: Born in Lubbock, Texas, April 23, 1963, the daughter of Harold and Catherine Altendorf.

Education: Graduated from Putnam City West High School in Oklahoma City, Oklahoma, in May 1981; received Bachelor of Science Degree in Agricultural Engineering from Oklahoma State University in December 1985; received Master of Science Degree in Agricultural Engineering from Oklahoma State University in December 1987; completed requirements for the Doctor of Philosophy degree in Agricultural Engineering at Oklahoma State University in December 1993.

Professional Experience: Employed by Oklahoma State University Vet Med Library from August 1982 to December 1984; Engineer Draftsperson at Oklahoma Department of Transportation for Summer 1983; Undergraduate and graduate research assistant in the Agricultural Engineering Department at Oklahoma State University from January 1985 through October 1987; Research Engineer in the Biosystems and Agricultural Engineering Department at Oklahoma State University from November 1987 to present.

Professional Memberships: ASAE, Alpha Epsilon, Tau Beta Pi, Registered Oklahoma Engineering Intern, Oklahoma Society of Professional Engineers, National Society of Professional Engineers.